605569
P. 224

DOE/NASA/0335-2
NASA CR-185240
GARRETT NO. 31-8071(2)

ADVANCED TURBINE TECHNOLOGY APPLICATIONS PROJECT (ATTAP)

1989 ANNUAL REPORT

Engineering Staff of
Garrett Auxiliary Power Division
A Unit of Allied-Signal Aerospace Company

February 1990

Prepared for
NATIONAL AERONAUTICS AND SPACE ADMINISTRATION
Lewis Research Center
Cleveland, Ohio 44135
Under Contract DEN3-335

for
U.S. DEPARTMENT OF ENERGY
Office of Transportation Systems
Heat Engine Propulsion Division
Washington, D.C. 20585

(NASA-CR-185240) ADVANCED TURBINE TECHNOLOGY APPLICATIONS PROJECT (ATTAP) Annual Report, 1989 (Garrett Turbine Engine Co.) 215 p CSCL 21E

N90-26728

Unclas
G3/85 0289161

DOE/NASA/0335-2
NASA CR-185240
GARRETT NO. 31-8071(2)

ADVANCED TURBINE TECHNOLOGY APPLICATIONS PROJECT (ATTAP)

1989 ANNUAL REPORT

Engineering Staff of
Garrett Auxiliary Power Division
A Unit of Allied-Signal Aerospace Company

February 1990

Prepared for
NATIONAL AERONAUTICS AND SPACE ADMINISTRATION
Lewis Research Center
Cleveland, Ohio 44135
Under Contract DEN3-335

for
U.S. DEPARTMENT OF ENERGY
Office of Transportation Systems
Heat Engine Propulsion Division
Washington, D.C. 20585

Disclaimer

This report was prepared as an account of work sponsored by an agency of the United States Government. Neither the United States Government nor any agency thereof, nor any of their employees, makes any warranty, express or implied, or assumes any legal liability or responsibility for the accuracy, completeness, or usefulness of any information, apparatus, product or process disclosed, or represents that its use would not infringe privately owned rights. Reference herein to any specific commercial product, process, or service by trade name, trademark, manufacturer, or otherwise, does not necessarily constitute or imply its endorsement, recommendation, or favoring by the United States Government or any agency thereof. The views and opinions of authors expressed herein do not necessarily state or reflect those of the United States Government or any agency thereof.

Printed in the United States of America

Available from
National Technical Information Service
U.S. Department of Commerce
5285 Port Royal Road
Springfield, VA 22161

NTIS Price Codes
Printed copy: A10
Microfiche copy: A01

TABLE OF CONTENTS

TABLE OF CONTENTS (Contd)

LIST OF FIGURES

LIST OF FIGURES (Contd)

LIST OF FIGURES (Contd)

LIST OF FIGURES (Contd)

LIST OF FIGURES (Contd)

LIST OF FIGURES (Contd)

LIST OF TABLES

LIST OF TABLES

LIST OF TABLES

LIST OF TABLES

ACRONYMS AND ABBREVIATIONS

AGT	Advanced Gas Turbine
ASME	American Society of Mechanical Engineers
ASTM	American Society for Testing Materials
atm	Atmosphere
ATTAP	Advanced Turbine Technology Applications Project
BOL	Broke-On-Loading
C	Celsius
cal	Calorie
CFDC	Combined Federal Driving Cycle
cm	Centimeter
CVD	Chemical Vapor Deposition
DOE	Department of Energy
ECU	Electronic Control Unit
EPIC	Elastic-Plastic Impact Computations (Computer Code)
F	Fahrenheit
FEM	Finite Element Model
FOD	Foreign Object Damage
FSH	Flow Separator Housing
GAPD	Garrett Auxiliary Power Division
GCCD	Garrett Ceramic Components Division
HIP	Hot-Isostatic Pressing
HP	High Pressure
in	Inch
hr	Hour
K_{IC}	Crack Growth Rate From Crack Origination Point
ksi	Thousands of Pounds Per Square Inch
LAS	Lithium Aluminum Silicate
lbs	Pounds
LP	Low Pressure
mg	Milligrams
MOR	Modulus of Rupture
mpg	Miles per Gallon

ACRONYMS AND ABBREVIATIONS (Contd)

NASA	National Aeronautics and Space Administration
NDE	Nondestructive Evaluation
ORNL	Oak Ridge National Laboratory
RBSN	Reaction-Bonded Silicon Nitride
RIT	Regenerator Inlet Temperature
RPD	Reference Powertrain Design
rpm	Revolutions Per Minute
SAE	Society of Automotive Engineers
SASC	Sintered Alpha Silicon Carbide
sec	Second
shp	Shaft Horsepower
SEM	Scanning Electron Microscope
Si_3N_4	Silcon Nitride
SiC	Silicon Carbide
SSN	Sintered Silicon Nitride
TiB_2	Titanium Diboride
TIPS	Turbine Inlet Particle Separator
TIT	Turbine Inlet Temperature
UDRI	University of Dayton Research Institute

1.0 SUMMARY

This report describes progress and work performed by Garrett Auxiliary Power Division (GAPD), a unit of Allied-Signal Aerospace Co., during Calendar Year 1989, to develop and demonstrate the technology of structural ceramics for automotive engines and other applications. This work was performed for the Department of Energy (DOE) under National Aeronautics and Space Administration (NASA) Contract DEN3-335, Advanced Turbine Technology Applications Project (ATTAP). This is the second in a series of technical summary reports being published on an annual basis over the course of the five-year contract.

1.1 Test Bed Engine Design, Analysis, and Materials Assessment

An analysis of the effect of regenerator inlet temperature (RIT) revealed that a reduction in RIT from 1093 to 982C (2000 to 1800F) had minimal impact on combined federal driving cycle (CFDC) fuel economy. The benefits of such a reduction in RIT include:

- Improved overall durability of the regenerator system
- Reduced oxidation/improved strength of components in the turbine discharge/combustor inlet areas

The RIT for the Reference Powertrain Design (RPD) was therefore reduced to take advantage of these benefits.

Improvements to the AGT101 advanced gas turbine test bed engine were necessary and included: regenerator seal durability, engine control system improvements, and combustor operation for easy light-off without risk of excessive carbon formation. The latter addressed the need to minimize the risk of impact to hot section components by loose carbon particles. In addition, alternate means of dealing with impact concerns are also being investigated. Specifically, turbine inlet particle separator (TIPS) development was continued and a potential redesign of certain hot section components (including the rotor and the stators) for increased impact tolerance was under consideration at the close of the report period.

Secondary issues and test bed improvements addressed by ongoing ATTAP work included:

- Spring durability in the combustor cap to maintain the required part stacking loads during extended operation
- Thermal insulation improvements to improve performance and inhibit erosion
- Ceramic seal improvements to separate the high-pressure combustor inlet air from the low-pressure turbine discharge stream

Other areas for improvement included:

- An improved design to address yielding of the metallic nut on the ceramic bolts to retain the ceramic turbine shroud
- Modifications to ceramic wave springs for better reliability
- An improved material for the exhaust housing to provide better high-temperature strength and resistance to corrosion over the current cast ductile iron housing

1.2 Ceramic Component Design

A large portion of this effort was devoted to the development of design methods for impact tolerance. Ballistic experiments continued at University of Dayton Research Institute (UDRI) to characterize the behavior of ceramic targets when impacted under various conditions. The distinction between structural impact failure (due to bending) and local impact damage (characterized by flaw propagation from the impact site) was recognized. Analytical work seeks to understand the phenomena that govern impact failure. The Elastic-Plastic Impact Computations (EPIC) code was used to make predictions of blade failure under impact, and these predictions compared favorably to physical test results.

The effect of pressure stresses on the ATTAP flow separator housing (FSH) was investigated for a baseline and several alternative configurations. These alternatives included stiffeners, increased flange thickness, and new means of supporting the FSH in the test bed engine. This work will continue into 1990.

1.3 Materials Characterization and Ceramic Component Fabrication

The three ceramic subcontractors (Norton/TRW Ceramics, Carborundum, and GCCD) continued work on development of fabrication techniques suited to the volume production of ATTAP components. This effort must demonstrate the ability to form materials into the required complex shapes without a reduction in the material properties demonstrated with test bars. Materials which had been assessed early in the ATTAP were further characterized to better define their capabilities in an engine environment.

A study was performed to verify that heat treatment can be effective in eliminating an intermediate temperature stability problem in certain materials. An investigation was also initiated to determine which, if any, other materials used in the ATTAP test bed engine exhibit a similar problem.

Thermal conductivity, an important property for resistance to thermal transient failure, was measured for eight materials, and the threshold for dissocation of NT154 under high vacuum and temperature conditions was assessed. This last was done to support high temperature spin testing, scheduled later in ATTAP.

1.4 Component Rig Testing

Combustor rig testing concentrated on evaluating the ability of the current combustor to operate successfully without creating carbon particles. Testing was performed at engine idle, cruise, and maximum power conditions using a variety of fuels. Progress continues in this area.

TIPS testing evaluated a design which uses combustor swirl to centrifuge damaging particles to the periphery of the combustor. Clean air then flows down the center to the turbine area. Refinements to this concept continue to be evaluated.

Testing of ceramic piston ring seals at the junction of the turbine shroud, transition duct, and FSH confirmed that the triple seal configuration had a better leakage characteristic than double seals. The triple seal design was adopted as a result of this testing.

Preliminary testing to confirm the ability to spin a disk under a soft vacuum (up to 1/3 atm) was performed. This activity complements dissocation testing of NT154, and will be used to determine the test matrix for heated spin pit tests later in ATTAP.

2.0 INTRODUCTION

This report is the second in a series of Annual Technical Summary Reports for ATTAP, authorized under the DOE sponsored NASA Contract DEN3-335. This report has been prepared by GAPD. Included as appendices are reports provided by Garrett Ceramic Components Division (GCCD), Norton/TRW Ceramics Co., and the Carborundum Co., all subcontractors to GAPD on ATTAP. The project is administered by Mr. Thomas Strom, Project Manager, NASA-Lewis Research Center, Cleveland, Ohio. This report presents plans and progress for Calender Year 1989.

Project effort conducted under this contract is part of the DOE Gas Turbine Highway Vehicle System Program. This program is oriented to provide the United States automotive industry the high-risk, long-range technology necessary to produce gas turbine engines for automobiles with reduced fuel consumption and reduced environmental impact.

The ATTAP test bed engine (Figure 1) is designed such that, when installed in a 3000-pound inertia weight automobile, it will provide:

- Low emissions
- Fuel economy of 42 mpg on diesel fuel
- Multifuel capability
- Competitive costs with current spark-ignition engines
- Noise and safety characteristics that meet federal standards

It is nominally a 100-shp engine, capable of speeds to 100,000 rpm and operation at turbine inlet temperatures (TIT) to 1371C (2500F) with a specific fuel consumption level of 0.3 pounds/hp-hr over much of the operating range.

The program is oriented toward developing the high-risk technology of ceramic structural component design and fabrication, such that industry can carry this technology forward to production in the 1990s. The ATTAP test bed engine, continued in use from the AGT101 Project, is being used for verification testing of the durability of ceramic components, and their suitability for service at Reference Powertrain Design (RPD) conditions.

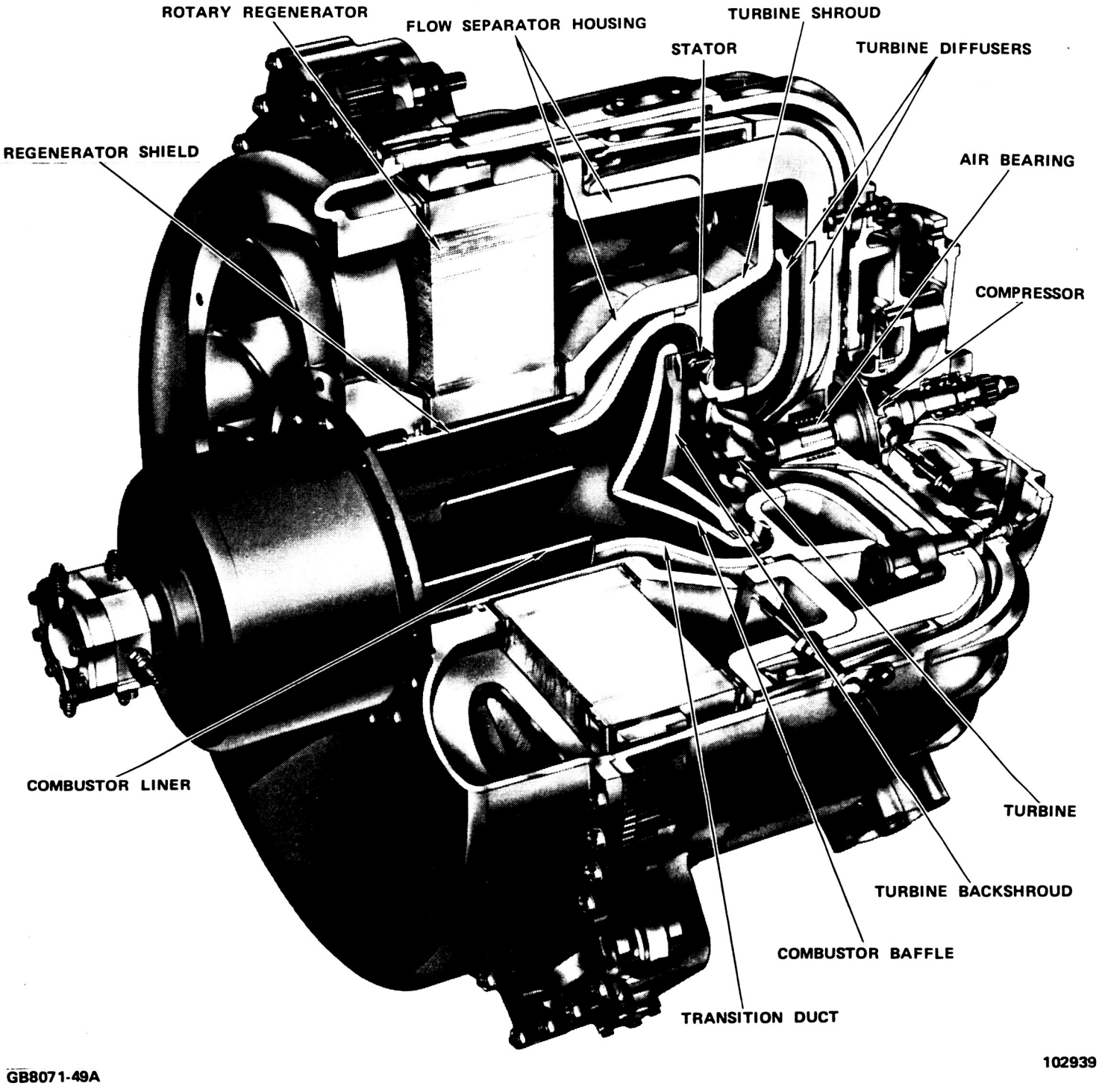

Figure 1. ATTAP Test Bed Engine.

The ATTAP schedule is depicted in Figure 2. The program continues technology work into Calendar Year 1992, culminating in the demonstration of ceramic engine operation for 300 hours under conditions simulating CFDC for automotive engines. In addition, a RPD Cost Analysis will be performed in late 1991, to provide the U.S. automotive industry with data on the costs of producing engines with structural ceramic materials.

This report reviews the efforts conducted in the second full year of ATTAP in development of ceramic technology, review and updating of the RPD, and improvements made to the test bed engine and test rigs. Appendices include progress reports made by the major ATTAP subcontractors to GAPD: Norton/TRW Ceramics, Carborundum Co., and GCCD.

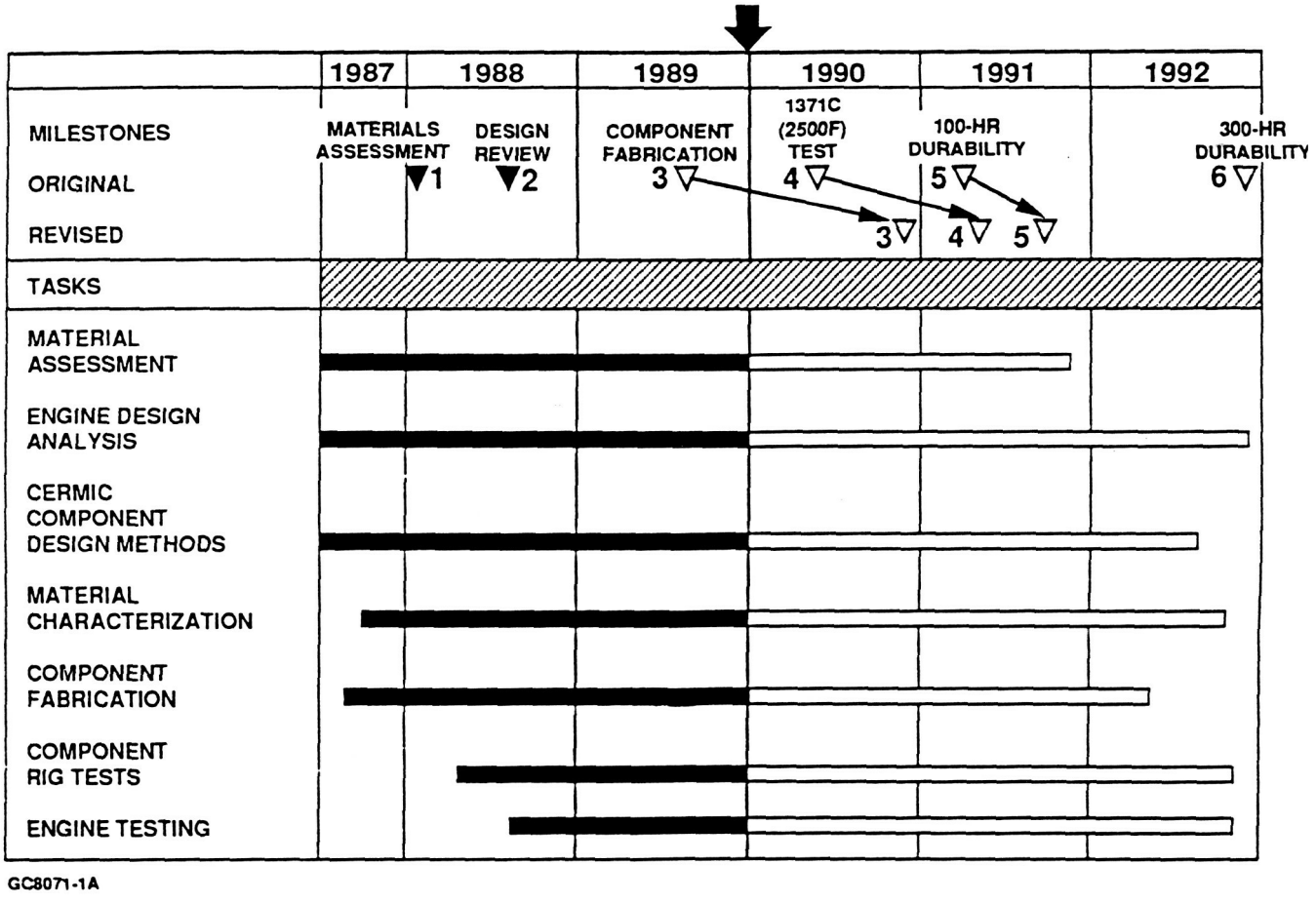

Figure 2. ATTAP Milestone Schedule.

3.0 TEST BED ENGINE DESIGN, ANALYSIS AND MATERIALS ASSESSMENT

3.1 Materials Assessment

No new materials were assessed.

3.2 Reference Powertrain Design (RPD)

A review was conducted of the effect of RIT on the performance of the AGT101 RPD. This review evaluated the impact of RIT on the projected performance of the engine cycle, on the durability of existing ceramic components, and the future development of the regenerator system.

The effect of RIT was evaluated using the AGT101 RPD engine performance/mission model, which studied the effect of varying RIT from the current design level of 816 to 1093C (1500 to 2000F) to determine the effect on CFDC fuel economy. Figure 3 shows the results of this work. A reduction in RIT from 1093 to 982C (2000 to 1800F) would reduce projected fuel economy by 1.1 mpg.

The benefits of reducing RIT to 982C (1800F) are significant. First, there will be improved durability of the regenerator system. Increased life can be expected from the regenerator core and the seal system as a direct benefit of the reduced operating temperatures at engine idle and cruise operating conditions. Second, the operating temperatures in the combustor inlet and turbine discharge areas will be reduced by 93C (200F) resulting in a corresponding reduction in the operating temperatures of the surrounding metallic and ceramic components. This results in reduced oxidation and improved strength of these components, while reducing heat loss.

3.3 Reference Powertrain Design Cost Analysis

The RPD Cost Analysis is scheduled for the final year of ATTAP.

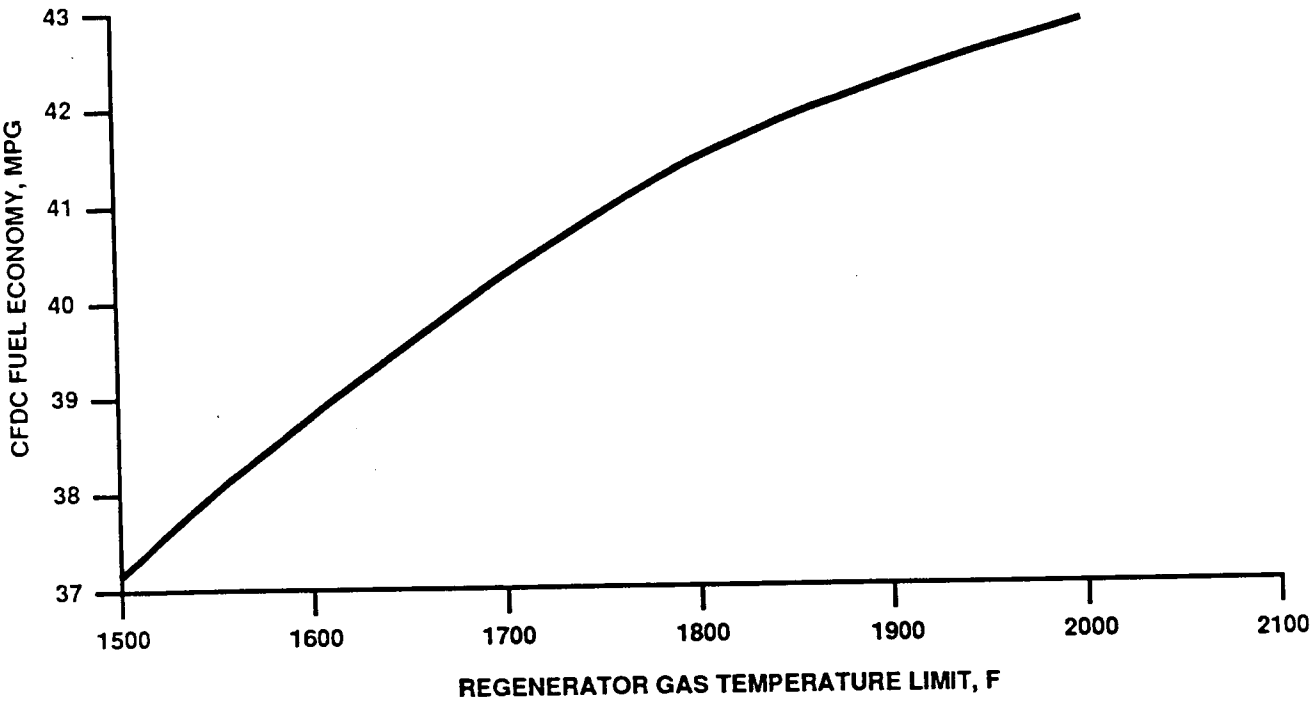

Figure 3. Effect of RIT on CFDC Fuel Economy.

3.4 Test Bed Improvements

Improvements in the ATTAP test bed engine design have progressed towards the goal of providing a reliable test bed for evaluating ceramic components at engine operating conditions representative of RPD. The combustor system has been improved to ensure reliable starting, smooth operation and the reduction of carbon formation. Complementary to the reduction of carbon formation, TIPS development has been investigating the conceptual feasibility of flow path geometries which can separate out solid particles before the ceramic rotating components suffer foreign object damage (FOD). Regenerator development activity has addressed the simultaneous concerns of seal leakage and seal durability at the elevated temperature operating conditions. Ceramic seal development is examining how to effectively seal interpath high-temperature gas leaks.

Other activities were undertaken to improve the high-temperature durability of existing test bed components, by addressing deficiencies noted in previous testing. This work included improving the material used in the exhaust housing, redesigning the combustor cap to reduce the temperature of the combustor springs, and a minor redesign of the ceramic bolt assembly used in the turbine shroud support. Detailed discussions of each of these issues follow.

3.4.1 Regenerator Metallic Seal

At the end of the 1988, regenerator seal shoe ceramic-coated/metallic-substrate specimens were evaluated to identify a suitable substrate with improved high-temperature strength over the original Inconel 601. Heat treatment at 1093C (2000F)* for one hour in air was performed on a baseline and two alternate specimens consisting of:

	Baseline	Alternate 1	Alternate 2
Substrate:	**Inconel 601**	**Inconel MA956**	**Haynes 230**
Bond Coat:	**NiCrAlY**	**FeCrAlY**	**NiCrAlY**
Intermediate Coat:	**I-00****	**I-00**	**I-00**
Top Coat:	**I-112****	**I-112**	**I-112**

****Ford Motor Co. coating designations**

Of the three specimens evaluated, the Haynes 230/NiCrAlY combination of substrate/bond coat appeared to be the most stable. The Inconel 601/NiCrAlY system exhibited warpage and coating spallation. The Inconel MA956/FeCrAlY specimens exhibited severe oxidation and corrosion.

Work continued into 1989 with metallographic and scanning electron microscopic (SEM) analyses. Interfacial attack was evident in all three cases (Figure 4). The Inconel 601 and Incoloy MA956 substrates exhibited the most substantial attack while the Haynes 230 base metal exhibited minimal attack. X-ray mapping performed at the coating/substrate interfaces showed chemical diffusion in all three substrates.

*This work was begun prior to the reduction in RIT to 982C (1800F) discussed in Section 3.2. Substrate comparisons are still valid.

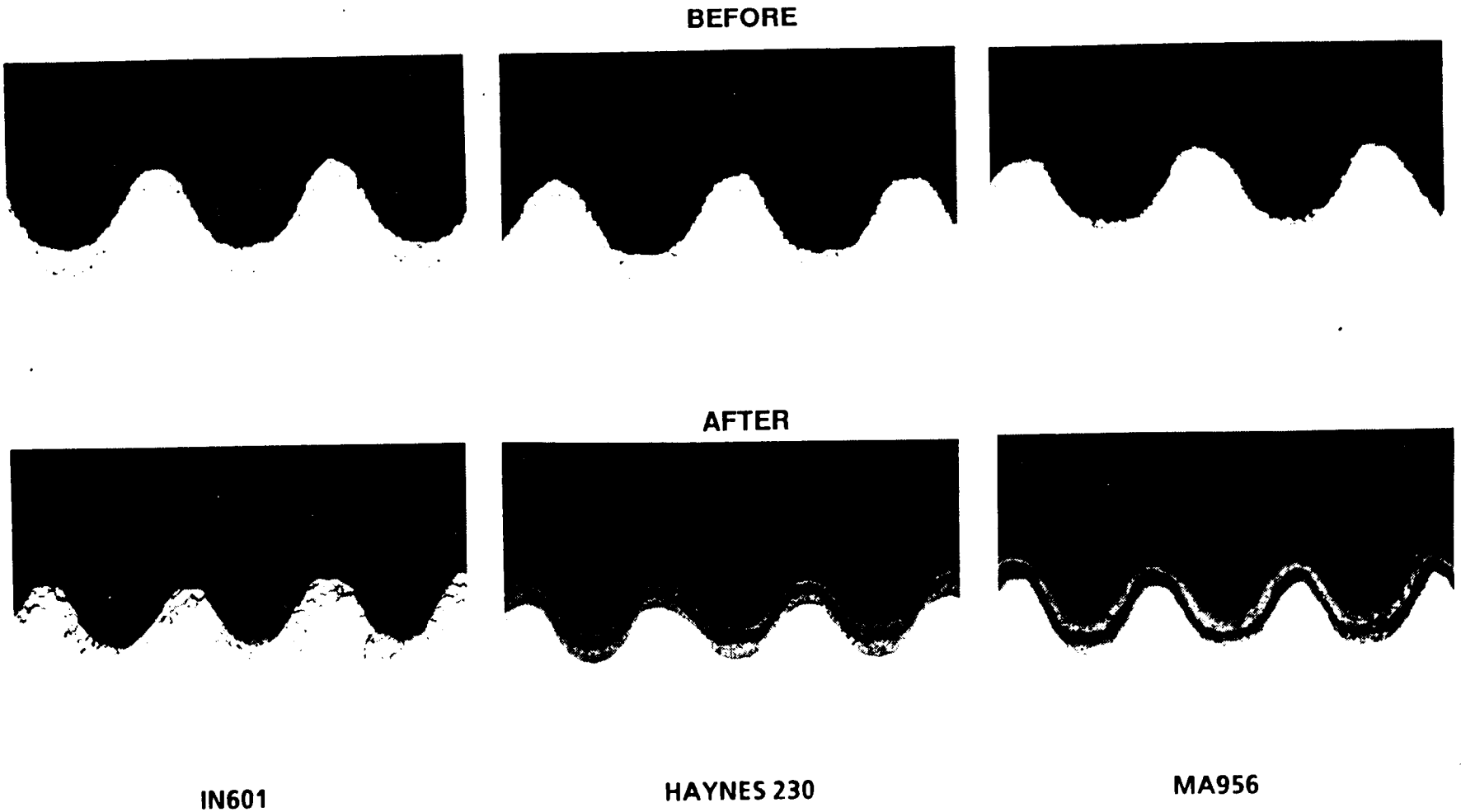

Figure 4. Regenerator Shoe Specimens Exhibited Interfacial Attack After a 2000F/1 Hour Heat Treament.

As the Haynes 230 exhibited the most stable behavior, seal specimens (Figure 5) were prepared for further testing. To inhibit chemical diffusion, these specimens included a ten micron chemical vapor deposition (CVD) alumina layer between the NiCrAlY bond coating and the I-00 layer. The coating/substrate configuration was:

Substrate:	**Haynes 230**
Bond Coat:	**NiCrAlY**
Diffusion Barrier:	**Al_2O_3 (CVD)**
Intermediate Coat:	**I-00**
Top Coat:	**I-112**

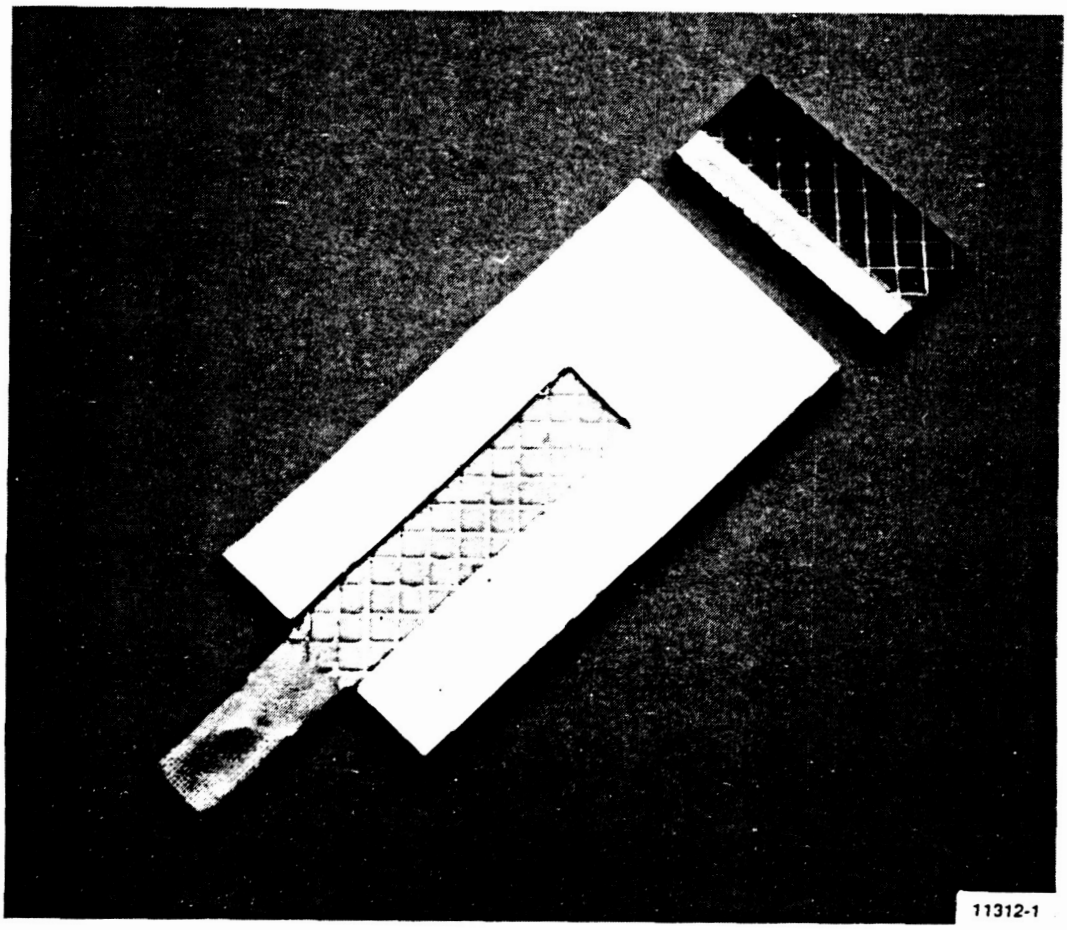

GB9-125-77

Figure 5. 3/4-Inch Coupons Were Cut From the Haynes 230 Test Specimens and Heat Treated for Compatibility Evaluation.

Coupons cut from these coated specimens were heat treated between 871 and 1093C (1600 and 2000F), in 56C (100F) intervals, for one hour in air to evaluate interfacial stability and to assess the effectiveness of the CVD alumina diffusion barrier in accommodating the chemical incompatability between the coatings and the nickel-based alloys.

All interfaces were stable up to 927C (1700F). At 982C (1800F), a reaction between the bond coating and the I-00 layer was evident. At 1038 and 1093C (1900 and 2000F), substrate attack was observed. Obviously, the CVD alumina layer was ineffective as a diffusion barrier, and appeared to degrade interfacial stability since the attack observed at 1093C (2000F) was more pronounced than previously observed in samples with no CVD alumina layer.

Specimens were exposed in a burner rig under thermal cyclic conditions [204-927C and 204-982C (400-1700F and 400-1800F)] to evaluate the bond coating thermal strain tolerances. These tests were inconclusive due to an inability to achieve the desired microstructure (microcracking) during the coating application.

Six sets of Haynes 230 regenerator seal assemblies were ordered to satisfy the hot regenerator rig and engine test hardware requirements over the next two years. As a result of the compatibility test outcome, only two seals will be coated with the baseline AGT101 substrate until further compatibility tests can be performed to define a superior coating system. These two sets of seals will be used in the initial regenerator rig tests and engine tests where short term seal shoe durability (up to 50 hours) will satisfy the test objectives.

Regenerator activities also included successfully bonding six regenerator core assemblies and ordering the hot regenerator rig hardware required to conduct testing in 1990. The ring gear/regenerator core bonding process is illustrated in Figures 6 and 7.

3.4.1.1 Integral Seal Development

The long term approach to a regenerator seal system which meets the 3500-hour/982C (1800F) design requirement is to eliminate the metallic components from the seal and apply the seal wear-face coating directly to the ceramic flow separator housing. Two studies were performed to support integral seal development:

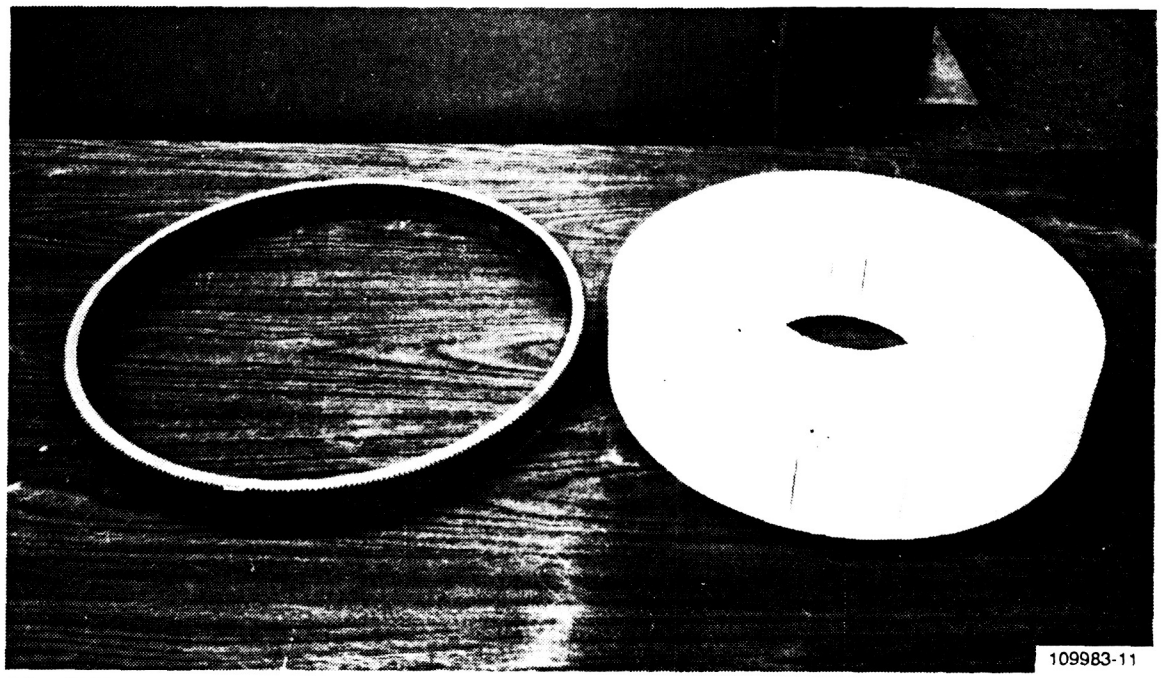

GB9-125-58

Figure 6. NGK Ceramic Regenerator Core and Ring Gear Prior to Bond Assembly Process.

- The thermal expansion and elastic properties of three candidate Ford seal coatings (I-00, I-39 and I-112) were measured to identify potential problems with substrate/coating expansion mismatch stresses

- I-112 coatings were applied to different ceramic substrates to assess potential compatibility problems

I-39 was the only composition which exhibited linear expansion characteristics to 1100C (2012F). Both the I-00 and I-112 compositions exhibited permanent shrinkage during testing. The dilatometer runs were repeated on the same I-00 and I-112 specimens to determine if additional shrinkage (sintering) would occur in subsequent runs. Both the I-00 and I-112 coatings exhibited greater stability in the repeat tests, but some additional shrinkage did occur. Recently, the coating supplier switched from spray dried powders to sintered I-00 and I-112 powders. The go-forward plans are to repeat this experiment on specimens prepared from the sintered powders.

ORIGINAL PAGE
BLACK AND WHITE PHOTOGRAPH

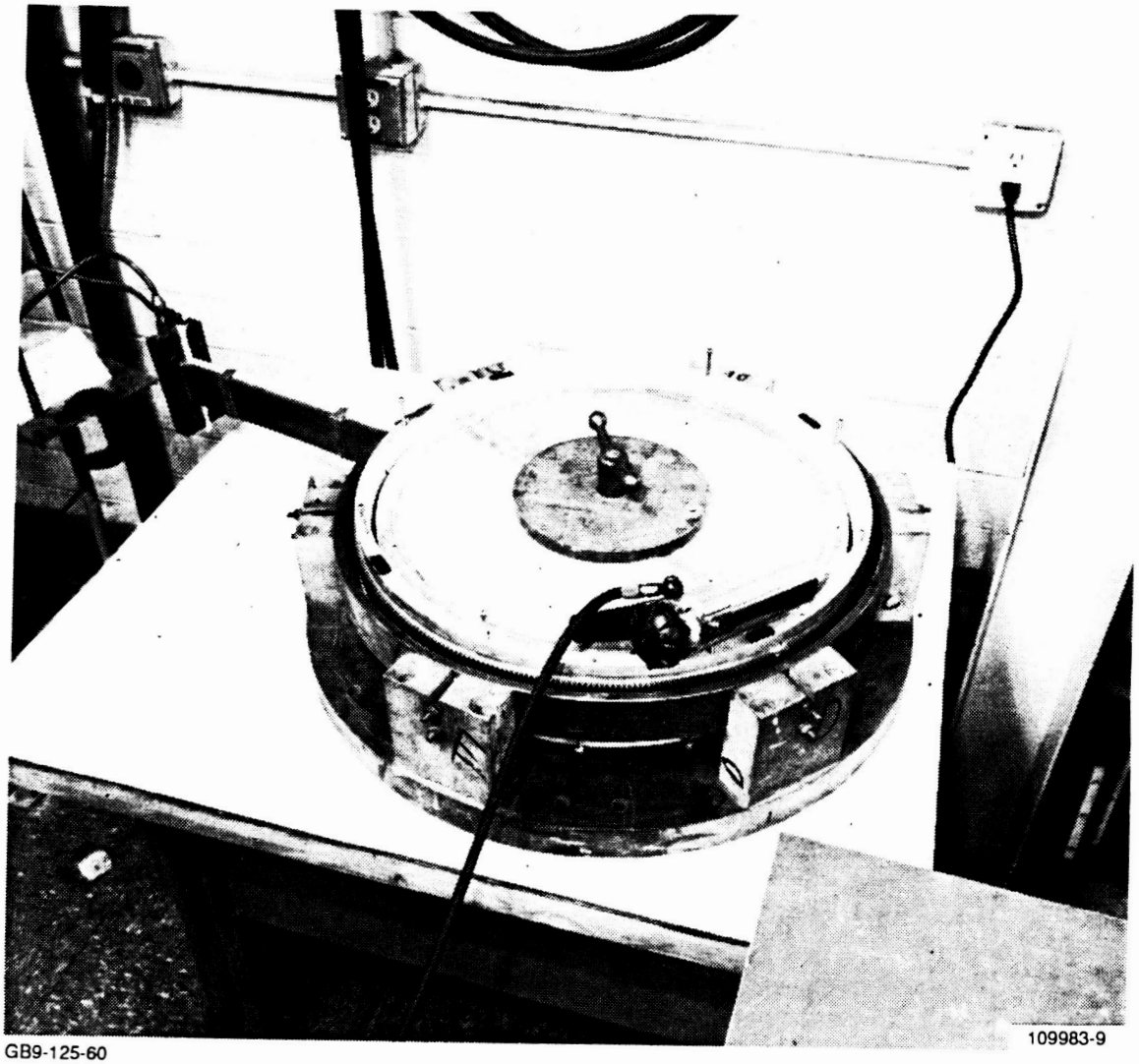

Figure 7. Ring Gear Is Bonded to the Regenerator Core With Silastic J Elastomer Cured in This Induction Heater Fixture.

The elastic properties were measured at room temperature using sonic velocities. Lov elastic moduli and Poisson's ratio indicate the I-112 coating was heavily microcracked. Hig attenuation in I-112 compared to the other coatings support that conclusion.

Thin I-112 coatings were applied to four different ceramic substrate materials to asses potential chemical compatibility problems: Lithium aluminum silicate (LAS) glass-ceramic GCCD reaction-bonded silicon nitride (RBSN), Kyocera SN251 silicon nitride (Si_3N_4), and NGI SN84 Si_3N_4. LAS is the current FSH material. The I-112 coatings were initially adherent t all substrate materials. Heat treatment studies similar to those performed for metallic sea studies are in progress.

An integral seal configuration was designed which eliminates the hot seal shoe/ diaphragm assembly and operates with the core bearing directly against the FSH. A concept verification test has been defined. The rig layout for this test was completed and detail component design was initiated in 1989. The test will be conducted in 1990.

3.4.2 Combustor Design

During 1989, a three-dimensional flow analysis of the combustor was performed incorporating the center flow TIPS hardware. This analysis was conducted at the engine's steady-state maximum power conditions and included evaluations of unburned fuel, pressure drop, temperature distribution and flow field distribution. The results, as depicted in Figure 8, indicate good combustion but further analysis needs to be conducted at other operating conditions. This analysis has been postponed until a decision has been made for TIPS and combustor geometries.

3.4.3 Seals

One of the critical sealing locations of the ATTAP test bed engine is at the FSH, transition duct, and turbine shroud junction. If the seal is not adequate in this area, there is a direct loss to the system due to air flowing from the compressor to the downstream side of the turbine. During the AGT101 program, seal improvements included changing the original single seal design to a dual seal configuration. Since then, a new triple seal design has been designed for use in the ATTAP engine (see Figure 9).

The triple seal configuration initially utilized SSN. The rings were designed with a split-end gap to account for thermal growth variation between the ring set and the FSH against which the rings seal. The rings were designed to have a closed gap at engine operating conditions.

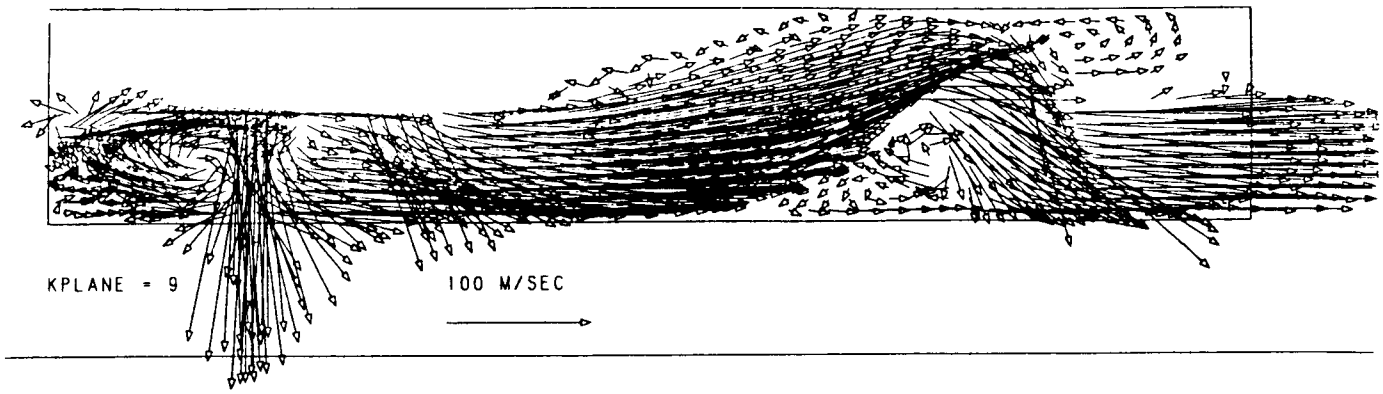

GB9-125-106

Figure 8. Combustor Flow Field Distribution.

During the past year, seals were constructed out of LAS material, the same material used for the FSH. As the disparity in growth is nil, these are made without an end gap. However, each seal must be custom fitted to a particular FSH for maximum sealing efficiency.

At the onset of this design change, it was believed that the triple seal configuration would provide approximately 15 percent less leakage over the dual seal used previously in the AGT101 configuration. Testing, as described in Section 6.7, confirmed the benefits of the triple seal.

The testing of both the dual and triple solid seals was completed in early September. As was expected, the results of the tests supported the theory that triple seals would allow less leakage than dual seals. Based on the findings, the triple seals will be incorporated into the next build of the ceramic ATTAP test bed engine.

3.4.4 Turbine Inlet Particle Separator (TIPS) Design

The TIPS test program's overall goal is to identify a means of separating particles from the gas stream in order to eliminate particle impact on the ceramic turbine rotor. Several designs have been evaluated during 1989 to maximize the separation efficiency and minimize the pressure drop across the TIPS. Since the development of this design relies heavily upon physical testing, the details of this work are reported with rig testing in Section 6.6.

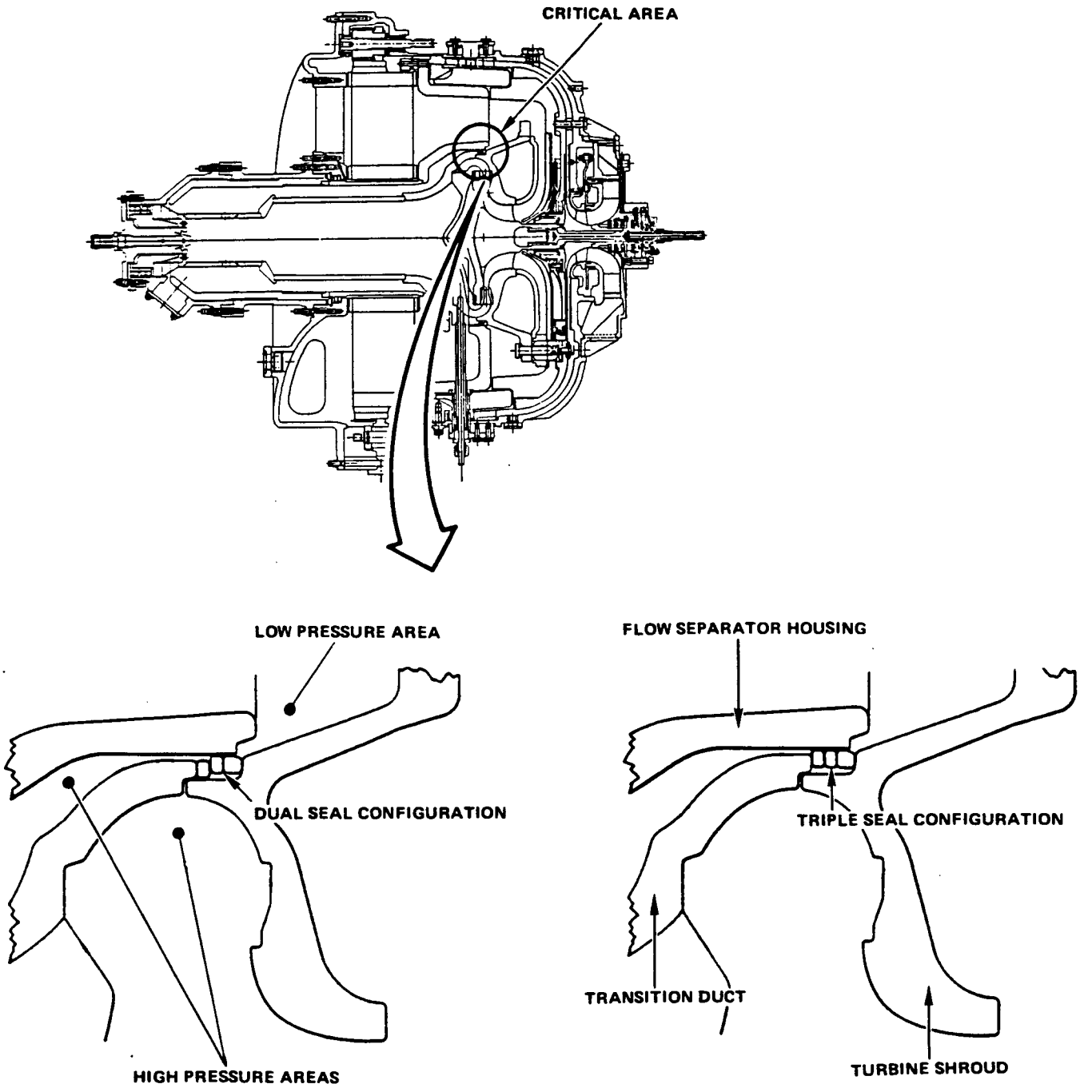

Figure 9. Critical Seal Location and Triple Seal Configuration.

3.4.5 Flow Separator Housing (FSH) Support

The current FSH mounting system uses a metallic ring support to restrain the housing axially against pressure loads at its peripheral flange, as shown in Figure 10. Since the LAS flow separator has low thermal expansion compared to the metal ring support, thermal growth mismatch during operation creates a sliding friction. There are two consequences: (1) The sliding friction generates tensile loads in the flow separator flange, and (2) the higher axial loads at the high pressure (HP) side of the flow separator make it tend to follow the movement of the ring support to the HP side, and to drift off-center during operation.

Analysis of the current flow separator full flange support system, and comparison with frictional coefficient test data, indicate a potential for frictional contact tensile stresses as high as 35 ksi in the flange. The characteristic strength of the LAS flow separator material is 12 ksi. Experience in the prior AGT101 Program confirms the likelihood of failure in this mode.

The proposed rocker assembly, Figure 11, uses a chrome-plated M-50 tool steel cylinder rolling between contact washers of like material to remove the contact tensile stress and friction that pulls the FSH on the HP side. The load distribution and stresses for a cylinder on a washer support system were evaluated with a 2-D finite element model. Loads were found to be very low, as shown in Figure 12, and the maximum stress in the flange was 3.6 ksi. The maximum stress location is indicated on the finite element model (FEM) used for this analysis, Figure 13.

Tests are planned to confirm the load capability of the FSH with the 3-point support. A test rig has been fabricated to test the design of an individual rocker support. After satisfactory completion of this test further testing will be done using a FSH with all the rockers in place.

3.4.6 Ceramic Bolt Assembly

The ceramic bolt assembly consists of a ceramic pilot bolt with a Hastelloy X locking nut whose separate jaws slip over the end of the pilot bolt. A retaining ring is placed over the jaws to keep them from separating. The ceramic bolt assembly, which secures the turbine shroud, is shown in relation to the ATTAP test bed engine in Figure 14.

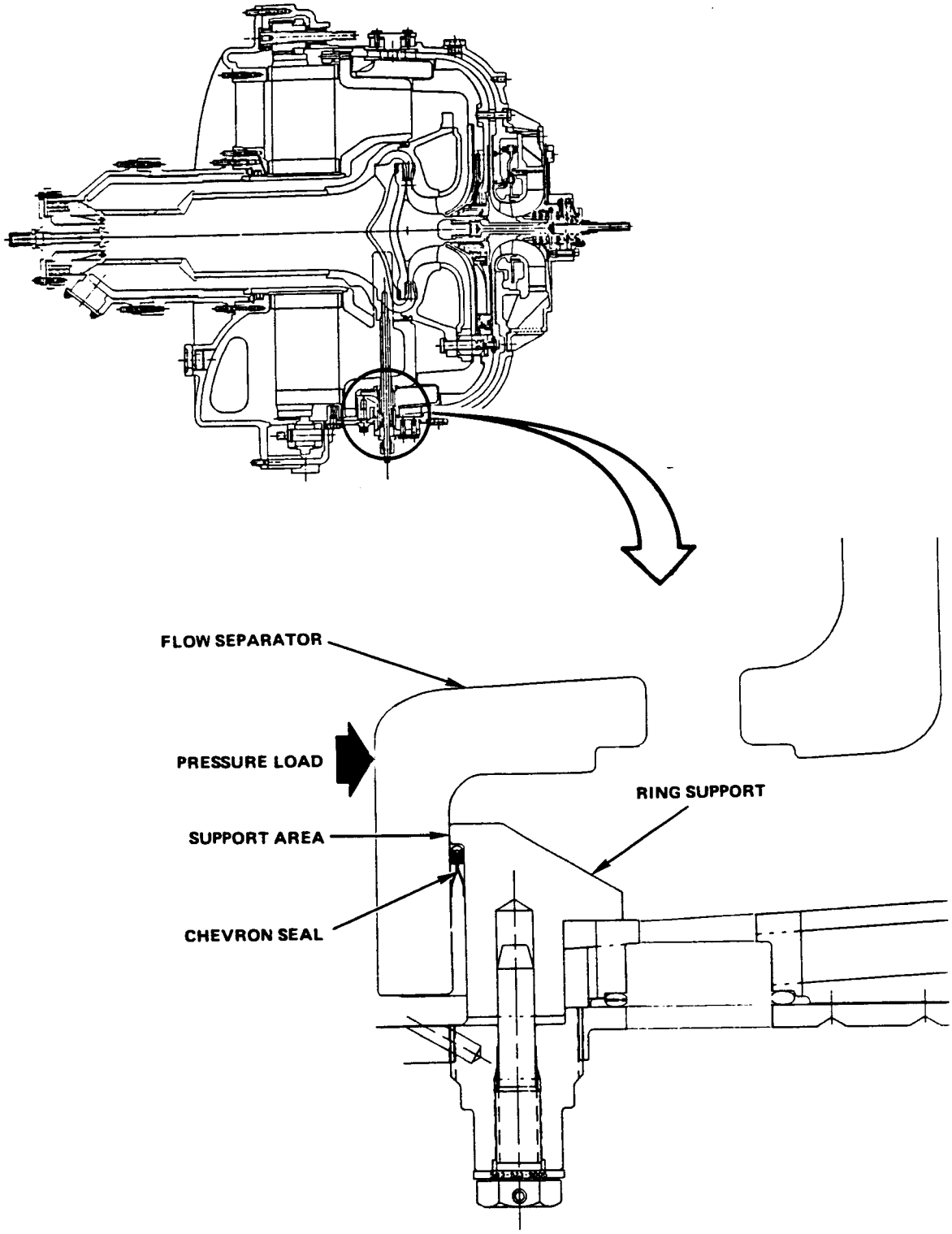

Figure 10. FSH Is Currently Supported by Full Ring Contact.

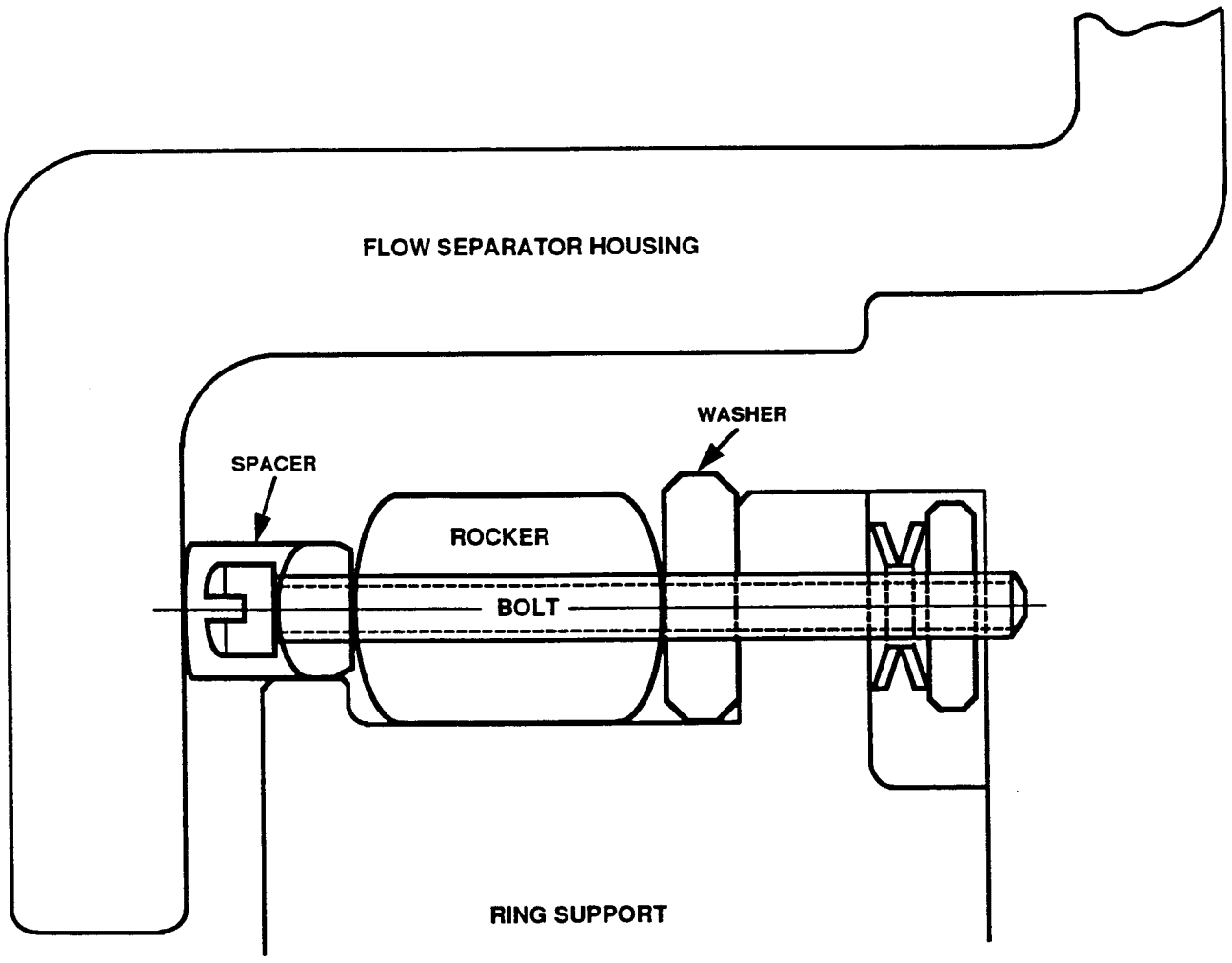

GC8071-4A

Figure 11. Proposed Flow Separator Support Configuration.

Through finite element analysis and testing, it was determined that the Hastelloy locking nut and retaining ring yield during proof loading of the bolt prior to engine assembly, and are unable to withstand stresses during engine operation at elevated temperatures. Thus, the bolt design was modified to prevent yielding and the subsequent bolt load relaxation.

The design changes shown in Figure 15 were made to prevent yielding of the locking nut and sleeve. By changing the material and the geometry of the locking nut and sleeve, component yielding during assembly is eliminated and integrity is maintained during engine operation. The thinner ceramic pilot bolt can easily tolerate the operating stresses of 17 ksi.

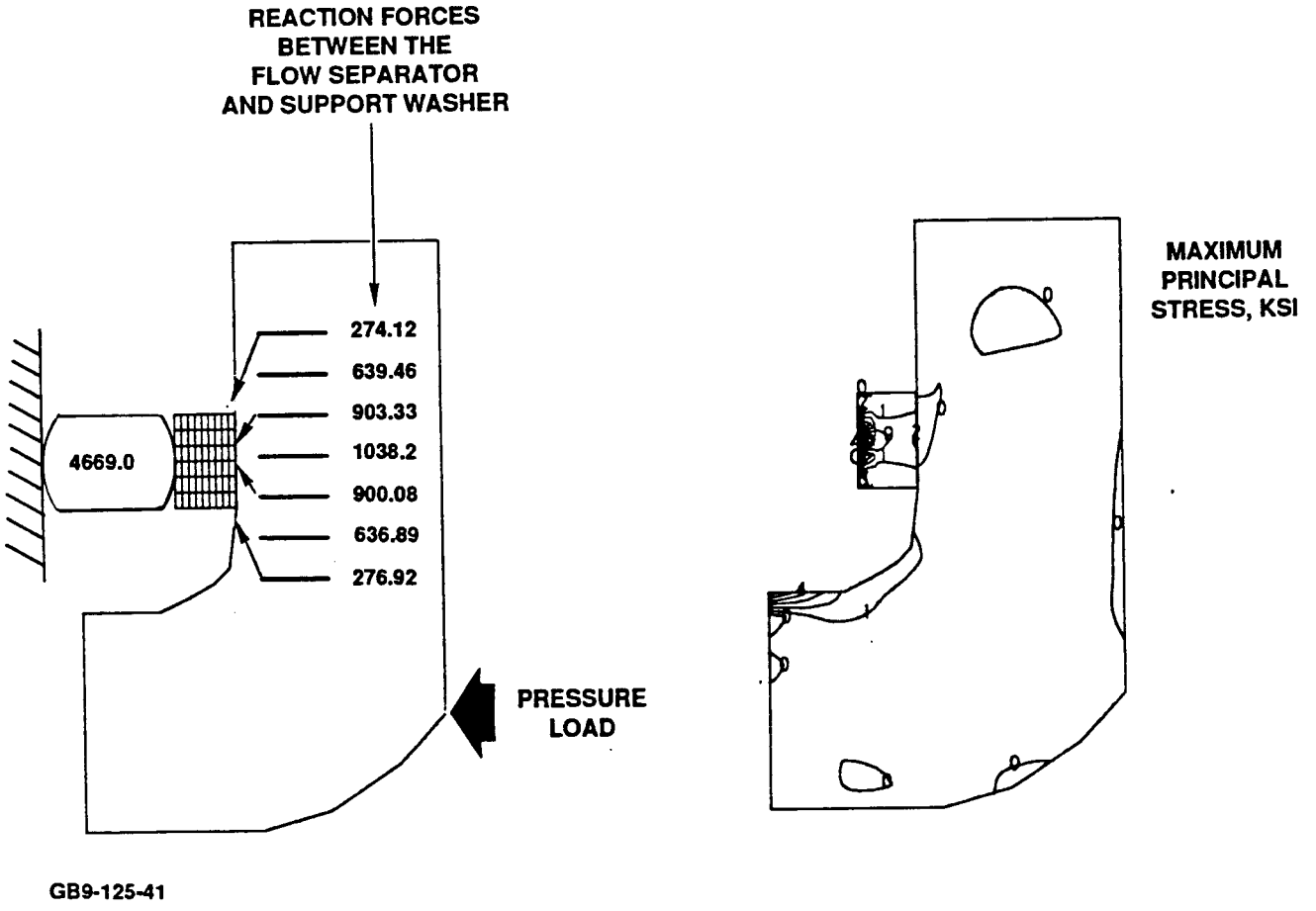

Figure 12. **Finite Element Modeling Shows Acceptable Load Distribution and Stresses.**

3.4.7 Miscellaneous Test Bed Improvements

3.4.7.1 Improved Combustor Cap

The combustor cap assembly was redesigned with the objective of reducing the combustor spring operating temperature. The combustor spring provides assembly loads for the hot section ceramic components. Similar springs, used in the combustor rig and early ceramic engines have relaxed at elevated temperatures.

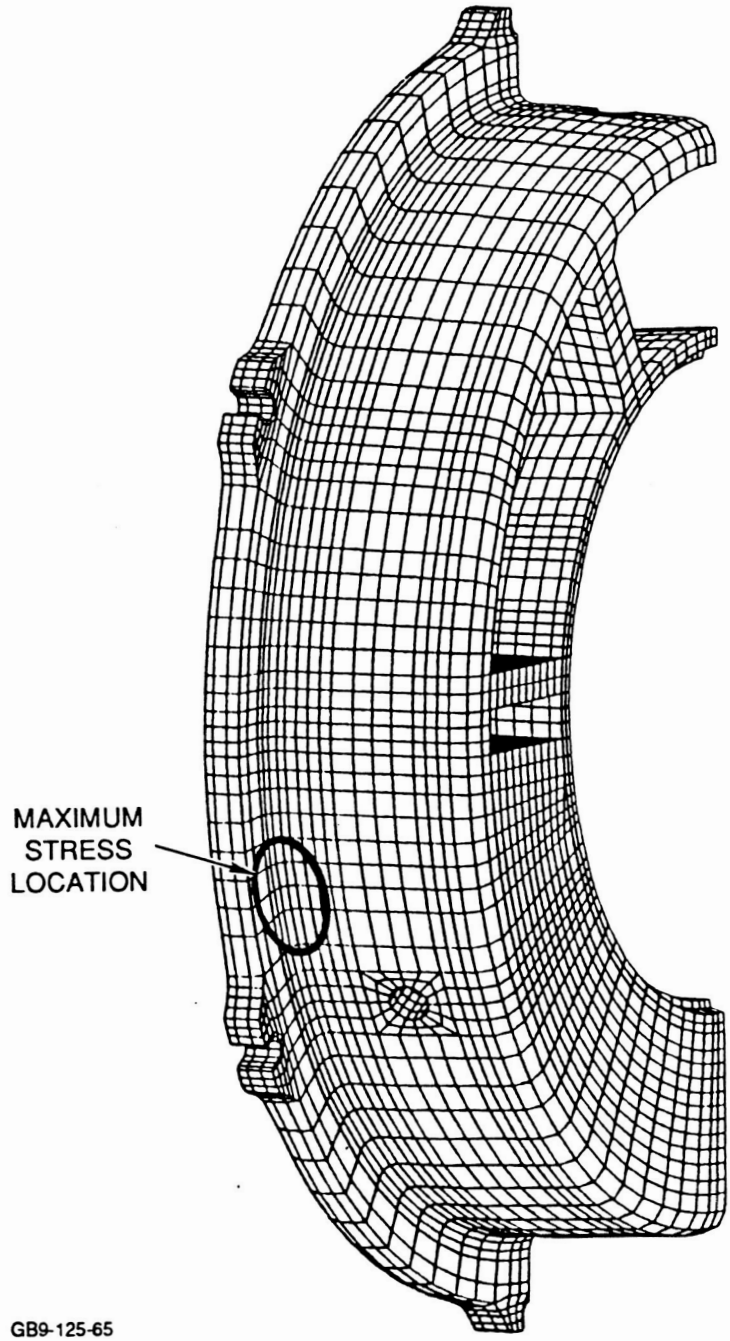

Figure 13. The Proposed 3-Point Rocker Assembly Is Calculated to Produce a Maximum Stress in the Flange of 3.6 ksi.

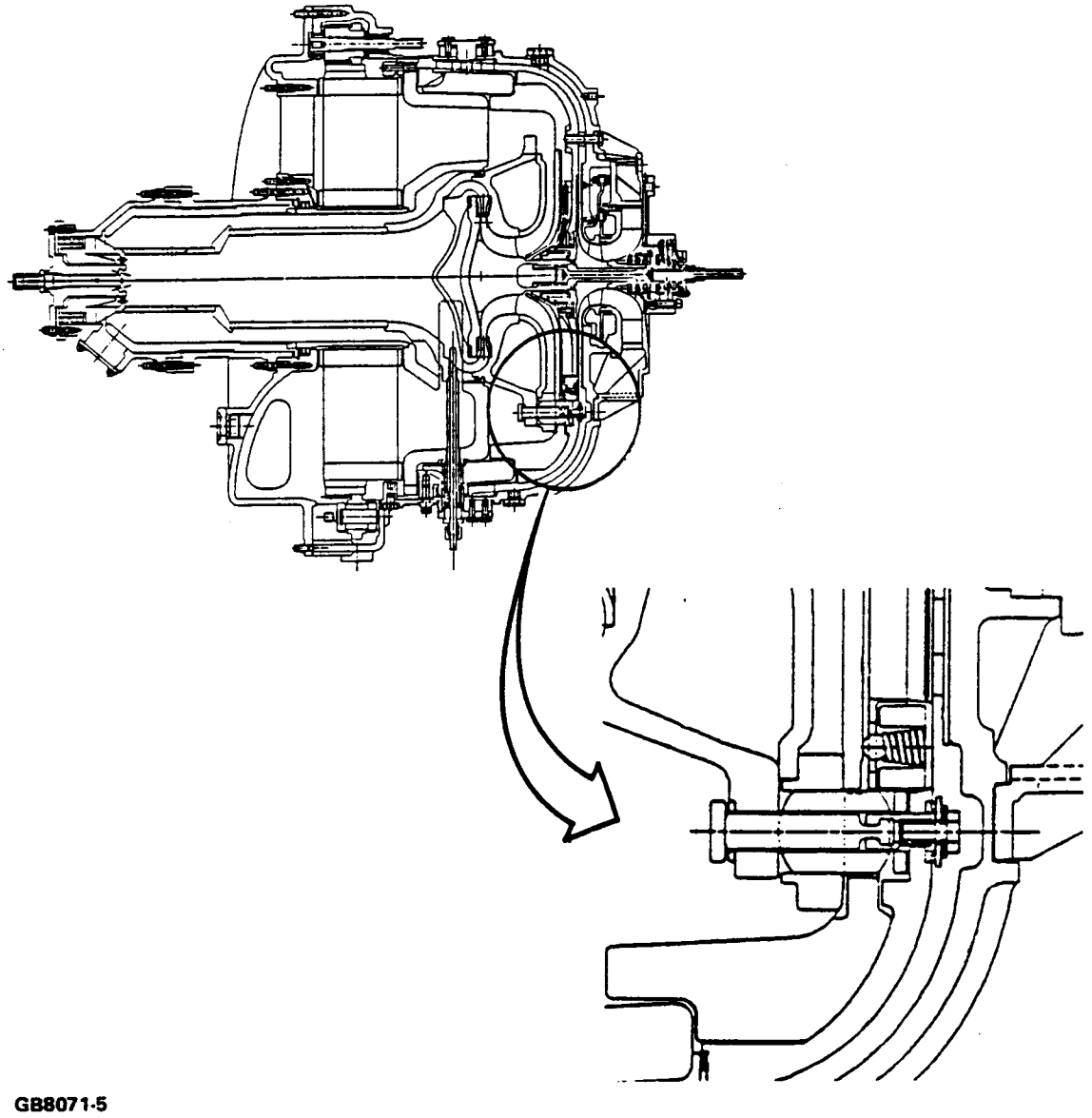

Figure 14. Three Ceramic Bolts Secure the Turbine Shroud.

A new combustor-housing design concept, shown in Figure 16 approaches this problem by increasing the amount of insulation around the spring assembly and surrounding the springs with cool external walls. The single spring from the previous design was replaced by several smaller springs, resulting in a more uniform loading of the structural stack, and the combustor cap material was changed from a cast ductile iron to a corrosion resistant steel (347). Analysis of the combustor assembly, which includes the spring assembly, has indicated that the maximum temperature of the springs under maximum power conditions will be 316C (600F).

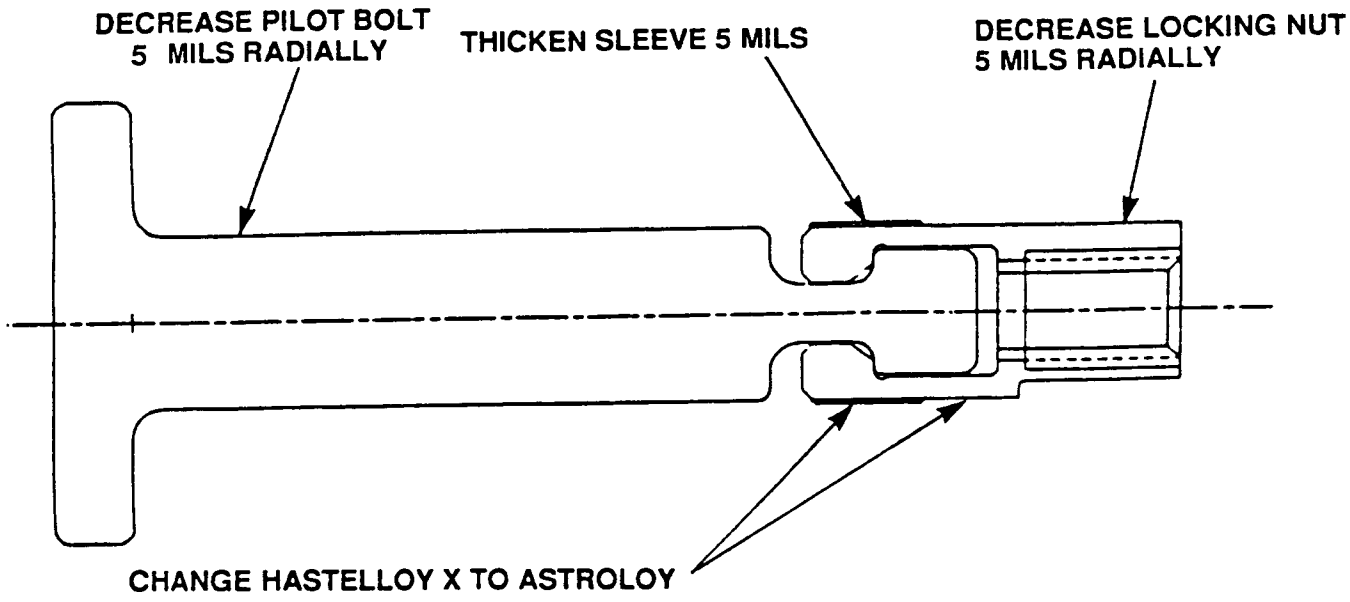

Figure 15. Design Changes Made to Prevent Yielding of the Locking Nut Jaws and Sleeve.

3.4.7.2 Exhaust Housing

The ATTAP test bed exhaust housings were fabricated at the onset of the AGT101 Project from cast ductile iron. As a result of testing in high-temperature rigs and engines during the AGT101 program, an undesirable amount of oxidation occurred in the regenerator shield seals area, and cracks were found in the low-pressure (LP) side struts in the exhaust housings. Although this did not cause a catastrophic failure, it was felt that this should be addressed before the test bed operating temperatures were increased to 1371C (2500F), where it could become catastrophic.

A review revealed that the exhaust housing operating temperatures reach 482 to 538C (900 to 1000F), and that cast ductile iron does not have sufficient creep strength or oxidation resistance at those temperatures. An alternate material was sought which could be used to fabricate the exhaust housing using the same casting tooling, and provide improved durability when operating at 538C (1000F). Ni-Resist D5B was selected for evaluation.

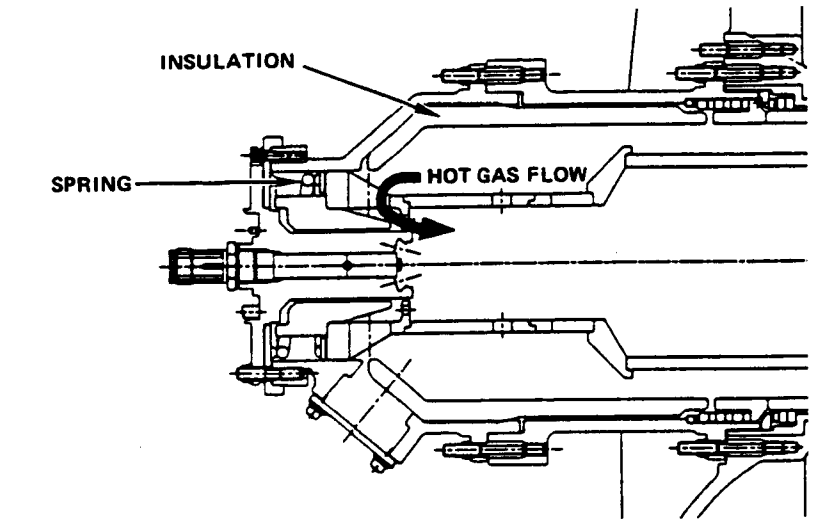

PREVIOUS COMBUSTOR CAP

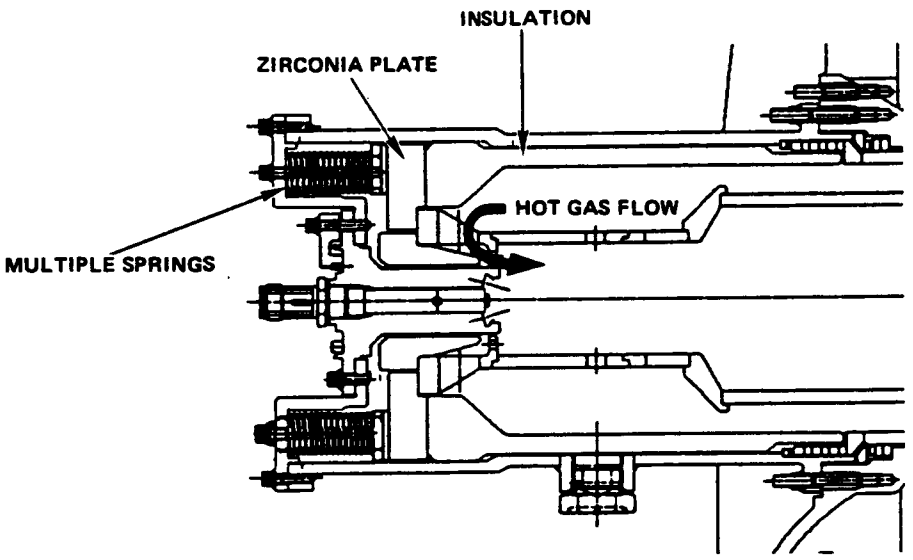

NEW COMBUSTOR CAP

GB8071-7

Figure 16. Combustor-Housing Design Concept.

This material has similar casting properties to the cast ductile iron, and improved oxidation resistance. It also has lower thermal expansion and higher thermal conductivity resulting in a more uniform temperature distribution (see Figure 17) and lower thermal stresses. Several castings were ordered for delivery in early 1990 and will be evaluated for engine and rig testing.

3.4.7.3 Regenerator Shield Seal System

The stack of two ceramic wave springs (and intermediate flat spacers) that load the regenerator shield against the flow separator were analyzed to determine if the travel available was sufficient to allow for thermal expansion under all engine operating conditions. The design was modified to incorporate three ceramic wave springs in place of the two-spring stack (and intermediate flat spacers), because engine data indicates a high degree of variability in the pocket dimension, and it has not been proven that the two-spring stack would always allow for sufficient travel. In this way, the variation in the pocket is assured never to exceed the travel available in the spring stack. The design change is illustrated in Figure 18, Views A and B.

3.4.7.4 New Wave Spring Design

Previous screen testing of wave springs has shown a sensitivity to the method used in load-compression testing, in that the springs can be easily overstressed during testing and suffer a failure which does not represent legitimate proof of service conditions. Another problem with these springs is the extreme sensitivity of the sintered alpha silicon carbide (SASC) spring load to changes in height (or pocket), such that the design needed to incorporate a backshroud that was custom-ground to give the required tolerance on the spring pocket. The change from a SSN material to SASC was made at a time when Si_3N_4 materials demonstrated creep behavior under engine test conditions. Current state-of-the-art Si_3N_4 materials are not expected to demonstrate creep behavior under engine test conditions.

To add more reliability to the test sequence, to reintroduce interchangeability of components in the stack at this area, and to increase overall reliability, the designs of the wave spring, the backshroud, and the baffle were improved. As shown in Figure 19, the spring pocket has been decreased from that anticipated for the SASC design, the spring

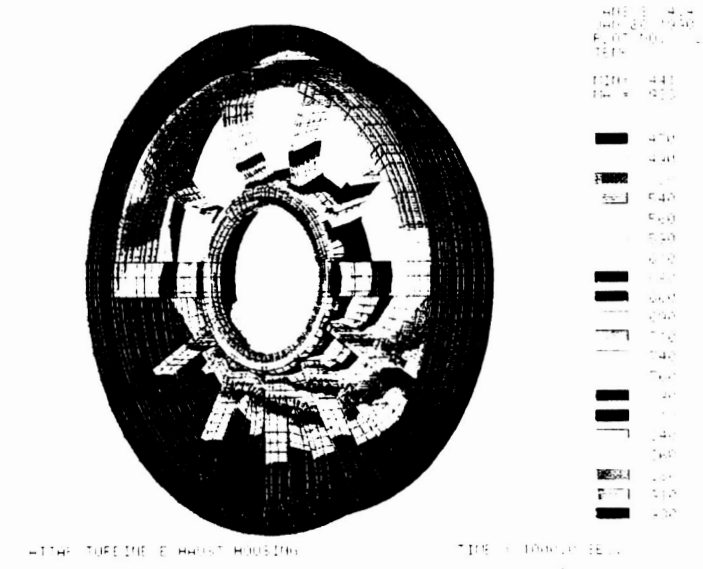

MAXIMUM POWER / T_{MAX} = 930 F, ΔT_{STRUTS} = 300 F

Ductile Iron

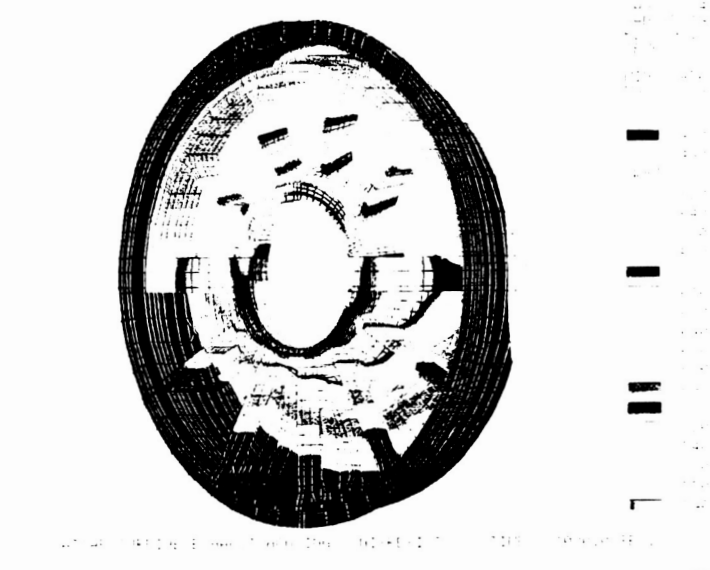

MAXIMUM POWER / T_{MAX} = 790 F, ΔT_{STRUTS} = 230 F

Ni-Resist D5-B

GB8071-8

Figure 17. Thermal Analysis Shows Reduced Temperatures and Gradients.

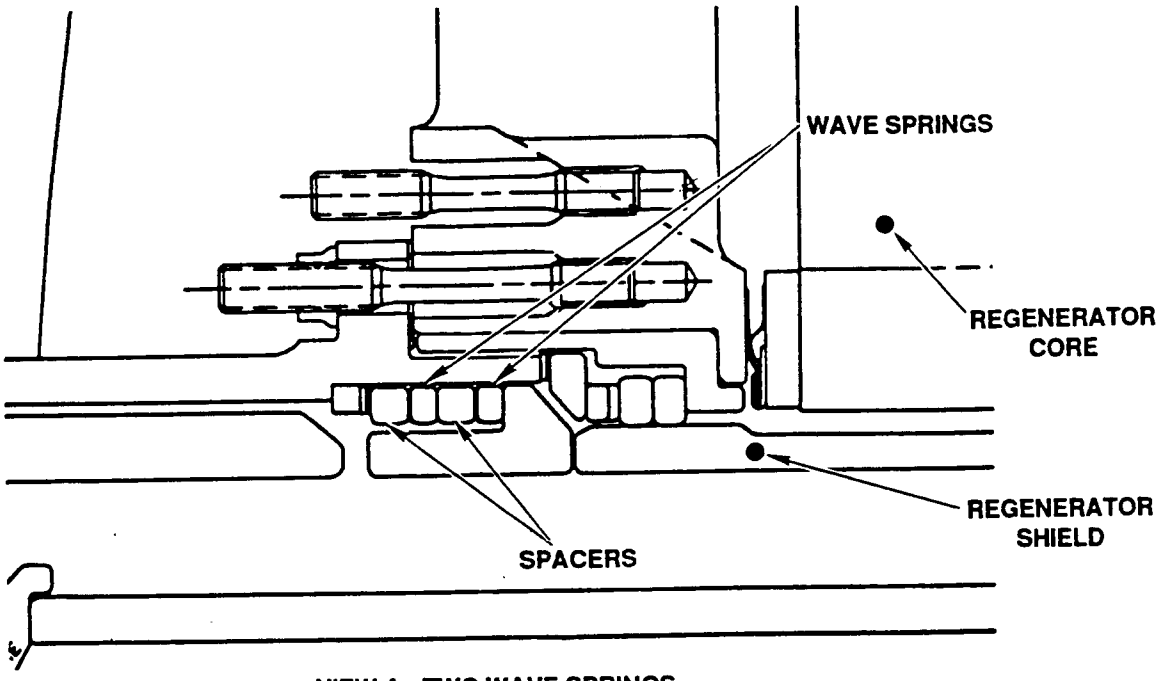

VIEW A - TWO WAVE SPRINGS

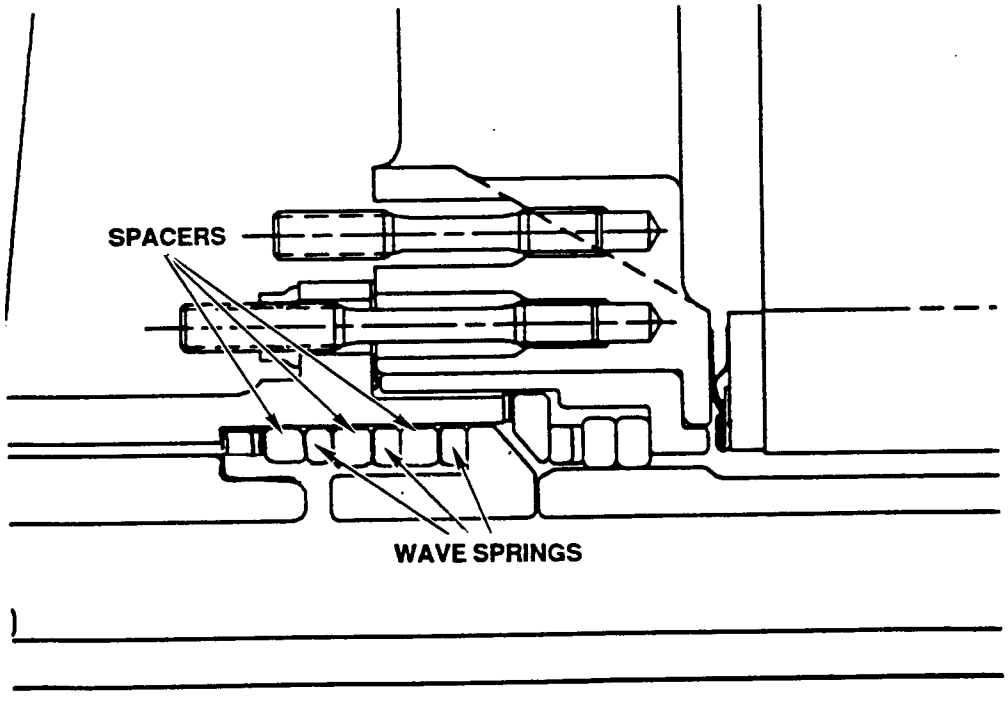

GB9-125-24

VIEW B - THREE WAVE SPRINGS

Figure 18. Wave Spring/Spacer Stack Configurations.

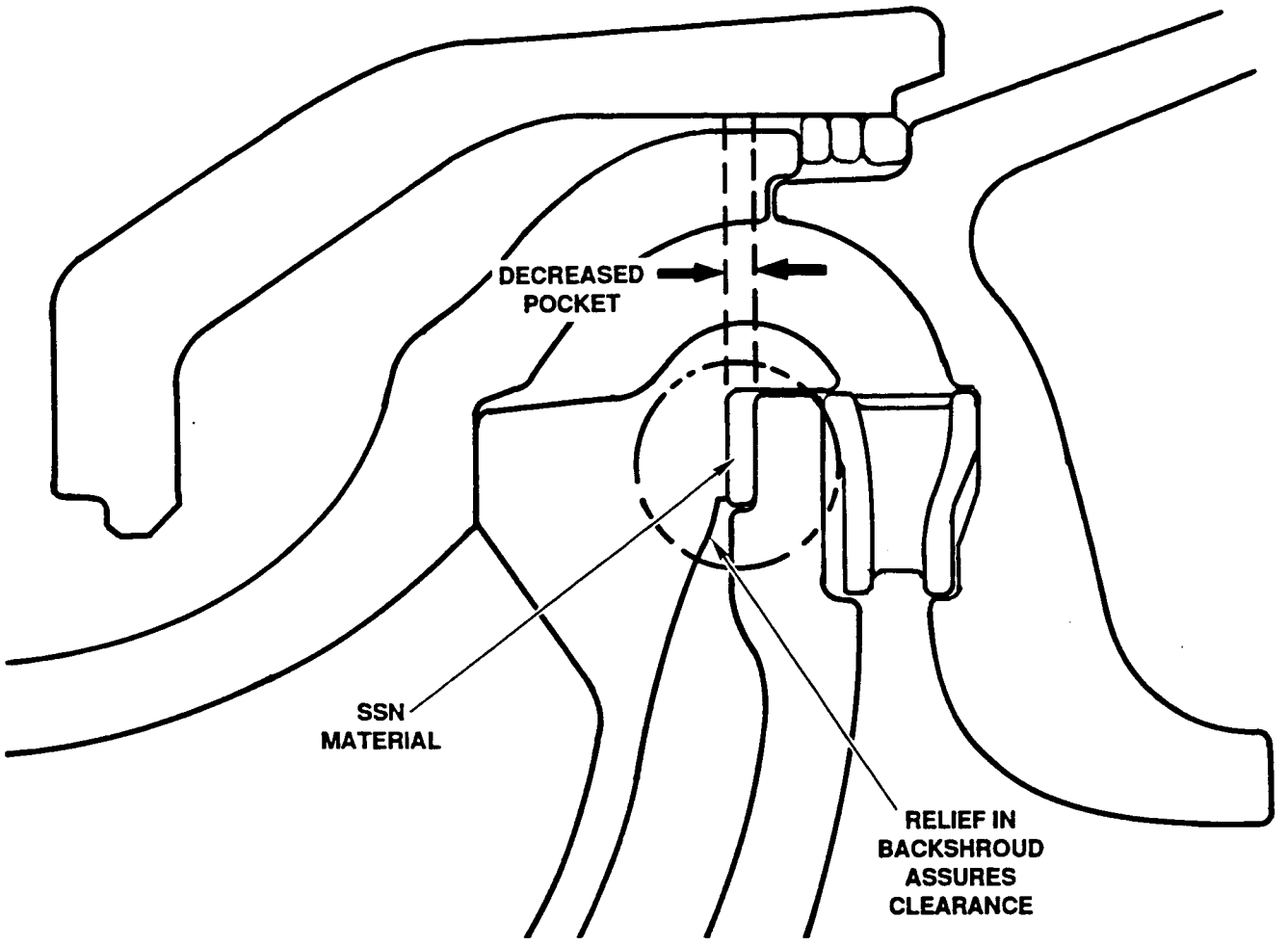

GB9-125-25

Figure 19. New Wave Spring Design Decreases Stress in Spring, Allows for Creep of Material.

material has been changed to SSN, and the baffle has been relieved to assure clearance for the spring travel. The wave spring design can accommodate a reduction in spring force due to relaxation of the spring (creep) down to a stress level of 10 ksi. Testing is planned to identify the threshold stress level at which current silicon nitrides will not creep.

The new spring design was ordered, and a new backshroud and baffle were fabricated by modifying existing hardware.

3.4.7.5 Impact Tolerant Designs

The potential for improving the impact tolerance of the ATTAP test bed engine was investigated. Components considered for redesign included the turbine rotor, turbine stators, and surrounding static structures. This approach has shown promise, and preliminary design work was begun on a modified rotor configuration.

4.0 CERAMIC COMPONENT DESIGN

4.1 Design Methods for Impact

Work has concentrated on the experimental observation and analytical modelling of two types of impact damage:

- o Local damage near the point of impact
- o Structural failure away from the point of impact due to bending stresses

Experimental work has guided the development of impact models for both modes of failure. Structural impact predictions use fast fracture methods, and local damage methods use micro-mechanical models integrated with FEM stress methods to predict damage evolution during the impact process.

The impact methods development work continues, in collaboration with UDRI.

4.1.1 Experimental Observations of Structural Impact

Ballistic impact tests were performed at UDRI to determine critical velocities (velocities that induce fractures) for the ATTAP radial turbine blade and the two axial turbine blade geometries (Figure 20). Tests were performed at room temperature and, selectively, at 1204C (2200F). These tests were performed with graphite spherical projectiles (to simulate combustor carbon) of 0.05, 0.10, 0.15, and 0.20-inch diameters.

These blade impact tests show the sensitivity of structural impact damage to projectile size. The 0.20-inch graphite projectiles fractured radial blades at ~120 ft/sec and the 0.05-inch projectiles required velocities above 2000 ft/sec to cause fracture. The critical velocities for the long axial blades and the radial blades are similar and the critical velocity for the short axial blades have approximately twice that for the radial blades.

These tests also indicate that elevated temperature and fracture toughness have little effect on structural impact resistance. Tests performed on rotors at 1204C (2200F) had nearly identical critical velocities to the tests performed at room temperature except for the 0.05-

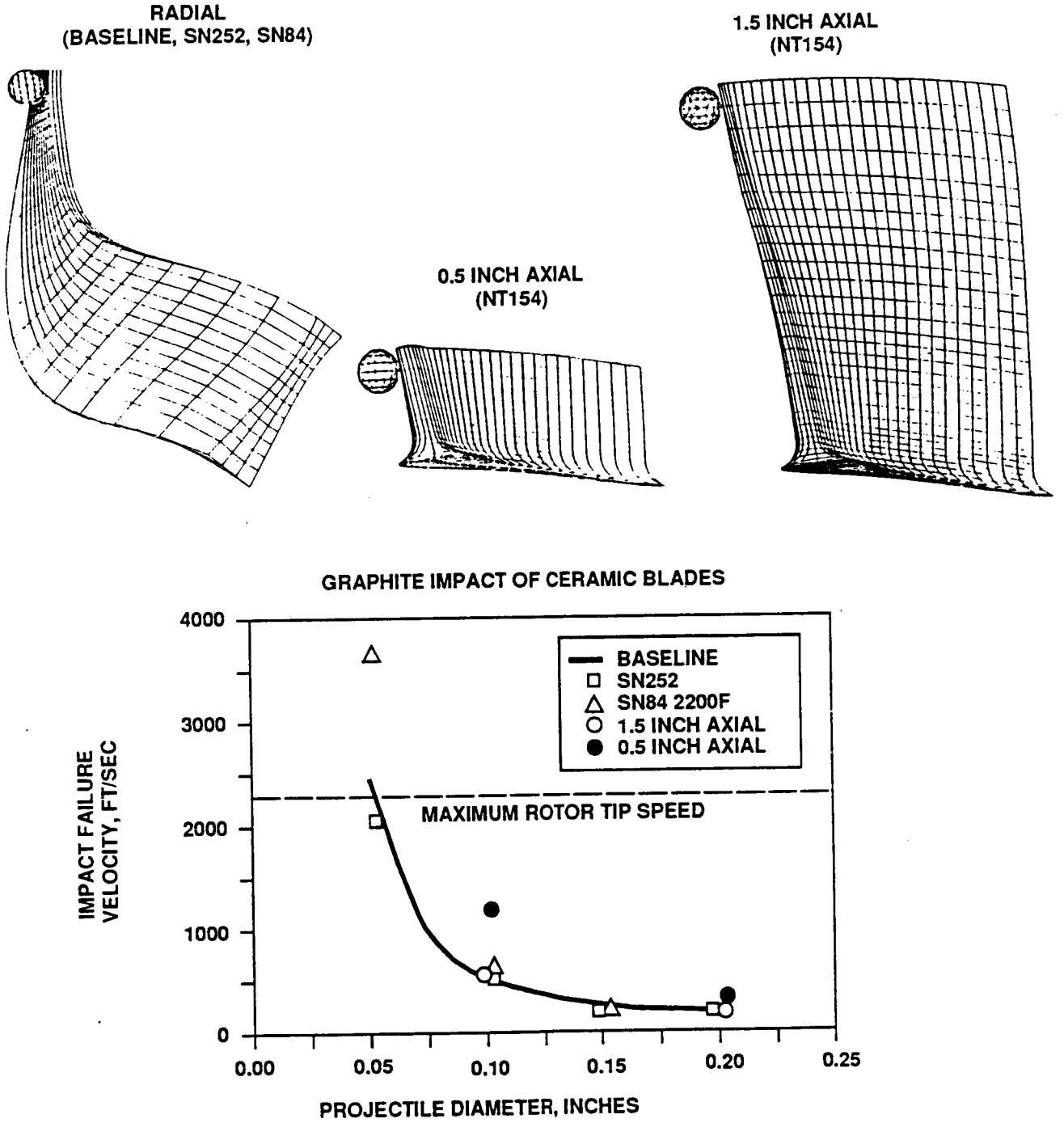

Figure 20. **Impact Tests Demonstrated Particle Size Influence on Failure Velocity for Three Blade Geometries.**

inch projectile impacts. The SN252 blades, which have critical velocities similar to the SN84 blades, have approximately 50 percent higher fracture toughness and similar strength to SN84. Although there are other differences between the SN84 and SN252 blades it appears that fracture toughness does not play a significant role in structural impact damage resistance.

High speed photographs were taken during each impact test to verify impact location and projectile integrity. Photographs from two ATTAP radial blade impact tests are shown in Figure 21. The 0.15-inch graphite projectile fractured the blade at 180 ft/sec, and the projectile remained intact. The 0.05-inch graphite projectile caused blade failure at 2550 ft/sec, and the projectile was pulverized.

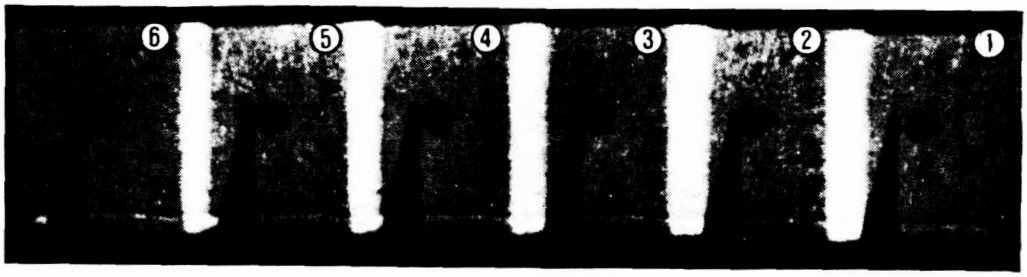

0.15 INCH GRAPHITE BALL
180 FT/SEC

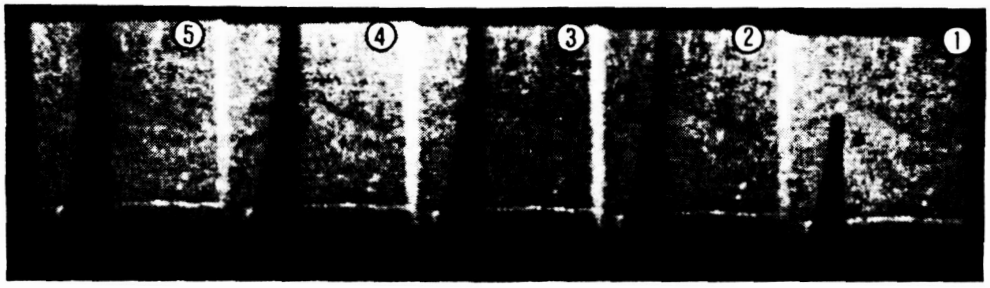

0.05 INCH GRAPHITE BALL
2550 FT/SEC

GB8071-19

Figure 21. Projectile Size Significantly Affects the Critical Velocity of SN84 Radial Turbine Blades.

The impact characteristics of carbon are also important for structural impact failure modeling. Impact bending stresses are produced by the forces applied to a blade by a carbon particle. An instrumented particle impact test was performed to measure the amplitude and duration of the forcing function. The target consisted of a ytterbium pressure gage epoxied between a two-inch cube and a 0.0625-inch thick plate. The plate was impacted at the gage location. The gage measured average pressure over the gage area, and recorded data on a digital oscilloscope (Figure 22).

Instrumented impact tests were performed with 0.05, 0.10, 0.15, and 0.20-inch graphite projectiles at velocities between 150 and 2100 ft/sec. At velocities above 500 ft/sec the projectiles fractured (usually pulverized). Pressure-time plots obtained from three impact tests are shown in Figure 23. These tests confirm that pressure is significantly influenced by impact velocity and particle size, and that impact duration decreases with increasing impact velocity.

These results are being used to develop a material model for carbon pulverization as described under model development.

4.1.2 Experimental Observations of Local Impact Damage

Tests were conducted to evaluate impact variables thought to affect ceramic impact behavior. The variables evaluated are listed in Table 1. The three specimen types used for these tests are shown in Figure 24. These tests were performed to determine the effect of each impact variable on critical velocity, the velocity that produced surface cracks visible with a 40X stereomicroscope. The critical velocities determined for each impact variable are compared in Figure 25.

Critical velocity was affected primarily by target material, target thickness, and projectile material. Silicon carbide (SiC) targets and targets with a 0.03-inch thickness, had approximately 1/3 the critical velocity of the baseline tests. The 0.03-inch thick specimens, however, failed from structural impact and not local damage, as shown in Figure 26. When a 52100 steel projectile was used, the critical velocity increased by more than a factor of three. Temperature is another variable worth noting. Impacts at 1316C (2400F) produced radial cracks at lower velocities than the circumferential (Figure 27). Surprisingly, a 45 degree impact angle did not significantly affect critical velocity.

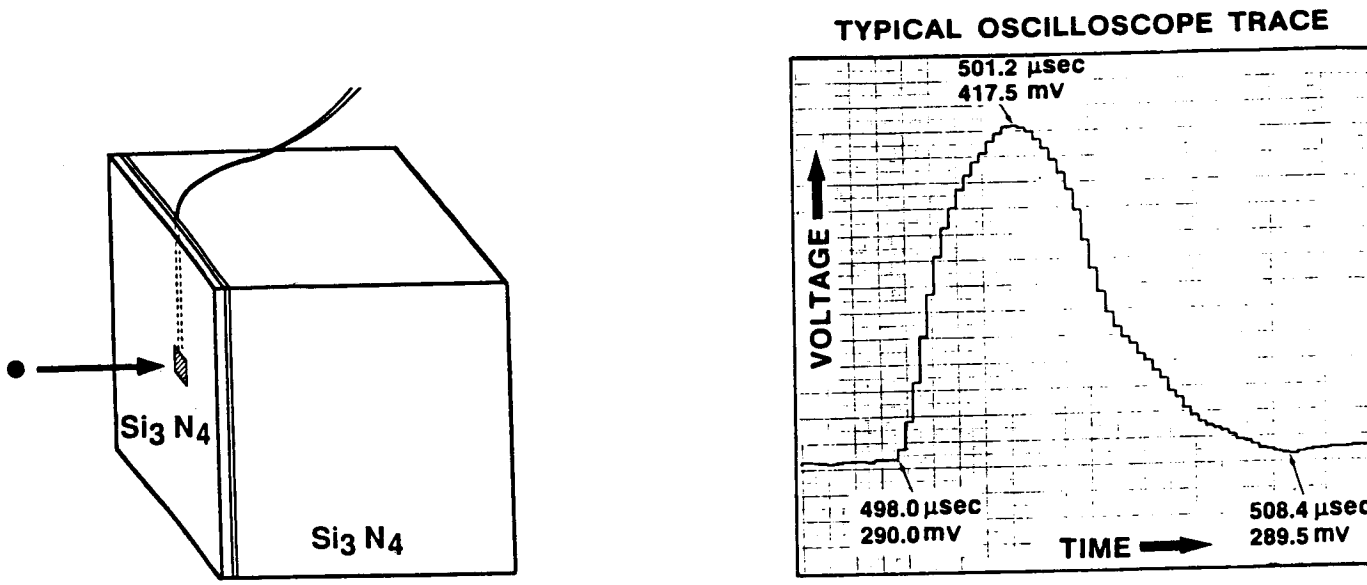

Figure 22. Instrumented Particle Impact Tests Were Performed to Evaluate Force Transferred by Projectile.

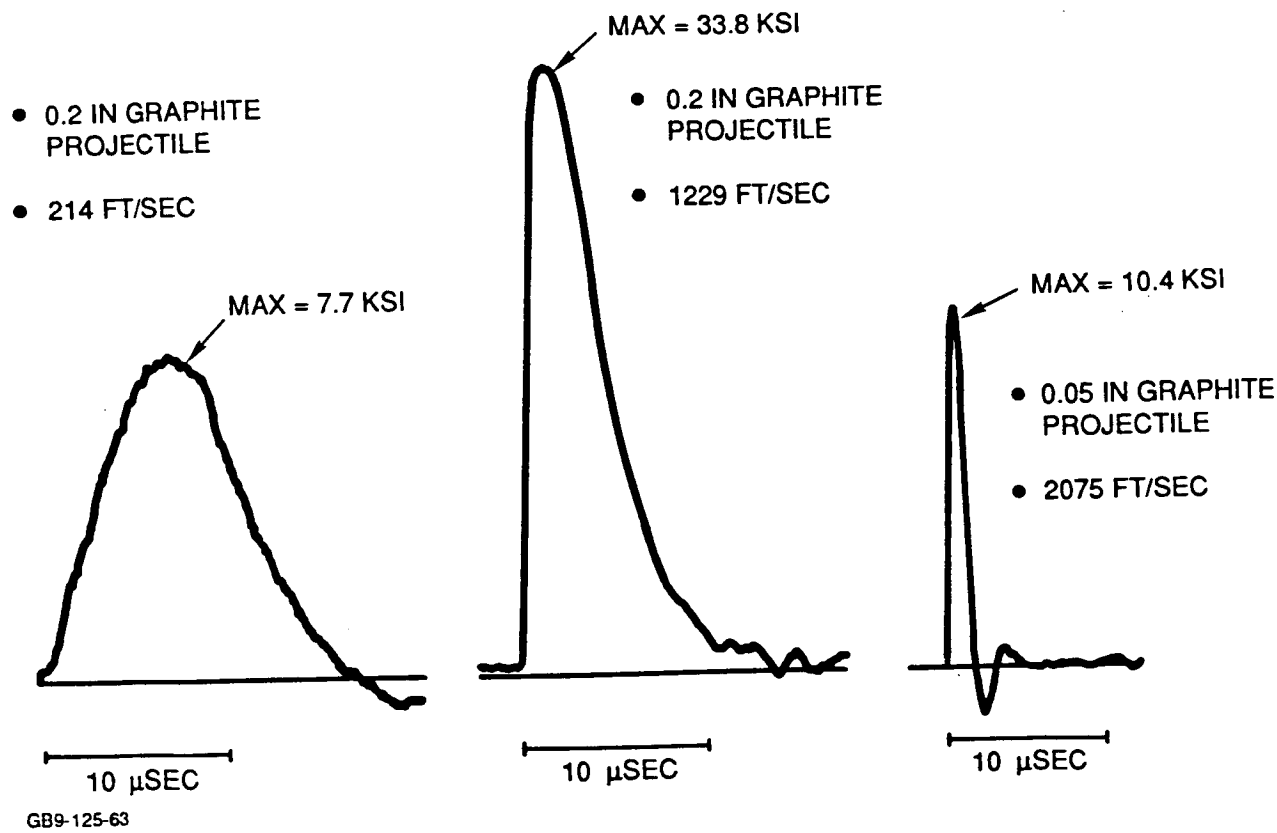

Figure 23. Pressure–Time Curves Obtained From Instrumented Particle Impact Tests.

TABLE 1. VARIABLES EVALUATED FOR EFFECT ON LOCAL IMPACT DAMAGE

Test Variable	Baseline Value
0.03-inch thickness	0.124-inch thickness
45 degree impact angle	90 degree impact angle
Impact on Edge	Impact on flat surface
Polished surface	As-machined surface
SiC target	Si_3N_4 target
1316C (2400F) temperature	Room temperature
52100 steel, 0.0625-inch projectile	NC132, 0.0625-inch projectile

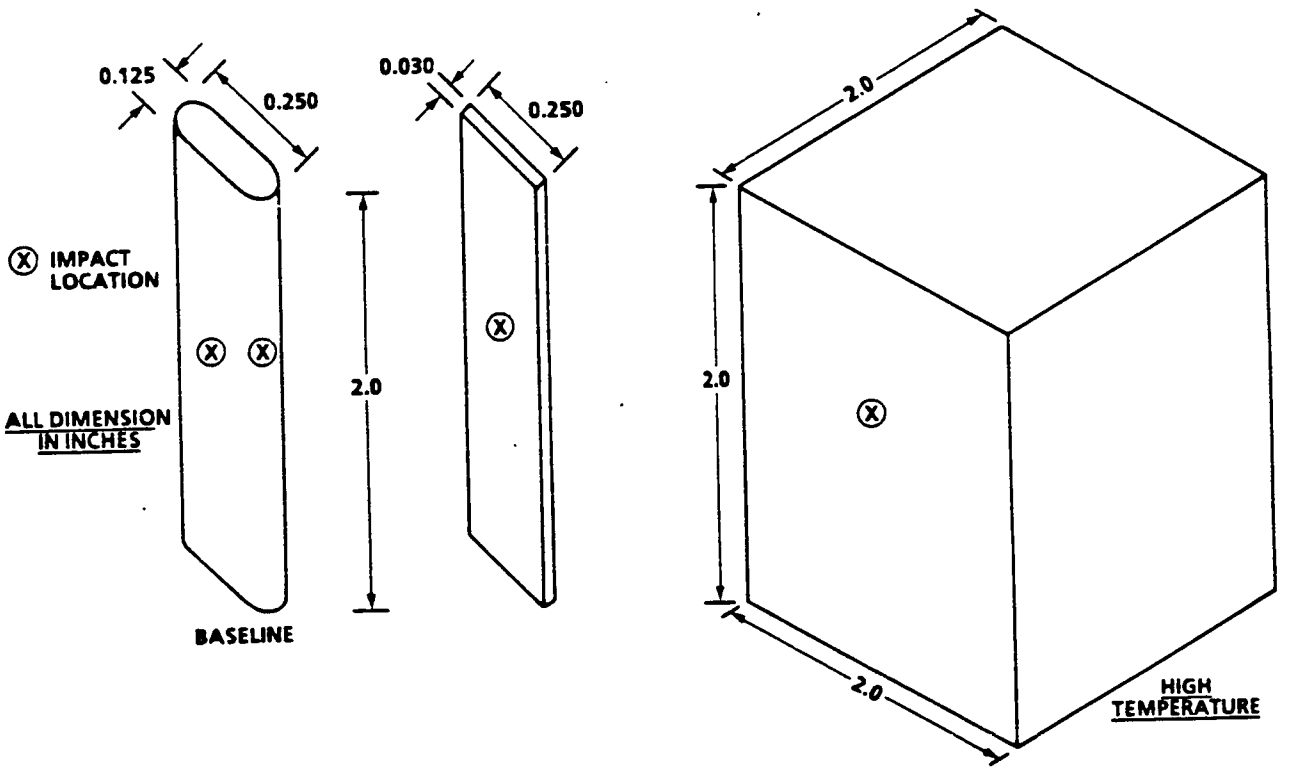

Figure 24. Three Specimen Geometries Were Used to Evaluate Impact Variables.

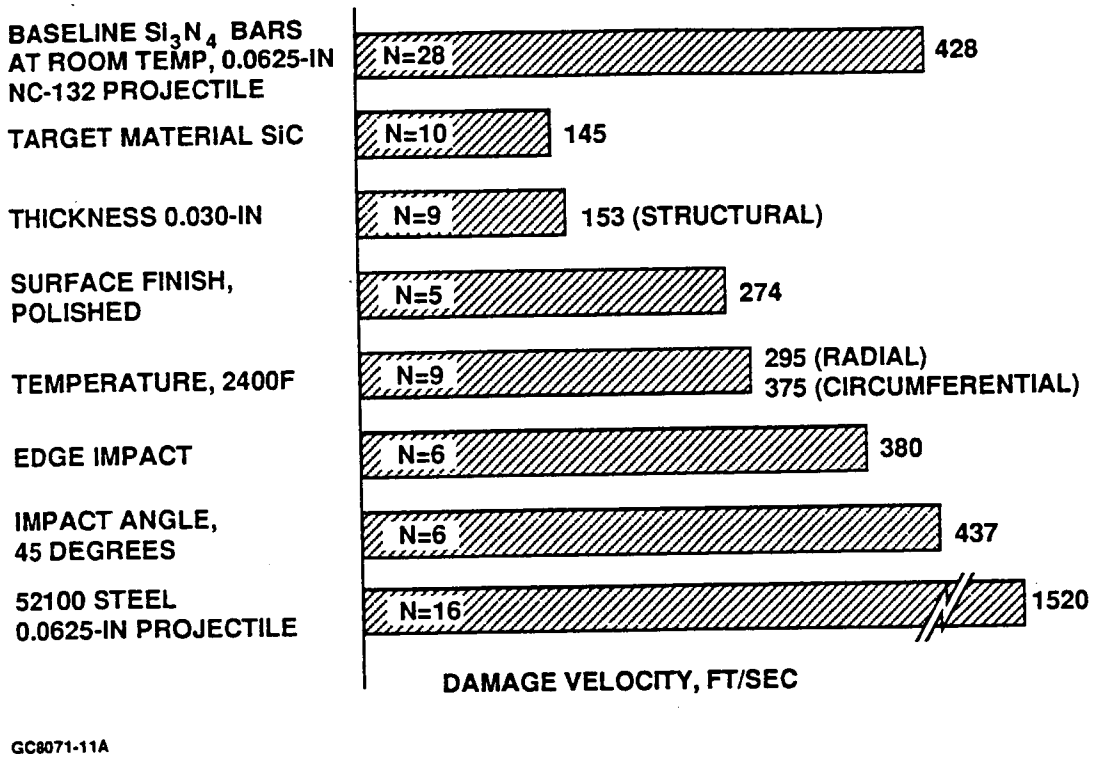

Figure 25. Damage Velocity and Damage Modes Were Affected by Several of the Impact Variables.

Results from impact tests and microscopic observations demonstrate that impact conditions can significantly influence the type and severity of local impact damage. The results are being used to direct model development.

4.1.3 Impact Stress Analyses

Although different damage and failure criteria are used for local and structural impact, stresses were calculated for both with the EPIC finite-element codes. EPIC can simulate an impact event by modeling the projectile and the target with a given initial impact velocity. Principles of conservation of mass, momentum, and energy are used to determine the momentum and the energy transfered during impact. Both the 2D and 3D versions of EPIC were installed at GAPD and used for specimen and blade impact stresses analyses.

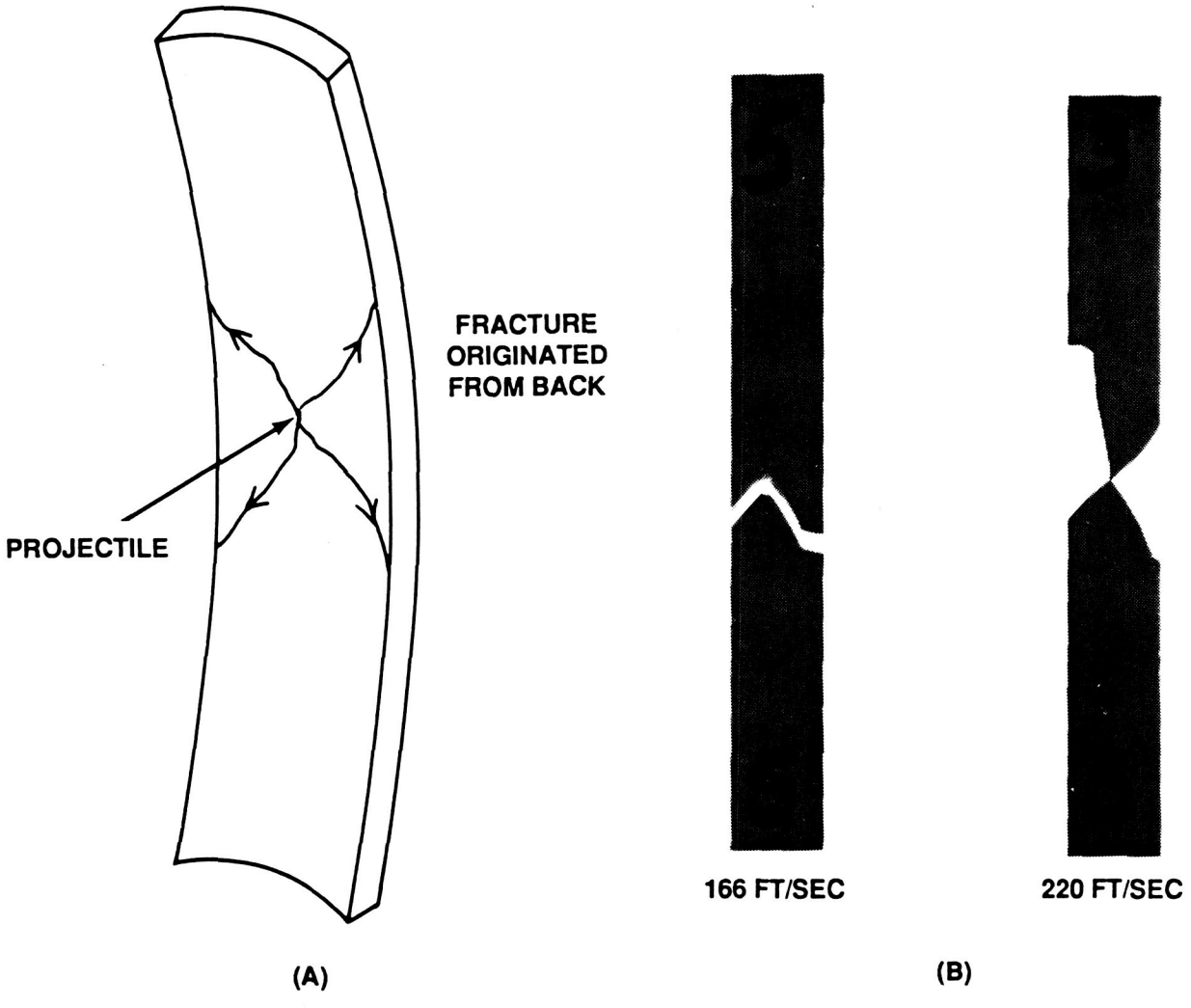

Figure 26. Thin Specimens Fractured at Low Impact Velocity Due to Bending.

EPIC stress analyses are applied differently for predicting structural failure or local damage. Separate approaches are used because structural and local impact typically occur at different times, locations, and from different stresses. Differences in the approaches are shown in Figure 28. Local damage is calculated during each time interval of the stress analysis, using micromechanics models. Structural failures are predicted with fast fracture methods after stresses are calculated. Progress was made in developing methods for both impact modes.

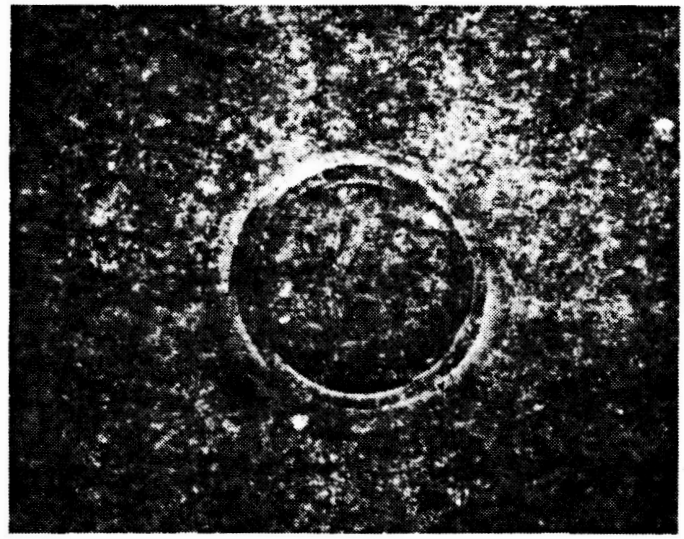

(A) CIRCUMFERENTIAL 100X

ROOM TEMPERATURE IMPACT
NC-132 SPHERE

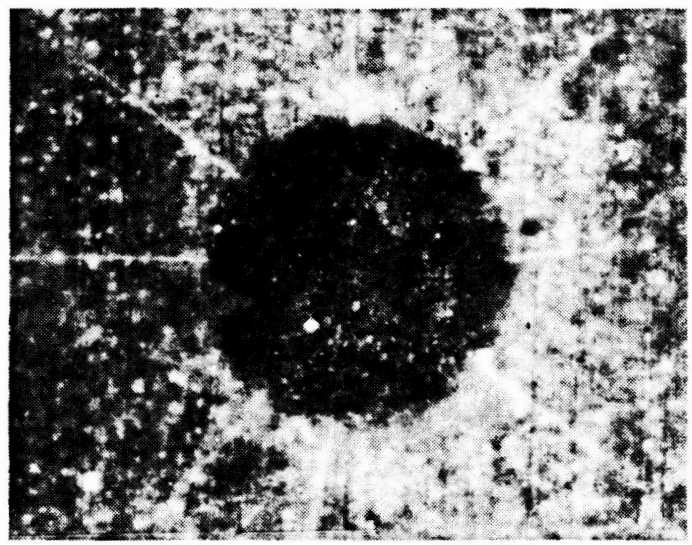

(B) RADIAL + CIRCUMFERENTIAL

2400F IMPACT
NC-132 SPHERE

0.010 IN

GB9-125-38

Figure 27. Type of Impact Damage Changes With Target Temperature.

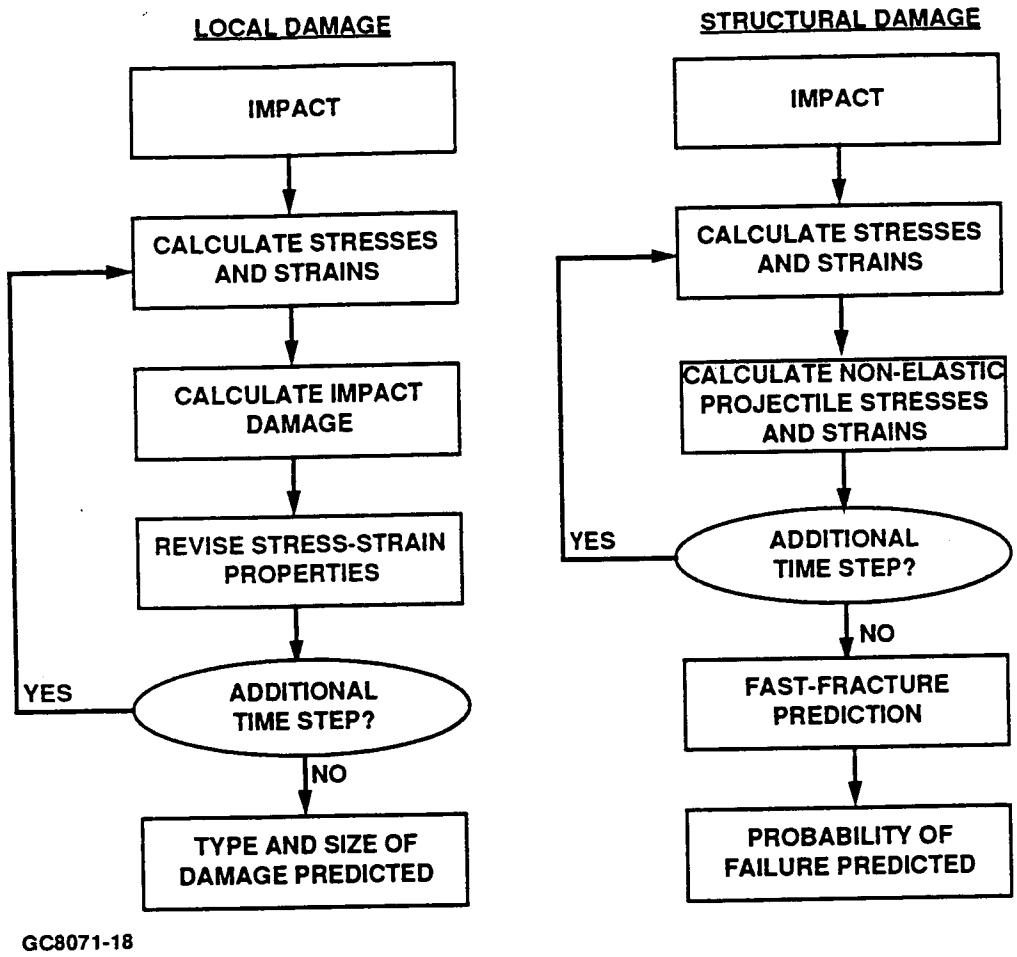

Figure 28. Different Analytical Methods Are Being Developed to Predict Structural Impact Failures and Local Impact Damage.

4.1.4 Structural Impact Failure Modeling

EPIC analyses indicate that structural impact failures are controlled by fast fracture strength. Impact stresses were calculated for the three blade geometries shown in Figure 20. Maximum principal stresses calculated with EPIC, at critical blade velocities, were in general agreement with the flexure strength of the test materials.

The EPIC blade analyses were performed assuming that the projectile and blade deform elastically. Maximum blade stresses calculated for projectiles with 0.1- and 0.2-inch diameters are listed in Table 2 along with the as-processed-surface flexure strengths of these materials. The stresses calculated for the radial and long axial blades were in agreement with the flexure strengths. The failure locations in both blades were near the predicted maximum stresses locations, as shown for the long axial blade in Figure 29.

TABLE 2. EPIC-3 PREDICTED IMPACT STRESSES

Conditions	Radial Blade	Long Axial Blade	Short Axial Blade
Impacted With 0.2-Inch Graphite Ball			
Critical Velocity From Test (ft/sec)	120	117	225
Impact Velocity in EPIC-3 Analysis (ft/sec)	120	120	225
Flexure Strength (Ksi)	55	47	47
Maximum Tensile Stress (Ksi)	58	46	105
Impact With 0.1-Inch Graphite Ball			
Critical Velocity From Test (ft/sec)	460	487	1115
Impact Velocity in EPIC-3 Analysis (ft/sec)	487	487	1115
Flexure Strength (Ksi)	55	47	47
Maximum Tensile Stress (Ksi)	56	48	105

NOTES: Material for the Radial Blades Is SN84
Material for the Axial Blades Is NT154

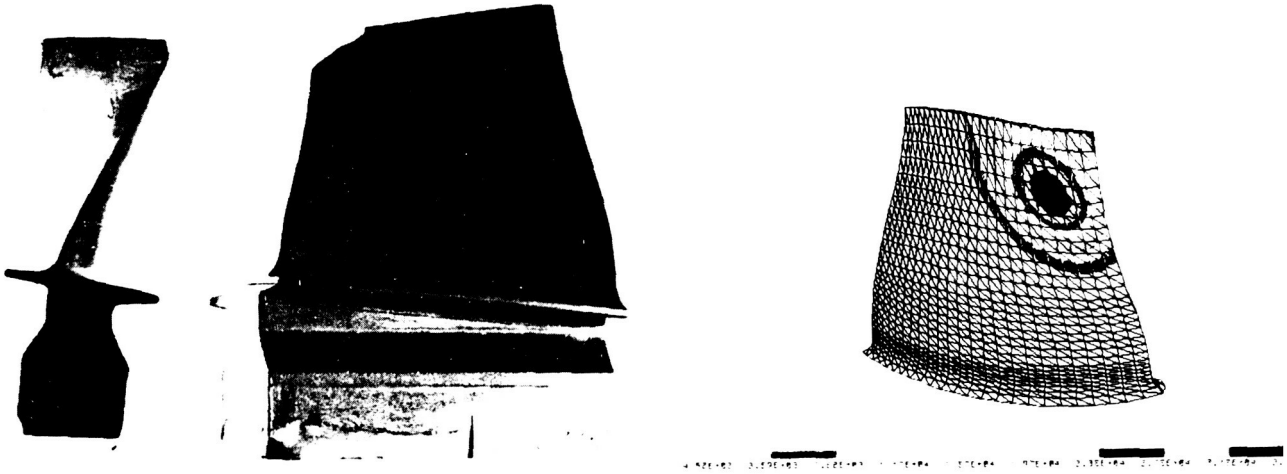

1.5 INCH BLADE LENGTH

(A) FRACTURED BLADE

(B) MAXIMUM TENSILE STRESS ON SUCTION SIDE

GB9-125-110

Figure 29. Photograph (A) Is a Long Axial Blade Fractured by a 0.10-Inch Graphite Sphere at ~500 ft/sec. Plot (B) Was Generated From an EPIC Simulation of a 0.10-Inch Graphite Sphere Impacting a Long Axial Blade at 487 ft/sec.

The stresses calculated for the short axial blade, however, did not at first agree. The calculated stresses were significantly higher than the flexure strengths, and were located in the blade root. It was later determined that this was largely due to the fact that the model considered the blade root as (absolutely) fixed, whereas the test piece included a dovetail section below the blade root. The implication is that the entire blade or target must be considered when predicting resistance to impact. Better agreement was obtained when a mass of material was added to the model, below the blade root.

Inelastic constitutive models for carbon are needed to predict higher velocity impacts which cause the carbon to pulverize. The instrumented particle impact tests described previously were performed to quantify the effect of projectile pulverization on the impacting forcing function. These tests, however, were inconclusive because measured pressures as a function of time were inconsistent with those predicted by EPIC. This inconsistency will be addressed using a different testing configuration in the 1990 efforts.

After the graphite fracture modeling is completed, fast-fracture methods will be combined with EPIC finite element methods to complete the structural impact failure methods.

4.1.5 Local Impact Damage Modeling

Candidate local impact damage models have been selected and are being incorporated into EPIC. Evaluation of these models has started by comparing predicted and observed local damage.

Stress and local damage are calculated concurrently because they are interdependent. As stresses develop during impact, damage occurs [likely in the form of microcracking[1]]. This microdamage changes the material's ability to carry load and effectively changes the elastic modulus in the damaged zone. As the impact process continues this change in modulus affects later stresses. To account for this concurrent stress-damage evolution, both stress and damage are calculated in each time interval of the analysis as indicated in Figure 30.

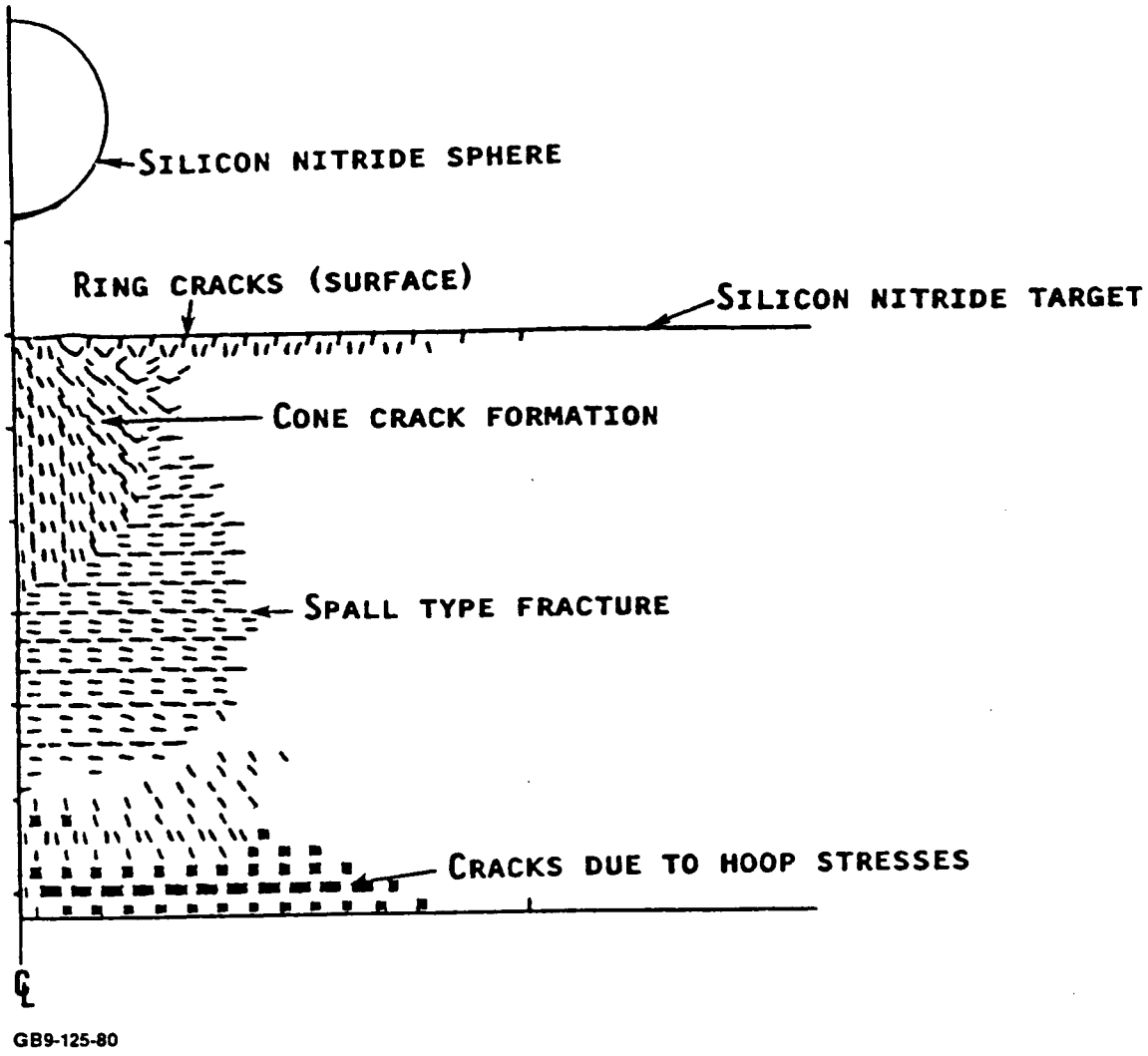

Figure 30. Example of Damage Predicted With EPIC Using the Griffith Fracture Criterion. This Damage Was Predicted for a 2300 ft/sec Impact.

The three candidate models[2, 3, 4] under consideration are:

- o **TCK** (Taylor, Chen, and Kuszmaul) - Assumes inelastic behavior for brittle materials under tension, and elastic and perfectly plastic behavior under compression. The inelasticity under tension is attributed to the nucleation and growth of microcracks. Crack density is determined by stress, strain rate, and toughness. The constitutive relationship between stress and strain is inelastic and isotropic.

- o **LKE** (Liaw, Kobayaski, and Emery) - A simpler model using a conventional finite element scheme to determine stress distribution from the global stiffness matrix. Cracks are formed when the maximum principal stress reaches the tensile strength and extend across the entire element perpendicular to the maximum principal stress.

- o **Margolin** - The most sophisticated model of the three. Griffith criterion is used to determine the flaw population. Material degradation is due to the growth of microcracks assumed to grow from a pre-existing flaw population, and is characterized by effective moduli at different locations along different orientations.

The TCK model has been added to EPIC and evaluation has begun. An example of local impact damage predicted with the TCK model with the Griffith fracture criteria is plotted in Figure 30. This plot was produced from a simulation of a Si_3N_4 ball impacting a Si_3N_4 plate at 2300 ft/sec. While the general location and direction of predicted damage agree with observations in the general model, development is ongoing to improve the accuracy of the number of cracks predicted and the velocity at which they occur.

After a local damage model has been developed that can predict damage for a wide range of specimen impact test data, the accuracy of the model will be confirmed with stator impact tests.

4.2 Ceramic Component Analysis

During 1989, an analysis was begun of the FSH to better understand its behavior in an operating environment, particularly with regard to the regenerator seal face. Finite element models, as shown in Figure 31, have been created representing various geometric modifications. These include the addition of stiffeners and an increase in flange thickness (as may be required for an improved hot side regenerator sealing system). Figures 32 and 33 illustrate the geometry variations under consideration. The analysis will indicate the effect of modifying the support mechanism for this component, the effect of modifications to the geometry, and the feasibility of substituting ceramic materials stronger than (the current) LAS for this large component.

Data from an upcoming engine test will be used to determine the thermal boundary conditions necessary to complete the analysis.

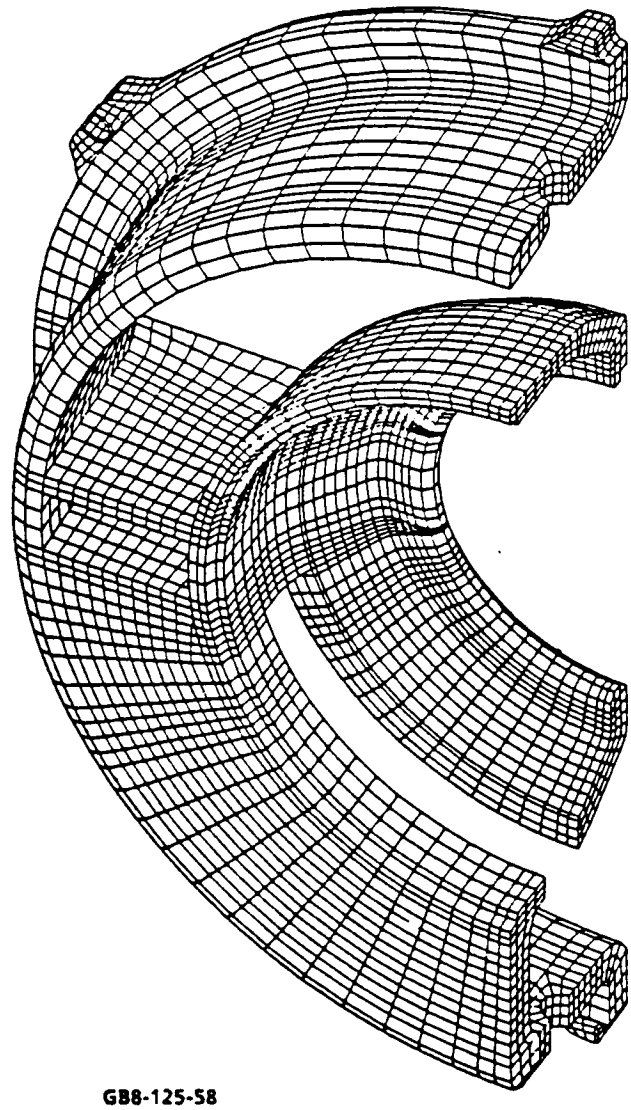

GB8-125-58

Figure 31. Flow Separator Housing Finite Element Model.

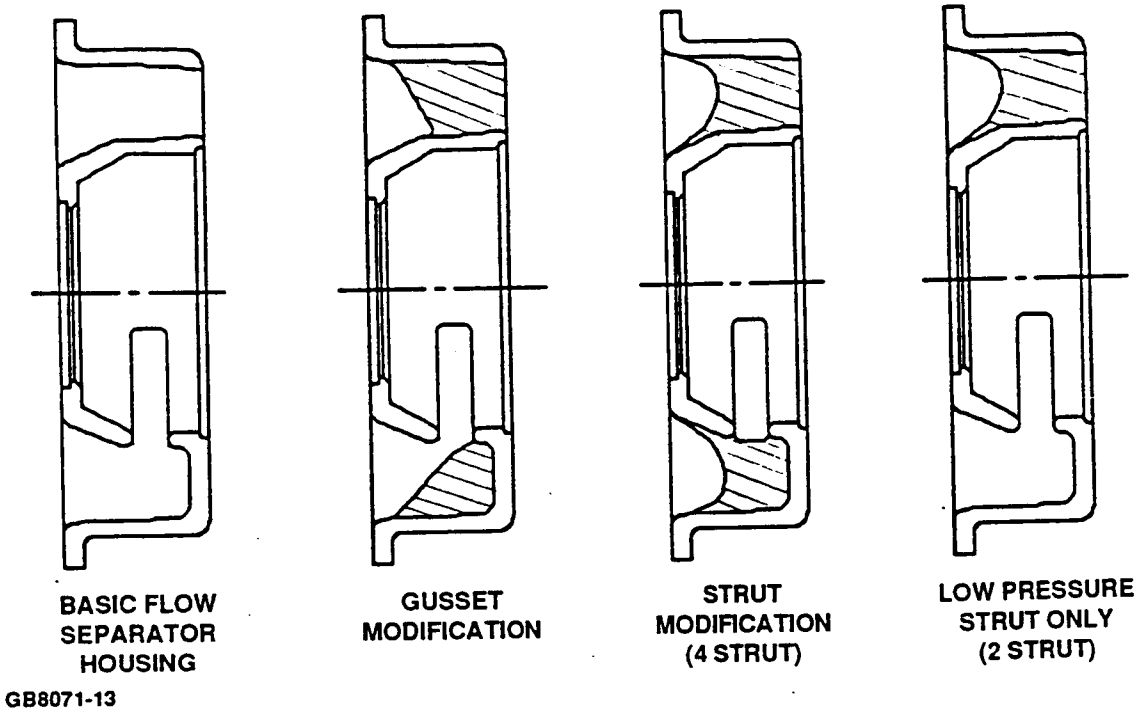

Figure 32. Stiffening Structures Added to Housing Model.

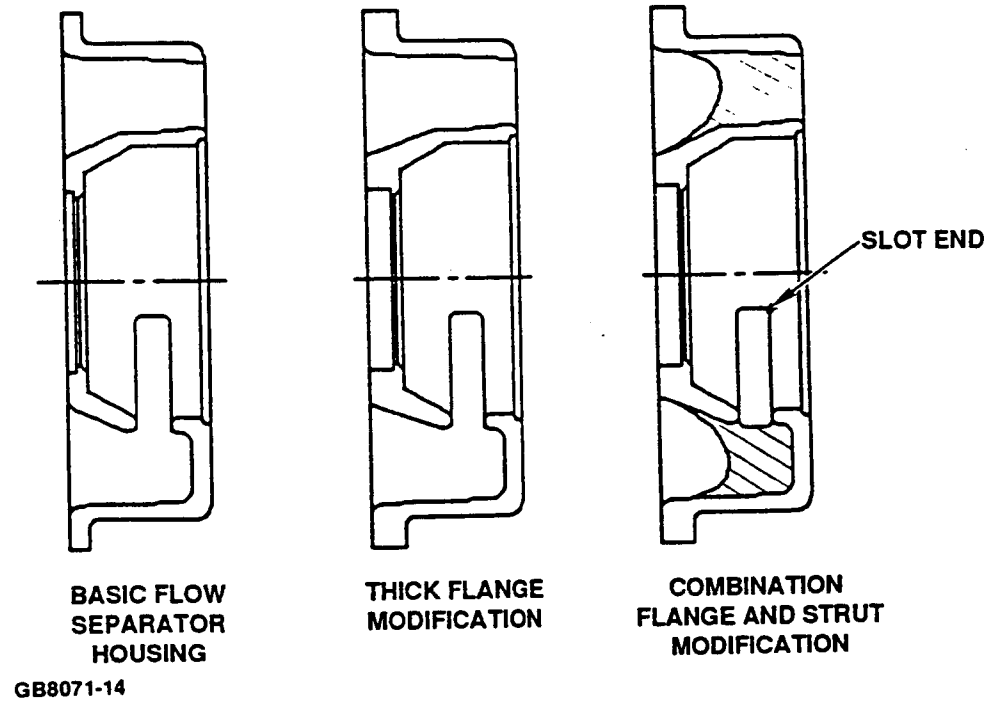

Figure 33. Flange and Strut Combination Housing Modifications.

REFERENCES

1. Margolin, L.G., "Microphysical Models for Inelastic Material Response", International Journal of Engineering Science, Vol. 22, No. 8-10, 1984, pp. 1171-1179.

2. Taylor, L.M., Chen, E., and Kuszmaul, J.S., "Microcrack-Induced Damage Accumulation in Brittle Rick under Dynamic Loading", Computer Methods in Applied Mechanics and Engineering, Vol. 55, 1986, pp. 301-320.

3. Liaw, B.M., Kobayaski, A.S., and Emery, A.F., "Theoretical Model of Impact Damage in Structural Ceramics", Journal of the American Ceramic Society, Vol. 67, No. 8, 1984, pp. 544-548.

4. Margolin, L.G., "A Generalized Griffith Criterior for Crack Propagation", Engineering Fracture Mechanics, Vol. 19, No. 3, 1984, pp. 539-543.

5.0 MATERIALS CHARACTERIZATION AND CERAMIC COMPONENT FABRICATION

5.1 Materials Characterization

5.1.1 Property Measurements

5.1.1.1 Carborundum Hexoloy ST

Carborundum Hexoloy ST, a 20 percent titanium diboride (TiB_2) particulate toughened alpha SiC, was evaluated for retained flexure strength and weight gain following an elevated temperature static exposure. Specimens were exposed at 1260, 1316, and 1371C (2300, 2400, and 2500F) for 25 and 100 hours prior to the flexure test. The baseline material strength of unexposed specimens was also measured. These data are plotted in Figure 34.

At 1316C (2400F), Hexoloy ST has a slight strength reduction after 25 hours of exposure and a 38-percent reduction following 100 hours of exposure. At 1371C (2500F), a strength reduction of 35 percent after only 25 hours and 61 percent after 100 hours may limit the use of Hexoloy ST at the higher temperatures. The weight gains measured are inversely proportional to the strength losses measured. The weight gain data is shown in Figure 35. The Hexoloy ST weight gain and strength reduction above 1316C (2400F) is due to oxidation of the TiB_2 particulates.

Hexoloy ST bars were coated with a proprietary silicon carboxide "black" glass coating, to seal the surface and prevent TiB_2 oxidation, and tested to determine if the coating would prevent the strength degradation and weight gain experienced by the uncoated specimens. The coated specimens were exposed for 25 and 100 hours in a static air furnace at temperatures of 1260, 1316, and 1371C (2300, 2400, and 2500F). Following exposure, the specimens were tested to measure the retained flexure strength and weight change. The coated Hexoloy ST behaved the same as the uncoated Hexoloy ST, showing large strength reductions and weight gains at 1316C (2400F) and above. The black-glass coating offered no improvement over the uncoated material.

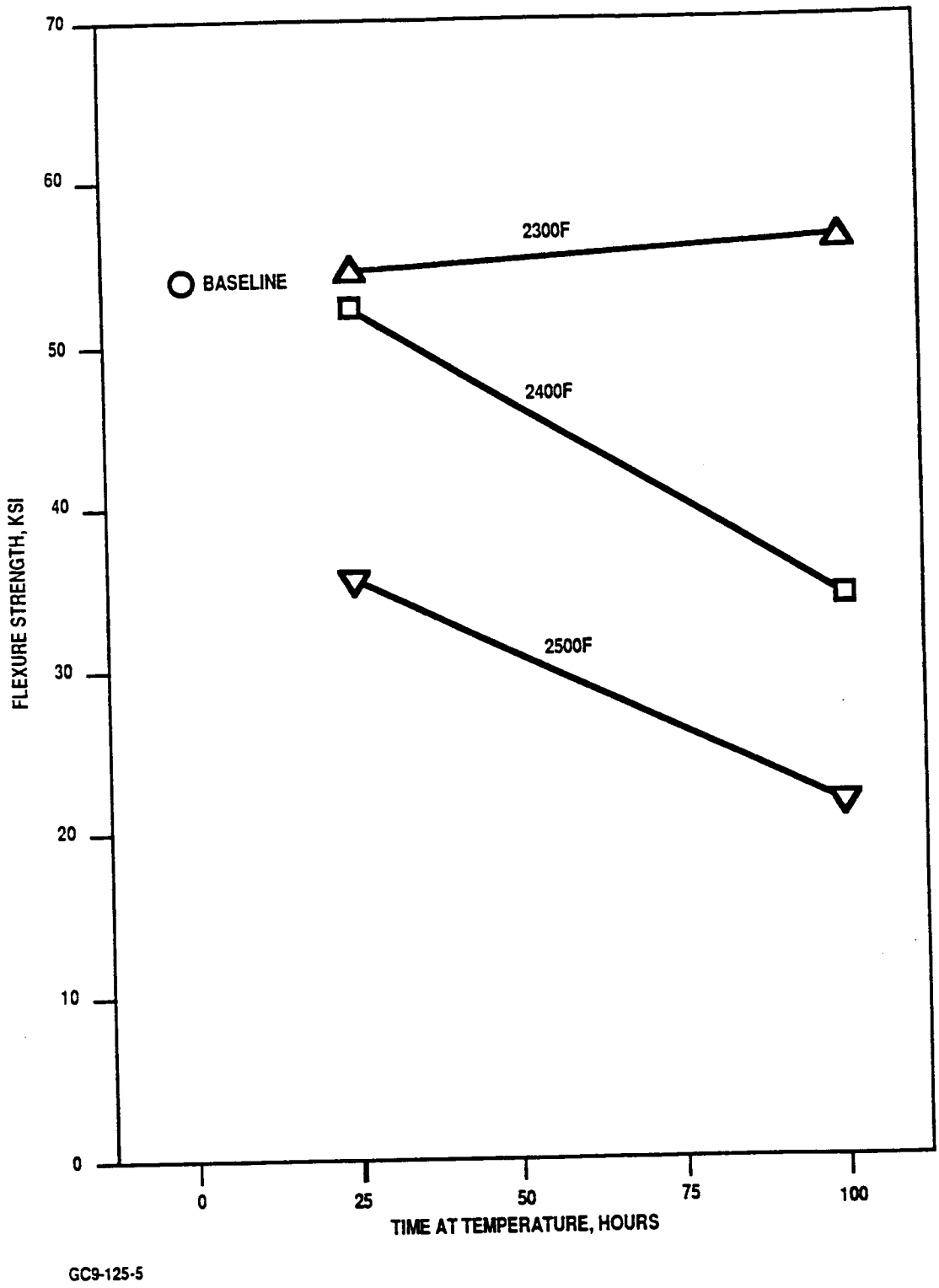

Figure 34. Retained Flexure Strength of Hexoloy ST After Static Oxidation Exposure.

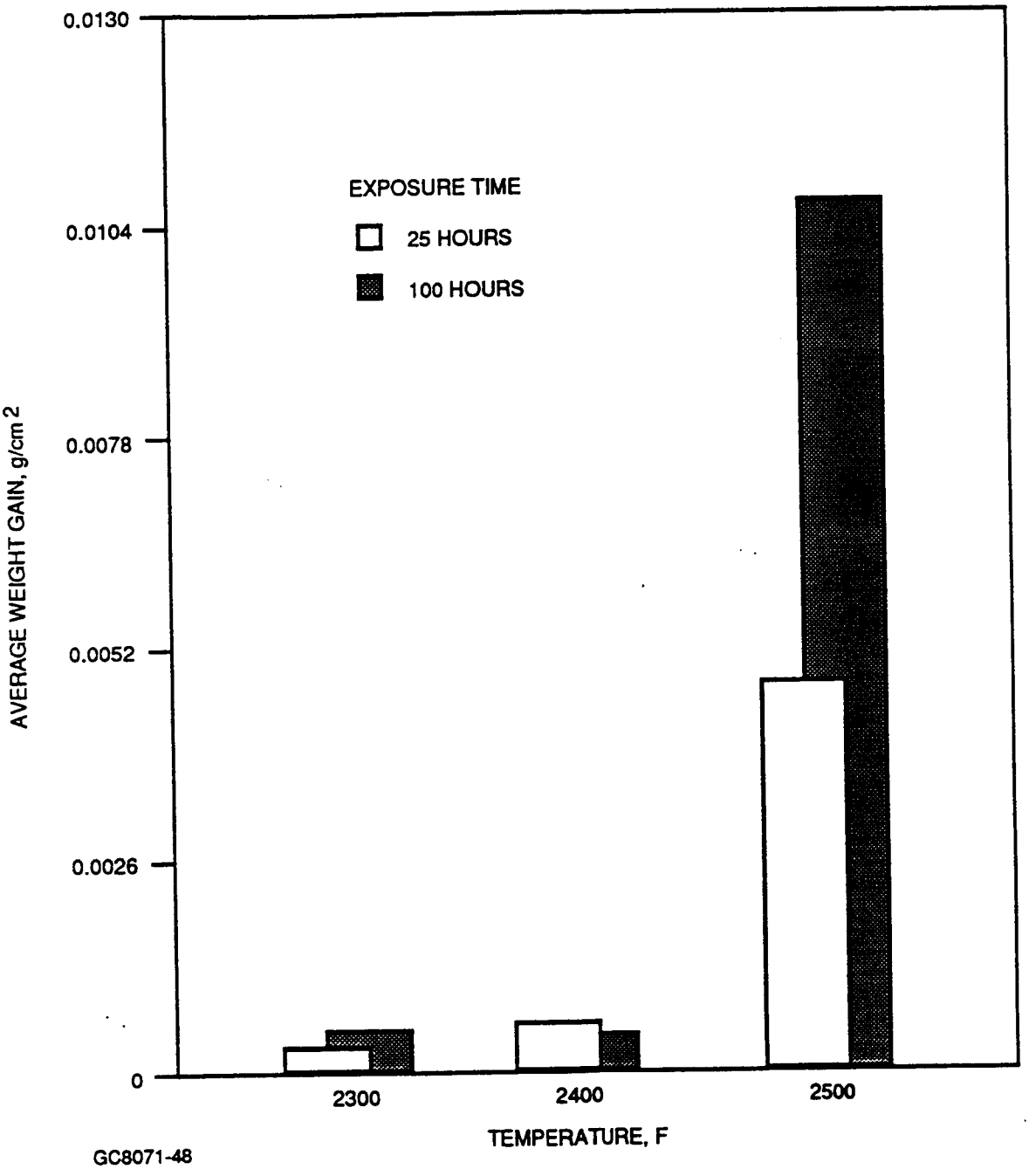

Figure 35. Weight Gain of Hexoloy ST After Elevated Temperature Static Oxidation Exposure.

5.1.1.2 Norton/TRW NT154 Rotor Hub Characterization

Nine NT154 rotor hubs were received from Norton/TRW. Ultrasonic, microfocus X-ray, and fluorescent penetrant inspections revealed no material flaws. The rotor hubs were cut into test specimens and heat treated at 982C (1800F) for 50 hours to heal surface machining flaws. The material was characterized for fast fracture strength, and fracture toughness. The results are presented in Table 3.

Measured average room temperature strength is 144.2 ksi. The strength decreases with increasing temperature to 91.5 ksi at 1371C (2500F). Good agreement was obtained between the specimens cut from rotor hubs and those fabricated as specimens and evaluated under the materials characterization effort (Figure 36).

TABLE 3. COMPONENT CHARACTERIZATION

Material: NT154 Rotor Hubs Date Received: 06/89

FAST FRACTURE:

Test Temp., F	Average MOR, ksi	Specimen Quantity	Weibull Modulus	Surface	Internal	Predominant Fracture Origins
Room	144.2	30	--	Fractography in Progress		
1000	149.3	10	--	Fractography in Progress		
1400	135.8	9	--	Fractography in Progress		
1800	120.6	9	--	Fractography in Progress		
2000	112.5	9	--	Fractography in Progress		
2200	107.4	30	--	Fractography in Progress		
2300	104.8	11	--	Fractography in Progress		
2400	99.7	10	--	Fractography in Progress		
2500	91.5	9	--	Fractography in Progress		

FRACTURE TOUGHNESS:

Test Temp., F	Average K_{IC} ksi/in$^{1/2}$	Specimen Quantity
Room	5.55	5
1800	4.84	5
2200	4.31	4
2500	4.08	4

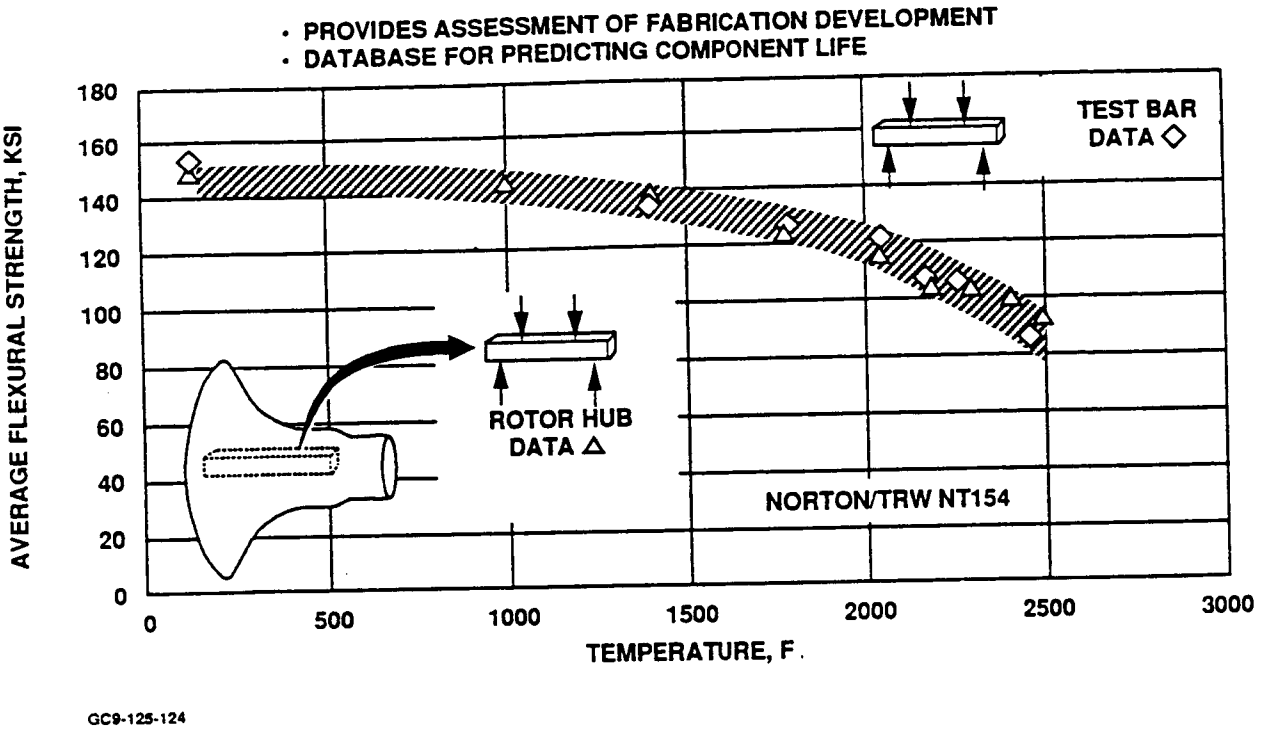

Figure 36. Component Material Characterization Verifies Hardware Quality.

Room temperature toughness is 5.55 ksi/in$^{1/2}$ decreasing to 4.84 ksi/in$^{1/2}$ at 982C (1800F), then 4.31 ksi/in$^{1/2}$ at 1204C (2200F), and 4.08 ksi/in$^{1/2}$ at 1371C (2500F). The fracture toughness values are approximately ten percent lower than those obtained on the materials characterization fabricated test specimens.

5.1.1.3 GCCD GN-10

Fast fracture and chevron notch fracture toughness testing was conducted on a slip cast GN-10 specimen. The data is presented in Table 4. Figure 37 shows the fast fracture data measured on the 1988 vintage GN-10 materials assessment specimens and the data from the 1989 material characterization. The more recent material is approximately ten percent lower in strength than the initial material evaluated. Visually, the materials characterization specimens had a mottled appearance. A fluorescent penetrant inspection and a microfocus X-ray inspection were performed. The mottled areas held the penetrant and were visible on the microfocus X-ray. This is an indication of a density variation within the materials. Visible on the surface were several cracks and many chips on the chamfers caused by abusive machining.

TABLE 4. MATERIALS CHARACTERIZATION OF GCCD GN-10

Material: GCCD GN-10 Machined, Slip Cast

Date Received: 3/89

Fast Fracture:

Test Temp., F	Average MOR, ksi	Specimen Quantity	Weibull Modulus	Surface	Internal	Predominant Fracture Origins
Room	109.5	30	8.8	90%	7%	Surface - Tensile surface and chamfer failures at machining flaws, chips Internal - Silicon inclusions
Room (lg)	92.1	30	6.9	63%	37%	
1400	106.3	10	--	70%	10%	
1800	105.0	10	--	70%	20%	
2000	102.9	10	--	90%	10%	
2200	95.4	30	18.8	70%	27%	
2300	88.8	10	--	90%	10%	
2400	78.7	10	--	80%	20%	
2500	64.6	10	--	100%	20%	

Fracture Toughness:

Test Temp., F	Average K_{IC} ksi/in$^{1/2}$	Specimen Quantity
Room	5.78	3
1800	5.22	4
2200	5.40	4
2500	10.58	4

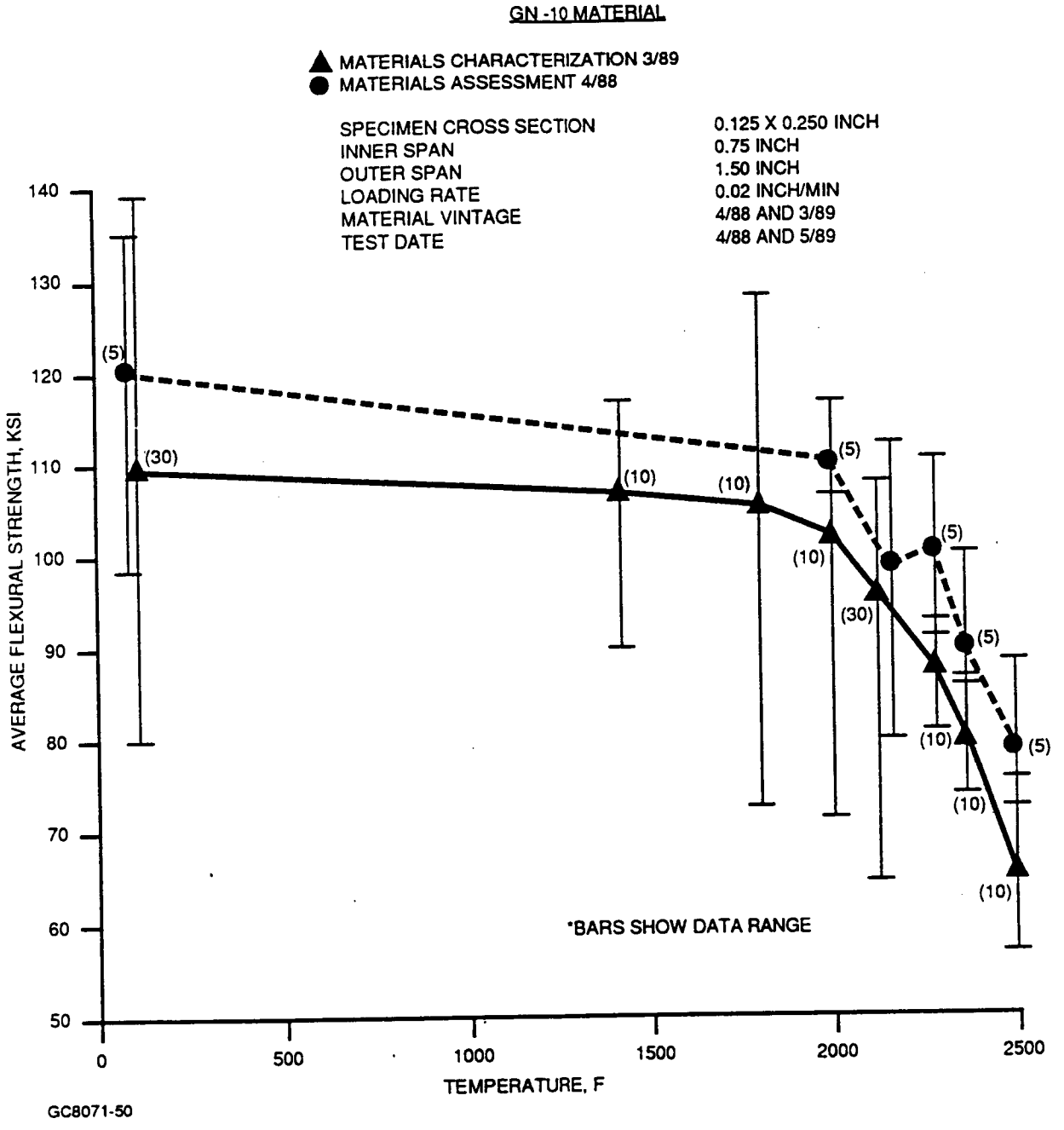

Figure 37. Comparison of GN-10 Materials Assessment and Materials Characterization Flexural Fast Fracture Data.

Fractography was performed on the fast fracture specimens to characterize the fracture initiating flaws. Approximately 20 percent of the specimens failed at internal silicon inclusions. The specimens which failed at the tensile surface usually failed at the chamfer, at chips or machining grooves. None of the resulting fractures were related to the detected mottling. GCCD is performing a machining study to eliminate abusive machining damage.

5.1.2 Nondestructive Evaluation (NDE)

The ATTAP NDE effort is an integral part of the materials characterization effort. Ceramic materials present unique NDE challenges as the materials are extremely sensitive to small anomalies (10-200 microns). These anomalies may be due to material property differences such as density or grain size variation, or discrete flaws such as voids, inclusions, and cracks. To produce engine quality hardware components, both NDE and proof testing are required to identify and eliminate detrimental material conditions. The NDE goals are:

- o To assess the ability of NDE as a materials characterization tool
- o To assess the detectability limits for discrete flaw types found in ceramic materials and components
- o To determine appropriate inspection techniques for ceramic material and components
- o To write NDE process specifications for ceramic materials.

In 1989, components and material characterization bars underwent NDE to support engine, rig, and other testing requirements. Fluorescent penetrant inspection procedures have been documented for both as-fabricated and machined surfaces. While defects are equally critical for both surfaces, the greater surface roughness of the as-fabricated surfaces prohibited the use of extremely high sensitivity penetrant materials due to excess penetrant background problems. Additional methods for surface inspection were then pursued.

A preliminary evaluation of the General Electric CAUM3000 Acoustic Microscopy was performed to determine the validity of acoustic microscopy for surface anomaly detection. Two ceramic impact test specimens were used to perform the evaluation, one with known surface and subsurface damage and the other with only surface damage from the indent. Typical acoustic images are shown in Figure 38. View A shows a specimen with known circumferential cracking at the impact. In addition subsurface cracks from a previous test are shown at the right edge of the specimen. View B shows a specimen that was impacted but did not crack. In this case, only the indent is visible at the impact sight, as well as ink marks on the surface from a permanent marker.

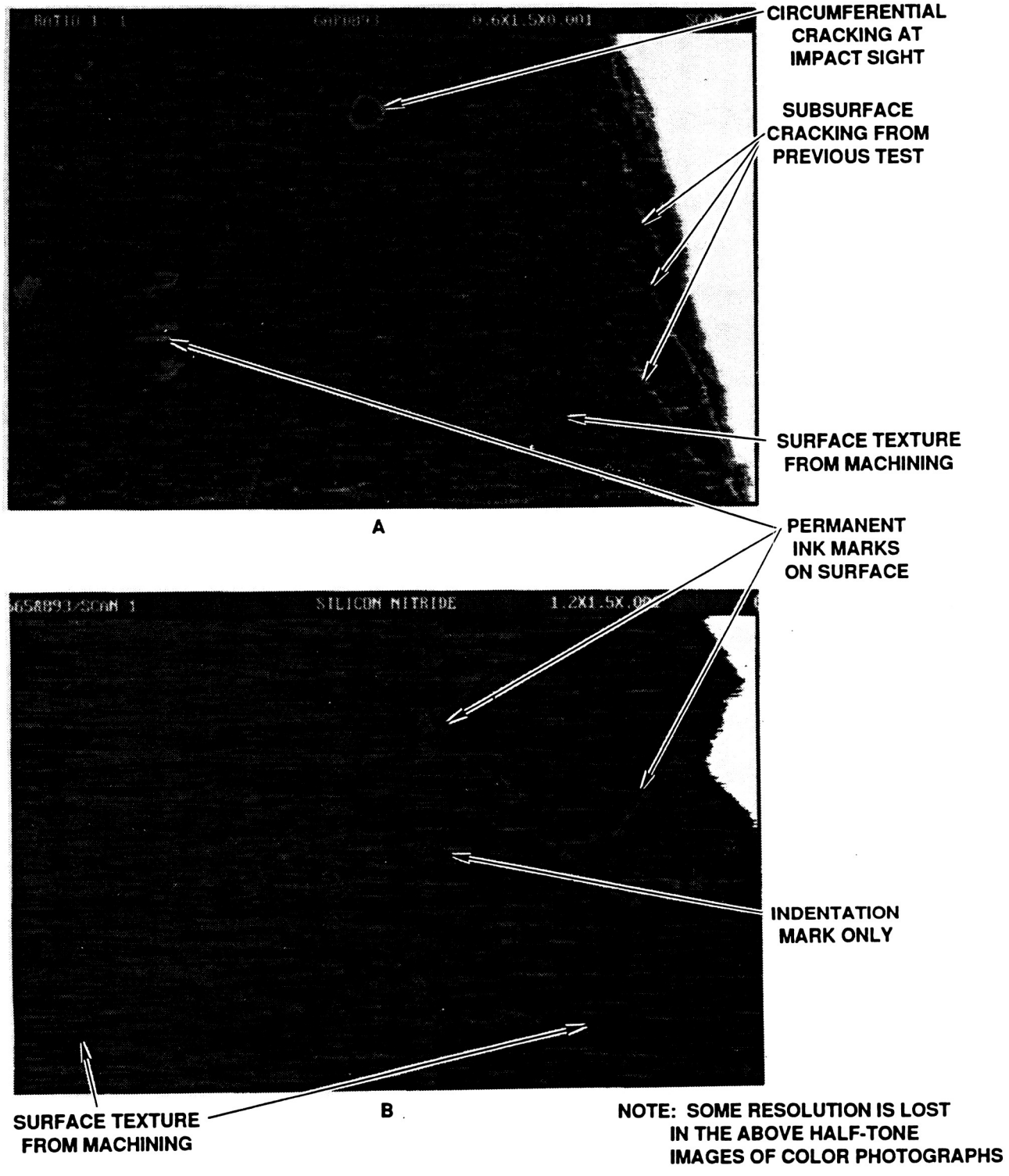

Figure 38. Typical Acoustical Images of Impacted Specimens by GE CAUM3000 Accoustic Microscope.

In both views, a definite pattern is visible that correlates to the machining marks on the specimen. The indications from the surface machining complicated the evaluation of the image and indicated a need for further development of this technique before it can be applied to component inspection. Further acoustic microscopy development is planned under the Oak Ridge National Laboratory (ORNL) Ceramic Life Predication Program.

Fluorescent penetrant inspection and film radiographic inspection of GN-10 materials characterization bars revealed a mottled condition that had been observed previously in other Si_3N_4 materials. The condition was visible in varying degrees by both inspection methods. The indications were documented for later correlation to fractographic data. Room temperature MOR bar testing did not show any correlation between the mottling and fracture origins. High temperature testing has not been completed but data will be correlated as it becomes available.

Radiographic inspection procedures for turbine rotors have been established and include a combination of film and real-time radiographic methods due to the complexity of the rotor shape. The procedures were developed using mock high density inclusions by taping 0.001- and 0.002-inch diameter wires on the hub and blades. Although these procedures are not ideal, they will be used until seeded standards become available in 1990 to refine the procedures. Limited ultrasonic inspections of the rotors was also performed. Ultrasonic inspections will also be extended and further quantified when seeded specimens become available in 1990.

Acoustic emission monitoring procedures for rig and engine testing were reviewed during 1989. Acoustic emission monitoring of rig and engine tests has been used previously to detect component failure during the test. The procedural review and monitoring of the rig tests identified a need to improve the acoustic emission detectability and reduce rig noise. Transducers, transducer location, and coupling methods have been targeted for further evaluation. A literature review of acoustic emission in ceramics provided additional theoretical analysis of the mechanisms of acoustic emission in ceramics. Acoustic emission monitoring of combustor baffle, stator segment, and transition duct thermal screening rigs support the proof-test requirements of ATTAP in 1989.

Further NDE efforts will concentrate on NDE technique optimization as the seeded specimens become available. The major NDE effort will be in ultrasonics and acoustic emission monitoring as Norton/TRW has completed extensive work in evaluation of fully dense components using both film and real-time microfocus radiographic techniques.

5.1.3 Miscellaneous Materials Issues

5.1.3.1 Intermediate Temperature Stability

The discovery of an intermediate temperature stability problem in Kyocera SN251/SN252 Si_3N_4 under another ceramic engine program prompted two activities under ATTAP:

- Establish a heat treatment for SN251/SN252 ATTAP components currently in-house to reduce intermediate temperature effects on the material properties
- Screen all ATTAP component materials to verify that intermediate temperature stability problems do not exist

Kyocera performed preliminary studies which identified a "flash-oxidation" heat treatment [1400C (2552F) for 1 hour in air] which improves the intermediate temperature stability of SN251/SN252. GAPD performed stress-rupture testing on Kyocera SN252 to evaluate this heat treatment. SN252 specimens were tested in the as-received condition, after flash-oxidation, and after flash-oxidation plus 982C (1800F) for 50 hours in air. In previous studies, the 982C (1800F) for 50 hours/air heat treatment significantly degraded the stress-rupture properties of SN251 and SN252. Testing was performed between 982 and 1371C (1800 and 2500F).

The results, shown in Table 5, showed that the flash-oxidation improved stress-rupture properties at 982C (1800F) and did not significantly impact stress-rupture life at higher temperatures. Flash-oxidation retarded the detrimental effects previously observed at 982C (1800F) and the times-to-failure for flash-oxidized and flash-oxidized plus 982C (1800F) exposed SN252 were virtually the same.

Post test inspection of the SN252 stress-rupture specimens was performed. The bars which received no heat treatment exhibited the "coring effect" or "skin effect" observed in previous studies when the intermediate temperature instability was first identified. This observation and the reduced stress rupture properties are consistent with previous tests.

TABLE 5. STRESS RUPTURE EVALUATION OF FLASH-OXIDIZED (2552F/1 HR/AIR)[1] KYOCERA SN252

Test Temperature	Stress	As-Received	Time to Failure	
			Flash-Oxidized	Flash-Oxidized + 1800F/50 Hrs/Air[2]
1800F	80 ksi			BOL[3]
	70 ksi	1 min 30 sec BOL	5 min 156.8 hr 1 min 164.5 hr	168.2 hr[2] 168.2 hr 0.1 hr
	65 ksi	BOL 8 min		
	60 ksi	11 min		
2200F	70 ksi		BOL	BOL 30 sec
	65 ksi 160.1 hr	184.4 hr BOL BOL	68.0 hr	167.1 hr
	60 ksi	BOL 160.2 hr BOL	3 min 161.4 hr 161.4 hr	161.8 hr
	55 ksi		161.9 hr	166.6 hr 163.4 hr 43.7 hr
2400F	60 ksi	35.5 hr		BOL
	55 ksi	160.9 hr 15.6 hr 123.9 hr 161.4 hr	11.7 hr 21.5 hr 1 min 54.7 hr	44.8 hr 60.6 hr BOL 19.9 hr
	50 ksi		BOL 163.2 hr 19.3 hr	165.6 hr

TABLE 5. STRESS RUPTURE EVALUATION OF FLASH-OXIDIZED (2552F/1 HR/AIR)[1] KYOCERA SN252 (Contd)

Test Temperature	Stress	As-Received	Time to Failure	
			Flash-Oxidized	Flash-Oxidized + 1800F/50 Hrs/Air[2]
2500F	55 ksi	1 hr 0.4 hr 2.2 hr	0.8 hr 1.0 hr 2.0 hr	1.0 hr 1.1 hr 0.8 hr
	50 ksi	7.3 hr 93.0 hr[5] 66.7 hr 10.6 hr 4.1 hr	2.2 hr 28.9 hr 0.6 hr	14.5 hr 8.6 hr 10.4 hr 166.5 hr
	45 ksi	165.8 hr	25.2 hr 56.8 hr 20.6 hr	162 hr 162 hr

(1) Heat treatment recommended by Kyocera to improve intermediate temperature stability of SN251/SN252.

(2) Heat treatment found previously to be detrimental to stress/rupture properties of SN251/SN252

(3) Broke-on-loading.

(4) ">" denotes test was terminated without specimen fracture.

(5) No fracture - specimen crept to limit switch.

As a side observation, creep was visually evident in all samples tested at 1204C (2200F) which survived more than a 40-hour exposure. At 1316C (2400F), creep effects were more pronounced, and the fracture surfaces of most specimens displayed evidence of slow crack growth.

To verify that intermediate stability problems do not exist in other ATTAP component materials, ceramic coupons are being screened in a gradient furnace between 427 and 1371C (800 and 2500F). Furnace runs involving the upper-half of the temperature range [927 to 1371C (1700 to 2500F)] have been completed. The weight gain data obtained does not suggest any intermediate temperature problems. Gradient furnace runs for the lower-half [427 to 871C (800 to 1600F)] were delayed by equipment problems which have been resolved. Gradient furnace exposures have been resumed, but no further data was available at the end of the reporting period.

5.1.3.2 Thermal Conductivity

Thermal conductivity data from room temperature to 1371C (2500F) for eight candidate Si_3N_4 and SiC materials was generated. The importance of thermal conductivity for thermal transient failure resistance of ceramic components has long been recognized. The data generated provided a more accurate thermal transient stress analysis and better understanding of the conductivity/material characteristics relationship.

The eight materials evaluated are listed below:

- o Carborundum Hexoloy SA
- o Carborundum Hexoloy ST
- o GCCD GN-10
- o Kyocera SN220M
- o Kyocera SN251
- o Norton/TRW NT154
- o NGK SN73
- o NGK SN84

The Energy Materials Testing Laboratory, Biddeford, ME, which uses the laser flash diffusivity/drop ice calorimetry specific heat method was selected to perform the measurements.

The equation below was used to calculate the thermal conductivity:

$$k = \alpha \, Cp \, \rho$$

where:

k	=	Thermal conductivity
α (alpha)	=	Thermal diffusivity
Cp	=	Specific heat
ρ (rho)	=	Bulk density

The specific heat of the material at each temperature was derived from the slope of the enthalpy-temperature curve. Enthalpy data throughout the temperature range was measured with a Bunsen-type drop ice calorimeter to generate the curve. The enthalpy/specific heat measurements made by the drop ice calorimetry method conform to American Society for Testing Materials (ASTM) D2766-83, with modifications to permit measurements to elevated temperatures.

Thermal diffusivity was measured with the laser-flash method. This method conforms to ASTM C-714-72, with modifications to permit accurate measurements at elevated temperatures. In this method a short duration of thermal energy (laser) is absorbed on one face of a disc specimen and the thermal response of the opposite face was monitored as a function of time and recorded with an oscilloscope. Thermal diffusivity was then calculated as a relation of this time function and the specimen thickness. The simplified relationship is:

$$\alpha = \frac{WL^2}{t_{1/2}}$$

where:

α = Thermal diffusivity, $cm^2\ sec^{-1}$

L = Specimen thickness, cm

$t_{1/2}$ = Time for backface temperature to reach one-half its maximum, sec

W = Parameter which is a function of heat loss from the specimen. For the ideal case of zero heat loss, the value of this parameter is 0.139.

Figure 39 shows the thermal conductivity of the six silicon nitrides. From room temperature to about 400C (752F), the SN251 has the highest thermal conductivity, followed by NT154 and GN-10. The thermal conductivities decreased as temperature increased and the values were close at 1371C (2500F).

For the silicon carbides, the Hexoloy SA had higher thermal conductivity at lower temperatures than Hexoloy ST as shown in Figure 40. The thermal conductivity of the two highest silicon nitrides, SN251 and NT154 are also plotted on the same graph for comparison.

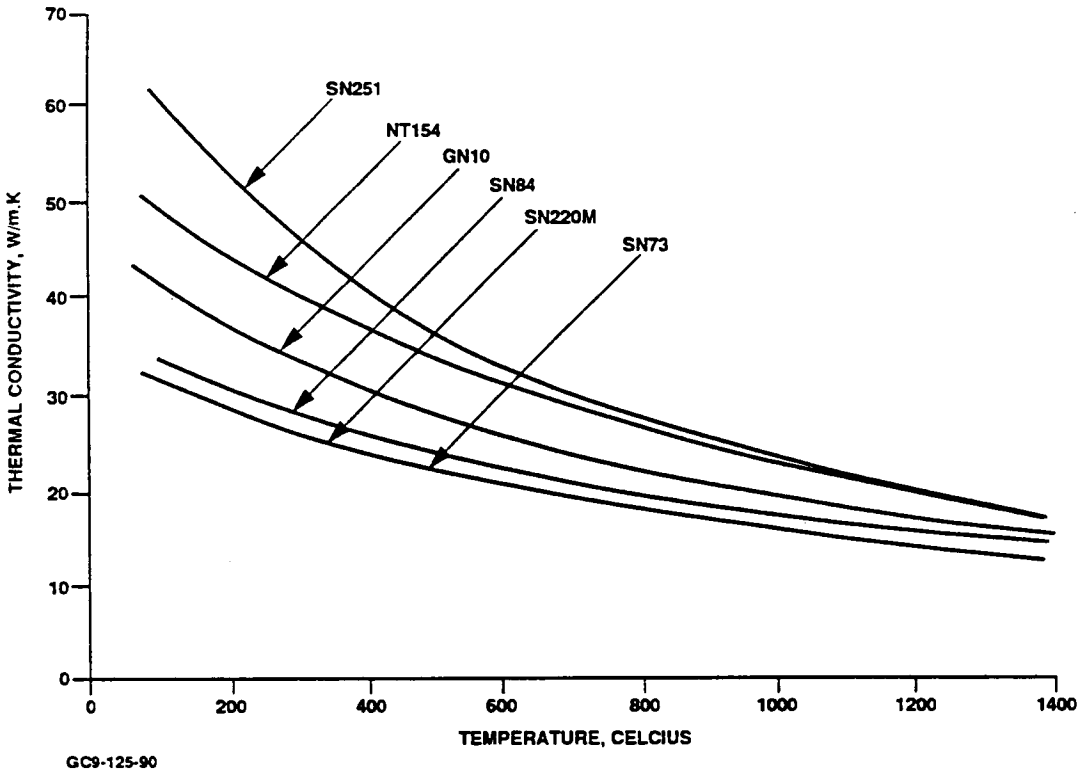

Figure 39. Thermal Conductivity Comparison of Six Silicon Nitrides.

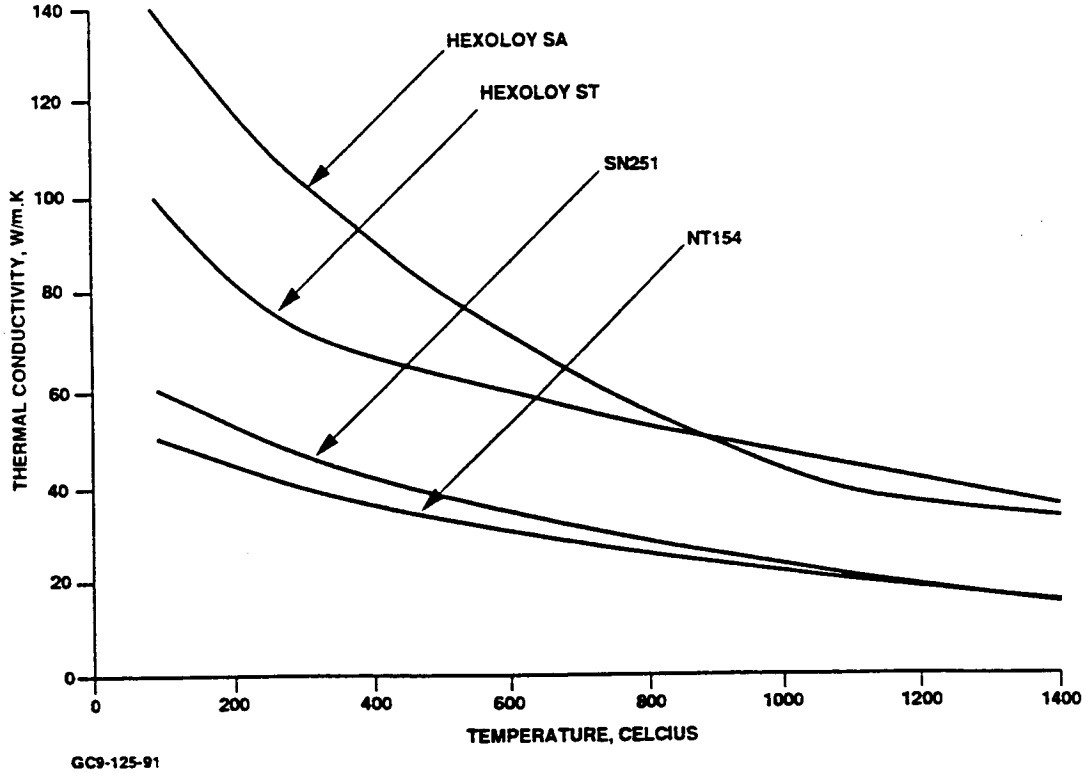

Figure 40. Thermal Conductivity Comparison of Two Silicon Carbides and Two Silicon Nitrides.

The change in thermal conductivity of the material probably can be attributed to the increase in thermal diffusivity alone. Figure 41 shows that the Si_3N_4 specific heats were virtually the same throughout the temperature range measured. The SiC specific heats were only slightly higher than Si_3N_4 specific heats (see Figure 42). The thermal diffusivity of the silicon nitrides and silicon carbides tested are shown in Figures 43 and 44 and show the same trend as the thermal conductivity data.

5.1.3.3 High Temperature Vacuum Exposures

ATTAP and the ORNL Ceramic Life Prediction Program plan to use an elevated temperature spin test to verify life prediction models. This testing is to be conducted at high temperatures under vacuum conditions, and an evaluation of NT154 sensitivity to these conditions is in order. This is because Si_3N_4 is susceptible to material loss and surface roughening at high temperatures and low pressure through dissociation and/or active oxidation. Tripp and Graham[1] showed that active oxidation should not occur above $P_{O2} = 10^{-7}$ atmospheres at 1400C (2552F), so active oxidation should not be of concern to the spin testing at a 200-micron vacuum (2.6×10^{-4} atm) However, the dissociation of Si_3N_4 is governed by the partial pressure of nitrogen, P_{N2}, according to:

$$P_{N2} = \exp \frac{\Delta G^{\circ}}{2RT}$$

where:

$G^{\circ} = -180{,}000 + 80.4T$ cal/gm mole for Si_3N_4 (Kubashewski and Evans).
R = the universal gas constant
T = temperature

Accordingly, at 1093 and 1371C (2000 and 2500F), P_{N_2} equals 2.4×10^{-6} and 6.6×10^{-4} atm, respectively. Dissociation will likely occur during the 200-micron (2.6×10^{-4} atm) exposures as the desired 1371C (2500F) test temperature is approached. The degree of this dissociation, and its influence on the material strength needed to be evaluated experimentally.

[1]Journal of the American Ceramic Society 59 9-10, Oct 1976.

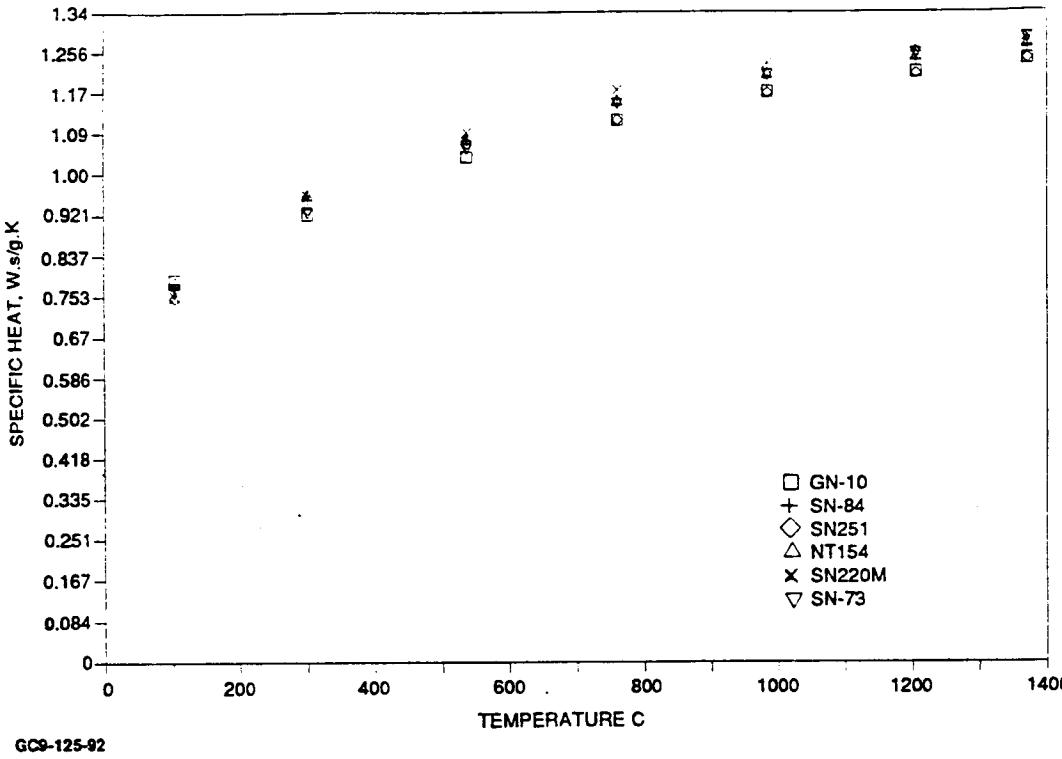

Figure 41. The Six Silicon Nitride Specific Heats Are Very Similar.

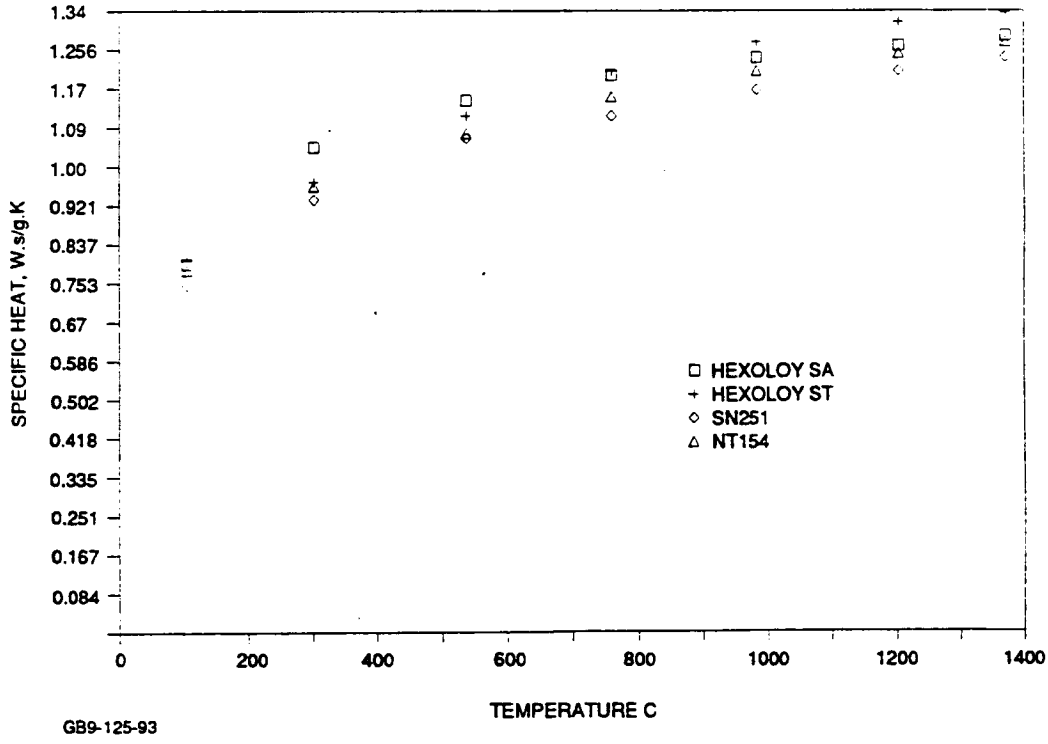

Figure 42. Specific Heat Comparison of Two Silicon Carbides and Two Silicon Nitrides.

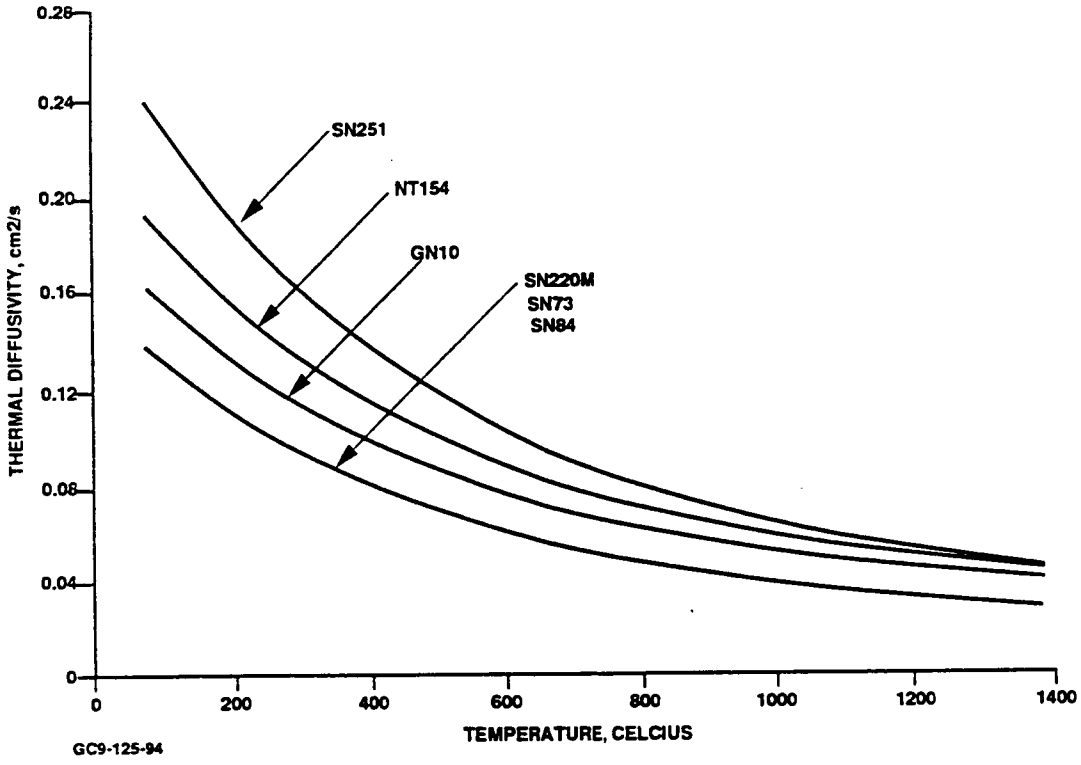

Figure 43. Thermal Diffusivity Comparison of Silicon Nitrides.

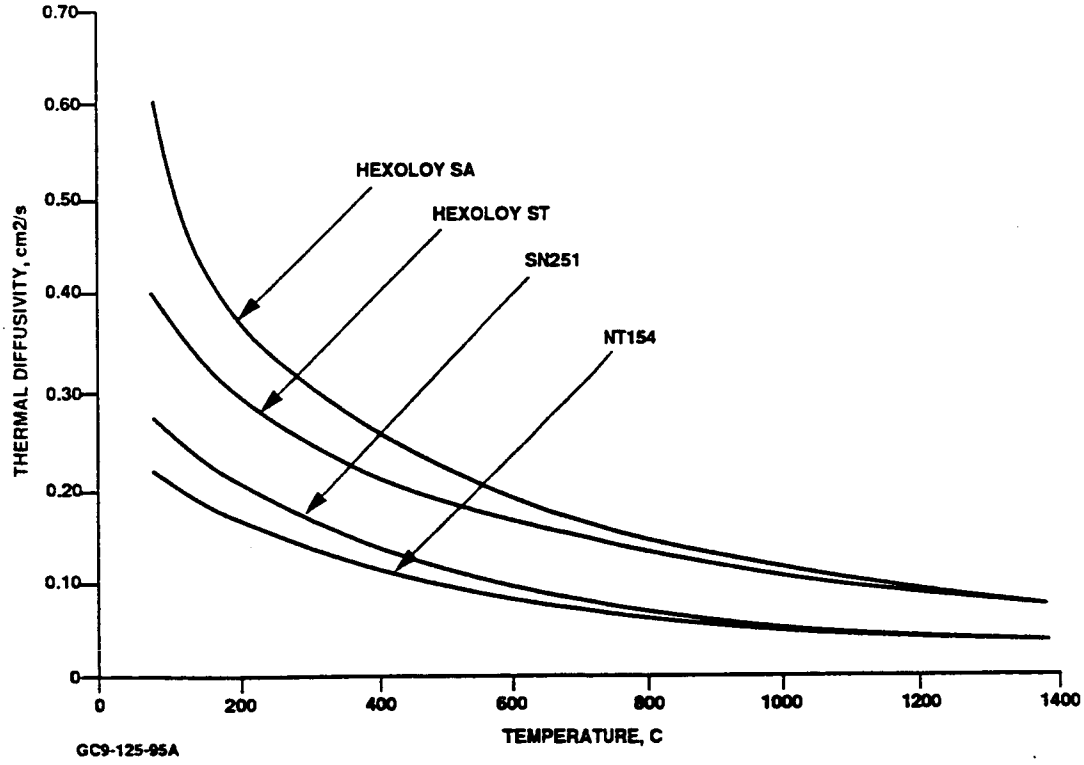

Figure 44. Thermal Diffusivity Comparison of Two Silicon Carbides and Two Silicon Nitrides.

This preliminary study was conducted to identify whether significant material degradation occurs under the anticipated spin pit vacuum and temperature conditions of 200 microns up to 1371C (2500F). If degradation were identified, more extensive evaluations would be required to determine its impact on the vacuum spin test, and to select suitable conditions for the test.

The approach was to expose Si_3N_4 test bars to the elevated temperature vacuum, and to measure retained strength and weight change. Flexure bars (1/4 x 1/8 x 2 inches) of both NT154 and RBSN were exposed. The NT154 bars had been pre-oxidized at 982C (1800F) for 50 hours to simulate component conditions for the spin disks and rotors. The RBSN was exposed in both as-nitrided and oxidized [1204C (2200F) for 2 hours] conditions to assess the oxide layer effect.

Exposures were performed for 20 hours at temperatures from 1093 to 1371C (2000 to 2500F) in 56C (100F) increments in an alumina retort, shown in Figures 45 and 46. The retort was inserted into a Lindberg furnace, and the vacuum was provided by a roughing pump. Because this vacuum pump normally produces a vacuum level of 5 microns, the desired 200-micron vacuum level was regulated by utilizing an air bleed valve. Both vacuum level and temperature were monitored throughout the exposures. After exposures and weight measurements, the bars were tested in 4-point flexure (outer span of 1.5 inch, inner span of 0.75 inch, cross-head speed of 0.02 in/min). Strength data for NT154 material was obtained only after exposures at 1148, 1260, and 1316C (2100, 2300, and 2400F) due to a limited supply of test bars. Additionally, because the RBSN specimens were obtained from several different batches of material, the flexure results were normalized by dividing the individual strength results by the appropriate batch baseline average strength. A scanning electron microscope (SEM) analysis of both fracture faces and exposed surfaces was performed.

The retained strength and weight change results for NT154 are summarized in Figures 47 and 48. These results showed a significant strength loss occurring after exposure to 1316C (2400F), which was matched by a loss in weight. A larger weight loss occurred at 1371C (2500F). Strength losses may be occurring as low as 1260C (2300F), however, no corroborating weight change was measured at this temperature. Visual examination of the bars exposed to 1316C (2400F) showed pit formation, and they had a dry appearance devoid of any oxide or glaze. Fractures originated at the pit locations. Bars exposed to 1204 and 1260C (2200 and

ORIGINAL PAGE
BLACK AND WHITE PHOTOGRAPH

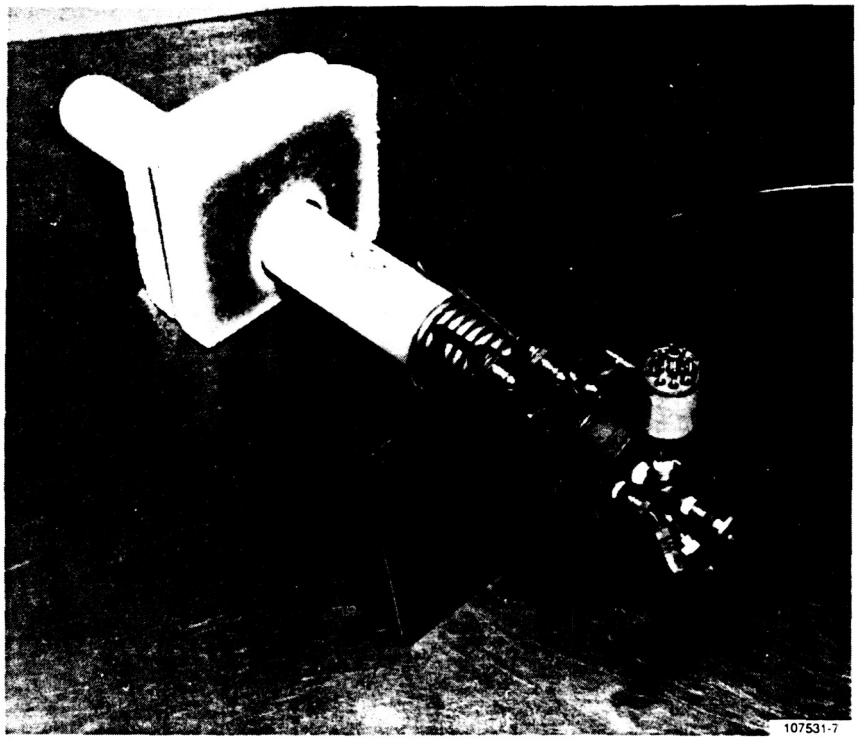

Figure 45. Instrumented Alumina Retort Used for Elevated Temperature Vacuum Exposure.

2300F) exhibited small dispersed glassy oxide spots on the exposed surfaces, and appear to have failed from these spots or from the machined surface.

The weight change and normalized retained strength results for the RBSN are presented in Figures 49 and 50. The strength results show a decreasing trend above 1148C (2100F), particularly for the as-nitrided material. This trend is less certain for the oxidized material. Both materials showed substantial strength loss at 1371C (2500F). As with the NT154, the RBSN did not exhibit a weight loss until exposure temperatures reached 1316C (2400F). Although the oxidized RBSN may have maintained more of its strength with increasing temperatures than the as-nitrided material, neither material lost weight until exposure temperatures reached 1316C (2400F).

SEM analysis of the vacuum heat-treated test bars was performed to better document the degradation which occurred. The change in surface topography of NT154 as a function of heat-treatment temperature is illustrated in Figure 51. The surface topography remains unchanged relative to the baseline up to the 1260C (2300F) vacuum exposure temperature. At

ORIGINAL PAGE
BLACK AND WHITE PHOTOGRAPH

GB9-125-68

Figure 46. Elevated Temperature Vacuum Test Retort, Furnace, Vacuum and, Temperature Monitors.

1316C (2400F), the surface oxide appears to have been stripped and pitting is evident in th bar surface. A fracture originating from a pit location is shown in Figure 52. Pitting wa observed at 1316C (2400F) for both as-nitrided and oxidized RBSN, as illustrated in Figur 53 and 54.

The results of this study supported the calculated prediction of material loss under th highest temperature vacuum conditions. Results also indicated that material loss is rap enough to degrade the material strength in only 20 hours. Because ATTAP spin testing

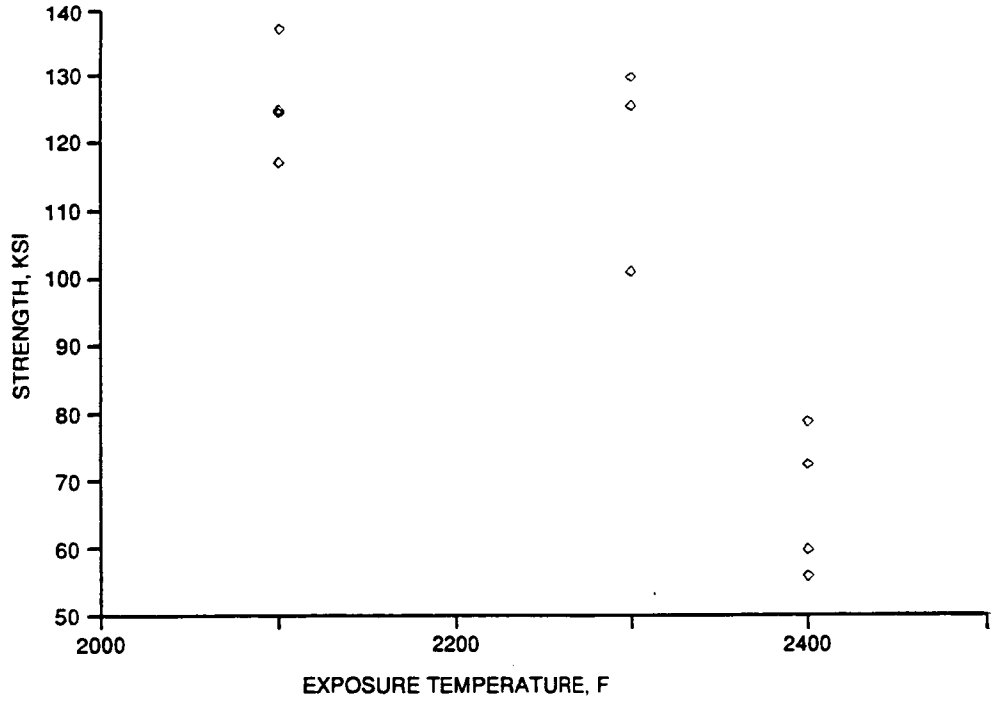

Figure 47. Retained Strength of NT154 After a 20-Hour Vacuum Exposure.

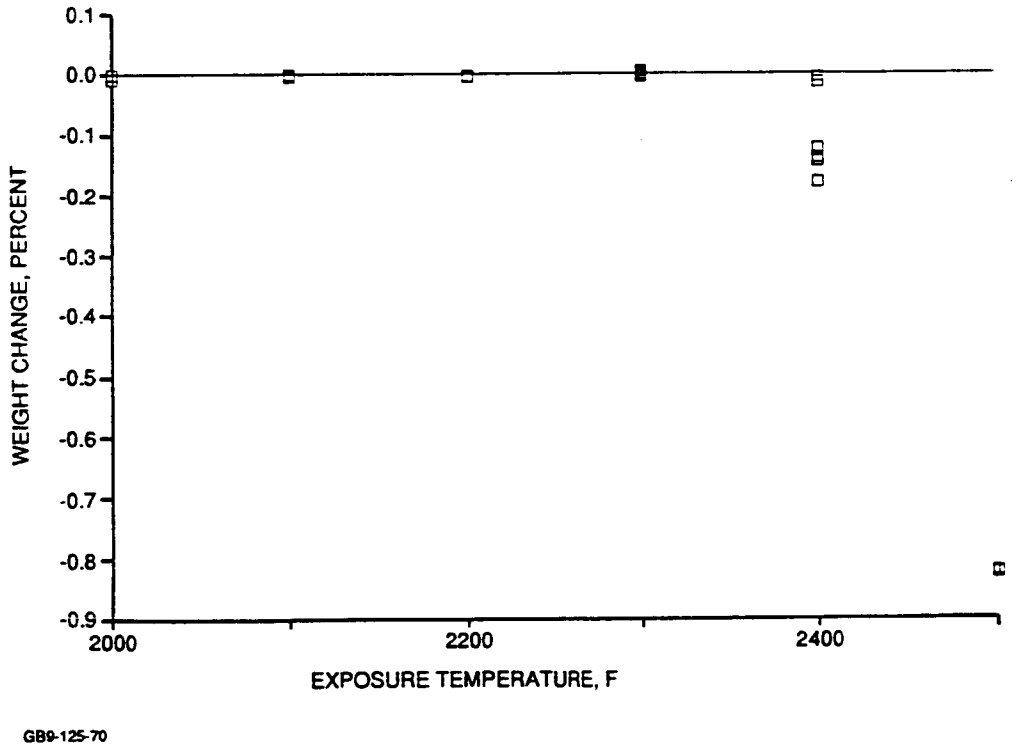

Figure 48. Weight Change Versus Exposure Temperature for NT154.

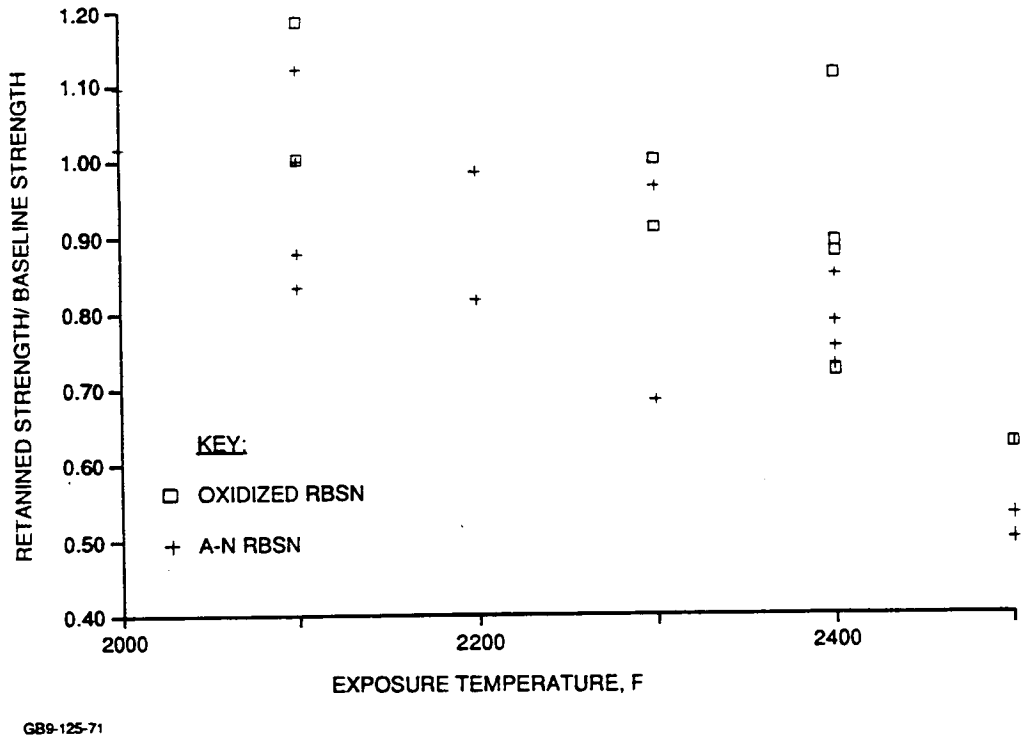

Figure 49. Normalized Retained Strength of RBSN After a 20-Hour Vacuum Exposure.

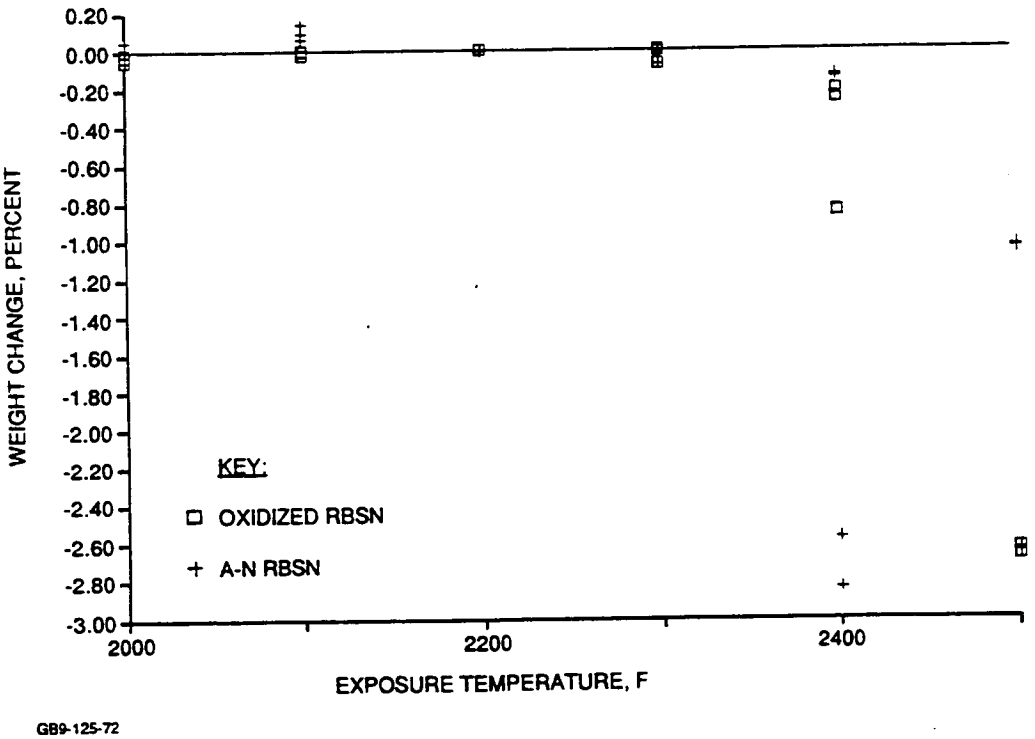

Figure 50. Weight Change Versus Exposure Temperature for RBSN.

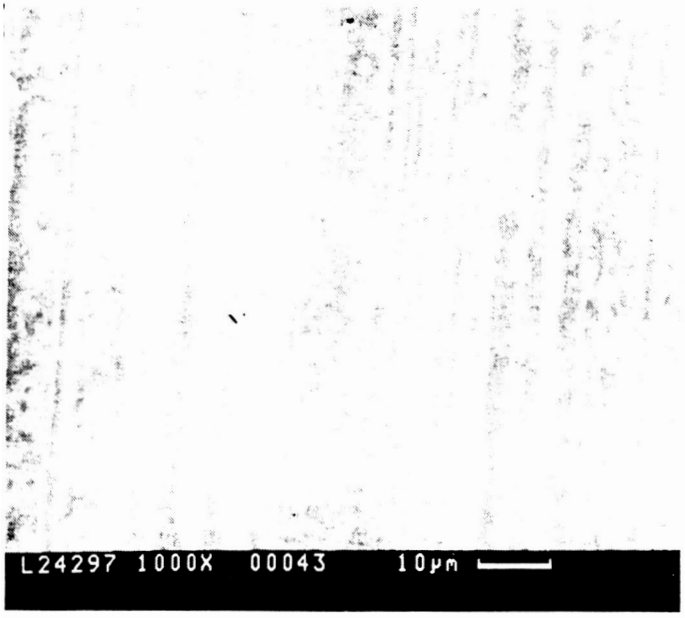

BASELINE NT154
(OXIDIZED)

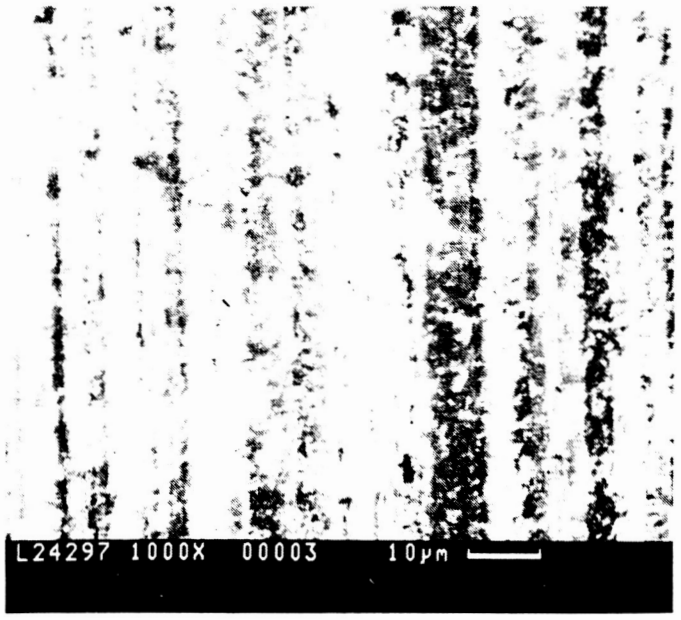

2100F VACUUM HEAT TREAT

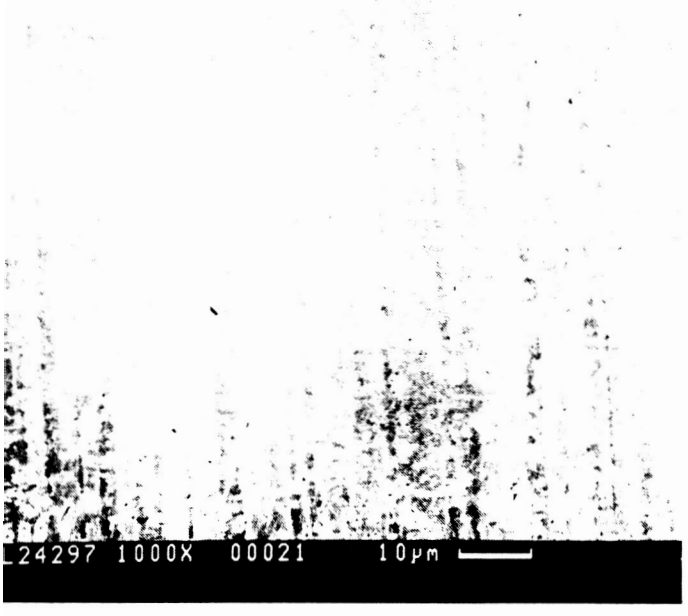

2300F VACUUM HEAT TREAT

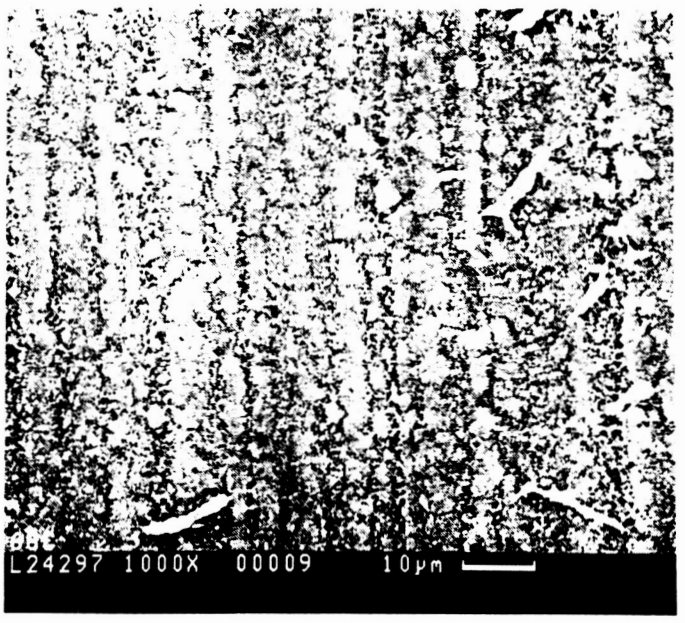

2400F VACUUM HEAT TREAT

GB9-125-97

ALL HEAT TREATMENT WERE 20 HOURS UNDER 200 MICRONS VACUUM

Figure 51. NT154 Exhibits No Change in Surface Topography Up to 1260C (2300F) Vacuum Exposure. Pitting Occurs at 1316C (2400F).

ORIGINAL PAGE IS
OF POOR QUALITY

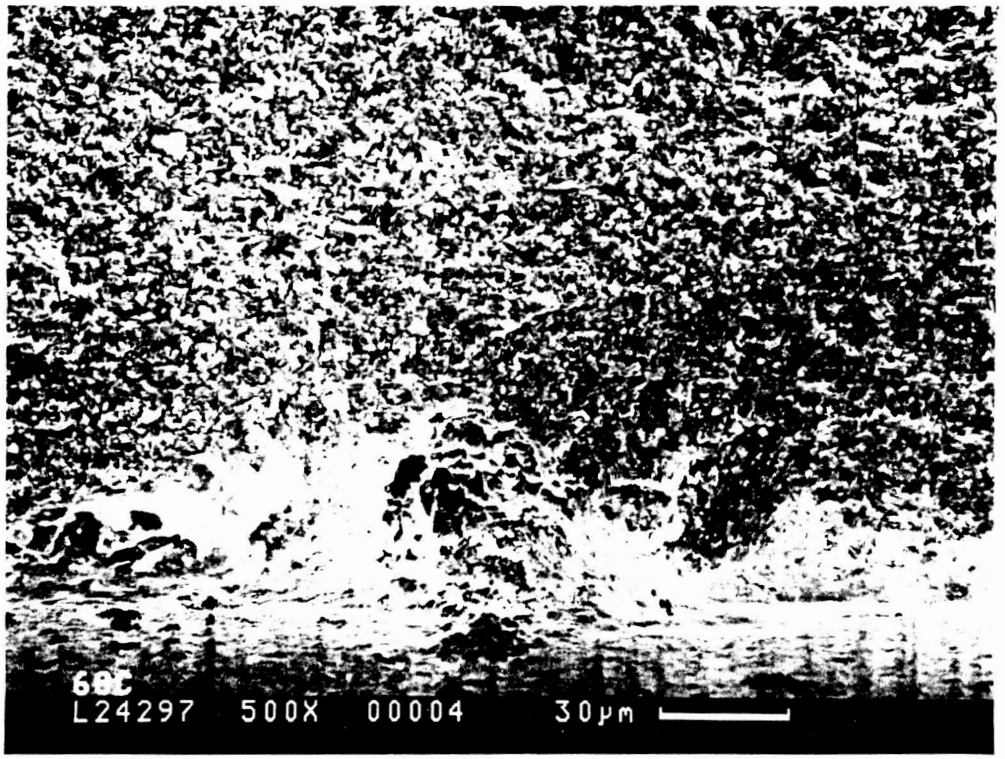

GB9-125-98

Figure 52. Fracture Originating From a Pit Location in NT154 Exposed to 1316C (2400F) Under a 200-Micron Vacuum.

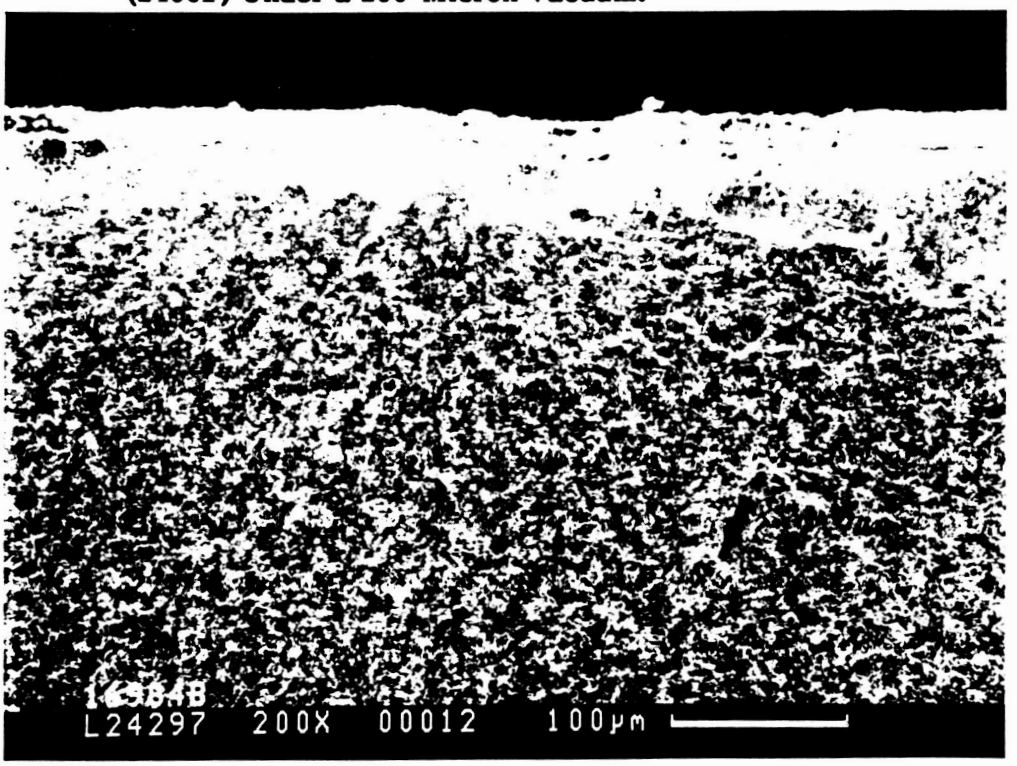

GB9-125-99

Figure 53. Fracture Originating From a Pit Location in As-Nitrided RBSN Exposed to 1316C (2400F) Under a 200-Micron Vacuum.

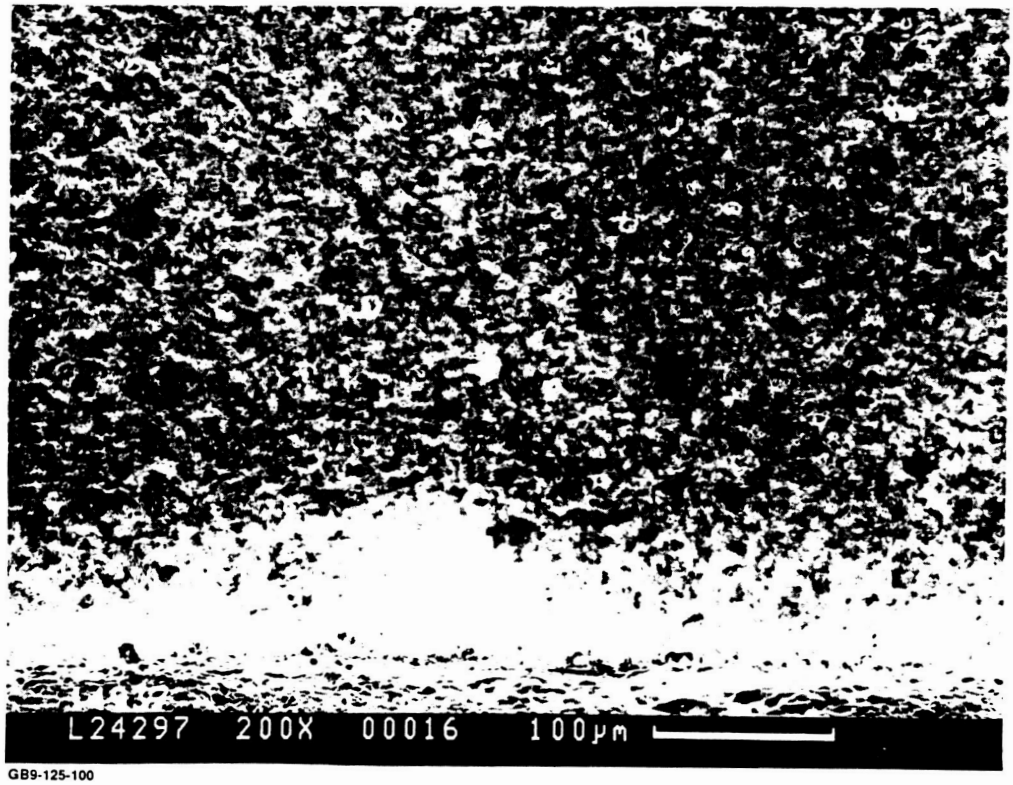

GB9-125-100

Figure 54. Fracture Originating From a Pit Location in Oxidized RBSN Exposed to 1316C (2400F) Under a 200-Micron Vacuum.

planned for longer times, e.g., 100 hours, additional studies were performed to identify whether the spin pit rpm goals could be met at higher pressure levels. Recent spin pit tests using a titanium wheel indicated the rpm goals could be met at pressure levels as high as 0.1 atm or more. Under these conditions, dissociation of Si_3N_4 is not thermodynamically predicted, so material and strength losses are not anticipated. High-temperature vacuum heat treatments under weaker vacuum conditions (0.01 and 0.10 atm) are in progress to verify the thermodynamic predictions.

5.2 Ceramic Component Fabrication

Activities of the three ATTAP ceramic component subcontractors (Norton/TRW, Carborundum, and GCCD) are detailed in the Appendices to this report. A brief synopsis of activities is presented in the following paragraphs. Figure 55 names and illustrates the components that each of the subcontractors worked on during the past year.

ORIGINAL PAGE IS
OF POOR QUALITY

NORTON/TRW

STATOR

GCCD AND NORTON/TRW

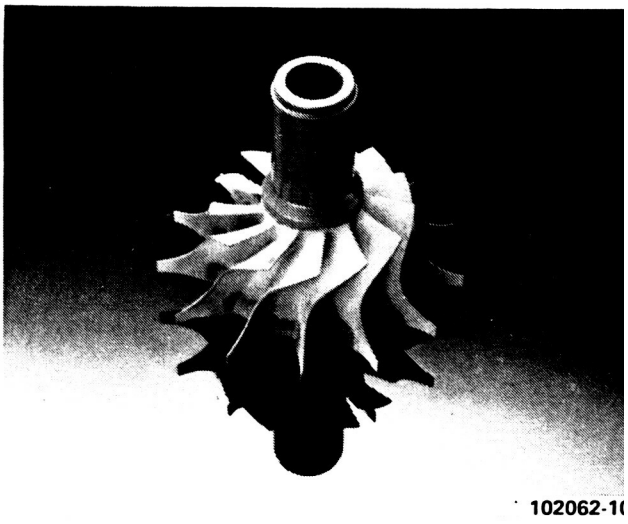

ROTOR

CARBORUNDUM

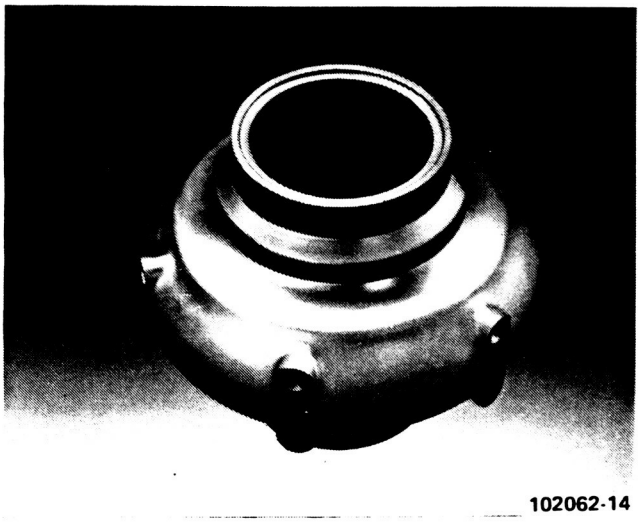

TRANSITION DUCT

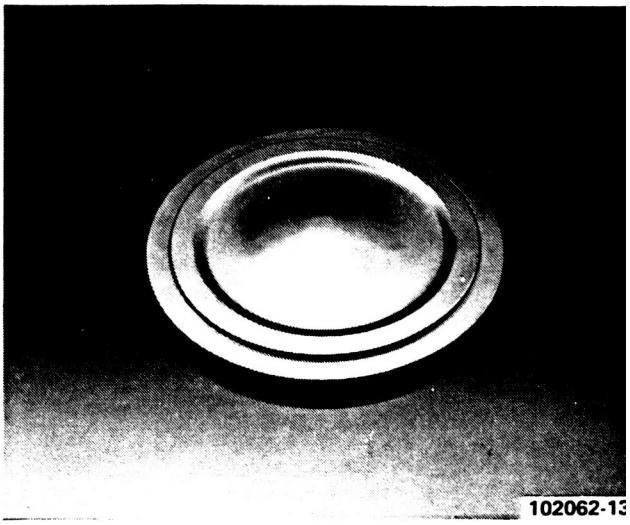

BACKSHROUD

GB8071-3

Figure 55. Fabrication Challenges Are Addressed by Subcontractors.

5.2.1 Norton/TRW Ceramics Company

Norton/TRW supplied nine rotor hubs for evaluation. These had material properties equivalent to the NT154 characterization bars (see also Section 5.1.1.2). In addition, new pressure slip casting equipment was acquired and installed to automate this process, and to make use of plastic molds for improved surface characteristics and mold life, over the traditional plaster mold.

Norton/TRW changed the fabrication approach for stators from injection molding to pressure slip casting. Norton/TRW was unsatisfied with the level of control that could be attained over metallic inclusions introduced during the injection molding process.

5.2.2 Carborundum Company

Carborundum continued work to evaluate two candidate compositions for injection molding of transition ducts. SX-05 was selected over SX-09 due to its relative ease of processing. Transition duct development made use of a subscale design which could be fabricated on the in-house injection molder. Flow analyses were performed to identify critical parameters governing the flow of material into the cavity, and at the end of 1989, a significant improvement in the visual quality of green components was demonstrated.

Work on the ram press approach to the fabrication of turbine backshrouds was hampered by the difficulty in identifying a baseline mix which could be successfully pressed and removed from the mold. The use of an outside source (a china tableware supplier) for the ram press operation limited Carborundum's control over the process. The ram press backshroud activity was discontinued by an agreement with GAPD due to the difficulties in transferring the ram pressing fabrication approach from the china industry to technical ceramics and to a pending design change affecting the backshroud component.

Wave spring activity was deleted from Carborundum's tasks early in 1989. Alternative materials can be employed for this part which offered advantages in spring compliance and increased assembly tolerances.

5.2.3 Garrett Ceramic Components Division (GCCD)

GCCD delivered four bladed rotors for evaluation early in 1989. The rotors were representative of the baseline rotor fabrication process, from which improvements were made throughout the course of the year. These first rotors were not cut up for property evaluation, but were kept on hand for comparison with later rotors fabricated by an improved process. Process improvements were pursued through the use of screening experiments and Taguchi designed experiments to identify critical parameters and the effect on the finished product.

GCCD was able to complete an accord with the Swedish firm ASEA for use of a proprietary glass-encapsulated hot-isostatic pressing (HIP) process. The license agreement will allow GCCD to speed development activities, it no longer being necessary to send components to Sweden for HIPping. The HIP process can now be further developed by GCCD to tailor it to the specific needs of gas turbine components.

5.3 Ceramic Component Preparation

Ceramic hardware is being prepared for engine and rig testing. Parts undergo dimensional inspections, NDE (i.e., fluorescent penetrant inspection, radiography, and magnified visual examination), and laser marking. The machining of flow path contours and touch-up machining of critical features is occasionally required, too. Heat treatment of certain ceramics is required to realize the maximum strength of the material. Information from these operations is fed back to the subcontractors, when appropriate, to enhance their ability to deliver engine- or rig-ready hardware.

6.0 COMPONENT RIG TESTING

6.1 Hot Spin Pit Design and Fabrication

The objective of this effort is to use data generated from test specimens to formulate methods to analytically predict ceramic component life, to refine these methods using the data from ceramic disks of the same material spun under both room temperature and heated conditions, and finally to verify the methods by similar testing of fully-bladed rotor components.

The spin tests were necessary to generate the biaxial stress fields that can demonstrate successful life prediction under more than just a uniaxial state of stress (as would be generated in a test specimen). Such spin testing at high rotational speeds was done in a near-complete vacuum so as to eliminate the effect of viscous drag, which can limit speed and affect the stability of the spinning member.

An actual gas turbine rotor would be subjected to temperatures and stresses of the same magnitude as spin testing would generate, but without the vacuum. During 1989, investigations were carried out to determine whether dissociation of the Si_3N_4 test material under the extremes of temperature and vacuum envisioned for the hot spin testing would yield false results in terms of the life of an actual component. These investigations consisted of heating specimens in a vacuum retort, and then checking for changes in weight and strength. This testing is reported fully under Section 5.1.3.3.

Additional testing was done in the spin pit at room temperature, with a titanium disk of a geometry nearly identical to that of the spin rotor. The objective was to quantify to what level the spin pit could be backfilled with gas to avoid dissociation without affecting the maximum desired test speed and without disrupting the rotating system dynamics. It was assumed that nitrogen would be used for this purpose, and this test was conducted by backfilling the spin pit with air to simulate nitrogen pressure. The pit can be backfilled as much as 1/3 atm without adversely affecting the rotor dynamics or overpowering the spin motor.

6.2 Combustor Rig Testing

Combustor rig testing concentrated on evaluating the ability of the current combustor configuration to operate successfully without creating carbon particles. This represents a means of addressing the risk of FOD to the gas turbine's hot section. Early in 1989, screening tests of newly-acquired ceramic combustor hardware were performed in this rig. Two sets of ceramic hardware were thermally screened by generating a 833C (1500F) difference between the combustor inlet and discharge airflow. This condition created a thermal stress state equivalent to 125 percent of normal engine start transient stresses. Both sets of hardware survived and are now qualified for engine and rig testing.

The next step in solving the coking problem was to evaluate this combustor design under actual ATTAP engine conditions. The conditions that were tested included the idle, cruise, and maximum power engine conditions. These conditions were maintained for two hours in the combustor rig using DF-2 as the fuel. The results of these tests indicated that coking occurred on the fuel nozzle lip at maximum power, and coking occurred in the pilot combustor at idle.

To prevent coking at maximum power, the fuel nozzle lip was removed, thus eliminating the coking surface. To solve the idle coking problem, rig insulation was ordered to prevent high heat loss through the rig. Retesting was performed with oxygen added to the inlet air. This was done to compensate for the oxygen depletion caused by a gas-fired inlet air heater. Unfortunately, the coking problem at idle still occurred.

An alternative fuel was sought to run the engine without coking. Ethanol and JP-4 were evaluated under the same idle, cruise and maximum power conditions. Ethanol was found not to coke at any of the engine conditions and light-off occurred under a variety of fuel flows, combustor flows, and air assist pressures. JP-4 accomplished the light-off easily but coking was found at the cruise condition in the pilot combustor. Therefore the metal and ceramic engine runs will use ethanol as a fuel until further combustor development yields a non-coking combustor, or until another means of addressing carbon-induced FOD can be identified.

Further combustor rig testing will concentrate on evaluating an updated nozzle design and an enlarged bore pilot combustor design. Both are intended to eliminate combustor coking over the operating range.

6.3 Regenerator Rig Testing

Regenerator seal development activities are reported under Section 3.4.1.

6.4 Structural Proof Testing

The NDE techniques to assure high reliability of ceramic components have not yet been fully identified or developed and it remains necessary to perform component proof tests to qualify ceramic hardware for use in the ATTAP test bed engine. These tests generally simulate a worst-case stress condition with a 25 percent overstress margin.

Information from these proof tests, when combined with results of prior NDE testing, can be valuable in determining the critical flaw characteristics. This provides a contribution to the establishment of specifications for ceramic components.

The proof tests conducted have been summarized in the following paragraphs.

6.4.1 Turbine Shroud and Support Structures Mechanical Proof Test

A 1818 kg (4000-pound) load was applied to the turbine shroud, rockers, and lower contact washers to represent 25 percent overstress of the maximum stress conditions in an engine due to pressure. The rig is shown in Figure 56. The test used an aluminum base to secure the turbine shroud and its supporting hardware and to provide stability. Metal shims were placed on the base and then ceramic hardware stacked in place starting with the lower contact washers and followed by the rockers and turbine shroud. This assembly was then bolted to the base to keep the proper alignment of the ceramic hardware.

To simulate the pressure condition, an aluminum disk with three equally spaced feet was placed feet down on the turbine shroud. When the load was applied by using a press and then measured by a load cell, the force was equally distributed through each foot in the load disk, transferred to the turbine shroud, and then through the rockers and contact washers, thus screening the ceramic hardware for mechanical overstress situations.

ORIGINAL PAGE
BLACK AND WHITE PHOTOGRAPH

Figure 56. 1818 kg (4000-Pound) Mechanical Load Test Rig.

Four turbine shrouds, sixteen rockers, and three lower contact washers were screened After visual inspections, none of the hardware showed any signs of damage. The rockers an lower contact washers were considered qualified for ATTAP engine testing. The turbin shrouds must also pass a thermal screening test before they will be considered qualified.

6.4.2 Turbine Shroud and Stator Thermal Proof Rig

Early in 1989, the turbine shroud and stator thermal proof rig was modified to provide the turbine shroud improved support. In the previous rig configuration, the turbine shroud rested directly on the rig insulation made of Babcock & Wilcox Kaowool® 3000 board stiffened with Zircar® alumina rigidizer and coated with Zircar® alumina cement. This system provided a semiresilient support for the shroud and insulated the metallic rig housing. However, with repeated use the insulation shrank, affecting the axial component stack and the assembly load on these components provided by the rig, as shown in View A, Figure 57.

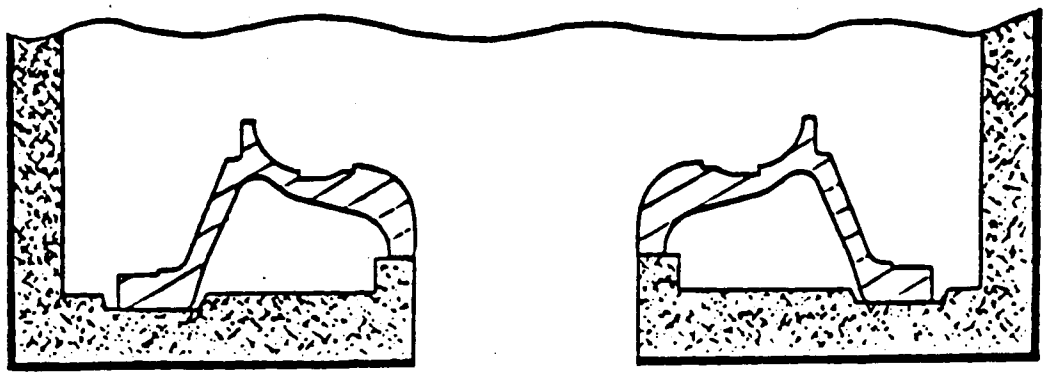

VIEW A
PREVIOUS CONFIGURATION

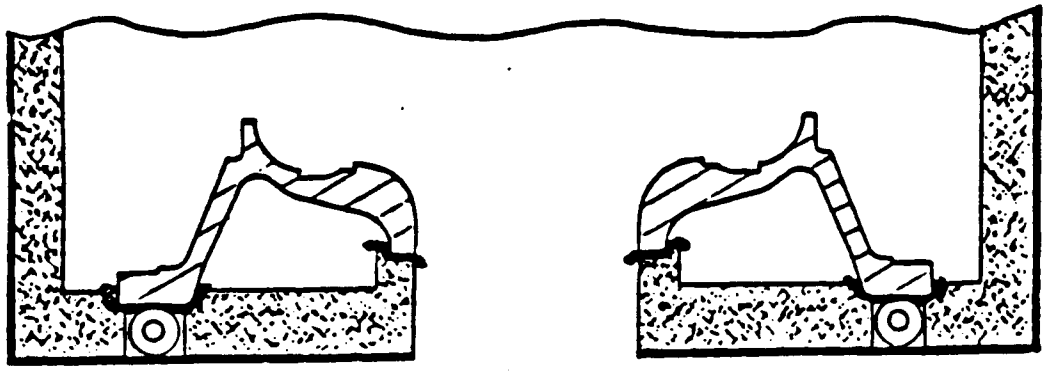

VIEW B
CURRENT CONFIGURATION

GB9-125-11

Figure 57. Turbine Shroud and Stator Thermal Proof Rig.

A modification to the rig is shown in View B, Figure 57. This configuration used a roller support made of Si_3N_4, under each foot of the turbine shroud. The rollers provided a rigid support for the component stack, yet allowed unrestrained differential thermal growth between the rig housing and the test components. A layer of Nextel• cloth, placed between the shroud feet and the rollers provided a resilient interface and helped protect against excessive contact loads caused by rig housing distortion.

The rig was to provide the ceramic hardware a 25 percent overstress of a cold start condition in a short amount of time. Cold start conditions are worse than maximum temperature conditions because the thermal gradient across the hardware is much more severe. Two different cycles, shown in Figure 58, were run twice in each screening tests. The turbine shroud was screened in the 888C (1630F) cycle while the stators were screened in the 1204C (2200F) cycle.

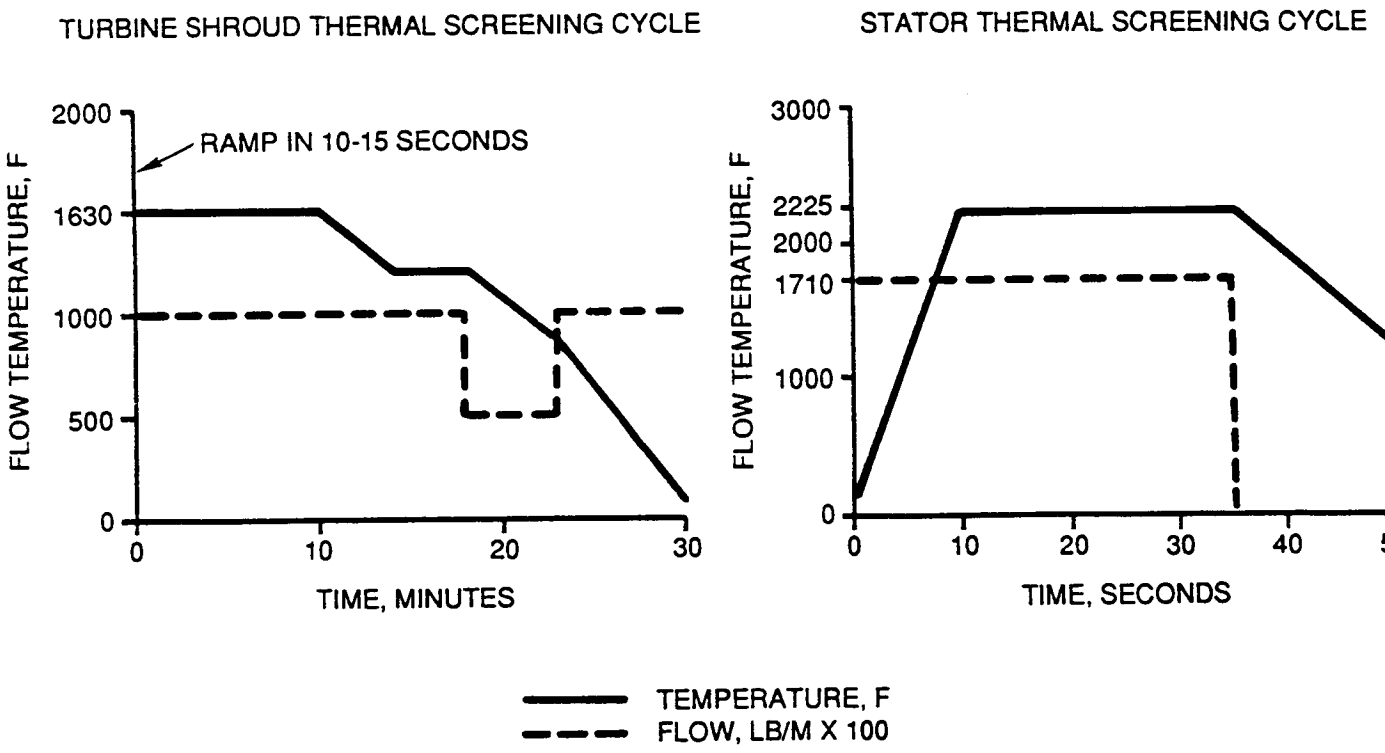

Figure 58. Turbine Shroud and Stator Thermal Screening Cycles.

In this rig test, the turbine shroud is not required to reach the engine operating temperatures to obtain screening stress levels. This is because the rig does not heat the back of the shroud as in the engine, thus a larger thermal gradient is created, resulting in higher stress levels.

The stators were screened in this same proof rig, but to a different thermal cycle. The rig flow path past the stators duplicates the engine condition, requiring a higher temperature and flow rate to provide the desired 25 percent overstress. Since the stators reach their worst stress condition within half a minute of light-off, the test time can be kept short to avoid a potentially damaging temperature gradient in the turbine shroud.

The thermal screening of four turbine shrouds and six stator sets was completed in 1989. Post test inspections did not reveal any thermally-induced damage to the hardware.

6.5 1371C (2500F) Test Rig

Preparation for the 1371C (2500F) rig is continuing. NT154 stators from Norton/TRW, and rig hardware from other suppliers is expected to arrive in mid-February 1990. All of the rig instrumentation, primarily thermocouples, has either been repaired or replaced.

Conax Buffalo Corporation is developing an innovative new temperature measurement system. This system, which utilizes fiber optics and a blackbody insert in a sapphire probe, could be used in the gas path of an engine to measure TIT. However, the system must first be tested in a low-risk, high-temperature rig before being placed in an engine. A cooperative effort is underway to test the probe in an already scheduled 1371C (2500F) rig test. This activity parallels the existing rig test plan and incurs no extra cost to the program.

6.6 Turbine Inlet Particle Separator (TIPS) Testing

Work in 1989 concentrated on testing the center flow TIPS design (Figure 59) and various refinements. This design uses swirled airflow from the combustor to centrifuge the particles outward in the combustor liner as they flow towards the turbine. A conical deflector and tubular splitter separate the particles from the clean airflow. Clean air is directed through the center of the splitter while carbon is trapped in the annulus between the splitter

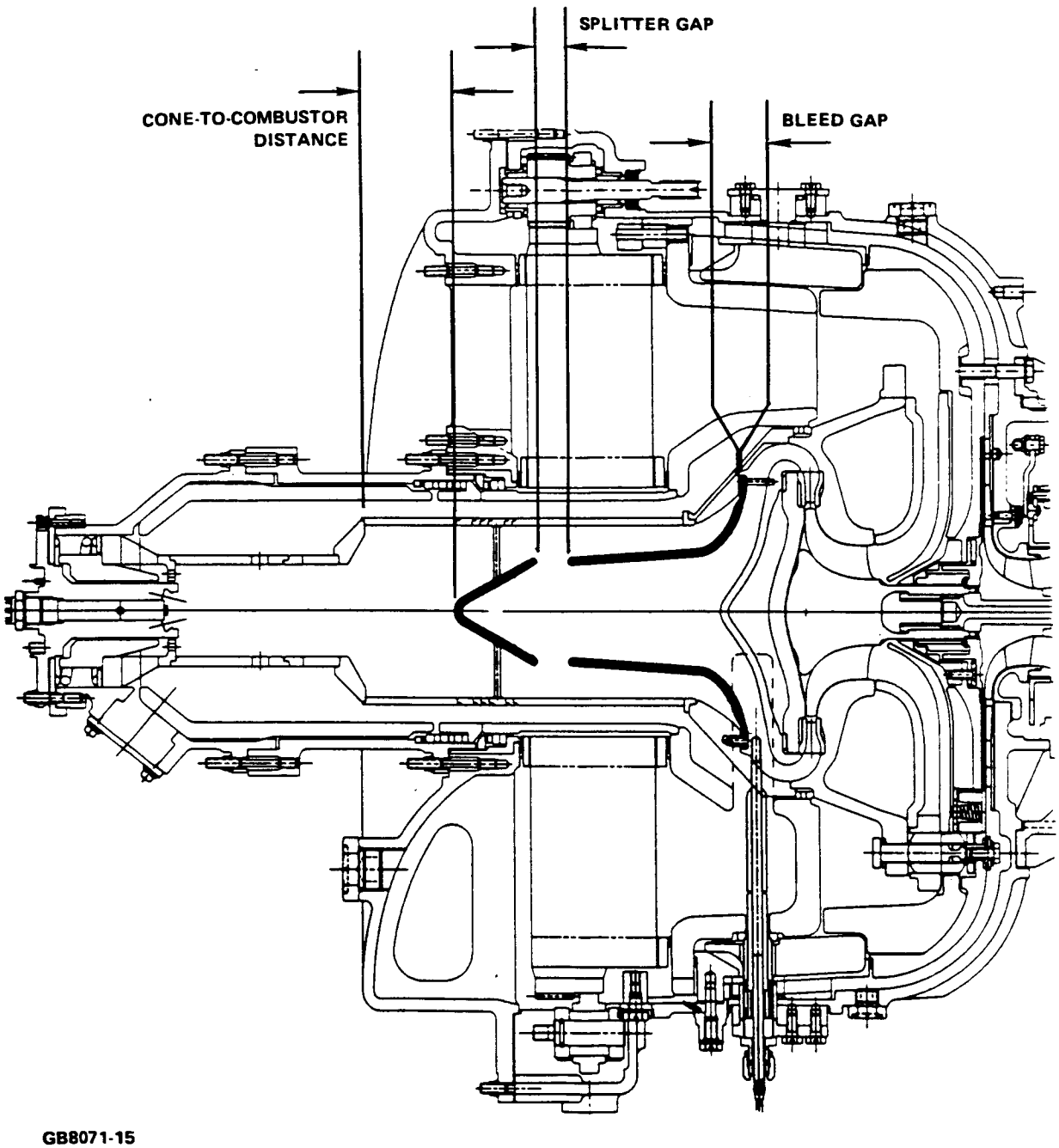

Figure 59. Center Flow TIPS Configuration.

and transition duct. Trajectory analysis and impact test results from UDRI were used to determine baseline splitter and bleed gaps for this configuration. This baseline configuration resulted in a separation efficiency of 97 percent with a pressure loss across the TIPS configuration of 3 percent.

Testing was performed according to a series of Taguchi test matrices to identify and optimize the critical parameters of the various design concepts. The test parameters identified for each design are shown in Figures 59, 60, and 61. Plexiglass components were used to permit flow visualization, via high-speed photography, of the most promising configurations. Trials were run at cold flow conditions comparable to engine flows during maximum power operation. Particle introduction was in the area corresponding to the fuel nozzle, and separation efficiency was measured by physically counting and weighing the trapped particles. A particle size of 0.180-inch diameter was chosen to facilitate the physical particle counts while still allowing good comparison of the various configurations.

Flow testing and high-speed photography of the initial or baseline center flow concept (Figure 59) determined that recirculation was occurring between the combustor liner and TIPS hardware. This recirculation suspended some of the particles around the splitter gap where they could be drawn into the turbine flow path.

To minimize the effect of the recirculation, a ramped-shroud center flow TIPS design was evaluated (Figure 60). This configuration did not perform as well as expected. While it did eliminate the recirculation in the combustor, it also created a small backflow near the TIPS which had a similar effect. Particles which struck the supporting spokes of the center cone lost axial velocity, and the backflow then entrained them in the area of the splitter, where they could be drawn into the primary flow path again.

To solve these problems, the center-supported center flow TIPS design (Figure 61) was generated. The inlet ramp was removed to resolve the backflow problem, and a tailored cone was provided to force the particles radially away from the splitter gap. To address the axial particle velocity loss, the radial spokes supporting the cones were replaced with struts that support the cone from the inside of the flow divider. This configuration will be tested in early 1990.

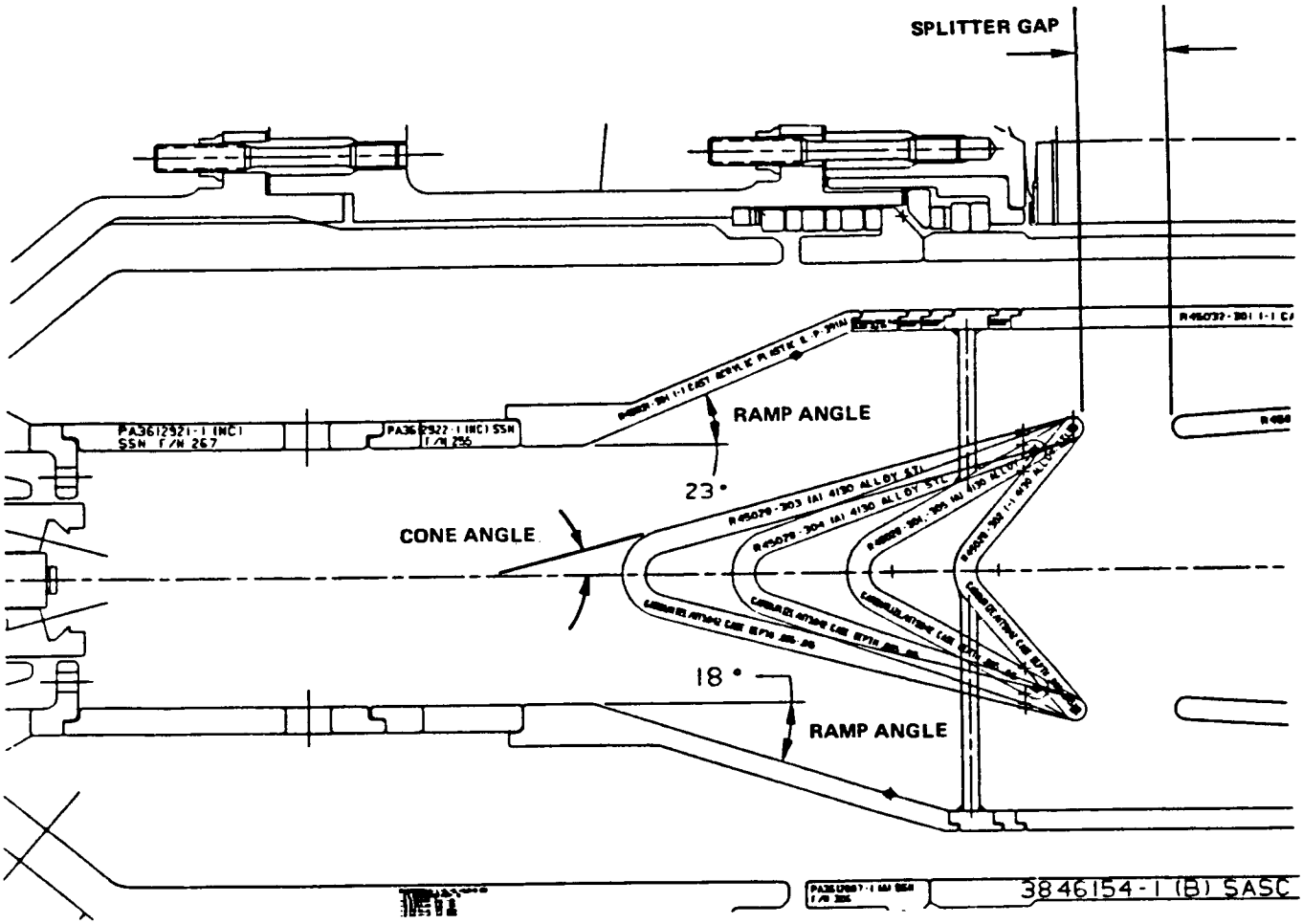

GB8071-16

Figure 60. Ramped-Shroud Center Flow TIPS Configuration.

6.7 Ceramic Seals Test Rig

Rig testing of FSH dual and triple seal configurations was completed in early September. After analyzing the data from the testing, it was determined that the triple seals worked better than the dual seals. A comparison chart can be seen in Figure 62. To make the comparison, the seal leakage was calculated as a function of engine speed. The graph shows that seal leakage is reduced by a factor of approximately 25 percent at an engine speed of 75,000 rpm.

ORIGINAL PAGE IS
OF POOR QUALITY

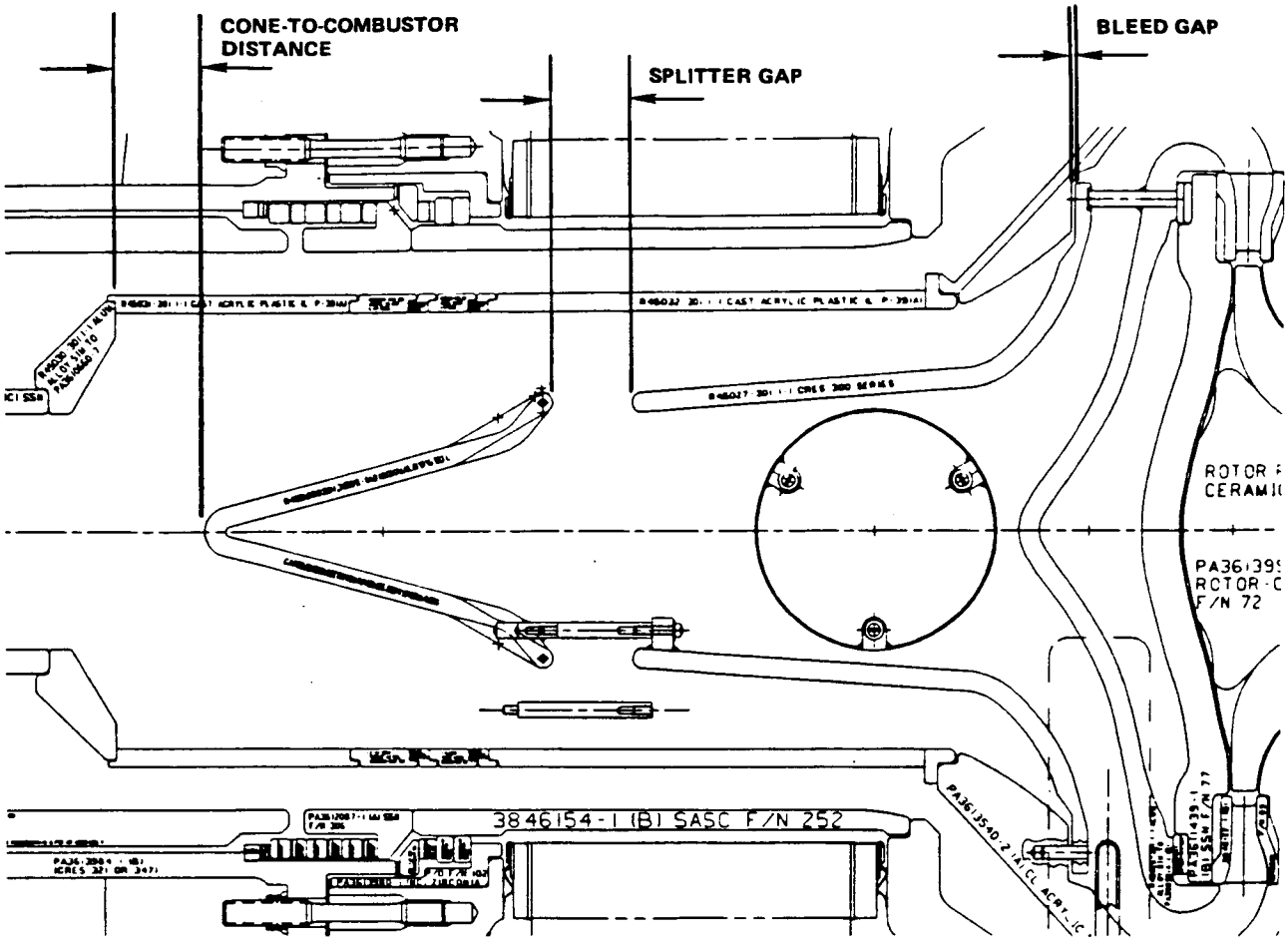

Figure 61. Center-Supported Center Flow TIPS Configuration.

Although this data showed a trend, it should be considered a guide rather than an absolute. The data was taken in a cold rig under ideal conditions while the conditions in an actual engine running at 75,000 rpm are less than ideal, so leakage cannot be assumed to be reduced by 25 percent. However, leakage will decrease when using triple seals and since any leakage reduction is desirable, triple seals will be used in the next ceramic ATTAP test bed engine.

ORIGINAL PAGE IS
OF POOR QUALITY

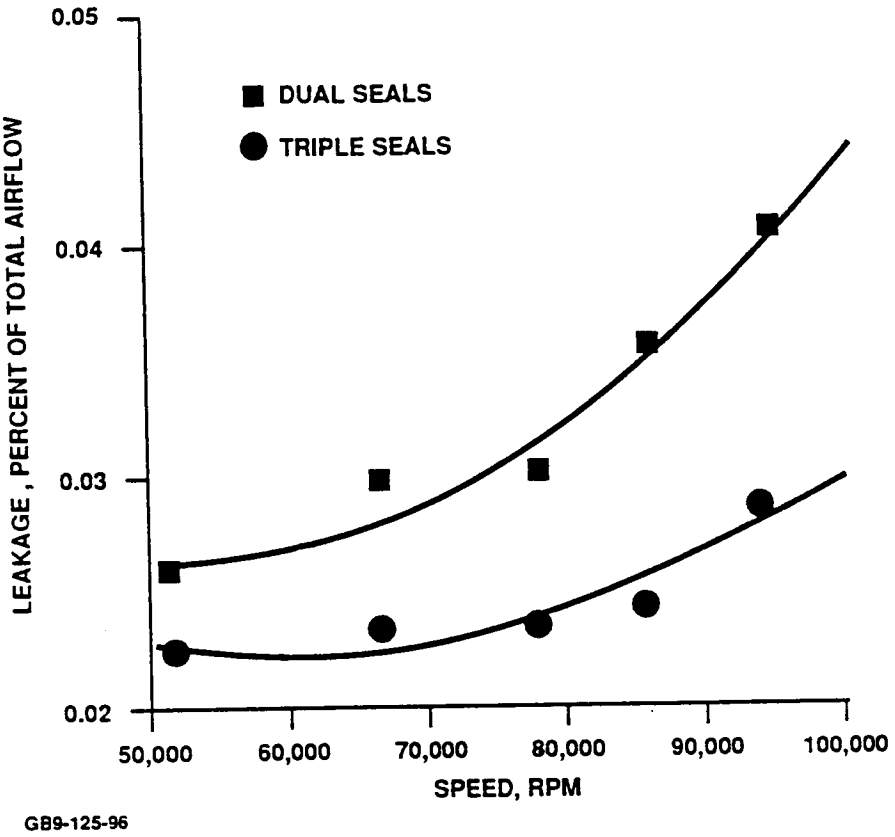

Figure 62. Seal Leakage Comparison as a Function of Engine Speed.

7.0 ENGINE TEST BED TRIALS

The metallic ATTAP engine test bed was assembled and tested to evaluate an improved electronic control unit (ECU). This test incorporated similar geometries with the ceramic ATTAP engine test bed, including the upstream combustor flow path insulation, the ceramic combustor, and a ceramic turbine rotor.

During this test the test bed was operated for 49 minutes at speeds up to 80 percent before the test was terminated due to excessive erosion of the flow path insulation. Insulation liners were designed to prevent further erosion and preparations were made to resume testing in early 1990.

8.0 PROJECT MANAGEMENT AND REPORTING

GAPD has provided the project management to assure that the 1989 project objectives were met within the available budget and in a timely fashion.

The ATTAP Milestone Schedule (Figure 63) shows that Milestones 3 - Turbine Stage Component Deliveries, 4 - RPD (2500F) Engine Test Bed Evaluation, and 5 - 100-Hour Test Bed Endurance Evaluation, will slip 16, 9, and 7 months, respectively. These slips are due to the increased efforts required by the subcontractors to develop the technology necessary to fabricate hardware that will meet RPD temperature requirements and the test bed engine specification, and the changes in turbine design for the ATTAP test bed engine.

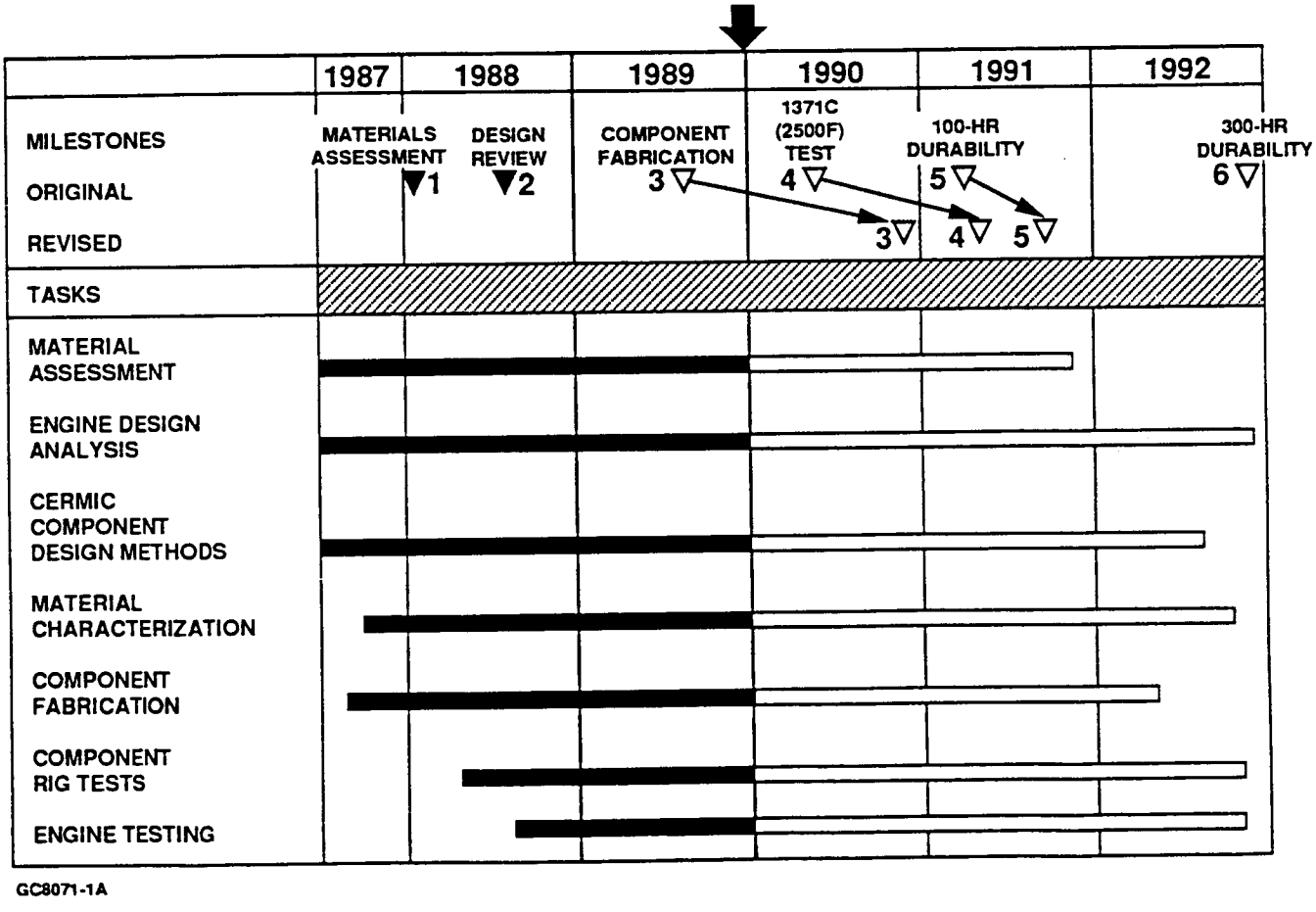

Figure 63. ATTAP Milestone Schedule.

GAPD issued six Bi-Monthly Technical Progress Reports during 1989 and attended five Bi-Monthly Review Meetings with NASA/DOE. In October 1989 GAPD and NASA met to discuss a change to the design of the ATTAP test bed engine. NASA concurred with the GAPD recommendation and gave the go-ahead to initiate the new design.

GAPD personnel attended the "Twenty-Seventh Automotive Technology Development Contractors' Coordination Meeting" in Dearborn, MI, October 23-26, 1989. Two presentations were made reporting on ATTAP accomplishments over the past year:

- "ATTAP/AGT101 - Year 2 Progress in Ceramic Technology Development" (GAPD Report No. 31-8440)
- "Impact Design Methods for Ceramic Turbine Blades" (GAPD Report No. 31-8441)

At the Dearborn meeting, two other presentations were made on the following ATTAP support programs:

- "Life Prediction Methodology for Ceramic Components of Advanced Heat Engines (GAPD Report No. 31-8421)
- "3500-Hour Durability of Commercial Ceramic Materials" (GAPD Report No. 31-8420)

GAPD made four more presentations on the ATTAP effort at the following technical society meetings:

- ASME International Gas Turbine Conference - Toronto
- ASME International Materials Week - Indianapolis
- American Ceramic Society - Anaheim
- Golden Gate Materials Technology Conference - Santa Clara

GAPD has submitted the following professional papers on the ATTAP effort for publication by the Society of Automotive Engineers (SAE):

- "Impact Damage of Sintered Silicon Nitride," by H. Fang and J. Cuccio (GAPD Report No. 31-7723).
- "AGT101/Advanced Turbine Technology Applications Project (ATTAP)," by G. Boyd and D. Kreiner (GAPD Report No. 31-7722).

APPENDIX I

ANNUAL TECHNICAL PROGRESS REPORT
NORTON/TRW CERAMICS COMPANY

ADVANCED TURBINE TECHNOLOGY APPLICATIONS PROJECT
COMPONENT DEVELOPMENT PROGRAM

Annual Technical Progress Report
for the period
January 1, 1989 to December 31, 1989
under
GAPD Purchase Order Nos. P1776307,
dated February 18, 1988,
and
P1772578, P1772588, P1772598, and P1772608
dated July 7, 1988.

Submitted by
NORTON/TRW CERAMICS
Goddard Road
Northboro, MA 01532-1545

Bryan J. McEntire
Program Manager

Report Date: February 26, 1990

Prepared for
NASA-LEWIS RESEARCH CENTER
Cleveland, OH 44135

Submitted to
Garrett Auxiliary Power Division
ALLIED SIGNAL AEROSPACE COMPANY
Phoenix, AZ 85034

TABLE OF CONTENTS

EXECUTIVE SUMMARY

This report presents a summary of Norton/TRW Ceramic's (NTC) work in support of the Advanced Turbine Technology Applications Project (ATTAP) for the 1989 program year. As a participant in ATTAP, NTC is responsible for the development of ceramic fabrication processes for the rotor and stator components of the AGT101 gas-turbine engine. Activities towards these objectives have centered on completion of seven tasks: (1) Design and Cost Analysis; (2) Forming Methods; (3) Process Engineering; (4) NDE; (5) Quality Assurance; (6) Deliverables; and (7) Project Management. For each task, all mutually-agreed-upon second-year program milestones were achieved.

During 1989, NTC continued to perform component development work using NT154 Si_3N_4. This material is a 4% Y_2O_3-doped Si_3N_4 prepared by HIP densification. Since its introduction in 1988, extensive characterization has been conducted at NTC, by GAPD, and several other independent testing laboratories. Physical, thermal, and mechanical properties continue to exceed program specifications, and are approaching overall ATTAP goals.

Component forming technology development continued during 1989. Casting and injection-molding were selected as the forming processes for the rotor and stator, respectively. Forming was integrated with other ancillary process operations including: (1) Powder Beneficiation; (2) Degas Heat-Treatments; (3) HIP, and (4) Post-HIP Heat-Treatments. Key process parameters and control ranges have been identified for these operations. At the end of 1989, most of these ancillary processes were defined and documented. Statistical process control (SPC) was implemented for these operations. Using these technologies, rotor-hubs and stators were formed, densified and characterized. An assessment of material properties for these two components, and their respective forming techniques has been made. Characteristic room-temperature strengths and Weibull Moduli were found to be ~920 MPa and ~19 and ~840 MPa and ~7 for rotors and stators, respectively. Process induced inclusions were found to be the dominant defects for the injection molding process; whereas the pressure-casting process was free of gross contamination. Based on these results, NTC has elected to curtail further work on injection molding in favor of pressure casting. In 1990, pressure casting will be the sole forming operation for both rotors and stators.

In the performance of this work, NTC continued to utilize Taguchi-based experimental design techniques for all process engineering activities. A comprehensive 1989 Work Plan for individual experiments was prepared and submitted to GAPD. Taguchi designs are advocated because of their ability to simultaneously achieve process robustness and reduce cost.

NDE efforts centered on the development of microfocus x-ray radiography (MFXR) inspection techniques. During 1989, a seeded-defect study was completed. From this work it was found that iron and agglomerate defects are detrimental to strength at all levels of contamination. Voids were only found to be harmful at sizes greater than ~400μm. However, the detection capability of the equipment was found to be insufficient in discerning all but very large strength limiting flaws. Based on these results, it was concluded that MFXR inspection is useful in process development; but is of limited applicability in assuring final component quality. Nevertheless, component inspection protocols were developed and implemented for green rotors and stators. In this mode, MFXR was successful in identifying process induced defects and voids within the injection molding process.

The key elements and schedule of a comprehensive quality assurance plan were identified and documented. Writing of a draft plan was completed. The plan was submitted to GAPD. Commentary on the plan was received, and revisions are currently in process. Full implementation of this plan coincides with completion of the experimental work prior to final component deliverables.

During 1990, efforts will focus on specific forming related problems for the rotor and stator. Development will emphasize the fabrication of components with appropriate form, feature and dimensional tolerance, while maintaining physical and mechanical properties. Due to component design changes currently contemplated by GAPD, activities during 1990 will utilize rotors and stators similar in geometry to the anticipated final designs. Because of these changes some schedule adjustments have been incorporated into the 1990 Work Plan; but overall achievement of ATTAP goals and final component milestones should be realized.

INTRODUCTION

Commercialization of advanced structural ceramics requires development of reliable component manufacturing processes. The Advanced Turbine Technology Applications Project (ATTAP) addresses this requirement. The ATTAP is a DOE-sponsored, 5-year ceramic component development program which utilizes the AGT101 gas-turbine engine as a functional test-bed. The goals of this program include: (1) The development and demonstration of reliable ceramic fabrication processes; (2) Production of the required ceramic components; (3) Evaluation of these components in actual engine tests; and (4) Preparation of a Ceramic Design Manual. The Design Manual will provide material specification and design methods for structural ceramics in gas-turbine engine applications.

As a participant in ATTAP, and subcontractor to the Garrett Auxiliary Power Division (GAPD) of Allied-Signal Aerospace Co., Norton/TRW Ceramics (NTC) is developing ceramic fabrication processes for the AGT101 stator and rotor. NTC has performed this work in accordance with the overall program schedule of the Statement of Work (SOW) as shown in Figure 64. Identified within the SOW are seven tasks: (1) Design and Cost Analysis; (2) Forming Methods; (3) Process Engineering; (4) NDE; (5) Quality Assurance; (6) Deliverables; and (7) Project Management.

From the SOW, a comprehensive 1989 Work Plan was developed. The schedule for the Work Plan is shown in Figure 65. The Work Plan further defines the technical approach of the program, extent of design and analysis, experiments, hardware, and activities directed at achievement of the program objectives and milestones. This report presents a summary of NTC's second-year developmental endeavors. Work reported includes: (1) Design information on NTC's NT154 Si_3N_4 used for component fabrication; (2) The completion of major developmental activities for all ancillary NT154 process operations (Powder Beneficiation, Degas, HIP, and Post-HIP Heat-Treatments); (3) Compilation and documentation of standard procedures for these operations along with the development and implementation of statistical process control methods; (4) Component fabrication development using pressure slip-casting (PSC) and injection molding (IM) for rotors and stators, respectively; (5) The completion of major efforts in NDE using microfocus x-ray radiography (MFXR); and (6) Definition, writing and submission of a quality plan.

DESIGN AND COST ANALYSIS

As part of the ATTAP SOW, NTC and GAPD agreed to a set of material specifications and goals. These are presented in Table 6. The material qualified for use within the program, NT154, is a 4% Y_2O_3-doped HIPed Si_3N_4. HIPing is accomplished using ASEA glass encapsulation techniques. During 1989, the data base for physical, thermal and mechanical properties of NT154 was extensively supplemented. Under the DOE Heat-Engines programs, samples of NT154 were supplied to GAPD under both the ATTAP and Life Prediction Program. Samples were also supplied to Oak Ridge National Laboratory (ORNL) [1], Ceramatec [2] and the University of Dayton Research Institute (UDRI) [3]. Flexural fast-fracture, tensile fast-fracture, creep-rupture, stress-rupture, and dynamic or cyclic fatigue studies have been completed by these various organizations. Typical complied physical, mechanical and thermal properties are summarized in Table 7. These data show that the material continues to exceed program specifications and meets many of the goals.

Figure 64- ATTAP Program Schedule For Norton/TRW Ceramics

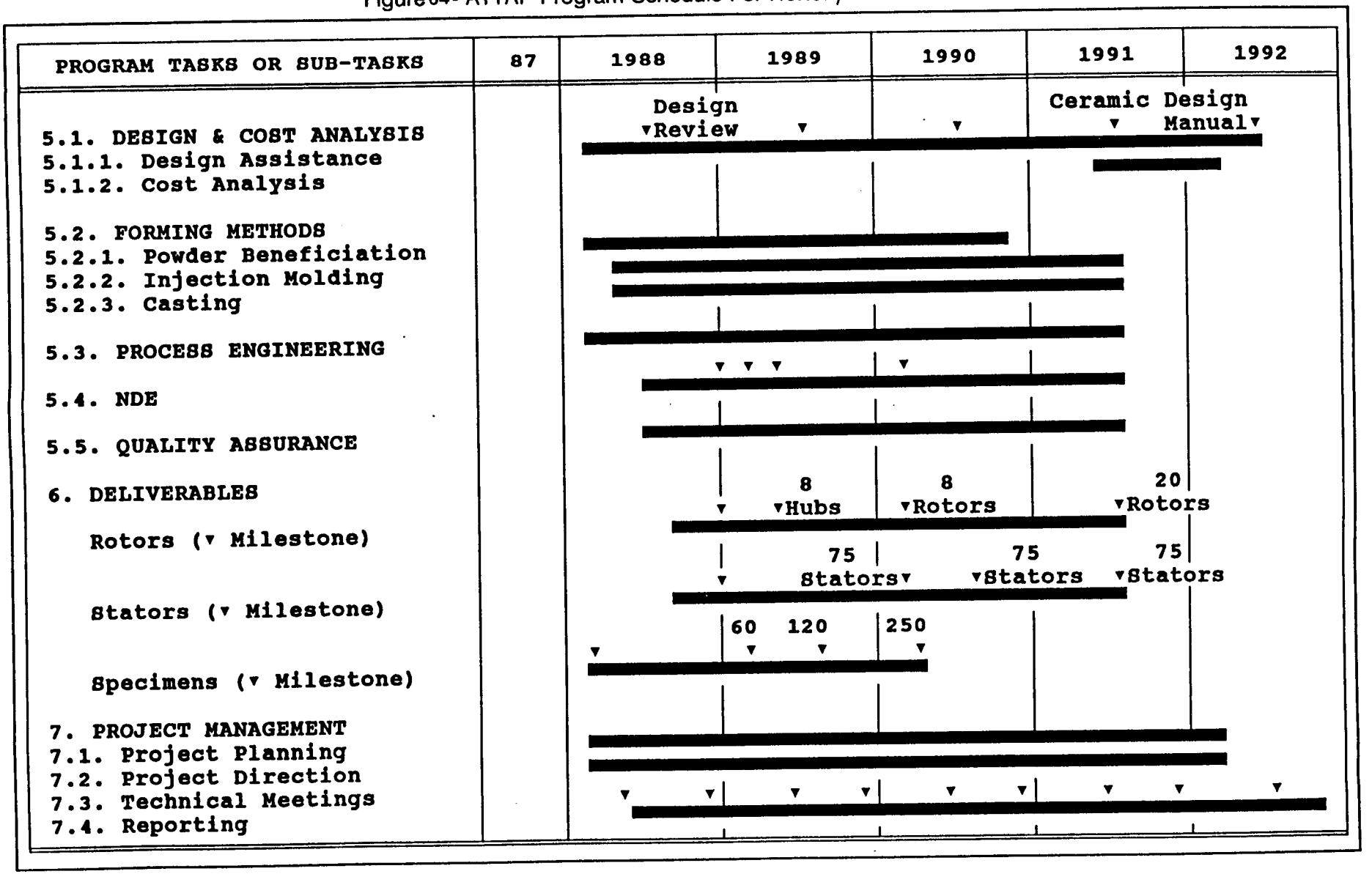

Figure 65- 1989 ATTAP Work Plan Schedule For Norton/TRW Ceramics

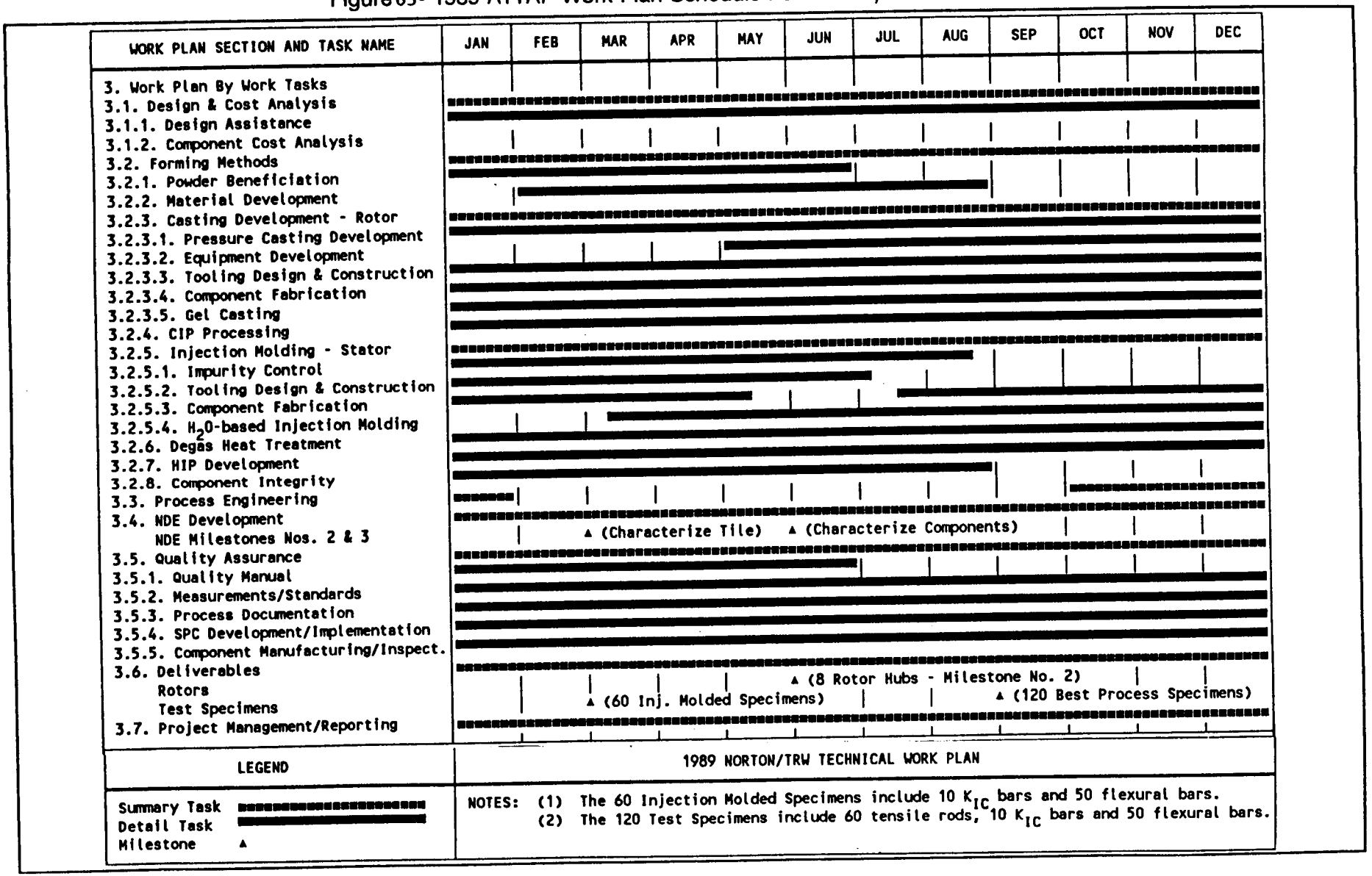

NT154 possesses excellent flexural fast-fracture behavior up to 1370°C, accompanied by an acceptable Weibull Modulus. Failure origins have been dominantly associated with surface related machining flaws and occasional minor impurities. Reported tensile strengths under fast-loading conditions parallel the flexural tests. Principal failure origins in tension have also been surface flaws. However, under slow-loading conditions, slow crack-growth and creep rupture at substantially lower stress levels have been observed. Despite this fact, the material demonstrates consistency in strength even after high-temperature exposure; and life in excess of 200 hours at 300 MPa under static flexural loading conditions.

Table 6
ATTAP Si_3N_4 Material Specifications And Goals

Measured Property	Specification	Goal
1. Density (% of Theoretical)	99.5%	99.5%
2. 22°C Flexural Strength (Mpa)	690	900
3. 1370°C Flexural Strength (Mpa)	517	690
4. Weibull Modulus	8	18
5. Fracture Toughness ($Mpa \cdot m^{1/2}$)	3.5	5
6. Flexural Stress Rupture Life (Hrs)		
1260°C - 350 Mpa	150	500
1370°C - 250 Mpa	150	500

FORMING METHODS

In accordance with the Work Plan, subtasks within the Forming Methods section include: (1) Powder Beneficiation; (2) Casting Development; (3) CIP Processing; (4) Injection Molding Development; (5) Degas Heat-Treatments; (6) HIP Development; and (7) Component Integrity Development.

A process flow chart for component fabrication is shown in Figure 66. Emphasis during the second program year was placed on powder processing, HIP densification, and post-HIP heat-treatment operations. Selection of appropriate processing parameters and control ranges for these operations were made. Using these techniques, an evaluation of component forming methods was completed. Each of the major areas in Figure 66 was linked to other areas through the forming operation. Experiments in Powder Beneficiation, Degas, HIP and Post-HIP Heat-Treatments were designed to allow interpretation of the results in light of the selected forming method. Cold isostatic pressing (CIP) was used in the program as a control. In each area, single or linked Taguchi experimental designs were implemented. Taguchi methods are advocated because of their ability to simultaneously

Table 7
Physical, Thermal and Mechanical Properties of NT154 Si_3N_4

Properties	Values
1. Density (g/cc)	3.232 ± 0.004
2. Elastic Modulus (GPa)	310 - 320
3. Shear Modulus (GPa)	126
4. Poisson's Ratio	0.273
5. Hardness (Kg/mm^2)	1620
6. Thermal Expansion Coefficient	3.93×10^{-6}/°C
7. Thermal Conductivity (W/m°K)	
(25°C)	37.6
(900°C)	20.7
(1400°C)	15.8
8. Typical 22°C Mechanical Properties	
Flexural Strength (MPa)	896 ± 55
Characteristic Strength (MPa)	917
Weibull Modulus	19
Fracture Toughness ($MPa \cdot m^{1/2}$)	4.7 - 5.5*
Tensile Strength (MPa)	900 - 920**
9. Typical 1370°C Mechanical Properties	
Flexural Strength (MPa)	579 ± 48
Characteristic Strength (MPa)	600
Weibull Modulus	11.4
Fracture Toughness (1300°C $MPa \cdot m^{1/2}$)	4.1*
Tensile Strength (MPa)	240 - 520***

* Chevron Notch or Controlled Flaw Methods.
** Includes CIP and Cast Samples, (ORNL Data).
*** Loading Rate Dependent, (ORNL Data).

achieve process robustness and reduce cost. In simple form, they are fractional factorial arrays which have advantages over traditional designs. Foremost among them is ease of use. Application and data analysis can be accomplished, in most instances, by relatively non-experts. Experiments can be designed in a global (i.e., "one-shot") or iterative manner. Because of these features, use of Taguchi methods leads to a high degree of experimental efficiency. Output includes significance, factor interaction testing, and experimental error. Response data can be plotted in the form of process maps. This is particularly effective in specifying process parameters and control limits.

Figure 66
NT154 Component Fabrication Flow Chart

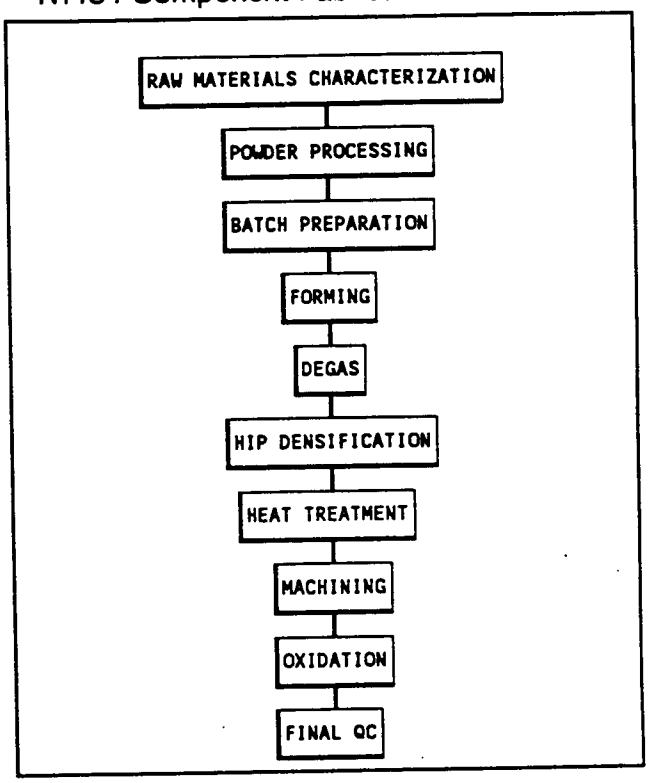

POWDER BENEFICIATION - Three experiments were planned and conducted in this area. The first two involved Taguchi arrays designed to ascertain important powder preparation variables. The third was a matched-pair experimental design used for the selection of milling equipment. The first experiment, a Taguchi L4 array, was completed during 1988 and reported previously.[4] The remaining two experiments, an L9 x L4 linked Taguchi array and the Milling Equipment Screening Test were completed during 1989.

L9 x L4 Powder Beneficiation Experiment - From the first Taguchi L4 array, several key factors were identified as significant for forming behavior and mechanical properties including: (1) Si_3N_4 Blend Source; (2) Milling Time; and (3) Forming Method. The Y_2O_3 blend source was found to not be a significant factor for any measured result. Output from this experiment was used as input to the second iterative Taguchi array--an L9 x L4 design. This experiment is presented in Figure 67. The experiment consists of an inside L9 powder beneficiation array coupled with an outside L4 HIP array. L9 factors included Si_3N_4 Blend Source, Milling Time, Solids Concentration, and the Interaction of Milling Time and Solids Concentration--each at three levels. The L4 factors were HIP Temperature, HIP Time and Cooling Rate--each at two levels. CIP and Slip-Casting were used as factors for component forming comparisons. The experiment required 72 separate trials. It represents one-sixth of a full-factorial array. An analysis of the effects of powder properties on green-forming has been compiled; and with the exception of complete stress-rupture data, physical and mechanical property results have also been acquired and analyzed. Presentation of these results, discussion and conclusions from this experiment are described in detail within the following paragraphs. The L9 portion of the experiment will be discussed first, then the L4, followed by a summary of the linked results of the two arrays and overall conclusions.

Initial results for green forming were presented in the 1988 annual report.[4] From this prior work, the Si_3N_4 blend source and milling time were found to be important in their effects

Figure 67
L9 x L4 Taguchi Powder Beneficiation Experiment

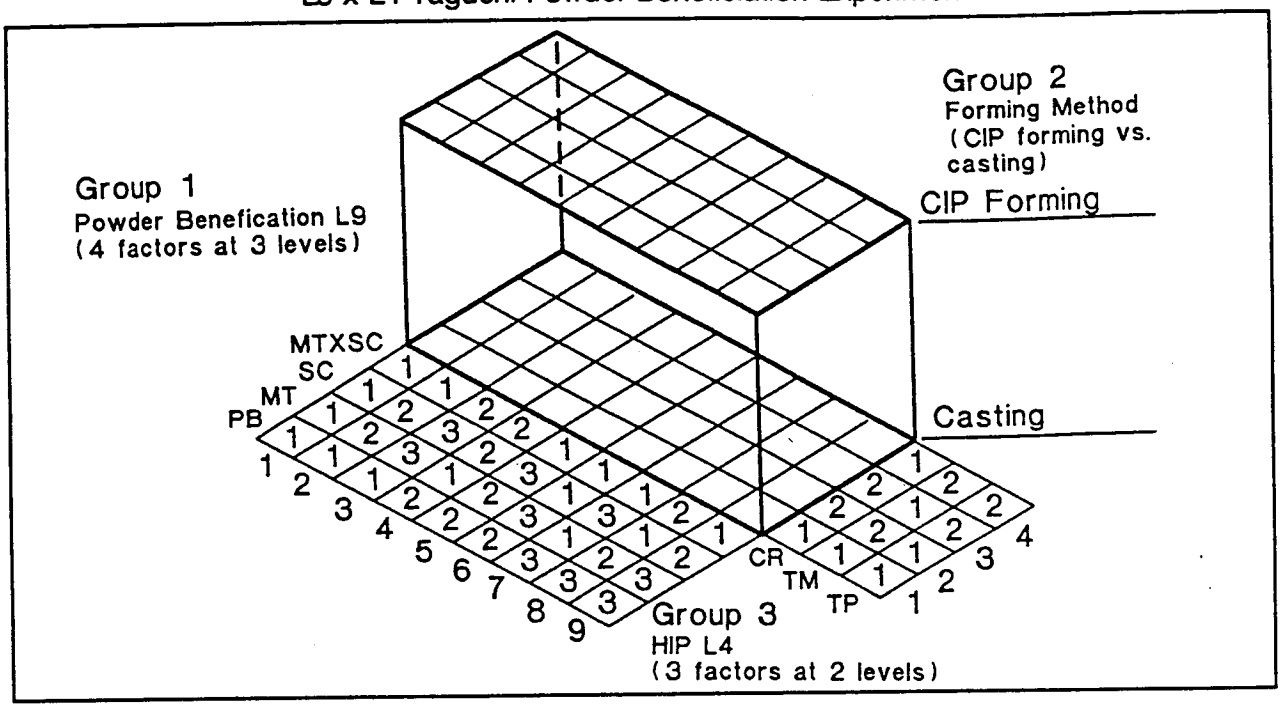

on particle size distribution, powder surface area and green density. For casting, it was noted that milling time carried more weight as a factor than did the initial blend. However, for either forming technique, green densities in excess of 1.80 g/cc (+55%) were routinely achieved. During 1989, the formability of selected powder blends was re-examined. Viscosity trials were conducted using standard formulations for both casting and injection-molding. It was found that powder blends possessing narrow size distributions and finer particles were the most difficult blends to incorporate into slips or molding mixes, respectively. Slurry or mix viscosities were ~1-5 times higher for the finest particle size blend. Conversely, acceptable viscosities were achieved using the coarse blends, or those possessing a broad distribution of particles.

Shown in Table 8 is the ANOVA for selected physical and mechanical properties from cast components for the L9 portion of the experiment. Level average data are presented in Table 9. Trends in CIP processed material were similar or identical to the casting process. Because of the complexity of the experiment, these data are representative of only one HIP condition. Of the four HIP conditions explored within the experiment, one was run at standard time, temperature and cooling rate. The remaining three were performed at alternative conditions--generally more severe than the standard. Data from the standard cycle are presented in Table 9. Overall results suggest that the

Table 8
L9 x L4 Powder Beneficiation Experiment
ANOVA For Slip-Cast Material
% Contribution

Response Variable	Blend	Mill Time	Solids Content	Blend x Mill Time	Error
Tile Density	77.71	0.0	12.47	3.32	6.50
22° C MOR	81.55	0.0	12.29	2.83	3.33
1370° C MOR	46.42	11.05	0.0	11.21	31.31
K_{IC}	55.57	0.0	19.59	0.0	24.84

Table 9
L9 x L4 Powder Beneficiation Experiment - Slip Cast NT154
Level Average Data For Selected Response Variables

Response Variable	Blend			Mill Time			Solids Content			Blend x Mill Time Interaction		
	A	B	C	Short	Avg.	Long	High	Med.	Low	1	2	3
Tile Density (g/cc)	3.223	3.219	3.211	3.217	3.218	3.218	3.220	3.219	3.215	3.220	3.217	3.217
22°C MOR (MPa)	983	923	784	895	908	887	940	859	891	912	905	872
(Ksi)	143	134	114	130	132	129	136	125	129	132	131	126
1370°C MOR (MPa)	575	513	548	534	542	580	570	542	544	-	-	-
(Ksi)	83	74	79	77	79	84	83	79	79	-	-	-
K_{IC} (MPa·m$^{1/2}$)	5.59	5.57	4.87	5.46	5.37	5.20	5.61	5.35	5.08	5.48	5.32	5.23

alternative HIP conditions were inferior to the standard schedule. Both room-temperature and 1370°C flexural strengths, as well as fracture toughness values decreased at the alternative conditions. Under standard conditions, values ranged from 786 MPa (114 Ksi) to 983 MPa (143 Ksi) for room-temperature, and 512 MPa (74 Ksi) to 580 MPa (84 Ksi) at 1370°C.

Shown in Figure 68 and Figure 69 are representative three dimensional surface plots of the effects of powder blend, milling time and solids concentration on flexural strength for cast NT154. These plots were constructed from the level average values of the L9 array. Both room-temperature and 1370°C graphs showed well-behaved surfaces. As is apparent from these figures and also the ANOVA, blend plays the major role in determining mechanical behavior. Milling time was a relatively unimportant factor for room-temperature strength, and mildly influential for 1370°C strength. Solids concentration played a role both for room and elevated-temperature strengths, but to a lesser extent than the powder blend. By specific selection of optimum conditions, values at room-temperature and 1370°C in excess of 1 GPa (145 Ksi) and 620 MPa (90 Ksi) were observed, respectively. Fracture toughness data for this

Figure 68
The Effect Of Powder Beneficiation Conditions
On Room Temperature Strength Of Cast NT154

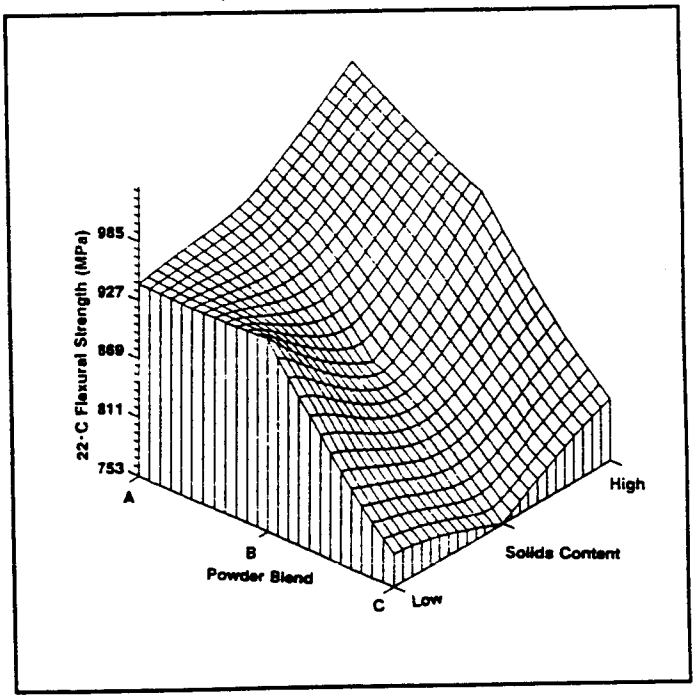

experiment were acquired using a controlled flaw method. Optimum values, (>6 MPa·m$^{1/2}$), corresponded to conditions which gave the highest strength.

Figure 69
The Effect Of Powder Beneficiation Conditions
On 1370°C Strength For Cast NT154

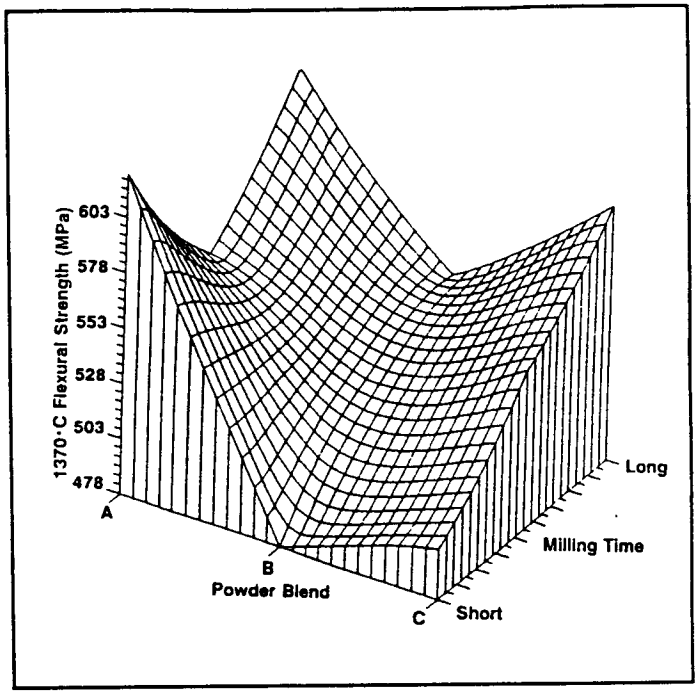

Time-dependent behavior of these materials was monitored by performing dynamic fatigue testing. Three sets of samples from each of the L9 trials were tested. Acquisition of this data was accomplished by measuring fracture strength at 1370°C under three different loading rates: 72.6 Kg/min, 7.26 Kg/min, and 0.726 Kg/min, (160 lbs/min, 16 lbs/min, and 1.6 lbs/min, respectively). For each L9 powder batch, an estimation of the slow-crack growth parameter was made. ANOVA results are presented in Table 10. The powder blend was clearly the most influential parameter determining slow crack-growth behavior in the material. Milling time may be significant, but its influence is equivalent to the error of the experiment. Solids content had no effect, and the interaction between powder blend and milling time was minimal. Level average data were utilized to generate a response surface plot of these results. Figure 70 shows slow crack growth exponents as a function of powder blend and milling time. The resistance to slow crack growth in NT154 is maximized by selection of powder blend "B" at short mill times. Powder blend "B" is of intermediate surface area, and possesses a broad size distribution of particles. In comparing these results with the 1370°C fast fracture data described earlier, conditions which led to high fast-fracture flexural strength did not necessarily provide the best time-dependent behavior. In fast-fracture, powder blend "B" gave intermediate or lower values regardless of comminution conditions. However, under time-dependent tests, just the opposite was true. The roles of powder surface area and oxygen content are key parameters affecting both high-temperature fast-fracture and time-dependent behavior. Correlation of intrinsic powder characteristics with mechanical behavior is addressed later in this section of the report.

Table 10
Powder L9 Experiment - ANOVA
For Slow Crack Growth Parameter
% Contribution

Powder Blend	51
Mill Time	20
Solids Content	0
Blend x Mill Time Interaction	9
Error	20

Analysis Is For Cast Material From Preferred HIP Conditions.

Overall, the L9 results suggest that preferred conditions for achieving an acceptable material for forming are also compatible with preferred conditions for attainment of adequate dense properties. Suggested process operations therefore include: (1) Short mixing/milling times; (2) High solids

concentration; and (3) Intermediate to broad powder blends.

Figure 70
Powder L9 Experiment - The Effect Of Powder Beneficiation Conditions On Slow-Crack Growth Behavior Of NT154 At 1370°C

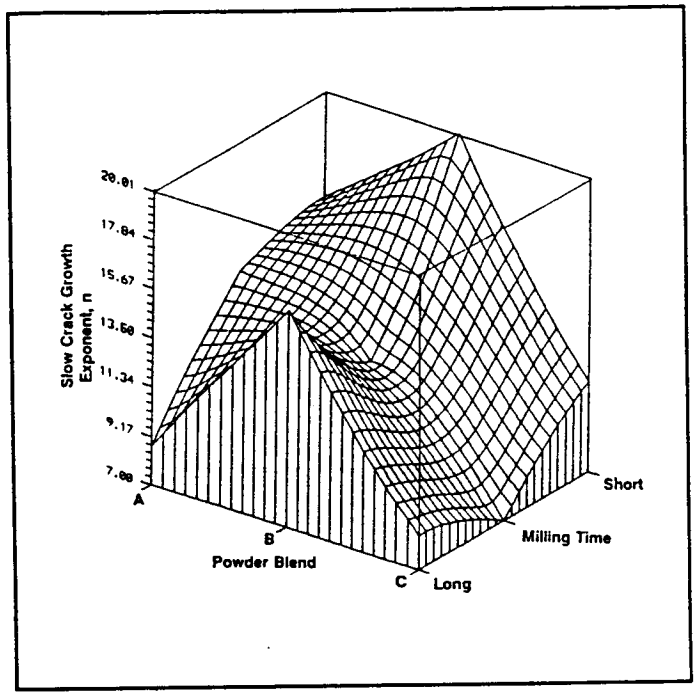

The L4 portion of the L9 x L4 experiment examined the effects of different HIP schedules on material properties. In general, the results from the L4 showed that the standard cycle was superior to any of the alternative conditions investigated. ANOVA and level average analyses for the L4 were compiled and are presented in Table 11 and Table 12. The data reveal that time, temperature, and cooling rate play various roles in determining mechanical properties. Cooling rate was shown to be highly significant, particularly for fracture toughness; whereas all three factors were important for 1370°C MOR and none were critical for 22°C strength. The large error term for room-temperature MOR data results from significant overlap of the standard deviations from the experimental trials. Failure origins for these test-bars were predominately associated with machining damage. Fracture-toughness was therefore considered to be a more critical measure of changes in room-temperature mechanical properties. Fracture toughness values ranged from ~5 MPa·m$^{1/2}$ to over 6 MPa·m$^{1/2}$ for the conditions studied within the experiment. Level average data revealed that lower HIP soak temperatures, shorter soak times, and faster cooling rates were preferred.

To amplify on the observed effect of HIP conditions on mechanical properties, several supplemental HIP schedules were added to the original L4 design. Because of the observation that time (i.e., soak time plus cooling rate) appeared to play the dominant role in mechanical property determination, shorter HIP times were investigated to determine if further improvements could be realized. Several alternative firing conditions were selected, and trials conducted. The original powders from the L9 array were utilized in these tests. Results of this work are presented in Table 13. From the data, it can be noted that for selected powder lots, both room-temperature and 1370°C flexural strengths were significantly increased by the use of shorter HIP times. Blends "A" and "B", which are comprised of moderate to high surface area powders and narrow to intermediate particle size distributions adequately densified during these tests. However, blend "C", which is comprised of primarily coarse powders did not densify to an acceptable level. For blends "A" and "B", room temperature flexural strengths in excess of program goals were achieved. Values >

Table 11
ANOVA For HIP L4 Experiment
% Contribution

Response Variable	Temperature	Time	Cooling Rate	Error
K_{IC}	0	3	73	24
22°C MOR	10	0	13	76
1370°C MOR	42	16	42	0

1GPa and 600 MPa for 22°C and 1370°C, respectively, were observed. Note that fracture toughness also increased. Values up to 6.5 MPa·$m^{1/2}$ were attained for powder blend "A". The results suggest that grain refinement, as well as aspect ratio modifications are quite sensitive to HIP conditions--particularly HIP time and cooling rate.

Table 12
Level Average Values For The HIP L4 Experiment

Response Variable	Temperature Low	Temperature High	Time Short	Time Long	Cooling Rate Fast	Cooling Rate Slow
K_{IC} (MPa·$m^{1/2}$)*	5.86	5.63	5.61	5.88	6.12	5.37
22°C MOR (MPa)	932	814	918	821	932	807
(Ksi)	135	118	133	119	135	117
1370°C MOR (MPa)	566	476	552	490	545	497
(Ksi)	82	69	80	71	79	72

* Controlled Flaw Technique.

From all conditions studied within the L9 x L4 array, response surface maps were generated to correlate selected important powder variables--particularly powder surface area and oxygen content--with HIP schedules. These correlations are presented in Figures 71 through 74. In Figure 71 controlled flaw toughness at room-temperature is plotted against HIP time and powder surface area. The response surface shows generally well behaved features for intermediate or long HIP times and moderate to high surface area powders. For both short HIP times and low surface area materials, significant drops in K_{IC} were observed, primarily attributable to inadequate densification. The largest values were obtained using high surface area powders of narrow size distribution, HIPed at relatively short times. A ~40% improvement in toughness was observed for this condition over coarser powder blends HIPed at longer times. Results for 22°C and 1370°C flexural strengths are given in Figure 72 and Figure 73, respectively. As expected, both these response variables paralleled the observed K_{IC} data. Use of short HIP times, along with fine powders, possessing high surface area and narrow size distributions pushed flexural strengths to >1 GPa (>145 Ksi) and >700 MPa (~102 Ksi) for room-temperature and 1370°C test conditions.

Time-dependent high-temperature behavior is shown in Figure 74. In this graph, material oxygen content for the nine powder batches is plotted against the slow-crack growth exponent. These data clearly demonstrate that high oxygen containing materials resulted in poorer durability. Those powder batches which contained high oxygen contents were generally derived from narrow size distribution high-surface area blends, or from extensively milled batches. For optimum values in slow-crack growth, low to intermediate surface area powders of a broad size distribution are preferred, despite the fact that such materials give lower fast fracture strengths. This result presents an interesting engineering paradox. Selected conditions which favor

Table 13
Powder L9 x HIP L4 Physical And Mechanical Properties For Lots HIPed At A Shorter Time

Powder Blend	Tile Density (g/cc)	Test Bar Density (g/cc)	22°C K_{IC} (MPa·$m^{1/2}$)	22°C Flexural Strength (MPa)	22°C Flexural Strength (Ksi)	1370°C Flexural Strength (MPa)	1370°C Flexural Strength (Ksi)
Powder Blend A:							
Slip Cast Material	3.225	3.228	6.3	1089	158	648	94
CIP Material	3.227	3.230	6.5	1089	158	641	93
Powder Blend B:							
Slip Cast Material	3.220	3.226	5.9	1034	150	641	93
CIP Material	3.220	3.230	5.8	938	136	607	88
Powder Blend C:	Material did not densify to acceptable levels.						

fast fracture strength do not coincide with optimum conditions for time-dependent strength. As a compromise, an intermediate set of powder processing and HIP conditions was therefore selected.

With the completion of this experiment, and the acquisition of an extensive data base on powders and HIP operations, a broader understanding of the roles for specific process variables was achieved. Conclusions from this experiment are as follows:

- An acceptable powder blend was identified. The blend possesses a broad particle size distribution and intermediate surface area. Because of these characteristics, the powder exhibits acceptable forming behavior. When densified at preferred conditions, excellent fast fracture and high-temperature durability are achieved. The selected blend represents a compromise between fast-fracture strengths and slow crack growth behavior. Ultra-high fast fracture strengths were sacrificed in favor of improved high-temperature time-dependent properties.

- Comminution conditions have been finalized and selected. Preferred operations include short milling time and high-solids contents. From earlier screening studies [4], it was learned that the Y_2O_3 blend source was non-critical. With the selection of the appropriate Si_3N_4 blend, the L9 x L4 results confirm that the principal purpose of the comminution operation is mixing.

- An appropriate HIP schedule was defined and selected. An intermediate temperature and time condition coupled with a rapid cooling rate are preferred. Selected conditions maximize density, fracture toughness and strength.

Figure 71
Powder Beneficiation L9 x L4 Experiment
22°C Controlled Flaw Toughness

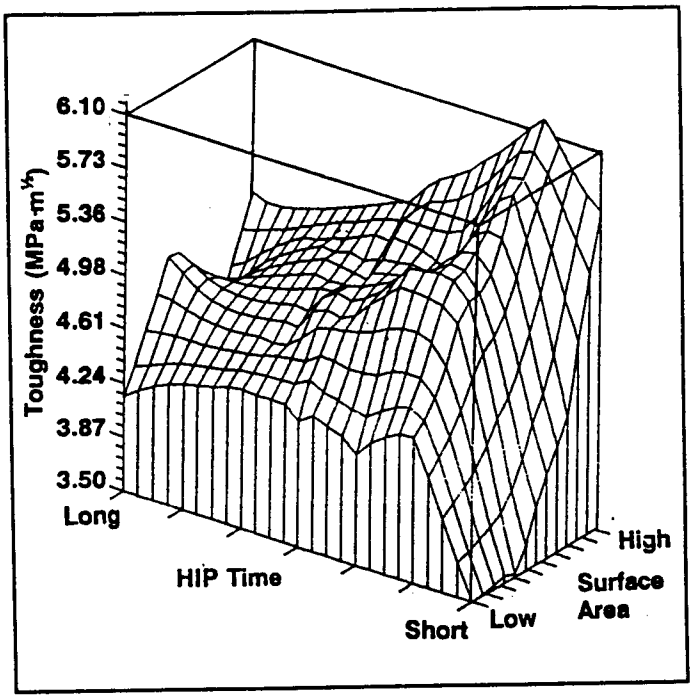

Figure 72
Powder Beneficiation L9 x L4 Experiment
Room Temperature Flexural Strength

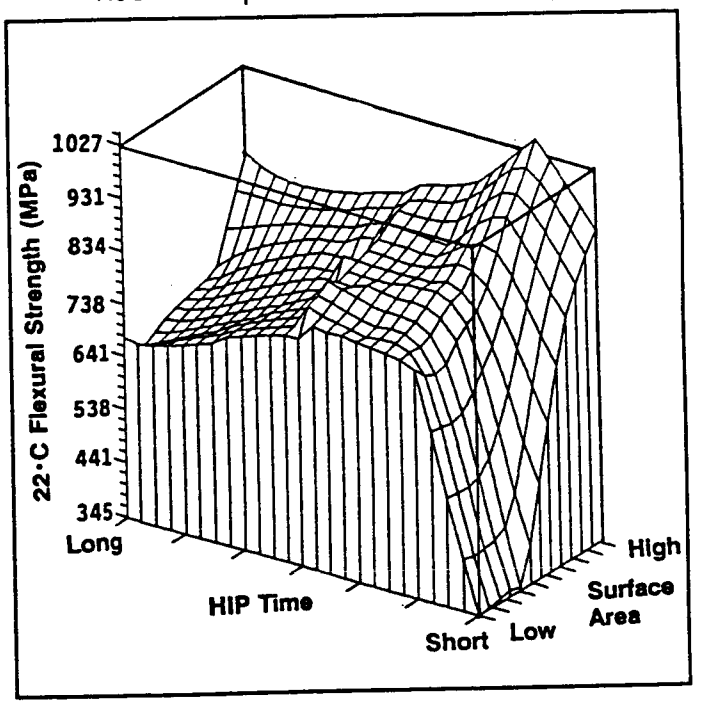

- Based on the response surface plots from the experiment, as well as on-going SPC, specifications and appropriate control ranges for powders (i.e., particle size, surface area, oxygen content and impurities) and HIP conditions (time, temperature and cooling rate) have been defined.

At the close of 1989, all preferred conditions from the experiment were incorporated into the standard NT154 process. Work continues to be conducted within clean room environments using high purity materials and equipment. SPC monitoring of these process operations, initiated at the beginning of the ATTAP will now oversee process conformance. Should process control problems arise, results from this Taguchi experiment will serve as a guide in fine-tuning the operations and in maintaining a high level of product quality.

Figure 73
Powder Beneficiation L9 x L4 Experiment
1370°C Flexural Strength

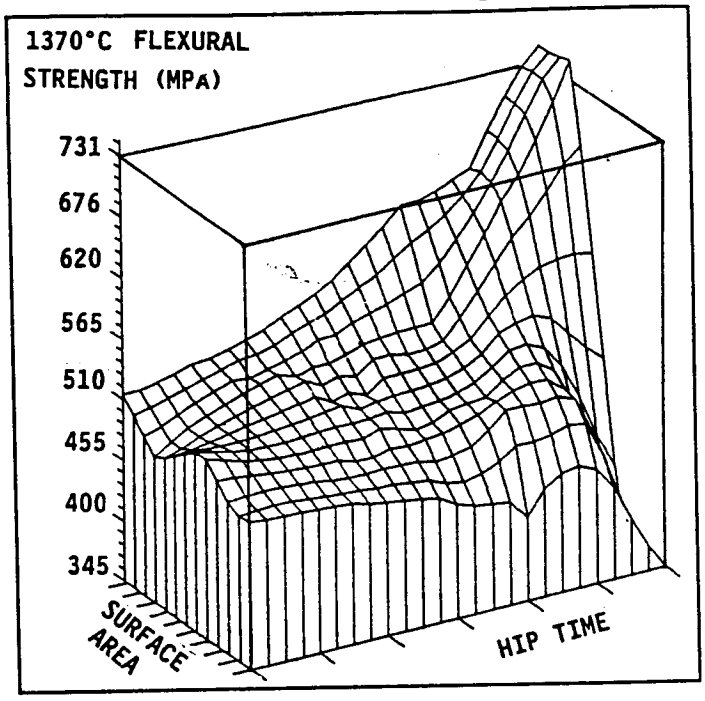

Milling Equipment Selection - The matched-pair milling equipment experiment involved a comparison of ball and vibratory comminution operations. The purpose of this experiment was to: (1) Examine alternative comminution equipment; (2) Scale the milling process from batches of ≤ to 15+ Kgs; and (3) Evaluate and select one process for powder production. The experiment was initiated in 1988 and completed early in 1989. Powder was prepared from both processes at scaled-up batch quantities of between 15 and 25 Kgs. Tile components were formed and densified from CIP, Injection Molding and Casting techniques. Mechanical property results are presented in

Figure 74
Powder Beneficiation L9 x L4 Experiment
Slow-Crack Growth Behavior at 1370°C

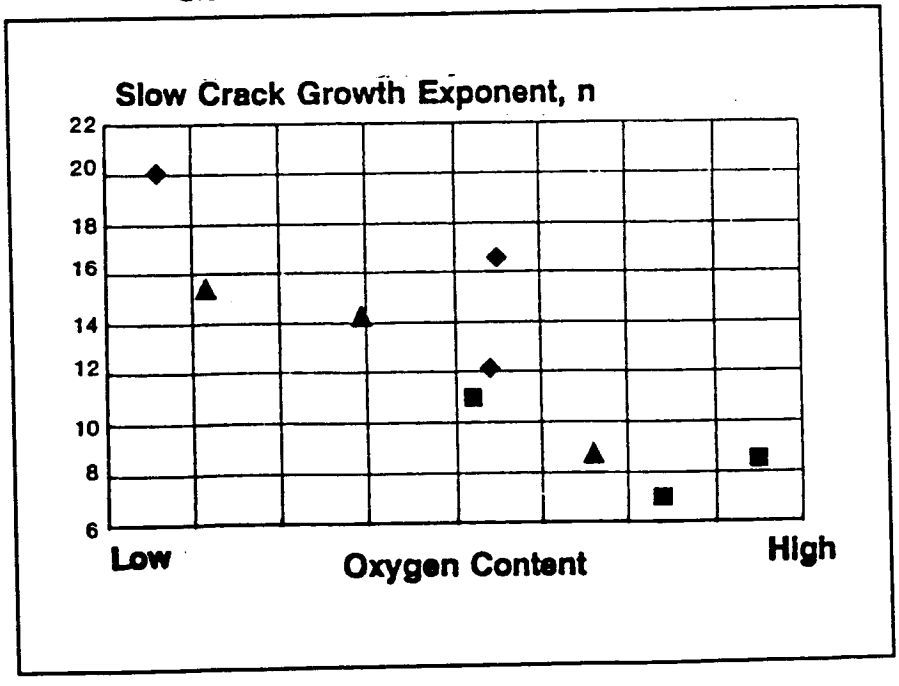

Table 14. Overall the two processes produced material of acceptable properties. HEX ball-milled materials generally provided superior properties at room-temperature. The one exception to this was the injection molding process, which showed equivalent strength and slightly higher average fracture toughness. At high-temperatures, the SWECO material showed improved properties. While conducting the trials with the vibratory grinding equipment, numerous problems were encountered associated with mixing and recirculation of the powder slurry. Settling occurred and stable equipment operation was difficult to achieve. Furthermore, the vibratory grinding operations yielded narrow-size distribution powders. Conversely, the ball milling operation prevented settling, provided intensive mixing concurrent with comminution and gave a broader size distribution of particles. Ball mills are simple devices of high reliability. Based on these qualitative processing factors and the overall equivalency of properties, the decision was made to exclusively utilize ball milling equipment for powder production. SWECO milling appears viable as a potential scale-up process, but further studies and equipment optimization are required.

Table 14
Milling Equipment Selection Experiment
Mechanical Property Results For CIP,
Slip-Cast and Injection Molded Components

Process and Properties		CIP	Slip-Cast	Injection Molding
I. SWECO Mill				
22°C MOR	(MPa)	726 ± 66	704 ± 97	803 ± 131
	(Ksi)	105 ± 63	102 ± 14	116 ± 19
Weibull Modulus		10.6	7.2	6.1
K_{IC} ($MPa \cdot m^{1/2}$)		4.1 ± 0.2	4.3 ± 0.7	5.6 ± 0.2
1370°C MOR	(MPa)	621	559	559
	(Ksi)	90	81	81
II. HEX Mill				
22°C MOR	(MPa)	851 ± 36	837 ± 93	830 ± 72
	(Ksi)	124 ± 5	121 ± 14	120 ± 11
Weibull Modulus		26.38	8.83	12.18
K_{IC} ($MPa \cdot m^{1/2}$)		5.5 ± 0.2	5.7 ± 0.2	5.3 ± 0.1
1370°C MOR	(MPa)	614	600	587
	(Ksi)	89	87	55

MOR and Weibull data are compiled from 30 samples.
K_{IC} values are representative of 5 individual tests each.

CASTING DEVELOPMENT - Casting was selected as the preferred method for forming the rotor. It is a proven process for complex shape fabrication. It requires minimal amounts of organic additives and therefore eliminates binder burn-out problems. During 1989, efforts in this area were directed at: (1) Slip-System Development; (2) Equipment Development; (3) Tooling Design and Construction; and (4) Component Fabrication.

Slip System Development - During 1989, casting experiments within the ATTAP concentrated on basic slip-preparation methods, additives and casting procedures using plaster molds. Limited Taguchi studies were conducted which examined the effects of slip composition and additives on casting rheology and component properties. Difficulties encountered during this work included impurities in critical casting additives and inconsistent cracking of rotor components--both hub and blade sections.

Prior to 1989, NTC identified a unique casting additive which improved our ability to form components. Several vendors for this additive were located and development work using their materials was initiated. Lots of this additive were characterized for their ability to form components and achieve adequate physical and mechanical properties. The additive proved to be very effective in component forming. A number of fully bladed AGT100* rotors were prepared and densified. However, during the course of this investigatory work, it was discovered that this

*A rotor master of Allison's AGT100 design was available and was used for initial development.

additive was toxic and carcinogenic. It was also learned that the preferred materials possessed undesirable levels of impurities--particularly iron and aluminum. According to the vendors, these impurities are either required in production of the additive, or result from wear from processing equipment. Handling safety and component mechanical properties were identified as two areas of major concern. To minimize handling exposure, NTC acquired specific safety equipment and implemented necessary procedures. Concurrently, chemical laundering of the additive was performed and an assessment of mechanical properties for NT154 containing the additive was made. A summary of flexural strengths for two preferred vendors of this additive is presented in Table15. Lots from both vendors (Lot Nos. 1-1, 1-2, 2-1 and 2-2) were investigated and developed during 1988. As shown in the Table, flexural strengths for these lots were both low and variable. Of particular concern were the poor high-temperature strengths. Iron was confirmed as a principal impurity at failure origins. Due to the inconsistency of these materials, NTC personnel visited Vendor No. 2 and negotiated a supply and quality improvement agreement. The agreement required refinement of both the functionality and purity of the additive. Lots of the improved additive were received during 1989, characterized and incorporated into casting batches. Mechanical property results from the improved additive are also shown in Table 15 as Lot No. 2-3 of Vendor No. 2. Impurities for this lot were well within acceptable tolerance. Significant advancements in strength were realized. In fact, strength levels were indistinguishable from baseline materials which did not contain the additive. However, despite these achievements the improved additive was not as effective as its lower purity predecessors in component forming. By removing impurities from the process used to produce the additive, the functional features which led to enhanced green strength were diminished. As a result, the additive did not provide the same level of green strength. Consequently, occasional hub and blade cracking during both casting or drying were observed. Screening experiments were conducted to adjust the slip-system and casting techniques in an effort to compensate for the lower inherent strength of the new additive. Modifications to the slip composition, mold designs, and casting procedures eliminated crack formation in hub sections; but blade cracking persisted. This additive and system were utilized to fabricate and deliver rotor hubs to GAPD in accordance with program milestones; but because of safety issues and blade-cracking problems, further work using this additive has been curtailed.

Table 15
Mechanical Properties Of NT154 Cast Tile Using Alternative Casting Additives

Source And % Of Additive	Additive Lot No.	Room Temperature MOR (MPa)	Room Temperature MOR (Ksi)	1370°C MOR (MPa)	1370°C MOR (Ksi)
Vendor No. 1					
% A	1-1	906 ± 125	131 ± 18	NA	NA
% B	1-2	794 ± 93	115 ± 14	487 ± 28	71 ± 4
% A	1-2	824 ± 88	120 ± 13	498 ± 13	72 ± 2
Vendor No. 2					
% C	2-1	835 ± 70	121 ± 10	518 ± 34	75 ± 5
% D	2-2	700 ± 54	102 ± 8	445 ± 16	64 ± 2
% B	2-2	724 ± 31	105 ± 4	447 ± 23	65 ± 3
Vendor No. 2 (New Material)					
%E	2-3	835 ± 86	122 ± 12	605 ± 11	88 ± 2
%A	2-3	894 ± 89	130 ± 13	684 ± 25	99 ± 4

All room temperature strength values are an average of 6-15 data points.
All high temperature strength values are an average of 5-7 data points.

Additional alternative binders and additives were explored in numerous screening experiments in an attempt to qualify a new system. From these tests, conducted over the course of the year, several classes of binders were identified as providing enhancements in green strength. Materials included both conventional organic binders and non-

conventional inorganic or mixed systems. Conventional binders were shown to be of value in improving the green strength of dried ware; but were incapable of preventing cracking during the drying operation itself. The non-conventional systems showed mixed success in controlling crack formation both in the "wet" and "dry" states; but issues surrounding the purity, morphology and chemical make-up of the non-conventional binders forced their early dismissal from the program. It was concluded that conventional binders may play a role in improving component forming, but additional experimental trials using a companion technology would be required in connection with their application.

Green cracking of cast components results from stresses which develop in the part during the drying process. Typically, this problem can be overcome with the use of highly controlled drying cycles in humidity ovens. However, this method requires drying cycles spanning up to several weeks for large cross-section components. The process is therefore costly and undesirable for mass-production. Despite this fact, a number of screening trials were conducted using an available humidity-controlled drying chamber and cast rotor hubs or tensile rod blanks. Component cracking was observed in all instances despite extreme care in environmental control. Gravimetric analyses were conducted to determine the water loss at which cracks formed. Cracks were observed to initiate at all stages of the weight loss cycle.

Table 16
Powder Treatment L8 Experiment Design

Process Variable	Level 1	Level 2
Treatment 1	on	off
Treatment 2	on	off
Treatment 3	1	2
Treatment 4	1	2
Slip Prep.	Mill	Blunge
Dispersant	1	2
Slip Solids	Low	High

Cracking during drying isn't as severe a problem with other ceramic materials, (i.e., whitewares and refractories) primarily because of the coarser nature of the particles generally used in these operations. Difficulties in forming are exacerbated with fine particles, particularly when the distribution approaches sub-micron levels. One concept developed during the year to overcome this problem was to modify the surface features and effective size distribution of the Si_3N_4 in order to mimic coarser distributions while retaining the requisite intrinsic powder characteristics needed for densification and mechanical strength. To test this concept, screening trials were conducted using both chemical and thermal techniques in an effort to modify the surface character of NT154 powders. These tests indicated that modified powders could potentially be successfully cast into thick cross-section components without cracking. Once this discovery was made, the effectiveness of various powder treatment methods was examined under a Taguchi experimental array. A Powder Treatment L8 Experiment was designed to clarify the effects of several powder treatment variables on drying behavior. A summary of the design is presented in Table 16. Various response variables monitored for this experiment included powder properties (particle size distribution, chemistry, surface area), slip behavior (viscosity, pH, specific gravity) and component characteristics (cast density, incidence of drying cracking). Components which showed acceptable drying behavior were carried through to the acquisition of mechanical property data. Primary efforts focused on casting of tensile rod blanks. Prior experience indicated that cracking found in tensile rods was similar to that observed in rotors. The experiment was initiated and completed during the year. An ANOVA for selected response variables is presented in Table 17. The results show that the slip preparation technique (i.e., blunge vs. mill) had the most pronounced effect on cracking. Two

other treatments (i.e., Nos. 1 and 4) also affected cracking, but were of lower significance. These same three treatment factors also influenced powder characteristics, slip behavior and green density. Collectively, the combination of these factors resulted in a modified effective particle size distribution and slip rheology. As a consequence, cracking was minimized. However, in no instance were totally crack free components obtained. Nevertheless, to amplify on these results, selected conditions were subjected to additional screening tests to determine if further improvements were possible. These screening tests included an examination of pH, conventional binders and additives, and solids loading. To expedite a pertinent evaluation of these tests, casting trials were conducted using a turbine blade component incorporating both a thick-base and thin-blade features. The selection of the turbine blade as the evaluation component was based on the fact that casting could be conducted rapidly, while the cross-sectional thickness variations could provide an assessment of cracking behavior in both thick and thin sections and feature control.

Table 17
ANOVA For Powder Treatment L8 Experiment
(% Contribution)

Response Variables	Treatment Factors 1	2	3	4	Blunge /Mill	Disper. Type	Solids Level	Error
Cracking	13.5	-	-	13.5	59.6	-	-	13.5
Effective Size Distribution	61.5	7.0	15.7	0.9	-	13.7	1.1	0.2
Surface Area	-	1.5	8.5	73.1	0.1	1.2	0.6	15.0
pH	-	0.9	18.0	0.1	7.1	64.6	9.0	0.3
Viscosity	31.1	23.0	0.1	-	29.1	9.7	6.3	0.6
Specific Gravity	-	9.5	44.5	33.4	1.6	4.8	4.8	1.4
Green Density	25.1	6.9	1.1	8.4	58.4	-	0.1	0.0

pH - Since pH was not a treatment factor within the L8 design, the first screening experiment was aimed at identifying the pH sensitivity of the preferred system. Ammonium-hydroxide (NH_4OH) was utilized to modify the pH while keeping all other factors constant. Response variables included pH, viscosity and green density. Results are presented in Table 18. A minimum in viscosity was observed at a pH of approximately 8.5, corresponding to a NH_4OH level at "C". At this pH condition, excellent green densities for components were achieved.

Binders and Additives - The second screening test re-examined the effects of pre-selected binders in connection with these modified powders and the range of pH conditions studied within the first screening test. For one particular binder at 1% concentration, viscosity and green density results are shown in Table 19. This particular binder did not have a pronounced effect on viscosity; but in general, green density values were lower than observed for compositions without the binder. The experiment was repeated with a second binder, but the viscosity levels for the second system were found to be too high. Components were cast from compositions both with and without binders. Quali-

Table 18
pH Screening Experiment - Effect Of pH
On Slip-Viscosity And Green Density

Slip Batch No.	% NH_4OH	pH	Viscosity (cps)	Green Density (g/cc)
308	A	8.05	61	2.05
309	B	8.14	54	2.06
310	C	8.46	35	2.06
311	D	9.43	124	2.00

tative results indicated that compositions containing binders were more prone to cracking. An additional screening test was conducted using a selected humectant as the additive. Results for this test are shown in Table 20. At high levels of the additive, high green densities were achieved in-spite of the higher viscosities observed for these slips. During casting trials, it was also noted that the presence of this humectant tended to make the slip "non-wetting" to plastics and metals. Because of this feature, cast components from these compositions were split from the molds with no gross surface flaws.

Table 19
Binder Screening Experiment - Effect Of pH On Slip Viscosity And Green Density

Slip Batch No.	% NH_4OH	pH	Viscosity (cps)	Green Density (g/cc)
312	A	9.05	56	2.02
313	B	8.80	47	2.01
314	C	8.85	49	2.01
315	D	9.97	80	2.00

Solids Loading - This screening test examined the effect of loading dilatancy on slip properties, cast density, and incidence of cracking. Results are presented in Table 21. For this test, significant improvements in cracking behavior were noted at higher solids loadings.

From the screening tests and the Powder Treatment L8 experiment, preferred slip-composition conditions were identified. They include: (1) High solids loading; (2) pH adjustments with NH_4OH to achieve minimum viscosity; (3) Elimination of binders; and (4) Utilization of a humectant. Casting trials conducted using preferred conditions resulted in crack-free turbine blade components. Extension of these preferred conditions for stators, tensile rods, and fully bladed-rotors is now part of NTC's 1990 Work Plan.

Table 20
Humectant Screening Experiment - Effect Of Humectant Content On Slip Properties and Green Density

Slip Batch No.	% NH_4OH	% Humectant	pH	Viscosity (cps)	Green Density (g/cc)
328	C	W	8.10	97	2.02
329	C	X	8.12	106	2.02
330	C	Y	8.01	109	2.04
331	C	Z	7.79	172	2.04

In addition to these efforts, NTC also examined gel-casting as a method for overcoming component cracking. Investigatory screening experiments were completed in two alternative gel casting systems: (1) Chemical cross-linking gels (ORNL Technology) [5]; and (2) Temperature activated gels.[6,7,8*] From this work it was concluded that chemical cross-linked gels are not viable for forming at this time. Solids loading for these systems is low--resulting in high drying and densification shrinkage. Some of the systems have significant health and environmental risks associated with their use. They require materials that are neurological toxins; or they need explosion proof process machinery and specialized air handling equipment unavailable in NTC's current facilities. Extensive development work is also required to optimize any one of these systems. As a result, it was decided to discontinue further work on chemically

* An Allied-Signal water-based injection molding technology was examined as part of the ATTAP. However, due to problems in license negotiations with Allied-Signal, work on the system using injection molding was dropped from the program. (Refer to the Injection Molding Development section of this report.)

cross-linked gel systems.

Table 21
Solids Loading Screening Experiment
Effect Of Solids Content On Slip Properties, Green Density, And Cracking Behavior

Slip Batch No.	% NH_4OH	% Solids	pH	Viscosity (cps)	Specific Gravity (g/cc)	Green Density (g/cc)	Degree Of Cracking
324	C	S	9.29	62	2.08	2.11	Cracked
325	C	T	8.82	76	2.12	2.03	Good
326	C	U	8.86	80	2.14	2.02	Good
327	C	V	8.82	159	2.20	1.98	Good

Temperature-activated gels were initially investigated as part of NTC's injection molding effort for the stator.* Work in this area indicated that similar gel-forming materials might be useful in the pressure casting process as well. In this sense, these gel-formers serve to enhance the "wet-strength" of the cast component. Several gel-forming additives were identified and screening trials initiated to examine their effectiveness. One system was found to provide sufficient wet-strength for casting rotor-hubs, tensile rod blanks and stators to prevent cracking. Further development using this particular additive in connection with modified size distribution powders is planned as part of NTC's 1990 effort.

Equipment Development - As part of NTC's commitment to pressure casting development, a commercially available automated pressure casting machine* was ordered during 1988, received, installed and commissioned during 1989. As part of the procurement of this equipment, NTC received porous plastic mold technology from the vendor. Using this information, an AGT101 rotor-hub mold was designed fabricated and installed on the equipment, and casting trials conducted. Due to machine design features, component casting times were short at casting pressures below full machine capability. Consequently, fully cast hubs were not achieved. Component cracking was also observed; and was assessed to be consistent with the behavior seen in laboratory trials. However, using the plastic mold, good form and feature definition were maintained. Minor machine modifications were required including: (1) Modification of the microprocessor-based program to allow greater flexibility in the selection, range and application of casting parameters; and (2) Alternations to the hydraulic system to allow for higher pressures on small molds. By year-end, these two issues had been resolved, but other minor problems with the microprocess programmer were encountered which forced additional delays in overall utilization and development of the equipment. These particular problems are expected to be corrected early in 1990. By the end of 1990, component forming is expected to transition to the automated equipment.

Tooling Design and Construction - Under the original 1989 Work Plan, NTC was to select tooling vendors and procure the necessary patterns, tools and fixtures to fabricate AGT101 rotor and stator components for engine testing at GAPD. However, during the year GAPD announced a change in the engine design from a radial to mixed-flow concept. As a result of this change, tooling procurement was delayed pending receipt of approved new turbine designs and drawings. As a consequence of this decision, work during 1989 focused on the utilization of available tools and fixtures for component development activities. Plaster or porous plastic molds were fabricated and utilized for a number of components including: (1) AGT101 rotor

* DG-60U, Dorst/Laufen Systems, Kochel A. See, Germany.

hubs; (2) AGT101 stators; (3) AGT100 rotors; (4) Tensile rods; (5) Tile and test-bar molds; and (6) Specialty molds to test warpage and shrinkage.

Table 22
Mechanical Properties For Co-Processed Tile With AGT101 Rotor Hubs

Mechanical Property	22°C	1370°C
Flexural Strength		
(MPa)	842 ± 69	555 ± 29
(Ksi)	122 ± 10	81 ± 4
Weibull Modulus:	18.5 ± 0.3	23.8 ± 0.4
No. of Samples	36	21

Component Fabrication - Effort in this area utilized process optimization work and tooling development to fabricate rotor hubs and stator components. During the year, nine rotor hubs were fabricated and delivered to GAPD for assessment in fulfillment of Rotor Milestone 3 of the SOW. Specimen property data from co-processed tile and cut-up rotors were also generated by NTC. Results are presented in Table 22 through Table 24. Production of these components occurred using two separate powder lots, five casting runs and two HIP runs. The observed variability is therefore expected to be representative of the current process. Strengths and Weibull moduli for these components exceeded program specifications and attained many of the overall property goals. The data for test bars cut from hubs are equivalent or superior to tile data, and are among the best values observed to date for this material.

During 1989, pressure slip-casting of stators in plaster molds was initiated due to recurrent impurity problems in injection molding. A pattern and case mold for this component were fabricated, from which a successful four segment plaster mold design was developed. Approximately 35 molds were prepared for trial castings. Using this design, initial trials resulted in defective cast components due to either cracking on de-molding or drying, or air entrapment. Correction of these problems was accomplished. Cracking on de-molding was alleviated by changes in de-molding protocols. A series of screening tests were then conducted to assess and eliminate the other problems. These tests consisted of the use of different fill pressures or rates, and different casting pressures. Selected conditions produced stator components free from gross defects. Using the conditions identified in the screening tests, 12 acceptable quality stators were cast. Five were sectioned for green density and variation. The remaining seven were degassed and HIPed. Density values and variations are shown in Table 25. Variations, both within each component and between components, are acceptably low. Components were successfully HIPed, and evaluated for defects, density, shrinkage and warpage. The results demonstrated that pressure slip-casting is a viable alternative for producing stators. For 1990, work in stator fabrication is being integrated with rotor developmental activities. Both components will be fabricated using pressure slip-casting techniques.

Table 23
AGT101 Rotor Hubs - Summary Of NT154 Mechanical Properties

Temperature (°C)	Fracture Toughness ($MPa \cdot m^{1/2}$)	Flexural Strength (MPa)	Flexural Strength (Ksi)	Weibull Modulus	No. of Samples
22	5.43 ± 0.09*	925 ± 70	134 ± 10	15.4 ± 0.4	30
1093	-	707 ± 50	101 ± 7	-	5
1204	5.06 ± 0.35*	683 ± 29	99 ± 4	-	5
1260	-	752 ± 42	109 ± 6	-	5
1316	-	693 ± 38	101 ± 6	-	5
1370	-	599 ± 28	87 ± 4	-	5

* Fracture Toughness by Chevron Notch Technique. No. of Samples = 3 at each temperature.

CIP PROCESSING - Work in this area was performed in conjunc-

Table 24
Stress Rupture Tests - AGT101 Rotor Hub Deliverables
Samples Cut From Rotor Hubs

Bar I.D. No.	1204°C 350 MPa	1204°C 400 MPa	1260°C 350 MPa	1260°C 400 MPa	1316°C 200 MPa	1316°C 250 MPa	1370°C 200 MPa	1370°C 250 MPa
2B4-57	161+							
2B4-56	161+							
2B4-58	161+							
2B4-59*		152+						
2B4-63		173+						
2B4-60			160+					
2B4-61			160+					
2B4-62			160+					
2B4-65				159+				
2B4-69				159+				
2B4-66					159+			
2B4-67**					—			
2A4-68					163+			
2A4-72						152+		
2A4-73						159+		
2A4-69							160+	
2A4-70							160+	
2A4-71							150+	
2A4-74								162+
2A4-79								162+

* Total test time of 152 hrs broken down as follows: 46.2 hrs @ 350 MPa/1204°C; 105.8 hrs @400 MPa/1204°C.
** Test aborted @ 123.1 hrs due to an equipment problem.

tion with other experiments to provide a baseline comparison for the component forming processes.

INJECTION MOLDING DEVELOPMENT - At the beginning of the ATTAP, injection molding was selected as the stator fabrication process. It was reasoned that this forming method was applicable to intricately shaped components of thin cross-section. For parts similar to that of the stator (i.e., ≤ 8 mm cross-section) binder removal was considered to be a less serious problem. During 1988, two iterative Taguchi experiments were initiated. The first experiment, an L8 design, identified basic mix composition, molding conditions and a binder removal schedule. The second array, an L4 x L9 was designed to optimize the

Table 25
Pressure Cast Stators Green Density Results

Variation Within Each Component:		Variation Within The Group:	
Part No.	Green Density (g/cc)	Section Location	Green Density (g/cc)
1	2.084 ± 0.071	Airfoil Trailing Edge	2.084 ± 0.082
2	2.092 ± 0.009	Airfoil Leading Edge	2.077 ± 0.007
3	2.085 ± 0.019	Platform Trailing Edge	2.093 ± 0.012
4	2.087 ± 0.017	Platform Leading Edge	2.087 ± 0.006
5	2.096 ± 0.011	Platform Trailing Edge*	2.096 ± 0.011
		Platform Leading Edge*	2.093 ± 0.012

* This is the platform opposite those shown earlier in the Table.

process for actual stator components. However, concurrent with performance of these experiments, significant impurity problems were encountered within the process. Because of this unexpected result, the 1989 Work Plan was altered to address impurity issues. Overall, planned sub-tasks with injection molding for 1989 included: (1) Impurity Control; (2) Component Fabrication; (3) Tooling Design and Construction; and (4) Aqueous-based Injection Molding.

Table 26
Green Weight And Density Variations For The L4 Injection Molding Experiment

Experiment	Green Weight (grams)	Green Density (g/cc)
L1	20.24 ± 0.09	2.268 ± 0.007
L2	20.31 ± 0.08	2.266 ± 0.004
L3	20.20 ± 0.12	2.271 ± 0.005
L4	20.20 ± 0.05	2.269 ± 0.005
D5	20.64 ± 0.08	2.280 ± 0.002
J6	20.74 ± 0.06	2.284 ± 0.002

Error estimates are expressed as ± 3 standard deviations.

Impurity Control - Two areas were targeted for improvements--binder raw materials and process equipment. To address impurities within the binder raw materials, two iterative L4 Taguchi arrays were initiated and completed. The first L4 was designed to examine different binder and lubricant sources and their impurity contributions. In conjunction with this experiment, two supplemental binder compositions were also evaluated. These supplemental compositions were investigated because under screening trials they appeared to provide components possessing a high degree of stiffness in the as-molded condition. (Molded stiffness was seen as desirable from the standpoint of dimensional control.) Initial results for green weight and green density of actual stators for this experiment are shown in Table 26. All compositions had low variations in both weight and density. However, the two supplemental compositions showed the smallest amount of variation coupled with the highest average weight and density. This suggests that these systems are perhaps less likely to incorporate shrinkage voids or air pockets. The high stiffness coupled with consistent green density were expected to yield parts of improved dimensional quality.

Molded tile from the experiment were examined for both low and high density inclusions via microfocus x-ray. Selected results from the experiment are shown in Table 27 for several conditions of the L4 array and the supplemental compositions. For high density indications, no significant differences were observed within the design. However, in comparison with the supplemental compositions, the original L4 materials showed a lower average number of counts per tile. High density indications were found to be aluminum, iron, or agglomerates comprised of either Si_3N_4, Al_2O_3, or ZrO_2. Small amounts of either aluminum or iron have been found within the binder raw materials. The agglomerates were believed to be remnants from the mixing or molding equipment, as a result of earlier experiments under prior contracts. The low density indications were generally small vacuum voids or internal cracks which probably occurred during part solidification. Of the compositions examined, the D5 composition had significantly smaller quantities of low density defects. From this experiment, it was concluded that: (1) The supplemental compositions provided more consistent green weights and densities and are therefore preferred; (2) A better filtration system was required in order to remove impurities from all incoming binder raw materials; and (3) One composition was identified as providing significantly lower

Table 27
Microfocus X-Ray Results For L4 Injection Molding Experiment

Experiment	High Density (counts)	Low Density (counts)
L1	6.5 ± 3.3	18.3 ± 6.2
L3	6.8 ± 4.6	7.8 ± 6.7
D5	14.3 ± 4.3	2.5 ± 1.9
J6	10.4 ± 2.6	22.0 ± 4.8

Error estimates are expressed as ± one standard deviation.

amounts of void and crack defects, (i.e., Composition D5). Because of the fact that substantial quantities of impurities were observed at all conditions of the L4 design, no further data acquisition or analyses for this experiment was performed. From this work, an improved binder filtration device was developed. The device utilizes sintered alumina filtration media and was capable of screening out all particulate contaminants above ~7 microns.* The device was tested and found to be an effective method of removing impurities from the binder.

Table 28
L4 Impurity Control Experiment
Initial Microfocus Results For High Density Indications

L4 Trial	Mixer Time	Pelletizer Passes	Counts Per Tile
L1	Regular	One	1,0
L1*	Regular	One	1,0,0,0
L2	Regular	Four	14,22
L3	Long	One	26,4
L4	Long	Four	7,3

* Repetition

In addition to the filtration system, considerable effort was put forth in the cleaning, modifying, and in some cases, remanufacturing of existing mixing or molding equipment to make it more wear resistant. Highly wear resistant materials, and coatings were incorporated into every facet of the operation. Using the improved filtration system and up-graded equipment, the second L4 experimental array was designed and conducted to verify correction of these problems. The experiment investigated sources of contamination from the equipment. Variables used within this experiment included: (1) Pelletizer passes, (2) Use of regrind material; and (3) Mixer time and speed. These factors specifically addressed the three pieces of equipment within the process where substantial impurity entrainment occurs. Tile were formed from the preferred mix-composition and microfocus X-ray counts were made for inclusions. Results of the experiment are presented in Table 28 . As can be seen from this limited amount of data, some improvements in impurity content were achieved. For the L1 condition, almost no inclusions were found; but in the remaining trials, substantial amounts of defects were observed. ANOVA for these data showed none of the treatment factors to be significant in controlling the incidence of inclusions. Results from this experiment further outlined difficulties in controlling process induced impurities for injection molding.

Component Fabrication - Developmental efforts in stator fabrication centered on the completion of the L4 x L9 experimental array initiated during 1988. This experiment was originally designed to understand the effects of material composition, solids-loading, and machine settings on dimensions and properties of actual stators. Preliminary data on the green-forming results for this experiment were reported previously.[4] Mechanical property data for the experiment are presented in Table 29 and Table 30 . No correlation between factors with the L4 x L9 experiment and mechanical properties were observed. For the flexural data, NTC incorporated a post-machining oxidation heat-treatment operation recommended by GAPD (980°C - 50 hrs). The data indicated that a reduction in strength occurs due to this heat-treatment. It is believed that the lower values may be the result of residual carbon present as a remnant of the injection molding process. Failure origins included 83% corner breaks. Non-heat-treated samples failed at corner breaks in only 30% of the population. The balance of the test bars failed from either machining flaws or inclusions. The large amount of corner breaks for the heat-treated bars could be the result of oxidation pit formation accelerated by the presence

* Norton Ceraflow Technology, Worcester, MA.

of residual carbon. Injection molded samples had a darker appearance than cast components, particularly within their interior. Repetitive flexural tests were conducted and confirmed a reduction in mechanical strength as a result of the post-grinding oxidation heat-treatment. For the stress rupture results, a majority of samples exceeded the 150 hr life requirement at temperature conditions ranging from 1204°C to 1370°C and stresses of up to 350 MPa. Of the twenty specimens tested, three failed at < 20 hrs life. These data demonstrate that the material has adequate high-temperature durability--although considerably more variability than the casting process.

Table 29
Mechanical Properties of Injection Molded NT154

Temperature (°C)	Flexural Strength (MPa)	Flexural Strength (Ksi)	Characteristic Strength (MPa)	Characteristic Strength (Ksi)	N
22	788 ± 147	114 ± 21	848	123	30
22*	899 ± 66	130 ± 10	931	135	10
1093	652 ± 55	95 ± 8	-	-	5
1204	681 ± 79	99 ± 11	-	-	5
1260	581 ± 58	84 ± 8	-	-	5
1316	531 ± 45	77 ± 7	-	-	5
1370**	480 ± 109	70 ± 16	-	-	5

* All samples except this group of 10 were subjected to a post-machining oxidation heat treatment (980°C - 50 hours) prior to testing.

** These data include one low sample break. Removal of the low value results in a 1370°C of 526 ± 48 MPa (76 ± 7 Ksi).

Data analyses for component dimensions and shrinkages for the L4 x L9 experiment are presented in Table 31. High error terms were encountered for all dimensional repose variables from the experiment. Only solids content was found to be a significant process factor. However, in this instance, the trends observed from the level average results were unexpected. Mixtures with lower solids loading had the smallest shrinkage. The converse would normally be expected, (i.e., lower solids loadings should yield larger shrinkage). When the nine separate L4 experiments were examined independently, the same effect was observed for all molding conditions. One possible explanation for this effect might be that lower solids loadings allowed greater penetration of, and reaction with the encapsulant glass during HIP densification. Thin cross-section parts, such as the stator would be more susceptible to this effect. Tile processed along with the stators did not show this problem. For high and low solids loadings, linear shrinkages were 15.0 ± 0.1% and 15.9 ± 0.1%, respectively. The experiment therefore suggests that elimination of the HIP reaction-layer is important in achieving close-tolerance net shape components.

Table 30
Stress Rupture Results For Injection-Molded NT154

	Temperature and Stress Conditions					
Specimen No.	1204°C 350 MPa	1260°C 350 MPa	1316°C 200 MPa	1370°C 250 MPa	1370°C 200 MPa	1370°C 250 MPa
34-AD-3	160+					
37-AD-6	19					
30-AD-1	158+					
20-AD-5	160+					
20-AD-1	150+					
31-AD-4		18				
24-AD-1		163+				
22-AD-3		160+				
21-AD-2		254+				
21-AD-6		8				
22-AD-4			168+			
23-AD-6			160+			
23-AD-7			150+			
30-AD-7				148+		
31-AD-1				150+		
29-AD-7					150+	
27-AD-6					150+	
27-AD-1					150+	
32-AD-6						217+
34-AD-2						150+

Table 31
Mold To HIPed Shrinkage
For The L4 x L9 Injection Molding Experiment

Component Dimensions	ANOVA - % Contribution: Solids Content	Binder/ Lubricant	Inter-action	Error
Gated Platform	54	18	2	22
Ungated Platform	14	39	0	42
Min. Platform Width	40	2	0	46
Max. Platform Width	62	4	3	30

	Level Average % Linear Shrinkage: Solids Content Low	Solids Content High	Binder/Lubricant Low	Binder/Lubricant High
Gated Platform	14.5	15.4	14.7	15.2
Ungated Platform	15.1	15.6	15.0	15.6
Min. Platform Width	13.4	15.1	14.0	14.4
Max. Platform Width	13.2	14.7	13.7	14.1

Note: Different levels of injection pressure or injection rate had less than 5% contribution to shrinkage.

Injection pressure, hold pressure, and injection velocity all had little or no contribution to dimensions or shrinkage. This is indicated by the high error terms of the ANOVA. The individual L9 experiments were also analyzed separately from each other. There was no correlation of processing factors on dimensions or shrinkage within the L9s either. The largest contributor to dimensions was injection pressure (ranging from 12% to 50%). However, the exact effect of this variable on shrinkage was different depending on the solids loading and binder/lubricant ratio. Part of this error for the ungated platform may be due to the gating design of the mold. The ungated platform is susceptible to changes in dimension due to short shot conditions. The large error terms in the ANOVA for both the total L4 x L9 and the separate L9s indicate that factors outside of the experiment were controlling. Overall, results from this experiment further suggested that near net-shape stator components are difficult to produce using an injection molding process. Undoubtedly, part of this difficult is the direct result of the HIP reaction layer, which can lead to component distortion during densification. However, the lack of significance and trends among the factors studied within the experiment imply that the process itself is inherently difficult to control.

Because of the observed problems with dimensional control, the additional stator development Taguchi experiments of the Work Plan were not performed. In lieu of these planned experiments, several small screening tests were conducted to assess whether improvements in dimensional control could be achieved. The first of these tests was a barrier coating experiment. The experiment was designed to determine the effects of a HIP barrier coating on part warpage. Twelve stators from the original L4 injection molding array were selected for this matched-pair test. Six received a barrier coating; six did not. After HIPing, warpage measurements were made. Calculated warpage factors were determined and are shown in Table 32 . Although the coatings were not perfect, and minor spots of glass penetration were observed, general glass penetration was eliminated. As can be seen from the data, the use of the coating significantly reduced platform warpage (i.e., "tip turn-out") for the trailing edge. The leading edge still showed a high degree of variability in warpage. The results were therefore encouraging because they suggested that part distortion can be improved by a reduction of glass penetration during HIP densification. However, due to the fact that warpage was still present, a major part of this distortion is probably due to the molding process itself.

The second screening experiment involved an examination of the effects of the degas heat-treatment and barrier-coatings in combination. This experiment was a simple paired comparison test to observe changes in component warpage for stators subjected to either the

standard degas cycle or not; and to further test the advantages of barrier coatings. Results from this experiment are presented in Table 33. Results from this test indicated that the smallest warpage and the least amount of variability was obtained when the degas operation was excluded from the stator fabrication process. (In lieu of the degas operation, components were subjected to standard binder removal schedules, and an air-fire treatment.) The barrier coating appeared to reduce platform warpage at the trailing edge, but increased it at the leading edge. The length of the airfoil was smallest for the coated condition--suggesting that the coating was effective in preventing attack by the encapsulant glass. However, due to the fact that warpage was still observed, component distortion appears to be more a function of the molding operation than the densification process.

Table 32
Platform Warpage Of Stators
Effect of Barrier Coatings

Warpage Expressed In % Change Of Dimension: 0% Indicates Parallel

Platform Measurement Location	Uncoated Stator	Coated Stator
Leading Edge	5.7 ± 0.4	3.8 ± 0.7
Trailing Edge	1.2 ± 0.5	2.1 ± 1.1
Midpoint Between Leading and Trailing Edges	1.5 ± 0.3	1.2 ± 0.3

Measurements taken from mold standards indicate that the mold may contribute up to 1% of total warpage.

Because of the extensive problems encountered in the injection molding process (i.e., impurities, strength reduction, component warpage, and lack of significance with respect to response variables), NTC elected to stop further work on this process. Under consultation with GAPD and with their concurrence, NTC switched all developmental activities for stators to the pressure casting process. In closing down the injection molding process, procedures for the preparation of mixes and molding of components were finalized and documented. NTC also intended to deliver a limited number of stators (≤ 75) from the various experiments to GAPD by year end. However, upon careful examination of these components, it was found that none were completely free of substantial defects, (i.e., cracks, voids, or high-density inclusions). Consequently, as an alternative, NTC suggested that stators from the pressure casting process be produced and delivered during the first quarter of 1990. Production of these components is currently underway.

Tooling Design and Construction - Due to GAPD's proposed design changes for the rotor and stator, no injection-molding tooling construction or development was conducted during the year. All experiments were performed using existing an AGT101 tooling transferred to NTC from Carborundum Co.

Aqueous Based Injection Molding - NTC performed a limited number of screening tests on a patented aqueous-based injection molding process.[8] This exploratory

Table 33
Effect Of Degas and Barrier Coatings On Stator
Platform Warpage And Dimensions

Measurement Location	Uncoated Degas	Uncoated No Degas	Coated & Degas
Across Trailing Edge	5.7 ± 0.4	3.4 ± 0.7	3.8 ± 0.7
Across Leading Edge			
Location A	1.2 ± 0.5	0.0 ± 0.1	2.1 ± 0.1
Location B	1.5 ± 0.3	1.0 ± 0.2	1.2 ± 0.3
Length Of Airfoil (mm)	37.49 ± 0.08	37.31 ± 0.03	37.24 ± 0.05

* 0% indicates Parallel.
Location A - Measured at the slash angle farthest from the leading edge.
Location B - Measured at the slash angle nearest the leading edge.

work was designed to investigate the potential for this process and validate component dimensions and properties. A number of trial AGT100 rotors were fabricated and densified using the technique. Reasonable shape and feature control were obtained. Difficulties were encountered in achieving high solids loadings, acceptable viscosities, mix stability and molding machine operation. It was reasoned that substantial additional work would be required to develop the system for use on Si_3N_4 turbine components. Concurrent with these efforts, negotiations for a potential license were initiated with the inventing organization. However, problems in these negotiations forced NTC to curtail further developmental work on this promising forming technique.

DEGAS HEAT TREATMENT - In accordance with the Work Plan, three Taguchi experiments were to be conducted in this area for 1989. They included an L9, L8 and L16 designs. The L9 experiment was initiated in 1988. The L8 followed in 1989. Both were completed by the end of the year. At the close of these experiments it was decided the L16 array was not required. Results and discussion of the two experiments are presented below.

Degas L9 Experiment - This experiment was designed to investigate and determine the effects of various degas schedules and/or atmosphere on final product properties. The degas operation is used to remove water and carbonaceous material from the body in preparation for HIP densification. The L9 experiment correlated time and temperature (each at three levels) with atmosphere (at two levels) and forming method (CIP, Cast and Injection-Molding) with physical and mechanical properties. The design of the experiment is shown in Table 34. ANOVA and level average results for the array were presented and discussed in the prior annual report.[4] From this earlier work, temperature and the interaction of time and temperature were found to be the critical controlling parameters. Atmosphere was of little or no significance. Excellent high temperature strengths were observed (> 700 MPa or 102 Ksi) for selected degas schedules. No physical or mechanical property differences were observed for the cast and CIP material used within the array. However, the injection molded material was significantly different. The difference was initially attributed to contaminants introduced with the binder raw materials. However, process induced inclusions, and residual carbon were subsequently suspected also. In general, the initial data revealed that longer times at higher temperatures gave improved materials. At these conditions fracture toughness (≥ 6 MPa·$m^{1/2}$) and 1370°C flexural strength (≥ 655 MPa or 95 Ksi) were maximized.

Table 34
Degas L9 Experimental Design

L9 Trial	Factors and Levels A	B	C	D	E
1	1	1	-	1	1-3
2	1	2	-	1	1-3
3	1	3	-	2	1-3
4	2	1	-	2	1-3
5	2	2	-	1	1-3
6	2	3	-	1	1-3
7	3	1	-	1	1-3
8	3	2	-	2	1-3
9	3	3	-	1	1-3

A = Time At Temperature.
B = Temperature.
C = A x B Interaction, or Error.
D = Atmosphere.
E = Forming Method: CIP, Cast, Injection Molding.

During 1989, stress rupture and dynamic fatigue tests were completed in an attempt to discern the effect of degas operational parameters on high temperature durability. Stress rupture testing was conducted using CIP samples for each condition of the experiment. Tests were performed at 1370°C, 300 MPa. Acceptable materials exhibited ≥ 200 hours life. Individual stress-rupture values for the experiment are presented in Table 35. As can be noted from the data, most samples exceeded the durability requirement. All values > 200 hrs were suspended from test without failure. The ANOVA for these data are presented in Table 36. As is readily apparent from ANOVA, the

effect of degas conditions on stress rupture life is obscured by the high contribution of the error term. Consequently, no useful process information was obtained from the selected stress-rupture test-condition. Additional tests at more severe conditions were not undertaken because of the extended time requirements for completion. Alternatively, dynamic fatigue testing was conceived and utilized to analyze the effect of processing differences on high temperature behavior. Three CIP samples were tested at three loading rates. After correcting the data for observed strain changes, the slow crack growth parameter, n, was calculated from the test results and used as a response factor in the ANOVA. Level average results are presented in Table 37. The ANOVA for these values is given in Table 38. Time, temperature, and their interaction accounted for all of the observed differences. Atmosphere was an insignificant factor; and unlike the ANOVA for the stress rupture data, error was inconsequential. From level average results for slow crack growth, preferred conditions for the degas heat-treatment operation were identified. They include a low temperature and short to intermediate-time schedule. Stress rupture results appeared to confirm this observation. There were no early failures at the lowest temperature condition or short and intermediate times. The only early failures were observed for the longest time condition--t_3.

Table 35
Stress Rupture Results For
The Degas L9 Experiment
1370°C - 300 MPa

L9 Trial	Treatment Factors Temp.	Time	Atmos.	Stress Rupture Life (Hrs)
1	T_1	t_1	N_2	214
1	T_1	t_1	N_2	239
1	T_1	t_1	N_2	311
2	T_1	t_2	N_2	216
2	T_1	t_2	N_2	204
3	T_1	t_3	N_2/H_2	312
3	T_1	t_3	N_2/H_2	216
4	T_2	t_1	N_2/H_2	329
4	T_2	t_1	N_2/H_2	207
5	T_2	t_2	N_2	186
5	T_2	t_2	N_2	209
6	T_2	t_3	N_2	255
6	T_2	t_3	N_2	200
6	T_2	t_3	N_2	33
7	T_3	t_1	N_2	162
7	T_3	t_1	N_2	262
8	T_3	t_2	N_2/H_2	255
8	T_3	t_2	N_2/H_2	353
8	T_3	t_2	N_2/H_2	214
9	T_3	t_3	N_2	59
9	T_3	t_3	N_2	209

The conclusions concerning an appropriate schedule for the degas operation based on dynamic fatigue and stress rupture data are at variance with earlier conclusions on fast-fracture. Preferred conditions for achieving optimum high-temperature flexural strengths include a high-temperature long-time schedule. The converse appears true for optimum time-dependent behavior. In resolving this apparent engineering paradox, NTC consulted with GAPD concerning an appropriate hierarchy of physical or mechanical property requirements. Foremost in this hierarchy was high-temperature durability. Consequently, NTC selected schedule conditions for the degas operation which optimized 1370°C stress rupture and minimized slow crack growth as measured by dynamic fatigue.

These results also show that dynamic fatigue is a good method for evaluating the relative high temperature behavior of NT154 process modifications. Process differences can be analyzed via Taguchi techniques to give clear indications of the effects of process changes on high-temperature durability. This data can be acquired and evaluated in approximately 1/3 the time required for stress rupture tests. Limited confirmation of results can then be performed using traditional stress-rupture testing.

Table 36
Degas L9 Experiment
ANOVA - Stress Rupture Life

Treatment Factor	% Contribution
Temperature	0
Time	4
Time x Temperature	0
Atmosphere	2
Error	94

Degas L8 Experiment - This L8 design was initiated in an effort to: (1) Evaluate the effects of degas conditions on the formation of the HIP reaction-layer; (2) Identify and select other parameters of potential importance within this unit operation; (3) Confirm the initial selection of degas conditions; and (4) Observe the effects of process changes on bulk and surface properties of components. The design of the experiment is shown in Table 39. In the experiment, the effects of component size, crucible type or powder bed, time, temperature and atmosphere on mechanical properties of as-fired and bulk ground samples were examined. Except for stress-rupture and dynamic fatigue tests, the experiment was completed during 1989. Shown in Table 40 are ANOVA and level average results for CIP tile and test-bar components processed for the experiment. In comparing these level average data, it must be remembered that both bulk and as-fired properties are analyzed together yielding average mechanical properties which appear to be much lower than normal. The difference between as-fired and bulk material characteristics is large. Because of this, these results tend to mask other observable differences within the experiment. Nevertheless, analyses of specific factors revealed trends in the data. Some of the more important conclusions for this experiment are as follows:

Table 37
Degas L9 Experiment
Level Average Data For Slow Crack Growth Exponent

Temperature			Time			Atmosphere	
T_1	T_2	T_3	t_1	t_2	t_3	N_2	N_2/H_2
13.0	8.5	10.4	12.6	11.6	7.6	10.7	10.4

- The condition of the test-bar surface (bulk vs. as-fired) was highly influential on all dense material properties. Level average room temperature flexural strengths decreased from 841 MPa (122 Ksi) to 490 MPa (71 Ksi), for bulk and as-fired test-bars, respectively. High temperature flexural strength also decreased from 600 MPa (87 Ksi) to 421 MPa (61 Ksi). However, toughness increased from 5.72 to 6.76 $MPa \cdot m^{1/2}$. These property alterations are primarily associated with the reaction-layer than forms on the component during HIP densification.

- Higher degas temperatures decreased the as-fired fast fracture strength even though an overall increase in fracture toughness was observed.

- The improvement in fracture toughness for as-fired components is perhaps an anomaly. Due to the reaction layer which forms on the component during HIP densification, the microstructure and surface morphology are significantly different from bulk characteristics. Initially, it was thought that due to the reaction with the glass, a surface compressive layer was formed. However, careful indentation studies coupled with annealing showed the near surface regions to be in slight tension (~2 Ksi), not compression. The high values are therefore considered to be the result of the controlled flaw testing technique employed to measure K_{IC}. Because of surface texture, non-uniform indents and crack-patterns were observed--leading to the anomalously high values.

Table 38
Degas L9 Experiment
ANOVA - Slow Crack Growth Exponent

Treatment Factor	% Contribution
Temperature	40
Time	55
Time x Temperature	1
Atmosphere	0
Error	4

- The reaction layer was minimized by a lower temperature degas. As-fired strengths at 1370°C were improved when using milder degas conditions.

- Temperature was most influential in altering boron content of the material. Degas time and vacuum schedule were not significant factors. Observed changes in chemistry are most likely due to the strong influence of the powder bed. Atmosphere was influential in reducing carbon content in the material. Powder bedding was very influential in altering oxygen and iron content of the material. Also, the use of a powder bed increased tile density, decreased toughness and fracture strength.

- The thickness of the tile controlled overall weight loss through the degas step. This suggests that removal of constituents from deep within large cross-sectional components is diffusion controlled, and may require extended soak times.

From the L9 and L8 experiments, sufficient information was obtained to eliminate the need for the planned L16 Taguchi array. Based on results from these experiments, time, temperature, atmosphere, settering, and other operational procedures have been defined and implemented. SPC methods for weight loss and chemistry are currently being utilized to monitor the process. NTC has acquired and will be utilizing an "on-line" gas analyzer to obtain "real-time" data for in-depth monitoring and statistical process control over this operation.

HIP DEVELOPMENT - Work in HIP development during 1989 involved: (1) The completion of the L4 portion of the L9 x L4 Powder Beneficiation Experiment; and (2) An investigation of various techniques and methods of minimizing the HIP reaction layer. A discussion of the L9 x L4 array was presented earlier. Work on reaction-layer development is discussed below. Efforts in this area included: (1) Barrier Coating Development; (2) Encapsulant Glass Engineering; (3) Decapsulation Methods; and (4) Abrasive Flow Machining Development.

Barrier Coating Development - This work was initiated as an exploratory effort to eliminate reaction of the encapsulant glass with the component during densification. Several parallel approaches to coating technology were investigated including CVD coatings of various compounds; and conventionally applied boron nitride coatings.

CVD coatings of Si_3N_4, BN, Tantalum and Niobium, or mixtures thereof were incorporated onto a number of green CIPed NT154 tile. HIPing was conducted for these tile. Although the coatings prevented penetration of the encapsulant glass, the components did not adequately densify. HIP densities were extremely low (<90%). The coatings apparently interfered with densification mechanisms or acted as a mechanical inhibitor of shrinkage.

Coating of components with boron nitride yielded the most success. Different BN materials and techniques for applying the coating were investigated. High purity, coarse BN powders proved to be most effective. Spray and dip coatings were investigated as application methods. After completing a number of screening trials, an L9 experiment was designed and initiated to optimize the process.

Table 39
Taguchi L8 Degas Experiment Design

Trial No.	Factors and Levels A	B	C	D	E	F	G
1	1	1	1	1	1	1	1
2	1	1	1	2	2	2	2
3	1	2	2	1	1	2	2
4	1	2	2	1	1	2	2
5	2	1	2	1	2	1	2
6	2	1	2	2	1	2	1
7	2	2	1	1	2	2	1
8	2	2	1	2	1	1	2

A = Time.
B = Temperature.
C = Atmosphere.
D = Vacuum/Time Schedule.
E = Crucible Type/Powder Bed.
F = Surface vs. Bulk Ground Bars.
G = Cross-Section Thickness.

Table 40

Degas L8 Experiment - ANOVA For Selected Response Variables
On CIP Tile and Test-Bars

A. ANOVA - % Contribution Of Process Factors On Various Response Variables

Response Variable	Temperature	Time	Atmosphere	Vacuum	Powder Bed	Bar Type	Thickness	Error
Oxygen Content	1	4	2	19	41	0	26	7
Carbon Content	13	13	50	13	0	11	0	0
Boron Content	60	18	0	4	9	4	2	2
Iron Content	0	17	3	4	46	0	22	8
Weight Loss	11	19	2	19	8	0	26	16
Tile Density	43	14	1	25	12	0	3	2
Test Bar Density	4	0	11	0	0	83	0	2
22°C MOR	0	0	5	0	1	93	0	1
1370°C MOR	0	8	2	0	3	80	2	5
K_{IC}	6	2	28	0	18	35	7	3

B. Level Average Data

Response Variable	Temperature		Time		Atmosphere		Vacuum		Powder Bed		Surface Type		Thickness	
	T_1	T_2	t_1	t_2	N_2	Ar	No	Yes	No	Yes	Bulk	As-HIP	Thin	Thick
Tile Density*	3.229	3.223	3.228	3.225	3.226	3.227	3.229	3.224	3.225	3.228	3.226	3.227	3.226	3.227
Test Bar Density*	3.230	3.227	3.229	3.228	3.231	3.226	3.228	3.228	3.229	3.228	3.235	3.222	3.228	3.229
Modulus Of Rupture														
22°C (MPa)	673	662	662	676	627	709	664	671	686	649	844	491	660	674
22°C (Ksi)	98	96	96	98	91	103	96	97	100	94	122	71	96	98
1370°C (MPa)	521	504	481	544	494	531	520	505	534	491	607	418	496	529
1370°C (Ksi)	76	73	70	79	72	77	75	73	77	71	88	61	72	77
K_{IC} (MPa$\sqrt{m}$)	6.01	6.46	6.38	6.09	5.77	6.70	6.18	6.29	6.61	5.86	5.72	6.76	6.47	6.00

* (g/cc)

Unfortunately, the experiment had to be terminated due to unforeseen problems with the application techniques. Problems encountered during these trials are summarized as follows:

- Application of coarse BN by spray coatings resulted in a poor as-HIPed surface features. The coating leaves a degree of texture on the part. This coating texture is subsequently "imprinted" onto the component during the HIP cycle. Although the reaction layer is prevented, surface roughness is markedly increased. From this observation, it was concluded that spray coatings are effective in preventing reaction, but must be applied in a more uniform manner.

- Dipping trials using fluid BN based mixes were completed. Reasonably thick layers of uniform density were built up by successive dipping and drying steps. However, the process was difficult to effectively reproduce on complex components of variable cross-section.

- Using selected techniques, reaction-layer free test tile were achieved. When the coatings were uniformly applied component warpage was minimized. However, flexural strengths for reaction-layer free materials were generally lower than for components with the reaction layer.

- To date, all complex-shaped barrier-coated components have shown moderate to severe warpage during HIP densification. The warpage is attributable to non-uniformity in coating thickness, or a density gradient within the coating. Each might lead to distortion during shrinkage of the component and coating.

Screening trials to investigate and verify alternative BN coating techniques in order to obtain more uniform coating layers on complex components are part of NTC's 1990 Work Plan.

Encapsulant Glass Engineering - In this area NTC performed several successive experiments with different glass materials. First, NTC contacted ASEA-CERAMA AB and conducted trials at their location on several new encapsulant glasses and barrier coats. Tile components were prepared and forwarded to their location, where several alternative glasses and barrier coats were tested. HIPing was also accomplished at ASEA. After completion, the tile components were returned, cut into test-bars and assessed for mechanical properties. For all encapsulants and barrier coatings tested, the as-fired surface mechanical properties were inferior to existing as-fired baseline data for NT154. Using the ASEA technology, room-temperature strength values dropped below 345 MPa (50 Ksi). Non-optimized baseline values for NT154 are ~552 MPa (80 Ksi). These new techniques from ASEA appear to not be useful for NT154.

Secondly, NTC performed exploratory tests by placing tile components within BN powder beds, and canning them into quartz ampoules. Of four tile attempted by this technique, only two densified. However, the dense components were severely warped, and unusable for assessment of mechanical properties. The technique appears to have limited applicability to complex-shaped components.

Finally, a program was initiated to investigate several alternative encapsulant glasses which would potentially be more chemically compatible to NT154. In this way, it is hoped that the detrimental effects of the reaction-layer can be minimized. To this end, a series of four candidate glass mixtures have been identified and prepared. Work on an evaluation of the behavior of these materials under temperature and pressure conditions was initiated. This work is planned for continuance into 1990.

Decapsulation Methods - NTC has acquired and installed a new low-pressure (<10 psi), high volume sand-blaster. This unit replaces the higher pressure equipment (>60 psi) previously used in the program. The unit allows continuous classification of the blasting media to insure consistency and control of the decapsulation operation. Installation of this equipment puts NTC in a position to assess the effects of different media type, grit size, and blast velocity on the surface integrity of components. To determine these effects and optimize this process, a Taguchi array will be designed and conducted using test-tile. Initiation of this experiment is expected as part of the 1990 Work Plan.

Abrasive Flow Machining - An L4 Taguchi array was designed and initiated during 1989 to determine whether the reaction layer could be effectively removed. The depth of the layer is less than ~0.13 mm (0.005"). This is well within the stock removal range of conventional abrasive flow machinery. A local vendor of this equipment was selected for performance of this test. Tile samples, possessing a reaction layer, were forwarded to this vendor; and experimental work initiated. Samples are being subjected to each of two different grit types, grit sizes, and time intervals (or number of passes). Following these treatments, "as-processed" test-bars will be characterized for mechanical properties. Work on this experiment is expected to be completed in early 1990.

COMPONENT INTEGRITY DEVELOPMENT - NTC's 1989 Work Plan called for the completion of an L16 Taguchi array. The objective of this experiment was to examine the effects of various post-HIP heat-treatment conditions on physical and mechanical properties. It was reasoned that improvements in both bulk and surface properties could be obtained by crystallization of the intergranular phase and by oxidation of the surface. Subsequent to the completion of the L16 array, a simple L4 array was designed and conducted to further investigate and verify appropriate oxidation conditions. The designs, results, and conclusions from these experiments are presented and discussed below.

L16 Component Integrity Experiment - Seven treatment factors were incorporated into this array--five as inside factors with two additional outside factors. The design is shown in Table 41. Within the experiment four temperature-time schedules were studied under different atmospheres. Oxidation was applied to half of the array; and component properties were assessed for as-fired and bulk-ground surfaces. Rotor-hubs were included within the experiment to test the applicability of the conditions to thick cross-sections. Work was conducted on CIP, Cast and Injection-Molded components. An assessment and comparison of mechanical properties from all three forming processes was accomplished by this design. The experiment was initiated during 1988 and completed in 1989.

To begin the experiment, baseline material properties for all three forming operations were acquired. Results are presented in Table 42. These data serve to highlight the differences between the various forming methods and offer a comparison standard for work conducted within the L16 array. Overall, the casting process produced the highest strengths and Weibull Moduli, regardless of surface condition. Injection-molded components showed acceptable strengths, but lower Weibull Moduli. In general, the CIP process fell in between the IM and PSC processes. Note also that ~35-37% reduction in strength for as-fired surfaces at room-temperature was observed for each forming technique. This difference is ~25-35% at 1370°C. The reduction in strength is attributable to surface roughness and the HIP reaction-layer.

For mechanical properties, the ANOVA for the L16 is shown in Table 43. The percent contribution of each factor is given for individual forming processes and combined data. Dynamic fatigue results are also included. However, in this instance, data were only collected for the CIP process. Data for both the injection molding and casting processes were expected to be similar, and therefore dynamic fatigue tests for these materials were not conducted.* Level average values for the experiment are presented in Table 44, Table 45 and Table 46. Due to the differences in as-fired and bulk-ground properties, the level average data have been separated based on specimen surface condition. A summary of pertinent results from the experiment is as follows:

Table 41
Component Integrity L16
Experiment Design

Trial No.	Inside Factors & Levels A	B	C	D	E	Outside Factors F	G
1	1	1	1	1	1	1-3	1
2	1	2	2	2	2	1-3	
3	1	3	3	1	1	1-3	
4	1	4	4	2	2	1-3	1
5	2	1	2	1	2	1-3	
6	2	2	1	2	1	1-3	
7	2	3	4	1	2	1-3	
8	2	4	3	2	1	1-3	
9	3	1	3	2	2	1-3	
10	3	2	4	1	1	1-3	
11	3	3	1	2	2	1-3	
12	3	4	2	1	1	1-3	
13	4	1	4	2	1	1-3	1
14	4	2	3	1	2	1-3	
15	4	3	2	2	1	1-3	
16	4	4	1	1	2	1-3	1

A = Temperature (T_1 through T_4).
B = Time (t_1 through t_4)
C = Atmosphere (Ar and N_2, Powder Bed).
D = Oxidation Treatment (On, Off).
E = Test Bar (As-Fired or Bulk).
F = Forming Method (CIP, Cast, IM).
G = Rotor Hub Component.

- For room temperature flexural strength, the oxidation treatment and test-bar surface condition were most influential. The oxidation treatment appears to repair machining damage (for ground test-bars) and may minimize the effects of any decomposition occurring during the inert atmosphere heat treatment. Test-bars with as-fired surfaces generally had much lower strengths than bulk ground material--as a result of surface roughness and the HIP reaction-layer. Oxidation did not have as influential a role for as-fired test-bars. Considerably variability (i.e., noise) was noted in room-temperature strengths. From physical observation of the samples, it is believed that several operative mechanisms could exist which explain this variation: (1) From x-ray diffraction, crystallization of the intergranular glass occurred at all temperatures. At the low-temperature condition, (T_1), the volumetric contraction of the intergranular glass accompanying crystallization may enlarge existing flaws, or stress the glass; (2) Healing of flaws and stress relief appear operative at moderate to high temperatures ($\geq T_2$). This is manifest by the general increase in strength for these conditions; and (3) Surface degradation or decomposition may occur at temperatures $> T_2$. Therefore, at the lowest heat-treatment temperature (T_1), the strength behavior is dominated by bulk material character. Conversely, surface character dominates at high temperatures (T_3 and T_4). At the intermediate temperature condition (T_2), a balance is found between these effects. The variability is therefore believed to be associated with the generation of surface flaws due to slight decomposition occurring during crystallization; which was subsequently healed for some of the experimental trials by the oxidation heat-treatment.

- For fracture toughness, the test-bar surface condition was clearly dominant. Soak temperature was moderately influential. As-fired test-bar surfaces have markedly higher toughness. This

* Specimens for the Casting and Injection-Molding Processes are available should the need arise to conduct dynamic fatigue tests on these forming operations.

is considered to be an anomaly of the test method as described previously.

- For 1370°C flexural strength, the test-bar surface condition was again clearly dominant. The forming method also played a role. For all three forming methods, bulk ground test-bars had higher 1370°C strengths than as-fired components. Yet, significant improvements in flexural strength were noted by the application of the crystallization heat-treatment. Figure 75 shows 1370°C flexural strength as a function of test-bar surface condition and soak temperature. For either type of test-bar, all heat-treatments improved strengths to above the non-treated baseline values.

- It is particularly noteworthy that at the highest heat-treatment temperature, strengths > 551 MPa (80 Ksi) were achieved with as-fired test bars. The result suggests that with the selection of an appropriate post-HIP heat-treatment, the strength of as-fired NT154 can be made constant at +551 MPa (+80 Ksi), regardless of test-temperature.

Table 42
Mechanical Properties For
CIP, Slip-Cast And Injection Molded Processes From The
Component L16 Experiment

Process and Properties	CIP	Slip-Cast	Injection Molding
I. Bulk-Ground Test Bars - 22°C			
Modulus of Rupture (MPa)	834 ± 103	893 ± 56	876 ± 119
(Ksi)	121 ± 15	130 ± 8	127 ± 17
Weibull Modulus	8.2	18.4	5.6
K_{IC} (MPa·m$^{1/2}$)	5.5 ± 0.1	5.6 ± 0.2	5.1 ± 0.5
II. Bulk-Ground Test Bars - 1370°C			
Modulus of Rupture (MPa)	525 ± 39	578 ± 50	573 ± 58
(Ksi)	76 ± 6	84 ± 7	83 ± 8
Weibull Modulus	14.7	12.7	10.5
III. As-Fired Test Bars - 22°C			
Modulus Of Rupture (MPa)	531 ± 39	583 ± 25	540 ± 52
(Ksi)	77 ± 6	85 ± 4	78 ± 8
Weibull Modulus	15.5	27.3	11.1
K_{IC} (MPa·m$^{1/2}$)	6.7 ± 1.1	7.3 ± 0.6	7.7 ± 0.8
IV. As-Fired Test Bars - 1370°C			
Modulus of Rupture (MPa)	394 ± 34	368 ± 35	395 ± 34
(Ksi)	57 ± 5	53 ± 5	57 ± 5
Weibull Modulus	12.7	11.5	12.7

Strength and Weibull data are for 20 - 30 samples for each forming method. Fracture Toughness values were compiled for 3 - 5 samples each.

- For the dynamic fatigue tests, time, atmosphere, oxidation, and surface condition affected slow-crack growth (SCG) behavior; while only time, atmosphere and surface condition were deemed significant in predicting time to failure. Predicted time to failure was estimated using the equation:

$$t = B \cdot S_i^{(n-2)} \cdot S_a^{(-n)}; \qquad [9]$$

where t = time to failure; B is a material constant, S_i is the inert material strength, and S_a is the applied stress. The value of the expression $S_i^{(n-2)}$ is determined for the y-intercept of the regression line of the dynamic fatigue data. Predicted failure times for "as-HIPed" surfaces are dramatically less than for bulk material, even though at some of the crystallization/oxidation conditions good SCG values were achieved. A plot of predicted time to failure versus treatment time indicates that optimum resistance to slow-crack growth is achieved at condition t_2. The graph of these data is given in Figure 76. The result also suggests that this treatment

Table 43
L16 Component Integrity Experiment - ANOVA
(% Contribution)

Response Variable and Forming Method	Experimental Factors: Temperature	Time	Atmosphere	Oxidation	Test Bar Surface	Forming Method	Error
I. Room Temperature MOR							
CIP Process	8	10	3	56	11	–	12
Casting Process	9	8	2	42	18	–	22
Injection Molding Process	6	5	10	14	51	–	13
Combined Processes	7	9	4	35	25	0	21
II. Fracture Toughness							
CIP Process	13	7	6	18	41	–	16
Casting Process	9	1	7	5	70	–	8
Injection Molding Process	17	3	3	0	69	–	8
Combined Processes	13	3	4	4	60	0	16
III. 1370°C MOR							
CIP Process	14	16	0	0	25	–	45
Casting Process	3	0	1	1	93	–	2
Injection Molding Process	0	2	6	5	81	–	6
Combined Processes	3	2	0	1	59	12	23
IV. 1370°C Dynamic Fatigue							
CIP Process	3	40	12	14	23	–	9
V. 1370°C Predicted Failure Time							
CIP Process	2	21	9	1	64	–	4

condition is preferred regardless of surface condition. However, the results also markedly demonstrate the differences between bulk and "as-processed" surfaces.

L4 Component Integrity Experiment - The ANOVA from the L16 array indicated that neither of the inert atmosphere environments studied within the design had any effect on the results. Similarly, temperature and time appeared to have minimal effects. Since the oxidation condition had a profound effect for 22°C strength, it was reasoned that subsequent treatment conditions should be investigated in an oxidizing environment. Hence, a simple L4 experiment was designed and conducted to examine the effect of various oxidation conditions on mechanical properties. The experimental factors studied within this design are shown in Table 47. The experiment was designed to answer the following questions:

- Can a high-temperature, short-time oxidation cycle be utilized in lieu of the inert atmosphere treatments of the L16 design? Is this "flash oxidation" cycle just as effective in bulk crystallization of the material? Is it as effective as oxidation cycles utilized within the L16 array?

- How effective is oxidation in repairing machining induced damage?

Data collection and analyses for mechanical properties were completed for this experiment. ANOVA for these response variables are presented in Table 48. The ANOVA showed that oxidation temperature and time were important for room temperature behavior.

Table 44 - L16 Component Integrity Experiment - Level Average Data From Bulk Ground Test-Bars

Response Variables	Temperature				Time				Atmosphere				Oxidation	
	T1	T2	T3	T4	t1	t2	t3	t4	N2	Ar	N_2Bed	ArBed	Yes	No
I. Bulk-Ground Test-Bars														
Room Temperature MOR														
CIP Process (MPa)	548	917	665	748	841	648	741	648	786	679	710	703	832	607
(Ksi)	80	133	97	109	122	94	108	94	114	99	103	102	121	88
Slip Cast Process (MPa)	569	889	634	717	789	627	734	658	703	755	638	714	803	602
(Ksi)	83	129	92	104	115	91	107	96	102	110	93	104	117	87
Inj. Mold Process (MPa)	707	920	662	776	848	786	734	696	845	782	648	789	848	684
(Ksi)	103	134	96	113	123	114	107	101	123	114	94	115	123	99
Overall Average (MPa)	608	909	654	747	826	687	737	668	778	739	665	735	828	631
(Ksi)	88	132	95	108	120	100	107	97	113	107	97	107	120	92
Fracture Toughness ($MPa \cdot m^{\frac{1}{2}}$)														
CIP Process	4.9	5.2	5.3	5.4	5.2	5.1	5.3	5.2	5.0	5.1	5.4	5.3	5.3	5.1
Slip Cast Process	4.9	5.3	5.4	5.5	5.3	5.2	5.4	5.2	5.0	5.1	5.4	5.5	5.4	5.1
Inj. Mold Process	4.8	5.1	5.0	5.3	5.0	4.9	5.1	5.2	4.7	5.2	5.1	5.2	5.2	4.9
Overall Average	4.9	5.2	5.2	5.4	5.2	5.0	5.2	5.2	4.9	5.1	5.3	5.3	5.3	5.0
1370 MOR														
CIP Process (MPa)	565	524	600	538	565	548	558	555	548	541	572	565	531	583
(Ksi)	82	76	87	78	82	80	81	81	80	79	83	82	77	85
Slip Cast Process (MPa)	596	576	610	579	576	600	610	576	593	579	607	583	577	603
(Ksi)	87	84	89	84	84	87	89	84	86	84	88	85	84	88
Inj. Mold Process (MPa)	583	565	627	638	596	607	596	614	548	600	610	655	602	605
(Ksi)	85	82	91	93	87	88	87	89	80	87	89	95	87	88
Overall Average (MPa)	581	555	612	585	579	585	588	581	563	573	596	601	570	597
(Ksi)	84	81	89	85	84	85	85	84	82	83	87	87	83	87

Table 45 - L16 Component Integrity Experiment - Level Average Data From As-Fired Test-Bars

Response Variables	Temperature				Time				Atmosphere				Oxidation	
	T1	T2	T3	T4	t1	t2	t3	t4	N2	Ar	N_2Bed	ArBed	Yes	No
II. As-Fired Test Bars														
Room Temperature MOR														
CIP Process (MPa)	686	538	724	596	645	624	638	627	662	658	610	603	705	562
(Ksi)	100	78	105	87	94	91	93	91	96	96	89	88	102	82
Slip Cast Process (MPa)	658	538	638	579	624	593	614	593	593	624	593	614	648	564
(Ksi)	96	78	93	84	91	86	89	86	86	91	86	89	94	82
Inj. Mold Process (MPa)	600	531	603	607	620	545	586	596	610	600	565	572	602	572
(Ksi)	87	77	88	88	90	79	85	87	89	87	82	83	87	83
Overall Average (MPa)	648	535	655	594	630	587	612	606	622	627	589	596	651	566
(Ksi)	94	78	95	86	91	85	89	88	90	91	86	87	95	82
Fracture Toughness ($MPa \cdot m^{\frac{1}{2}}$)														
CIP Process	6.2	5.7	5.4	6.5	6.3	5.3	6.4	5.3	6.2	5.7	5.9	5.4	5.8	5.8
Slip Cast Process	7.1	7.2	7.4	7.4	7.3	7.1	7.2	7.4	7.7	7.1	7.2	6.9	7.3	7.2
Inj. Mold Process	6.8	6.0	6.7	6.4	6.4	6.4	6.8	6.6	6.4	6.7	6.1	7.0	6.7	6.3
Overall Average	6.7	6.3	6.5	6.7	6.6	6.3	6.8	6.4	6.7	6.5	6.4	6.4	6.6	6.4
1370 MOR														
CIP Process (MPa)	414	421	493	538	465	434	486	534	552	479	421	469	453	507
(Ksi)	60	61	72	78	68	63	71	78	80	70	61	68	66	74
Slip Cast Process (MPa)	396	421	476	534	455	431	476	479	527	483	403	427	436	484
(Ksi)	58	61	69	78	66	63	69	70	77	70	59	62	63	70
Inj. Mold Process (MPa)	434	352	462	524	462	393	496	472	524	462	393	445	448	464
(Ksi)	63	51	67	76	67	57	72	69	76	67	57	65	65	67
Overall Average (MPa)	415	398	477	532	461	419	486	495	534	475	406	447	446	485
(Ksi)	60	58	69	77	67	61	71	72	78	69	59	65	65	70

Table 46
L16 Component Integrity Experiment
Level Average Values For 1370°C Durability Tests

	Temperature				Time				Oxidation		Test Bar Surface	
	T_1	T_2	T_3	T_4	t_1	t_2	t_3	t_4	Yes	No	As-Fired	Bulk
Slow Crack Growth Exponent	21	18	17	19	14	27	20	14	22	16	15	23
Predicted Time To Failure (mins)	7207	215	18	41782	26	48947	202	49	21002	3609	3	24608

Crystallization was either unimportant, or played only a minor role in determining room-temperature behavior. Conversely, crystallization and oxidation temperature dominated the 1370°C flexural strength results. For combined data, it is interesting to note that the crystallization heat-treatment and not test bar surface condition was most influential. Toughness was controlled by oxidation soak temperature. However, for combined results, test-bar surface was dominant.

In general, room temperature strengths averaged approximately 827 MPa (120 Ksi), 620 MPa (90 Ksi), and 896 MPa (130 Ksi) for transverse ground, as-fired and longitudinal ground test-bars, respectively. At best, only minor improvements were observed over longer-term, lower temperature oxidation conditions. Likewise toughness did not change appreciably after crystallization or oxidation heat-treatments. These data indicate that high-temperature "flash oxidation" treatments are perhaps not as desirable as longer-time lower-temperature oxidation conditions. However, substantial improvements were noted in 1370°C strength when the crystallization heat-treatment was applied. Figure 77 shows a dramatic rise in "as-fired" surface strengths through application of a post-HIP crystallization heat-treatment. Regardless of subsequent oxidation conditions, 1370°C flexural strength improved to > 580 MPa (84 Ksi) for "as-fired" surfaces when the crystallization heat-treatment was employed. Figure 78 presents similar information for transverse ground flexural bars. Strengths > 620 MPa (90 Ksi) were observed for these components after the crystallization heat-treatment. It appears that regardless of surface condition, 1370°C flexural strength can be markedly improved by the utilization of selected crystallization and oxidation heat-treatments.

Based on information gained within the L16 and L4 designs, a follow-up screening test was conducted to verify the intergranular phase composition and durability of the material under longer-term oxidation conditions. Results from the test are given in Table 49. In this test, crystallized and non-crystallized materials were both oxidized for 100 hours at 980°C. Before oxidation, the baseline material showed no presence of extraneous yttrium-silicate phases, while the crystallized material showed gamma-$Y_2Si_2O_7$.

Table 47
Factors For The L4 Component Integrity Experiment

Inside Factors:

A = Pre-Oxidation Heat-Treatment Condition.
B = Oxidation Temperature.
C = Oxidation Time.

Outside Factors:

D = Test-Bar Surface Condition
1. As-fired.
2. Longitudinal Bulk Ground.
3. Transverse Bulk Ground.

In general, no change in phase composition was noted for low-temperature oxidation heat-treatments. The data demonstrate that room-temperature flexural strength only improves after the oxidation heat-treatment, regardless of the existence of a crystallization operation. The oxidation step simply heals surface damage associated with either the crystallization heat-treatment, machining, or both. A two-step heat-treatment operation therefore appears necessary. In the first step, crystallization of the intergranular phase is performed at moderate temperatures under an inert environment. The second step involves an oxidizing heat-treatment to repair damage resulting from machining or from the crystallization heat-treatment itself.

Figure 75
Component Integrity L16 Experiment
1370°C Flexural Strength

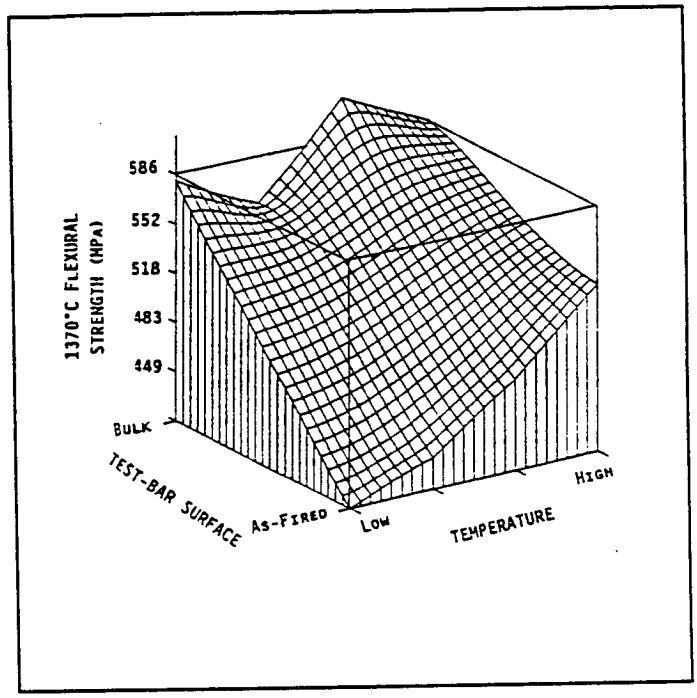

In summary, these component integrity experiments demonstrated that significant improvements in property uniformity can be achieved through selective post-HIP heat-treatment operations. A two step-process is advocated involving a crystallization heat-treatment under an inert environment, followed by an oxidation treatment. These two operations tend to optimize both room-temperature and 1370°C flexural properties. Respective strengths of approximately ~1 GPa (~145 Ksi) and +620 MPa (+90 Ksi) can be expected at each test-temperature. Utilization of the crystallization treatment significantly improves "as-fired" surface strengths. In fact, flexural strengths for "as-fired" surfaces were demonstrated to be insensitive to test-temperature. Values of +550 MPa (+80 Ksi) were observed from 22°C to 1370°C. While this is a helpful improvement, dynamic fatigue studies also indicated that the durability of test-bars with "as-fired" surfaces was significantly

Figure 76
L16 Component Integrity Experiment - Predicted Failure Times

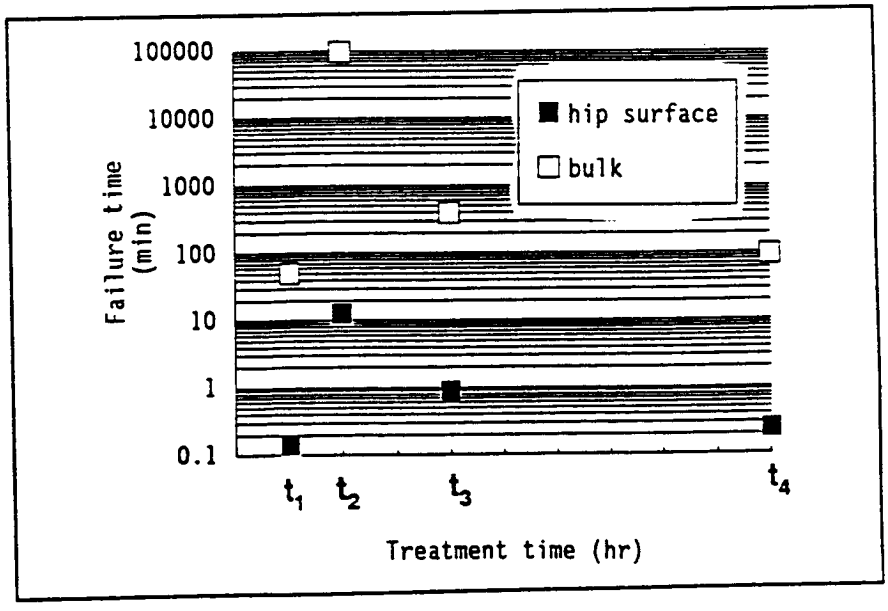

below bulk-ground material. The results therefore strongly suggest that for the production of "net-shape" components, solutions are needed for the HIP reaction layer. Work in this area is a primary thrust for NTC in 1990.

Table 48
Component Integrity L4 Experiment
ANOVA For Fracture Toughness and 1370°C Flexural Strength
(% Contribution)

Factor	Transverse Ground	As-Fired Surface	Longitudinal Ground	Combined
22° Flexural Strength				
Pre-Oxidation Crystallization	0	2	38	1
Oxidation Temperature	36	90	87	0
Oxidation Time	58	0	24	8
Test-Bar Surface Condition	N/A	N/A	N/A	63
Experimental Error	6	8	9	28
Controlled Flaw Toughness				
Pre-Oxidation Crystallization	0	0	38	1
Oxidation Temperature	23	18	59	1
Oxidation Time	73	43	0	0
Test-Bar Surface Condition	N/A	N/A	N/A	86
Experimental Error	4	39	3	12
1370°C Flexural Strength				
Pre-Oxidation Crystallization	26	98	0	45
Oxidation Temperature	29	1	67	2
Oxidation Time	0	0	24	0
Test-Bar Surface Condition	N/A	N/A	N/A	24
Experimental Error	45	1	9	29

PROCESS ENGINEERING

NTC submitted an overall 1989 Work Plan to GAPD. The plan provided general details for the experimental activities described in this report. Several changes in the plan were incorporated during the year to take advantage of new technology or address problems. NTC continues to utilize Taguchi-based experiment design methods for most of its experimental plans. This method is advocated because of its simplicity, ease of analysis, and cost-effective methodology.

NDE DEVELOPMENT

During 1989, NTC completed all major efforts on NDE. NDE activities within the ATTAP utilized microfocus x-ray radiography, (MFXR). Two areas were addressed: (1) Seeded Defect Studies; and (2) Component Inspection Protocol Development.

SEEDED DEFECT STUDIES - During 1988, all of the seeded defect tile identified under the Work Plan were fabricated. Three types of defects were chosen: (1) Iron inclusions; (2) Voids or porosity; and (3) Si_3N_4 agglomerates. Seed sizes ranged from 29 to 180 μm for the iron inclusions; 98 to 464 μm for the voids; and 66 to 315 μm for agglomerates. A volumetric seeding technique using pressure casting was developed for the fabrication of these components. In 1989, MFXR procedures were developed and green components characterized. These tile were subsequently densified, and re-assessed for defect detectability.

Film microfocus results for each series seeded defect tile are shown in Table 50 through Table 52. The defect detectability data for both film and real-time microfocus x-ray characterization is summarized in Table 53.

Defect detectability results for the spherical Fe-Al inclusion seeded defect tile, presented

in Table 50 show green body point probability of detection values (i.e., No. of seeds detected/calculated total No. of seeds) ranging from 0 to 0.51 over a thickness sensitivity ranging from 0.22 % to 1.53 %. Qualitatively, these high density inclusions are readily detectable in green tile down to 51 microns or 0.46 % thickness sensitivity. There appears to be a discrepancy between the quantitative point probability of detection and the qualitative results. The detection probabilities were lower than expected compared to films which showed high contrast, well defined seed images. One explanation for this apparent discrepancy is the possibility that the seeds partially settled out of the slip batches prior to casting, resulting in a much lower total number of seeds per tile. Another explanation is that seed location in the tile cross section is an important factor in addition to thickness sensitivity, resulting in the detection of seeds in a planar section of the tile only. In support of this second mechanism, the point probability of detection values for green tile from this study are in excellent agreement with prior published results.[10]

The film microfocus results for the spherical Fe-Al inclusions in HIPed NT154 tile are listed in Table 50 as well, and show a similar difference between qualitative and quantitative defect detectability. These high density inclusions are readily detected down to 88 microns or 1.23 % thickness sensitivity. As measured by destructive analysis of tile cross sections, the effective seed diameters increased in size by approximately a factor of three during HIP densification. The HIP-reacted seeds appeared as dark inclusions with a non-circular morphology. SEM characterization and elemental Fe dot maps verified that the compositional diameter of reacted seeds was in agreement with the effective, visually apparent seed diameter. The

Figure 77
Component Integrity L4 Experiment
1370°C Strength For "As-Fired" Surfaces

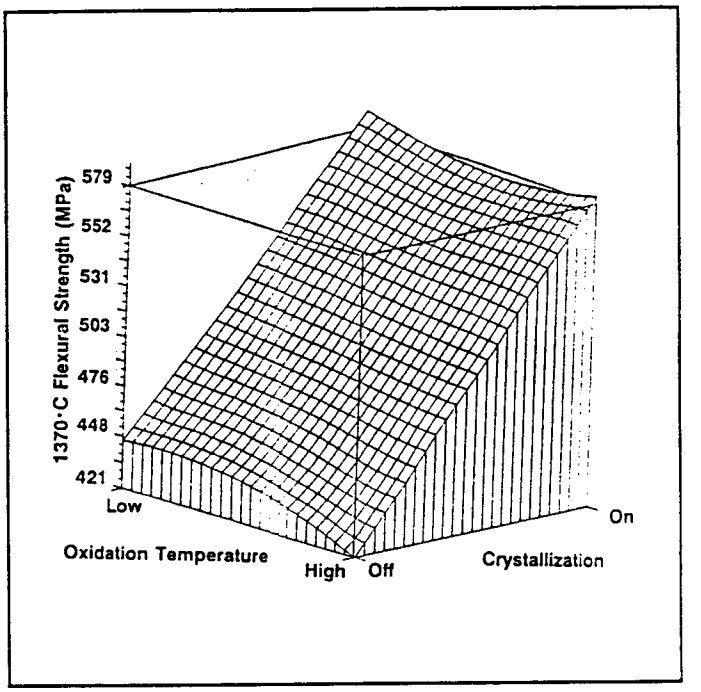

Figure 78
Component Integrity L4 Experiment
1370°C Strength For "Transverse Ground" Surfaces

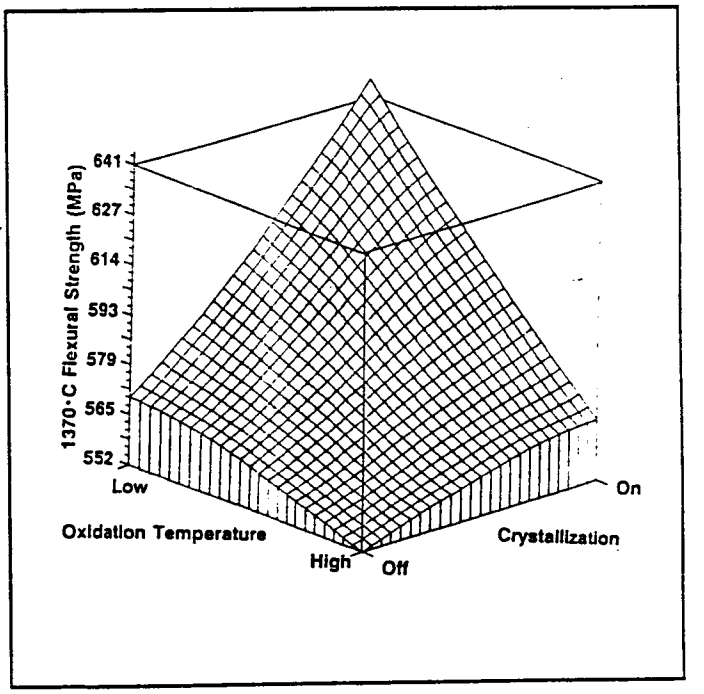

defect detectability of Fe-Al inclusions using this effective seed diameter is 274μm or 3.83 % thickness sensitivity.

Table 49
Component Integrity Follow-Up
Screening Experiment
Room-Temperature Flexural Strength

		Before Oxidation	After Oxidation
Baseline, Non-Crystallized	(MPa)	895 ± 55	993 ± 69
	(Ksi)	129 ± 8	144 ± 10
Pre-Crystallized in N_2	(MPa)	730 ± 165	972 ± 35
	(Ksi)	106 ± 24	141 ± 5

The impact of the seeded Fe-Al inclusions on room temperature flexural strength is shown in Figure 79. The presence of seeded defects results in a significant decrease in strength with respect to the 910 MPa (132 Ksi) baseline average. SEM photomicrographs of representative test bar fracture surfaces showed fracture origins to be clusters of relatively large beta Si_3N_4 grains. It appears that the Fe-Al inclusions dissolve during HIPing into the glassy phase and stimulate localized exaggerated grain growth. The size of the region of large grains decreased at smaller Fe-Al seed sizes, until the reacted inclusions appeared as relatively small microstructural inhomogeneities. The room temperature flexural strength decreased by only 69-103 MPa (10-15 Ksi) over Fe-Al inclusion diameters ranging from 51 microns to 180 microns.

Using a defect detectability limit of 0.5 % for Fe-Al inclusions in green material, and an estimated 30 micron inclusion diameter threshold for impact on room temperature flexural strength, one can inspect up to a 6 mm thickness for strength limiting high density inclusions. This means that airfoils and other thin cross sections inspected by MFXR may be screened for the presence of > 30 micron diameter high density inclusions.

Defect detectability data for tile seeded with spherical pores is listed in Table 51 and shows a qualitative cutoff in green tile at 200 microns or 1.71 % thickness sensitivity. The quantitative point probabilities of detection appear to be in error by a scaler quantity, perhaps from a combination of seed diameter, density, and batching errors. Normalizing probabilities using a multiplication factor of 0.79 brings the data in line with qualitative observations.

After HIP densification, spherical pore seeded defect tile showed no low density indications by film microfocus x-ray radiography. Pores with diameters up to 468 microns appear to heal during densification. There was no readily apparent evidence of incompletely healed pores or scars upon inspecting bulk-ground surfaces of these samples.

The impact of seeded pores on room temperature flexural strength is presented in Figure 80. In this case, the MOR data shows: (1) No significant decrease in strength over the non-seeded baseline, and (2) An independent relationship between pore size and flexural strength. No seeded pores or healed defects were observed by fractographic analysis and polished section inspection, which leads to the conclusion that pores up to 464 microns completely heal during HIP densification. Test bar fracture origins were surface flaws or small microstructural inhomogeneities (≤ 10 microns), which is typical of standard NT154 material. From these data, it can be summarized that green components with thicknesses up to ~ 30 mm may be screened for internal pores or forming voids > 464 microns in diameter. Below this level, their presence is inconsequential; and may not be grounds for rejecting a component.

Table 50
Film Microfocus x-Ray Radiography Characterization
Spherical Fe-Al Inclusions

Seed Diameter (μm)	Body Type	Thickness Sens. (%)	Total No. of Seeds	Seeds Detected ? (Magnification)	No. of Seeds Detected	Point Probability of Detection (Pi)
180	green	1.40	41	Yes (2X)	17	0.415
180	green	1.35	211	Yes (2x)	65	0.308
180	green	1.53	185	Yes (2x)	94	0.508
180	green	1.43	1166	Yes (2x)	492	0.422
129	green	1.07	2483 (DA)	Yes (2x)	DNC	-
129	green	1.07	274	Yes (2x)	127	0.474
88	green	0.73	5870 (DA)	Yes (2x)	DNC	-
88	green	0.73	326	Yes (2x)	87	0.267
69	green	0.62	12900 (DA)	Yes (2x); Yes (4x)	DNC	-
69	green	0.62	259	No (2x); Yes (4x)	0; 12	0; 0.046
51	green	0.46	24152 (DA)	No (2x); Yes (4x)	DNC	-
51	green	0.46	541	No (2x); Yes (4x)	0; 97	0; 0.179
28	green	0.22	2521	No (2x); No (7x)	0	0
28	green	0.22	474	No (2x); No (7x)	0	0
180 [429]	dense	2.51 [5.98]	787	Yes (2x)	DNC	-
180 [429]	dense	2.51 [5.98]	134	Yes (2x)	46	0.343
180 [429]	dense	2.51 [5.98]	26	No (2x)	0	0
129 [355]	dense	1.80 [4.95]	1663 (DA)	Yes (2x)	DNC	-
129 [355]	dense	1.80 [4.95]	183	Yes (2x)	60	0.327
88 [274]	dense	1.23 [3.83]	3961 (DA)	Yes (2x)	DNC	-
88 [274]	dense	1.23 [3.83]	220	Yes (2x)	87	0.354
69 [199]	dense	0.96 [2.77]	9619 (DA)	No (2x); Yes (4x)	DNC	-
69 [199]	dense	0.96 [2.77]	193	No (2x); Yes (4x)	0	0
51 [203]	dense	0.71 [2.83]	17690 (DA)	No (2x); Yes (4x)	DNC	-
51 [203]	dense	0.71 [2.83]	396 (DA)	No (2x); No (4x)	0	0
28 [82]	dense	0.39 [1.14]	216 (DA)	No (2x); No (7x)	0	0
28 [82]	dense	0.39 [1.14]	36	No (2x); No (7x)	0	0

Table 51
Film Microfocus X-Ray Radiography Characterization
Spherical Pores

Seed Diameter (μm)	Body Type	Thickness Sens. (%)	Total No. of Seeds	Seeds Detected ? (Magnification)	No. of Seeds Detected	Point Probability of Detection (Pi)
468	green	4.42	108	Yes (2x)	131	1.213 [0.964]
468	green	4.42	632 (DA)	Yes (2x)	DNC	-
324	green	2.71	2662 (DA)	Yes (2x)	DNC	1.298 [1.031]
324	green	2.71	228	Yes (2x)	296	-
281	green	2.31	3234 (DA)	Yes (2x)	DNC	1.265 [1.005]
281	green	2.31	294	Yes (2x)	372	-
200	green	1.71	11358 (DA)	Yes (2x)	DNC	1.171 [0.930]
200	green	1.71	222	Yes (2x); Yes (4x)	260	-
136	green	1.15	28256 (DA)	No (2x); Yes (4x)	DNC	0
136	green	1.15	234	No (2x); No (4x)	0	0
98	green	0.84	1504 (DA)	No (2x); No (2x)	0	0
98	green	0.084	147	No (2x); No (2x)	0	0
All Sizes	dense	7.1 mm Thickness	Same as Above	No	0	0

Notes:
(1) Number in brackets are normalized P_I values.
(2) DA = Destructive Analysis Sample.
(3) DNC = Did Not Count.

Table 52
Film Microfocus X-Ray Radiography Characterization
Dense Si_3N_4 Agglomerates

Seed Diameter (μm)	Body Type	Thickness Sens. (%)	Total No. of Seeds	Seeds Detected ? (Magnification)	No. of Seeds Detected	Point Probability of Detection (Pi)
315	green	2.08	1306 (DA)	Yes (2x)	240	0.184
315	green	2.93	156	Yes (2x)	29	0.186
324	green	1.88	2107 (DA)	Yes (2x)	DNC	-
324	green	1.88	191	Yes (2x)	16	0.084
176	green	2.31	* (DA)	No (2x)	0	-
176	green	2.31	*	No (2x)	0	0
125	green	1.71	* (DA)	No (2x)	0	0
125	green	1.71	*	No (2x); No (4x)	0	0
78	green	1.15	* (DA)	No (2x); No (4x)	0	0
78	green	1.15	*	No (2x); No (4x)	0	0
66	green	0.84	* (DA)	No (2x); No (2x)	0	0
66	green	0.084	*	No (2x); No (2x)	0	0
All Sizes	dense	7.1 mm thickness	Same As Above	No	0	0

Notes: (1) * = Did not calculate actual seed count.
(2) DA = Destructive Analysis Sample.
(3) DNC = Did Not Count.

Green tile seeded with dense Si_3N_4 agglomerates were detected down to 226 microns or 1.88 % thickness sensitivity. In this case, even the largest seed size of 315 microns or 2.93 % thickness sensitivity was below the threshold of reliable defect detection. The dense Si_3N_4 agglomerate seeds were not detected at all in the corresponding HIPed tile.

Table 53
Seeded Defect Study Summary

Seed Type	Defect Detectability	
	Film	Real-Time
Spherical Fe-Al Inclusions		
Green	51μm (0.46%)	129μm (1.07%)
Dense	88μm (1.23%)	>180μm (>2.51%)
Dense	274μm (3.83%)	>429μm (>5.98%)
Spherical Pores		
Green	200μm (1.71%)	324μm (2.71%)
Dense	-	-
Dense Si_3N_4 Agglomerates		
Dense	226 μm (1.88%)	>315μm (>2.93%)

* - Based on reacted effective seed diameter.

The impact of dense Si_3N_4 agglomerates on room-temperature flexural strength is shown in Figure 81. The agglomerates simulated in this study were made by grinding and sizing HIPed milling media. The presence of these agglomerates resulted in a significant decrease in strength with respect to the non-seeded average baseline. SEM evaluations of fracture surfaces confirmed that the seeded defects were the fracture origins. A reduction in room-temperature strength of ~20% for seeds in the size range of 66 to 315 μm was observed. In terms of the effectiveness of microfocus x-ray radiography, only thin cross-sections of green material can be inspected for this type of defect. Using film methods, a defect detectability limit of 1.88% was obtained for green seeded defect tile. Assuming as a best case that the strength-limiting Si_3N_4 agglomerate is 66μm in diameter, microfocus inspection for this type of defect in a component is only possible at up to ~3.5 mm thickness. MFXR is therefore of very limited value in locating defects of this type for either rotors or stators.

Overall, the flexural strength data demonstrates that Fe-Al and agglomerate defects have a significant impact on mechanical properties, while pores disappear upon HIP densification. No attempt was made to determine the impact of seeded defects on high temperature flexural strength.

Qualitative real-time microfocus x-ray studies were conducted concurrent with the film results presented earlier. Exposure conditions ranged from 50 to 60 Kv and 0.3 to 0.4 Ma. Image enhancement using still 256 frame averaging improved the clarity and contrast of seeds detected in the real-time operation, but it did not appear to have a significant impact on decreasing the thickness sensitivity threshold for reliable defect detection. For spherical Fe-Al inclusions in green tile, defect detectability dropped to 129 microns or 1.07 % thickness sensitivity, which corresponds to a factor of 2.5 decrease in defect detectability compared to film characterization. These high density inclusions were not detected at all in HIPed tile up to a thickness sensitivity of 2.51 %. The results are in qualitative agreement with previous studies using real-time microfocus radiography to characterize Fe inclusions in green Si3N4.[10] Spherical pores in green tile were detected in real-time microfocus radiography down to 324 microns or 2.71 % thickness sensitivity, representing a factor of 1.6 decrease in defect detectability over the film procedure.

Figure 79
Fe/Al Inclusion Seeded Defects - Impact On Room Temperature Flexural Strength

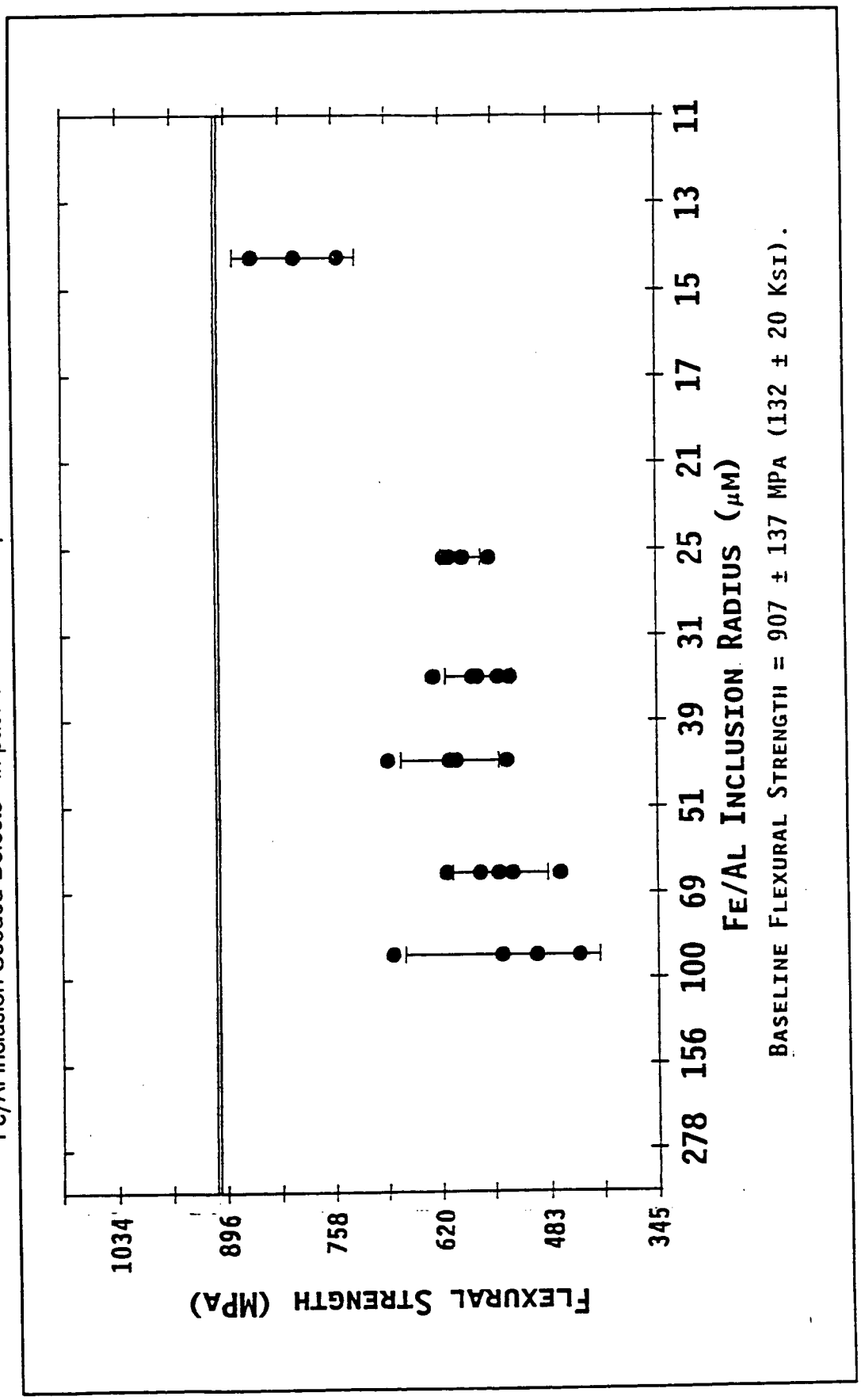

Figure 80
Spherical Pore Seeded Defects - Impact On Room Temperature Flexural Strength

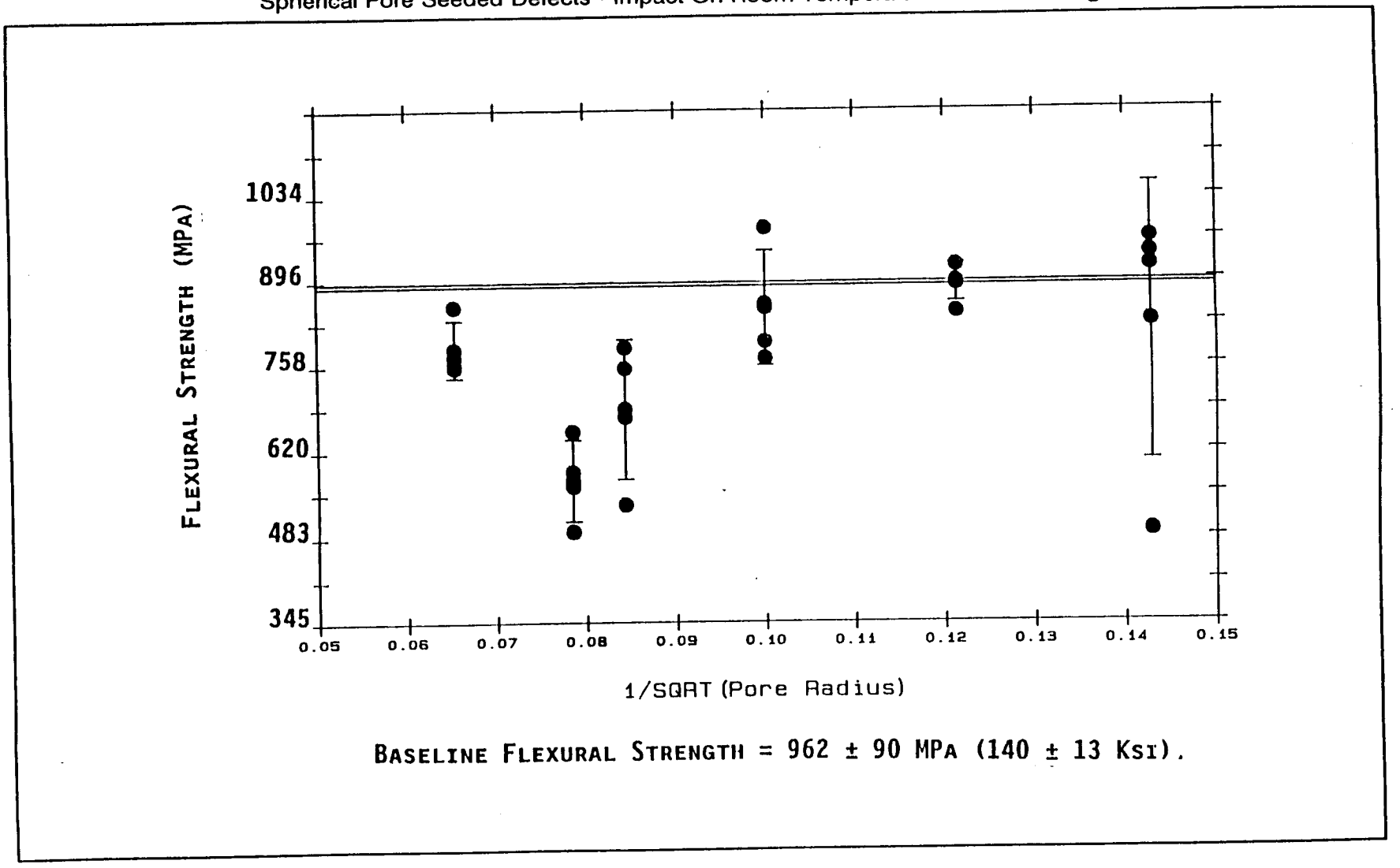

BASELINE FLEXURAL STRENGTH = 962 ± 90 MPA (140 ± 13 KSI).

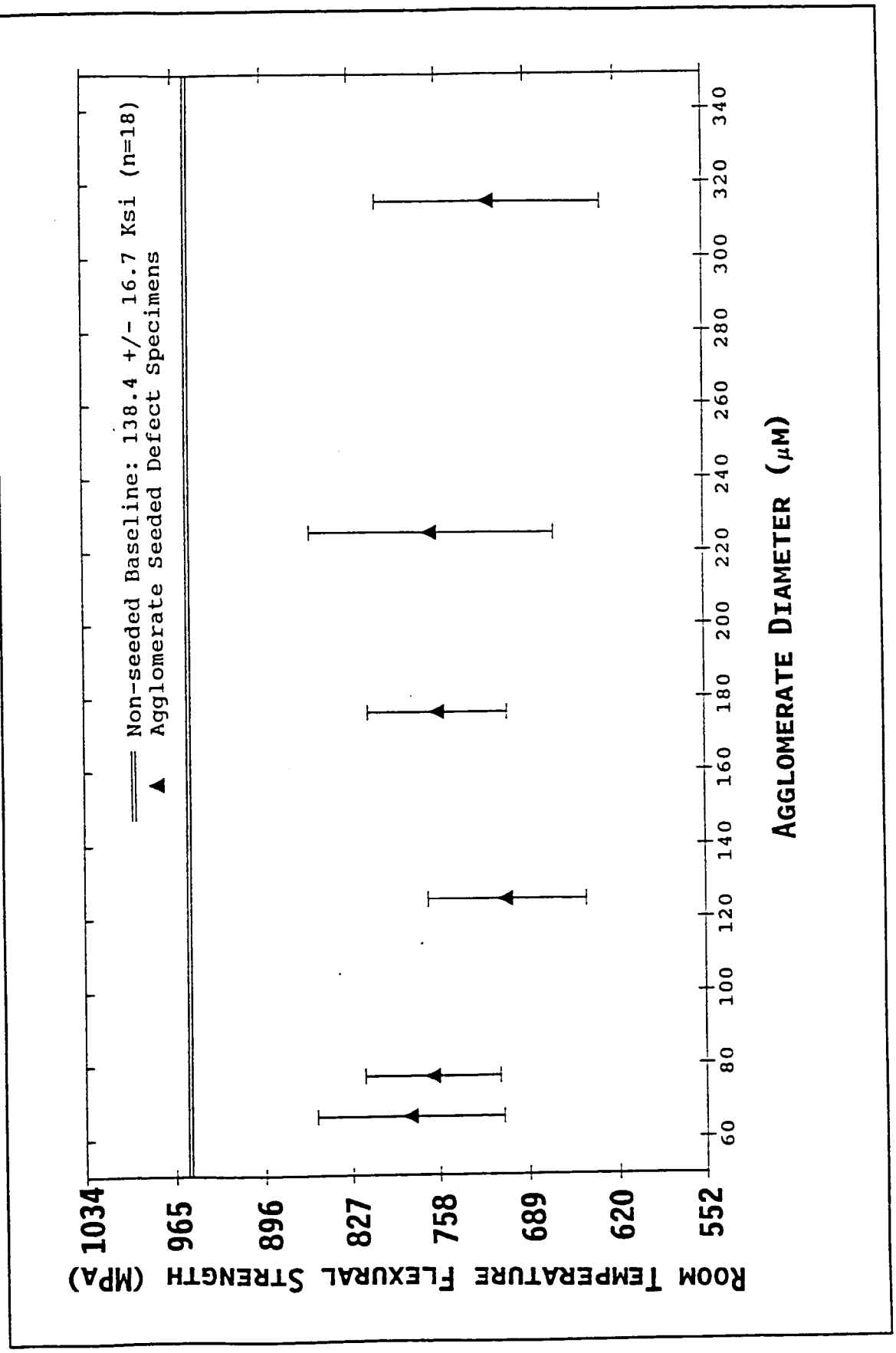

Figure 81 - Si^3N_4 Agglomerate Defects - Impact On Room Temperature Flexural Strength

The volumetric-seeding seeded defect tile study has verified the thickness sensitivity cutoff for reliable defect detection of typical high density and low density bulk inclusions. This information was used in the design of seeded defect stators and rotor hubs for the development of component specific microfocus x-ray radiography inspection procedures. It is clear from the sizes of readily detected defects as well as current experience, that "on-line QC" microfocus x-ray radiography will be insufficient in assuring component strength. Rather than working on incremental improvements in microfocus x-ray defect detectability, the emphasis has moved to areas that have a higher likelihood of success in assuring component strength,-- such as process SPC and other prevention measures. Future efforts in microfocus NDE development are geared toward establishing and maintaining day-to-day repeatability and reproducibility for component inspection.

COMPONENT INSPECTION PROTOCOL DEVELOPMENT - Film microfocus x-radiography inspection protocols were defined for green and dense AGT101 rotor hubs and stators. Parameters for inspection protocol for each component were developed, and are specified as part of the written component inspection procedures. These procedures, in draft form, were incorporated into NTC's quality plan and documentation control system. Using seeded defect components, all of the film microfocus x-radiography inspection routines were verified with respect to the previously defined defect detectability limits.

QUALITY ASSURANCE

Efforts in quality assurance were directed at: (1) Documentation of the Quality System; (2) Measurement Techniques and Standards Development; and (3) SPC Development and Implementation; and (4) Component Manufacturing and Inspection Plans.

DOCUMENTATION OF THE QUALITY SYSTEM - A draft ATTAP Quality Plan/Manual was prepared and submitted to GAPD for review. GAPD completed its initial review of the document and has returned it to NTC with constructive commentary. This document is a comprehensive plan in conformance with MIL-STD-9858A.

MEASUREMENT TECHNIQUES AND STANDARDS DEVELOPMENT - During the year, a liquid dye penetrant system for ATTAP related work was received and installed. Qualification of the system was completed. Magnaflux ZL27A, a post emulsifiable penetrant, and Magnaflux ZL54A, a water washable penetrant were recommended by GAPD and selected for use in inspecting bulk-ground and as-processed surfaces, respectively. Ni-Cr standard panels with cracks ranging from 10 to 50 microns were used in the qualification.

A density measurement station capable of 0.01% accuracy was received and installed. This equipment was needed to reduce vibration as well as minimizing operator error. NBS traceable standards were acquired and are being routinely used for the density measurement equipment. HIPed Si_3N_4 spherical bearings with NBS certified density values were also acquired and are used to assess the accuracy of density measurements for NT154 samples. For green components, an NBS certified silicon single crystal standard was procured and is used to assess accuracy of green components.

SPC DEVELOPMENT AND IMPLEMENTATION - By year-end, standard SPC methods were initiated or implemented for all ancillary NT154 operations including: (1) Raw Materials

Characterization; (2) Powder Beneficiation; (3) Degas; (4) HIP; and (5) Post-HIP Heat-Treatments.

The SPC charts implemented to date have been used to identify a number of process upsets and their underlying assignable causes. SPC charts for batch-to-batch processed powder have shown that Si_3N_4 raw material lot changes are the most frequent cause of an out of control signal. Based on our understanding of these process upsets, tighter specifications on physical and chemical properties of raw materials have been requested.

Mechanical properties are monitored for each processed powder batch. One complication identified in performing this SPC is the confounding effect of downstream process variability. To resolve this conflict, analysis of variance (ANOVA) calculations were performed on mechanical properties data sets from consecutive processed powder batches. Separate ANOVA analyses were performed using (1) Powder Batch, and (2) Process Path (defined as a unique degas furnace run/HIP run combination) as the blocking factors. As an example of this technique, a chart depicting historical changes for both blocking factors is shown in Figure 82 for controlled flaw fracture toughness. ANOVA confirmed that there are statistically significant differences between powder batches and process paths. Average values and ranges within the chart are shown for each powder batch. The large boxes show the process path groups for several powder batches. From these data, the impact of process path on mechanical properties is thought to be primarily due to run-to-run variations in the HIP, and not from prior powder processing or other heat-treatment steps.

The goal of this SPC activity is to: (1) In connection with designed experiments--define the critical material and process parameters; (2) Develop the appropriate measurement techniques and procedures; and (3) Identify and correct out-of-control situations.

COMPONENT MANUFACTURING AND INSPECTION PLANS - A format for the ATTAP rotor and stator component operations sheets was established, and procedures written. Operations sheets for all ATTAP deliverables were drafted, finalized and approved. A process documentation system was devised and implemented which defines the use of operation sheets in conveying work instructions and specifications for each step of component fabrication. The objective of this system was to coordinate individual work station records with component-specific operations sheets, and to establish the mechanism for material transfer between each process step. SPC for each process step was developed as part of work station records, and was included in this system.

DELIVERABLES

Nine rotor hubs were fabricated and delivered to GAPD during the year in fulfillment of the second Rotor Milestone of the SOW. By mutual agreement with GAPD, due to problems with the injection molding process, delivery of injection molded test specimens was initially delayed, then dropped as a deliverable requirement. Also, because of changes in rotor and stator component geometries, NTC and GAPD agreed to delay shipment of additional pressure slip-cast test-specimens, (tensile rods and flexural bars). Delivery of required samples will coincide with rotor and stator component deliverables during 1990.

Figure 82
NT154 Controlled Flaw Fracture Toughness
Batch And Process SPC Data

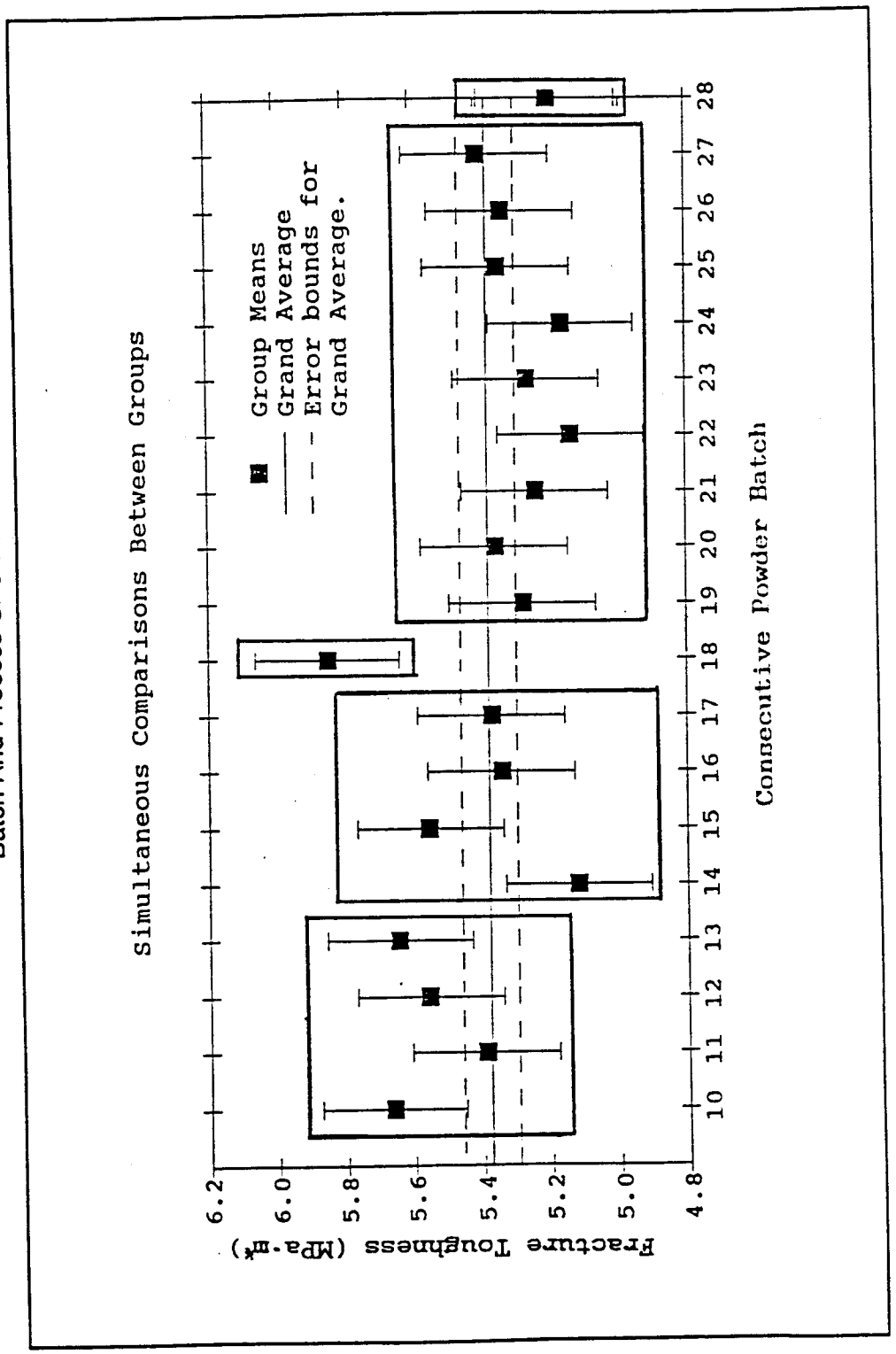

PROJECT MANAGEMENT

NTC submitted a detailed 1989 and preliminary 1990 Work Plan along with several submissions of cost-support information as requested by GAPD. Monthly reports and other technical information were supplied in accordance with defined schedules, or at GAPD's request.

NTC participated in the 27th DOE Contractor's Coordination Meeting in Dearborn, MI, on October 23-26, 1989. B. J. McEntire presented a review of this program during the meeting entitled, "Silicon Nitride Component Development For Advanced Gas Turbine Engines".

SUMMARY AND CONCLUSIONS

Norton/TRW Ceramics has successfully completed the second-year's effort of the ATTAP program. Process and component development work continued for the AGT101 rotor and stator. All mutually-agreeable second-year milestones and program objectives were achieved. Significant accomplishments are summarized below.

- NT154 continues to be extensively developed and characterized. A significant data-base has now been generated for this material both by NTC, GAPD, and by several independent testing laboratories. Component properties continue to exceed program specifications. Excellent strength characteristics at room and elevated temperatures are observed along with adequate static stress rupture behavior. Further improvements in material properties are expected as a natural consequence of process development work within the program.

- All powder beneficiation development was completed. Appropriate material and comminution conditions were investigated for their effects on forming and material properties. Powder blends, milling time, solids concentration, and other conditions were selected to provide a moderate to coarse material of a broad size distribution. Vibratory and bail-milling operations were compared. Ball-milling was selected because of reliability, intensive mixing action, and broad particle size output. Impurity pick-up was minimized through the use of high-purity powders and media under clean-room conditions. SPC has been implemented for this operation.

- Casting development continued for the rotor. Developmental work centered on the selection of appropriate additives, the development of slip-formulation and casting procedures. Laboratory pressure casting apparatus and plaster molds were utilized. From these techniques, rotor hubs were successfully cast, densified, characterized, and delivered to GAPD for evaluation. Mechanical properties for these components met all program requirements, and exceeded comparable properties from co-processed test-tile. Room-temperature strength and Weibull Modulus were ~925 MPa (134 Ksi) and 15, respectively. At 1370°C, a flexural strength of ~600 MPa (87 Ksi) was observed. Comparative data for the three forming processes investigated within the program suggest that pressure slip-casting is preferred. The highest strength levels (>1 GPa) and Weibull Moduli (up to 19) have been observed for this process. NTC has acquired and installed automated pressure-casting equipment for scale-up of this operation. Appropriate porous plastic mold technology has also been brought in-house. This equipment and mold technology is slated for development and eventual production of rotor and stator hardware for the engine tests at the end of the program.

- Injection molding was being developed for the stator. Experimental endeavors were directed at characterizing and improving binder formulation, molding parameters, equipment and binder removal conditions. However, in general flexural strength and Weibull Moduli acquired from components for this process were significantly lower than for the pressure-casting process. Particulate impurities from binder raw materials and process equipment were identified as strength limiting defects. Improvements to the process equipment and filtration of the binder were employed. Yet, despite NTC's best efforts, "defect-free" components were never routinely achieved. Additionally, the process showed significant variability with respect to shrinkage, warpage and overall dimensions. Because of these problems, NTC elected to discontinue further efforts on injection molding and focus resources on the casting operation. Future stator development work will therefore be performed using pressure slip-casting.

- Various degas heat-treatments were thoroughly investigated for their effect on physical and mechanical properties. Appropriate conditions were identified and selected. Preferred conditions maximize the high-temperature durability of the material while maintaining adequate flexural strength at both room and elevated temperatures. SPC has been implemented for this operation.

- HIP development experiments were linked to the powder beneficiation process. All essential experimental activities were completed. Quantitative data for these experiments were complied and evaluated. From this, specific HIP conditions were selected. Of these, time and cooling rate were found to have profound effects on mechanical properties. Shorter times and faster cooling rates maximized fracture toughness (>6 MPa$\cdot$m$^{1/2}$) and flexural strength. SPC has been implemented for this process. Various additional studies were initiated to eliminate problems associated with the HIP reaction-layer. Boron Nitride was identified as the preferred material for barrier coatings. However, trials using this material have not been totally successful. Component coverage and protection has been adequate and distortion minimal for simple tile shapes. However, coating uniforming has been difficult to achieve, and moderate warpage is observed for complex shapes. Current work is directed at solving this problem. Removal of the reaction-layer by abrasive flow machining was investigated; and a glass engineering approach to minimize the reaction-layer was also started. Work in these areas will also continue in 1990.

- Two post-HIP Component Integrity experiments were completed. These experiments were designed to address the effects of surface condition and post-HIP heat-treatment parameters on the mechanical integrity of components. The specific intent of these tests was to utilize crystallization of the intergranular glass phase--to improve high-temperature strength; and oxidation of the surface--to repair machining damage. By selection of preferred crystallization conditions, significant improvements in flexural fast-fracture on as-HIPed surfaces was observed. Oxidation operations were also highly effective in improving machined component strength. A two-step approach to post-HIP component heat-treatments is therefore recommended. Operational conditions and procedures for each were selected. SPC has been initiated for this operation.

- NDE development utilized microfocus x-ray radiography (MFXR). A seeded defect study was completed. From this an assessment of detectability limits was made and inspection protocols developed for the rotor and stator. It was concluded that MFXR is only of limited use as an inspection tool. Due to a lack of its ability to find "critical strength limiting flaws", NTC has

elected to restrict its application to green components only. In this capacity, it serves a useful purpose as a process development tool. MFXR was extensively utilized in the assessment and characterization of defects within the injection-molding process. Its use in this role will continue; but further developmental efforts for dense components have been discontinued.

- A draft Quality Assurance Manual/Plan was prepared and submitted to GAPD. Measurement techniques and standards were implemented for several critical inspection operations, including density, strength, dimensions and MFXR. Component specific operation sheets and procedures were implemented for each deliverable component. Documentation of the process continued through the writing of standard procedures and specifications based on results from the Taguchi experiments. SPC has been implemented for most of these key operations. Complete implementation quality plan and SPC are slated to coincide with the culmination of the process developmental work prior to delivery of the final components.

Continued effort in each of the above areas is scheduled for the 1990 program year. Work will shift to an emphasis on component specific problems for the rotor and stator.

ACKNOWLEDGEMENT

Work accomplished during the 1989 program year represents the combined efforts of a number of individuals. The following principal engineers are gratefully recognized for their key contributions: R. L. Yeckley--Materials Development, A. P. Taglialavore--Powder Beneficiation Degas and HIP Development, D. N. Heichel--Casting Development, J. W. Johnson--Injection Molding Development, J. E. Holowczak--Casting and Injection Molding Development; and E. Bright--NDE and Quality Assurance. Additionally, G. Janulewicz, D. Moylan, J. Gulcius, G. Manoogian, B. McGeary, W. Hackett, D. Karsberg, S. FitzGerald, and G. Watson are acknowledged and appreciated for detailed performance of the technical plan. Appreciation is expressed to G. A. Fryburg, T. G. Kalamasz, P. K. Caneen, C. Brown, M. G. Bingham, L. F. Russell, J. P. Reed, S. Sherman, L. Lynch and K. Mitchell for their technical support and services in consultation, machining, tooling, experiment design and presentation graphics. The Characterization and Analysis Groups of Norton Company are acknowledged for their work in chemical analysis, x-ray diffraction, microfocus x-ray characterization, mechanical property testing, and electron microscopy. E. M. MacKinnon, G. D. Roberts, R. T. Foy, D. L. Sterner, and M. J. Sweeney are appreciated for cost analysis, accounting and secretarial services. Special thanks go to Drs. C. L. Quackenbush and R. R. Wills who constructively reviewed program objectives, plans, and reports; and to J. M. Garwood, and F. P. Teta for government contract administration review and support. D. Kreiner, G. Boyd, L. Lindberg, J. Minter, and B. Morey, J. Smyth and D. Carruthers of GAPD are acknowledged and thanked for technical guidance, analyses, program direction and support. Finally, appreciation is expressed to Norton Company, TRW, GAPD, NASA and DOE for financial support.

REFERENCES

1. K. C. Liu and C. R. Brinkman, "Cycline Fatigue of Toughened Ceramics," Ceramic Technology for Advanced Heat Engines Project - Semiannual Progress Report for October 1988 Through March 1989, (Oak Ridge, TN: ORNL Publication No. ORNL/TM-11239), 351-360.

2. D. W. Richerson, "Fractography of Advanced Silicon Nitride Materials for Turbine Applications," Final Report, Submitted to Naval Sea Systems Command, Contract No. N00024-88-C-5112, Washington, D.C., (Salt Lake City, UT: Ceramatec Report No. 8963201, April 1989).

3. N. L. Hecht, D. E. McCullum, S. Goodrich, and L. Chuck, "Mechanical Properties Characterization of High Performance Ceramics," 27th Automotive Technology Development Contractors' Coordination Meeting, October 23-26, 1989, (Dearborn, MI: SAE Press), in press.

4. B. J. McEntire, "ATTAP Annual Technical Progress Report For The Period February 1, 1988 To December 31, 1988," (Cleveland, OH: NASA LeRC, January 26, 1989).

5. M. A. Janney, "Gel-Casting: A New Complex Shape Forming Technology," (Private Communication).

6. E. Blaha, "Casting Slip," U.S. Patent No. 2,527,390, (Oct. 24, 1950).

7. G. Q. Weaver and B. G. Nelson, "Molding Refractory and Metal Shapes By Slip Casting," U.S. Patent No. 4,341,725, (July 27, 1982).

8. A. J. Fanelli and R. D. Silvers, "Process For Injection Molding Ceramic Composition Employing An Agaroid Gel-Forming Material To Add Green Strength To A Preform," U. S. Patent No. 4,734,237, (Mar. 29, 1988).

9. B. J. Pletka, and S. M. Wiederhorn, "A Comparison of Failure Predictions By Strength And Fracture Mechanics Techniques," J. Mat. Sci., [17], (1982), 1247-1268.

10. K. E. Amin and T. P. Leo, "Radiographic Detectability Limits For Seeded Defects In Both Green And HIPed Silicon Nitride," Conference Proceedings On Non-Destructive Testing Of High Performance Ceramics, ASNT/ACerS, (Boston, MA: August 25-27, 1987), 211-232.

APPENDIX II

ANNUAL TECHNICAL PROGRESS REPORT
CARBORUNDUM COMPANY

Advanced Turbine Technology Applications Program
(ATTAP)
Contract DEN3-335
Ceramic Component Development

Second Annual Technical Progress Report

January 1, 1989 through December 31, 1989

Introduction

The Carborundum Company (formerly the Standard Oil Engineered Materials Company), Structural Ceramics Division, presents its second annual technical progress report under the ceramic component development subcontract. This subcontract is part of the U.S. Department of Energy-sponsored and NASA-administered 5 year contract DEN3-335, Advanced Turbine Technology Applications Project (ATTAP), awarded to Garrett Auxiliary Power Division, Phoenix, AZ, with Dr. J. R. Smyth, as Project Manager. This report covers work performed during the period of January 1, 1989 through December 31, 1989.

Carborundum's principal objective as a major subcontractor was the development of ceramic component fabrication processes through detailed analyses of materials and processes, controlled experimentation, and destructive and nondestructive evaluation of green and finished components. The goal of this development program was to achieve increased reliability and reproducibility on near net shape turbine engine components.

The original GAPD ATTAP workplan addressed five AGT 101 engine components - a transition duct, a backshroud, and three wave springs. As of November 8, 1989, the transition duct was the only remaining component on which development work was continuing. This report summarizes the work completed on each of the components during this reporting period. It is a continuation of the No. 1 annual for 1988 and summarizes the six bimonthly reports issued during 1989.

1.0 Transition Duct (CBBA)

The ATTAP goal for the transition duct is the development and demonstration of a capability to reproducibly injection mold and sinter a large and relatively complex sintered alpha silicon carbide (Hexoloy SA or SA SiC) component.

Several possible process/product limitations have been identified. Quantifying and dealing with these issues, shown below, has become the ATTAP objective for the transition duct.

Defects/inclusions
Dimensional control/tolerance predictability
Reproducibility
NDE capability

Last year's workplan noted that the current limitations are interrelated because dimensional and tolerance control are dependent upon fabrication of stress-free molded ducts. This stress-free condition is, in turn, dependent upon the flow characteristics of the molding compound and optimization of the tooling and molding parameters. A uniform green density and SiC distribution and isotropic particle orientation are required to produce stress-free molded and baked components. A controlled sintering process is required to optimize final component properties.

Carborundum for the past several years has been injection molding parts with two different compounds, designated SX-05 and SX-09. Although the average MOR values of as-fired, machined, and machined/annealed test bars suggested the same population, it appeared prudent to re-examine the relative merits of each material to select one for further process optimization. In addition, the identification and source of injection molding component inclusions were investigated as well as binder removal procedures.

The capacity required for molding the transition duct exceeded that of our in-house equipment. We identified external equipment which we could use. However, those molding machines were not instrumented to the degree that our equipment is. Our Reed 250 ton machine is instrumented to monitor in real-time, store data, calculate, and plot position, pressure, temperature, and velocity as a function of time. It was therefore decided to fabricate a subscale duct tool and conduct molding experiments in-house. In addition to providing full process control, the in-house approach significantly reduced material requirements. The weight of a subscale duct configuration is 1.1 pounds versus 7.5 pounds for the full sized configuration originally proposed. Prior to fabricating the subscale duct tool, a flow analysis was conducted to assess potential flow problems and to define potential sprue and gate configurations. In addition, a cooling analysis was run to determine the best location and size of cooling lines to provide uniform duct cooling.

Once optimum subscale molding parameters are identified, additional flow modeling of the full size duct will be conducted with this information as input. Recommended tooling revisions will be made and full size ducts will be molded off site utilizing the best control parameter values identified in the subscale experiments.

The 1989 ATTAP transition duct tasks addressing the current injection molding process and product limitations were identified as follows:

I. SX-05 Versus SX-09 Composition Comparison and Selection
II. Subscale Transition Duct Experiments
III. Extended Transition Duct Molding Trials
IV. Fabrication of Engine Quality Components

Task 1 SX-05 Versus SX-09 Composition Comparison and Selection

Compound Comparison and Selection

The compound selection goal was to select one of the two baseline compounds after fabricating and evaluating test bars from three batches of each compound.

A large lot of submicron powder (145-2) was put aside for all 1989 task processing requirements. Three batches each of SX-05 and SX-09 were milled, mixed, and compounded separately. Pairs of SX-05 and SX-09 batches were processed at three different time periods through the mixing step and both an initial and second pass compounding step to diminish the effect of outside environmental factors.

Twenty billets and 300 small and large test bars were molded for subsequent processing and MOR testing. All green parts were X-rayed. The test bars were sintered in a continuous furnace. The billets were sintered in a periodic furnace arranged in a 6x6 latin square plan to eliminate constant differences among layers and the differences among the six positions within a layer.

RT MOR was measured on the as-fired small bars, the machined/annealed large bars, and the machined/annealed bars cut from billets. The MOR, standard deviation, and Weibull modulus, are shown in Table 54.

Table 54

SX-05 Versus SX-09 MOR Results

MIX	SX-05			SX-09		
BATCH	1	2	3	1	2	3
As-fired Bars						
MOR (ksi)	47.6	47.9	43.1	43.8	46.3	43.9
s (ksi)	6.7	7.7	7.2	5.6	6.5	6.7
m	7.3	6.2	6.0	8.0	7.4	6.9
Machined Bars						
MOR (ksi)	67.0	62.4	63.4	62.4	60.6	67.6
s (ksi)	7.6	9.3	8.4	10.3	8.0	4.9
m	8.5	6.4	7.8	4.9	7.4	15.0
Billet Bars						
MOR (ksi)	67.6	62.0	51.8	57.4	49.4	47.8
s (ksi)	10.7	16.6	13.5	10.1	12.2	12.1
m	6.4	3.4	3.7	4.8	3.9	3.4

Figure 83 shows the 95% confidence limits (CLs) for all bar sets. The as-fired group average strength of 45.4 ksi is contained within all six CLs suggesting that all groups are from the same population. The machined/annealed test bars, at 63.9 ksi, are 41% stronger on average than the as-fired bars. Except for one set (09-3), five

sets are statistically from the same population. The MOR values of bars machined from billets vary considerably, ranging from 48 (09-3) to 68 (05-1).

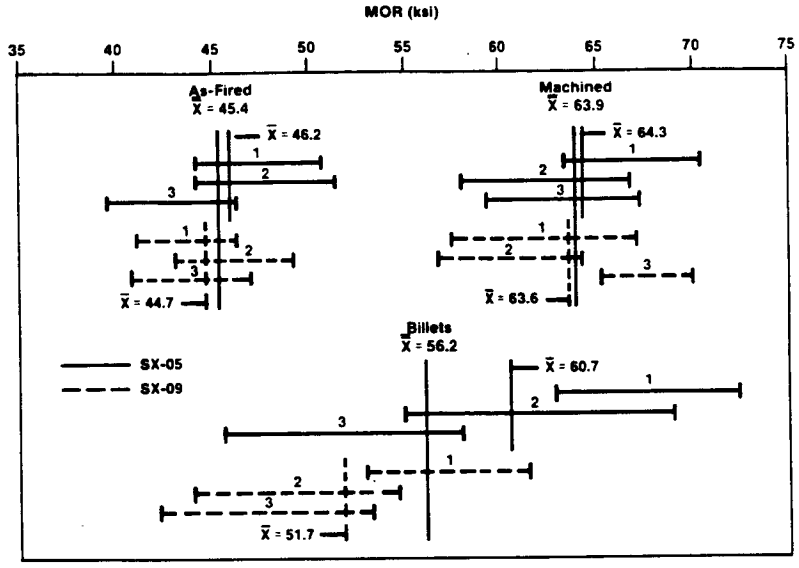

Figure 83. 95% Confidence Limits on Test Bars

The correlation is strong between average number of inclusions in the four green billets from which MOR bars were subsequently machined with a lower average number of inclusions resulting in a higher strength as shown in Table 55.

Table 55

Correlation of Billet MOR with No. Inclusions in Green Billets

Mix	Average Inclusions	MOR (ksi)
05-2	2.00	62.0
09-1	2.75	57.4
05-3	10.50	51.8
09-3	14.25	47.8
09-2	22.00	49.4

In all three test bar scenarios, the average MOR of three SX-05 batches was higher than that of the SX-09, although the average variability was higher on 05 than 09. The robustness of both mixes was rather poor, particularly for billet test bars. Carborundum proposed using 05 for future development and engine quality components because of its higher MOR and fabrication ease.

Complete fractography was conducted to identify failure origins. One as-fired sample (05-2 low) contained obvious flaws (Figure 84). Failure origins in other test specimens were not readily identified (Figure 85). In all six samples, the failure origins were located on the surface near an edge. Exaggerated grain growth was suspected as the primary reason for surface failure.

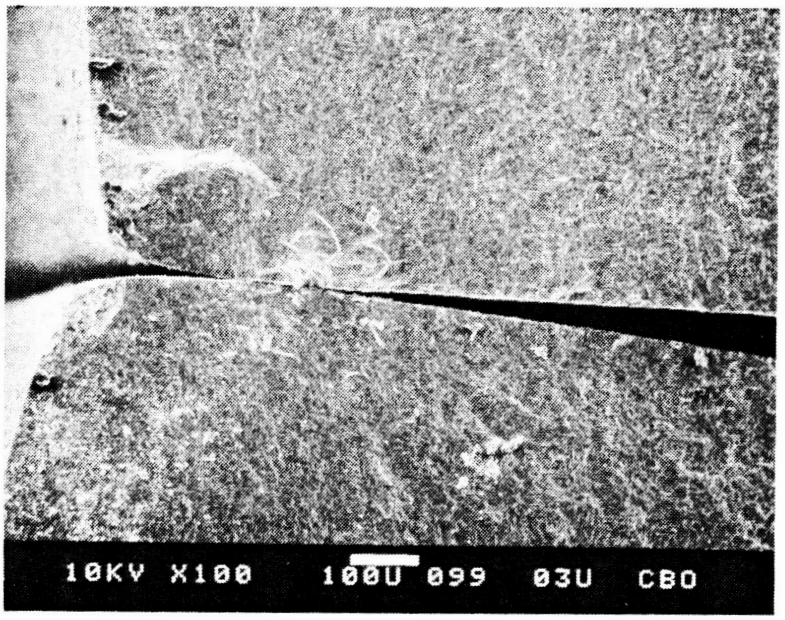

Figure 84. Obvious Edge Damage Surface Flaw

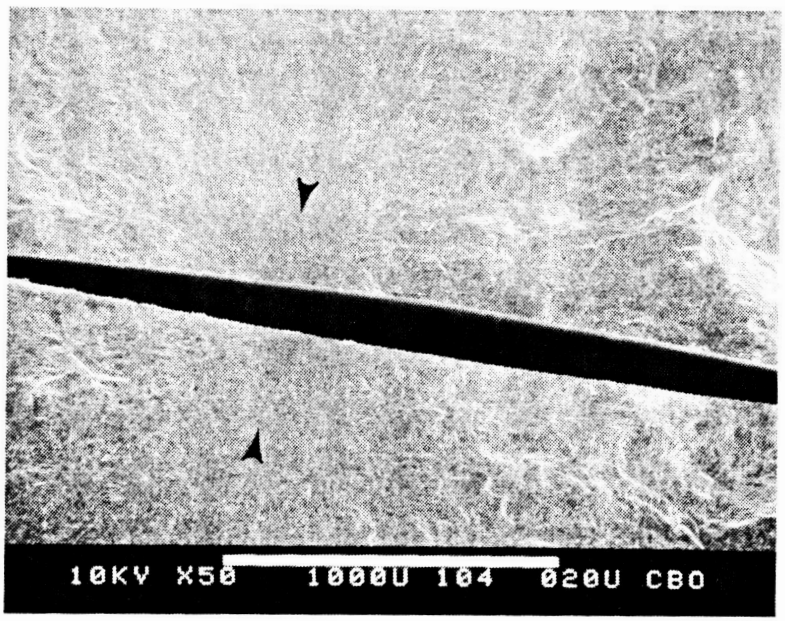

Figure 85. Unclear Surface Flaw Failure Origin

The primary reason for failure of the machined/annealed bars and the machined/annealed bars cut from billets was poorly sintered regions or processing flaws at or near the surface (Figure 86). Poorly sintered or porous regions were evident on bars from all MOR ranges; the primary difference was that the defect size was smaller in the higher strength bars. Forty (40) flaws were identified from 32 locations (including chamfer) on a total of 35 bars. Figure 87 shows log flexural strength versus log flaw size, for all MOR values. The plot is a relatively straight line; with equivalent flaw size, the strength values increase as the flaw location shifts from the surface inward.

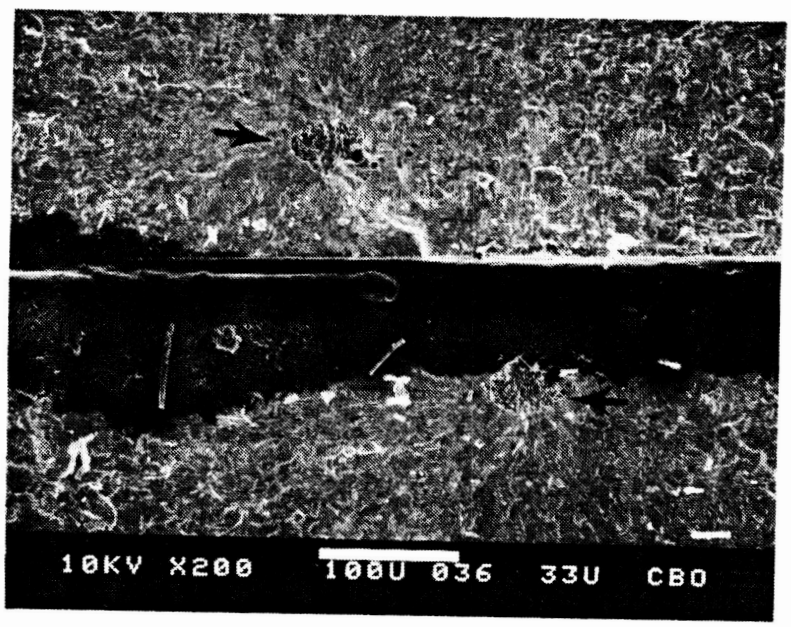

Figure86. Poorly Sintered Region 75μm From Surface; Strength of Bar 61.7 ksi

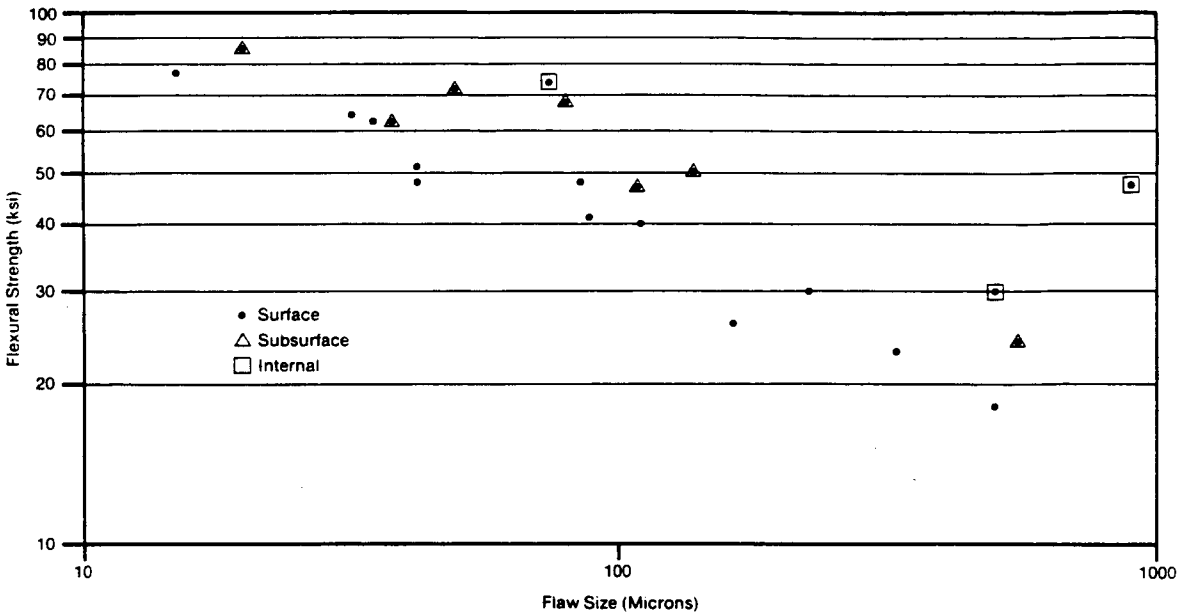

Figure 87. Log Flexural Strength Versus Log Flaw Size

Compound Preparation Evaluation

High density inclusions are typically observed by X-ray in injection molded components. The goal of this subtask was to determine the nature and source of inclusions and to identify removal procedures. Figure 88 is a flow chart of injection molding steps and the experimental methodology used.

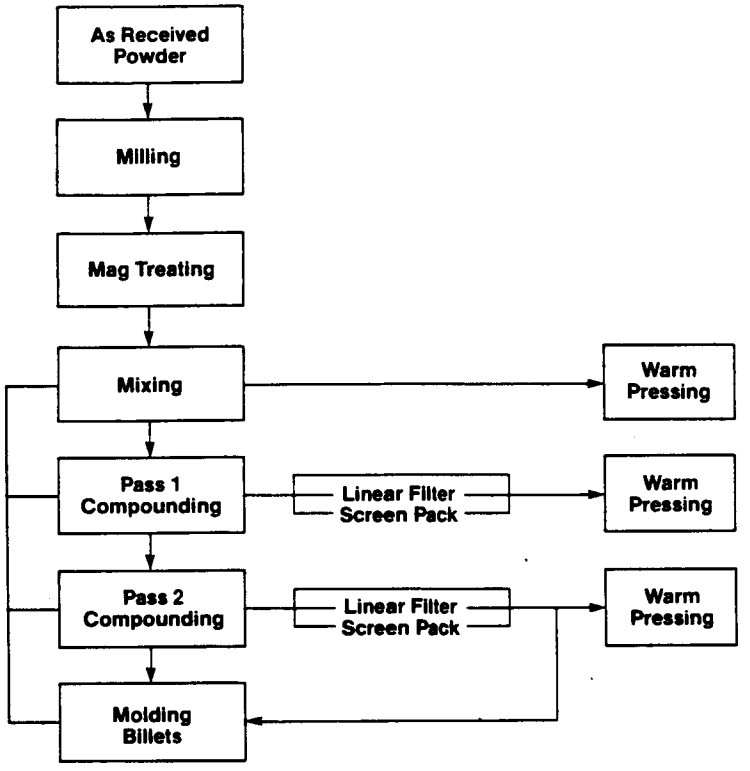

Figure 88. Compound Preparation Evaluation Flow Chart

Preliminary inclusion sources were first addressed. The ball mill covering, which was not made from a galvanized or stainless steel material to prevent oxidation, was lined with 1/8" thick rubber. The grease initially used to lubricate the screw retaining bolts contained metallic particulates and became fluid at the injection molding temperatures, and was replaced by a grease which is not liquid at the operative barrel temperatures.

Five billets were molded from each of six batches (three SX-05 and three SX-09) after mixing and after each of two conventional compounding steps as shown on the left in Figure 88. The X-ray results as shown in Table 56 were variable. The number of inclusions in SX-09 was, in all but one comparison, higher than in SX-05. The number of inclusions in the third SX-09 batch was excessive after mixing and after Pass 2 compounding. Analysis of the screen pack inclusions by SEM/EDS indicates these inclusions were SiC chips which most likely result from dry ball milling media. The results for Sample 09-3, i.e., the magnitude of the inclusion count for mixing and Pass 1 compounding are difficult to understand, and may possibly reflect a sampling problem.

Table 56

Inclusions Per Billet in SX-05 and SX-09 Samples

	05-1	09-1	05-2	09-2	05-3	09-3
Mix	1	4	1	4	5	244
Pass 1	2	1	1	30	2	6
Pass 2	1	2	1	4	6	90

In the original contamination study, the potential effect of cross contamination by molding was not taken into account. A second program was initiated to identify and to eliminate the contamination. In this second program, a mix was subdivided into thirds to evaluate the effect of filters. One third was compounded twice as a control. A second third was compounded twice through a linear filter to remove .010" and larger inclusions. The final third was compounded twice through a 250M screen pack to remove .0025" and larger inclusions. Two plates each were then warm pressed after mixing, Pass 1 compounding, and Pass 2 compounding. The results in Table 57 show that the use of a screen pack eliminated the observed inclusions. Once again a sampling error is assumed to be the cause of the apparent minor inconsistencies in Table 57.

Table 57

X-Ray Inclusions Warm Pressed Plates

		Incls/ Billet
Mixing		0
Pass 1	Compounding	
	Conventional	0
	Linear Filter	1.0
	Screen Pack	0
Pass 2	Compounding	
	Conventional	2.5
	Linear Filter	1.0
	Screen Pack	0

Twenty additional billets (and 300 small and large test bars for subsequent processing and MOR testing) were molded for each of the three Pass 2 compounding scenarios (bottom arrow Figure 88), 10 each with and without a 250M screen pack. Figure 89 displays the X-ray results of the green billets from the three different compounding scenarios. The detectable inclusions are greatly reduced when a screen pack is used in compounding and virtually eliminated using a screen pack during molding. Subsequent demonstrations revealed that minor sink marks occur when a screen pack is used in molding large shapes, probably because of the pressure drop differential. This required further investigation on the transition duct.

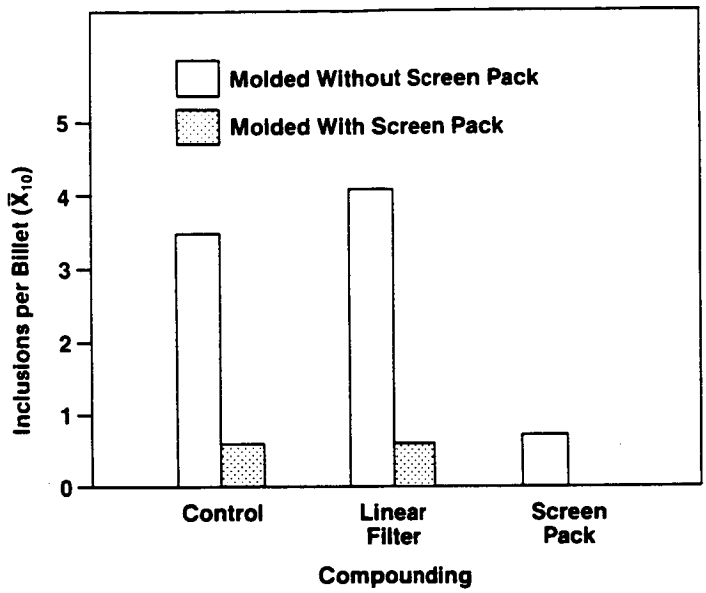

Figure 89. Inclusions Per Billet SX-05

The screen packs were dismantled and microscopically examined. The inclusions, mostly SA SiC chips from milling, were retained in all the incoming screens. The detrimental effect of high density inclusions in green billets on subsequent MOR was described in the previous section.

Task II. Subscale Transition Duct Experiments

Subscale transition ducts were fabricated in-house to control and monitor all molding parameters. Optimized molding conditions would be subsequently translated to full scale molding off site. The approach was to 1) conduct a flow analysis and cooling analysis, 2) construct a tool based on those analyses and verify through molding, and 3) outline an experimental design and run.

The flow analysis goal was to optimize specific molding variables which keep shear rates and shear stresses as low and uniform as possible. A flow analysis was conducted on a transition duct configuration having about 17% of the volume of a full size duct (Figure 90), a size designed to produce a molded part weighing about 500g. The results demonstrated that the 11/32" sprue bushing was preferable to the smaller 5/32" sprue bushing, and that flow imbalance was addressed by altering thicknesses within the gate. The gate balance was improved by reducing the gate thickness on the airflow diverter and thermocouple port side. This restricted the flow into this side which, because of its increased thickness, provided less resistance to flow once material entered that section.

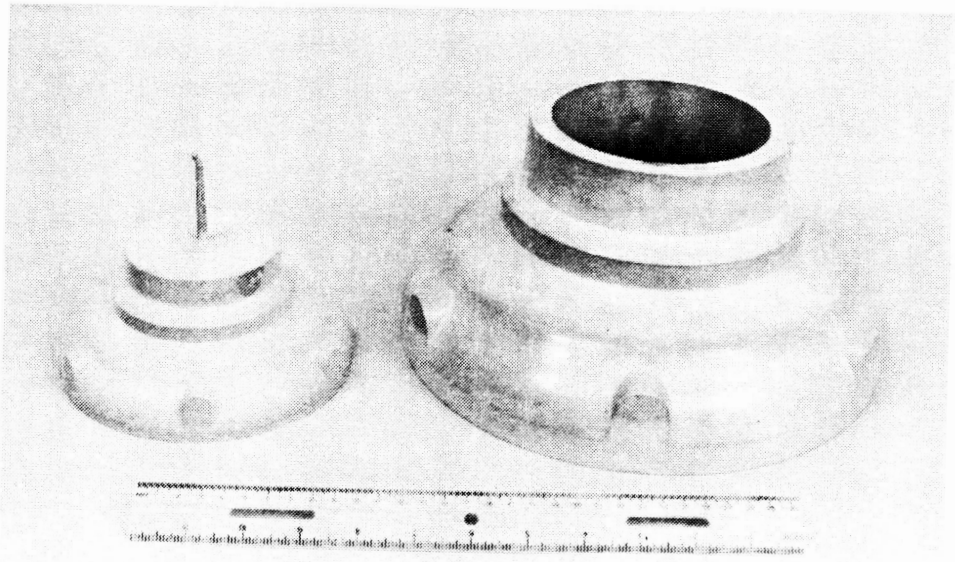

Figure 90. Subscale and Full Size Molded Transition Ducts

The cooling analysis goal was to provide uniform duct cooling in the tool. The approach was to design the tool with proposed cooling lines and then to run the cooling analysis and incorporate the recommended changes. The tool is designed first to locate leader pins, push-out pins, rings, and other items, and then to design around those mechanical requirements.

The original tooling configuration (Figure 91) had four separate in and out cavity lines and four vertical core baffles symmetrically located high up in the core, two of which are shown.

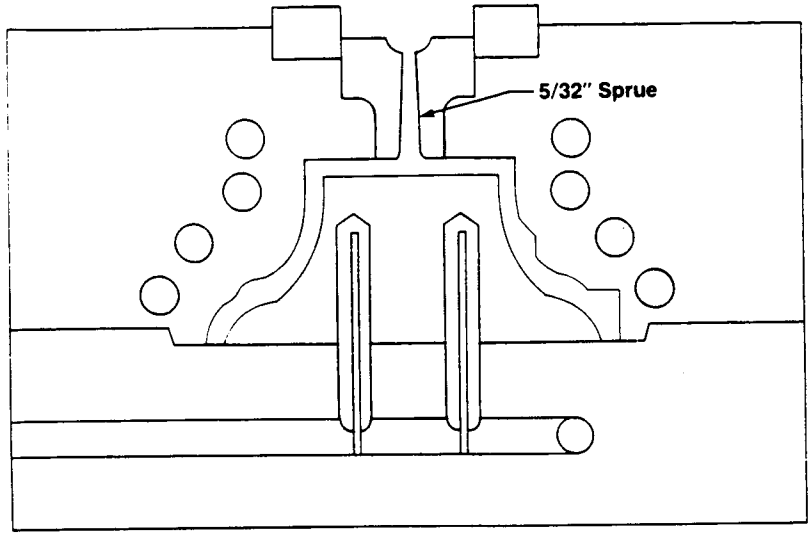

Figure 91. Original Cooling Configuration

The modified cooling configuration (Figure 92) shows the cavity lines unchanged, but the core cooling was changed from four vertical baffles near the center to eight in a circle farther down. In this way, cooling is concentrated on the thicker sections to increase the cooling rate through the plastic there to permit the part to cool uniformly through its cross section.

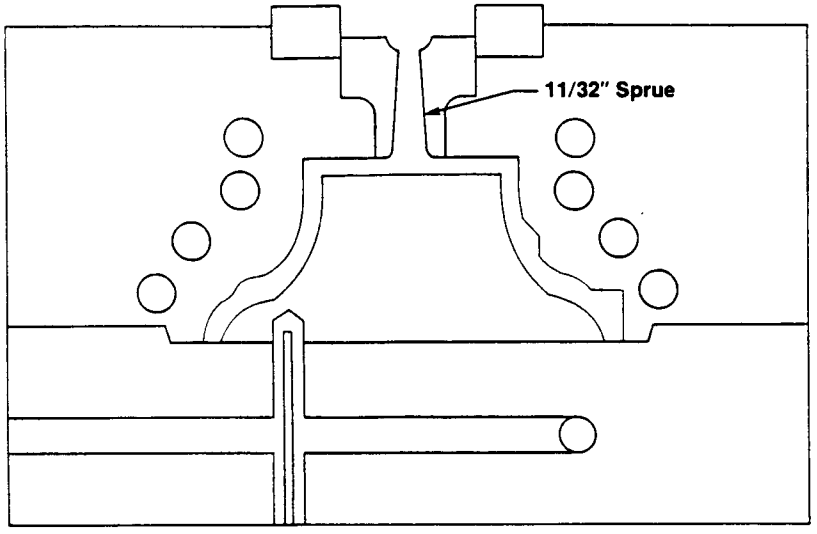

Figure 92. Modified Cooling Configuration

Using the flow analysis and cooling analysis input, the subscale duct tool was fabricated with two sprue configuration options (5/32" and 11/32") and two gate configuration options (uniform gate and balanced gate). The short shots with the uniform gate corroborated the flow analysis findings: the last place to fill is opposite the airflow diverter and thermocouple ports. The increased thickness on the airflow diverter side provides less resistance to flow once material enters that section and therefore fills first.

The subscale tool was originally designed to provide uniform duct cooling using conventional injection molding practices. Subsequent success with another component with respect to knit line reduction and improved surface appearance suggested heating the mold to a higher temperature followed by cooling in the same molding cycle. The original approach was to modify and upgrade a two-zone hot oil system using the previously described channels for heating and then cooling. An alternate, more efficient method was subsequently used which proved to be more adaptable to a production cycle. Two alternate cavity lines were heated with hot oil from one zone; the other two were cooled with water. The eight vertical core baffles were heated with hot oil from the other zone and spiral cooling lines in the core center were cooled with water. The cooling analysis suggested this alternative for thermal cycling of the tool.

A 2^{8-4} Taguchi L16 design was formulated to minimize confounding in what are perceived to be the most important main effects and also to get interactions for important main effects. The factors and the linear graph are shown in Figure 93.

A: Mold Temperature
B: Velocity
C: Back Pressure
D: Sprue Size
E: Gate Configuration
F: Pack Time
G: Hold Time
H: Melt Temperature

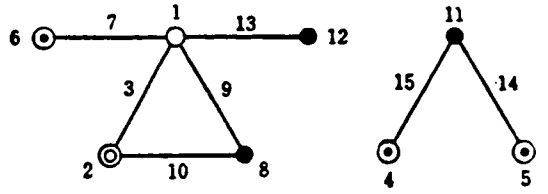

Figure 93. 2^{8-4} Taguchi L16 Factors and Linear Graph

The response variables include flow lines, sink marks, blisters, and mottling, the latter recorded as a percentage of the surface that is mottled. The percent contribution from ANOVA of molding factors on the four response variables is set forth in Table 58. The balance of the contribution is assigned to the interaction columns.

Table 58

Percent Contribution of Molding Factors on Response Variables

	Response Variable				
Factor	Flow Lines	Sink Marks	Blisters	Mottling	Green Weight
A: Mold Temperature	51	11	2	80	23
B: Velocity	8	0	4	2	1
C: Back Pressure	0	12	0	0	25
D: Sprue Size	0	13	16	0	8
E: Gate Configuration	2	0	0	0	7
F: Pack Time	0	11	0	0	9
G: Hold Time	4	9	2	0	13
H. Melt Temperature	2	0	53	2	5
Error	12	18	27	9	7
TOTAL	79	74	54	93	98

Mold temperature is the most important factor for flow lines and mottling. Higher temperatures significantly reduced the flow line number and virtually eliminated mottling. Sink marks are the result of failing to pack out the material long enough before the gate freezes. At high mold temperatures, long pack and/or hold times are required.

In experiments of this type, compromises are often required when trying to minimize all problems. Table 59 shows the factor levels for minimizing four response variables and maximizing green weight and the process average for each. A variety of compromise levels are also given. The goal was to minimize the first four response variables and possibly maximize green weight for dimensional control. The best process average for flow lines corresponds to Trial 13 whereas Trial 14 actually produced the fewest flow lines. The best compromise is given in Line 4.

Table 59

Best Process Average Factor Levels

Factor	Flow Lines	Sink Marks	Blisters	Mottling	Green Weight
A	2	1	1	2	1
B	2	2	1	2	1
C	1	2	2	1	2
D	2	1	1	2	1
E	2	2	2	2	1
F	1	2	1	2	2
G	1	2	1	1	2
H	1	1	1	1	1
Best Process Average	7.2	-1.6	-1.2	-5.8	523.2
A B C D E F G H					
1) 2 2 1 2 2 1 1 1(1)	7.2	2.1	4.3	-1.9	501.3
2) 2 2 1 2 2 2 2 2(2)	28.3	0.8	6.8	7.1	505.4
3) 2 2 1 1 2 2 2 1	21.1	-0.1	2.5	0.2	510.3
4) 2 2 1 1 2 2 1 1	8.6	0.5	1.4	-3.8	506.9

(1) Best for flow lines
(2) Best trial for flow lines

As of the end of this reporting period, the molding of all of the L16 experimental subscale transition ducts was completed. The as-molded inspection and analysis was subsequently performed to complete that portion of the experiment.

2.0 Turbine Backshroud (CBBB)

Hexoloy ST (a titanium diboride particulate reinforced pressureless sintered alpha SiC) was chosen as an advanced material for this application instead of SA SiC because of its increased fracture toughness and increased strength.

Ram Pressing

Ram pressing was identified as a potential near net shape forming process for this component. This process is used commercially for high volume production of chinaware and particularly for large area contoured dish-like configurations with thin uniform cross sections, ideally fitting the backshroud's requirements.

Although the ram press process requires specialized equipment for material preparation and forming, it is well established within the traditional ceramics industry. A local chinaware manufacturer allowed Carborundum to utilize their ram pressing equipment for this program.

Initial development activities related to binder and lubricant composition were conducted in-house on small scale equipment. When specific compositions were scaled up and processed in larger scale equipment of various types, the same viscosity versus shear relationships were not duplicated.

The information gained during the previous program provided insight for the formulation of an experimental plan based upon the processing of full scale components of a configuration simulating a backshroud.

An experimental program addressing more fundamental powder issues was designed and approved for the program year. This design focussed on feedstock preparation and carbon source and included binder, water content and mixing variables carried out on production scale equipment. The revised workplan consisted of the following tasks.

Task I:	Composition Development - SA SiC
Task II:	Fabrication of Ram Pressed SA SiC Backshrouds
Task III:	Composition Development - ST
Task IV:	Fabrication of Ram Pressed ST Backshrouds
Task V:	Fabrication of Engine Quality Components

SA SiC was selected for initial ram pressing process development because Carborundum had acquired substantial experience in aqueous processing of sintered alpha silicon carbide for slip casting and extrusion. It was anticipated that successful ram pressing of SA SiC could be readily adapted to the very similar Hexoloy ST material.

Early in this reporting period, strength tests on ST were conducted after oxidation and exposure to a turbine engine environment. Substantial and not unexpected strength degradation was exhibited below the 2500°F maximum operating temperature.

The oxidation problem was anticipated and a parallel effort had been initiated to CVD coat the Hexoloy ST with a more oxidation resistant coating of silicon carbide.

This coating technology had been demonstrated on a laboratory basis to be an effective oxidation barrier. However, the scale-up to an off-site vendor for larger components or larger numbers of test bars was not completely successful. Coating inconsistencies resulted in large strength variations which would be unacceptable in backshroud components.

The turbine backshroud program, therefore, was revised to concentrate on the delivery of engine quality Hexoloy SA SiC components only.

If the higher fracture toughness of ST is required and the scale-up of the CVD SiC coating is completed, the program was to be redirected to adapt the SA SiC forming technology to ST backshrouds.

The specific tasks in the 1989 workplan were revised to include the following:

Task I:	Composition Development - SA SiC
Task II:	Fabrication of Ram Pressed SA SiC Backshrouds
Task III:	Fabrication of Engine Quality Components

Task I - Composition Development - SA SiC

The objective of this task was to develop a mix with the following properties: 1) high yield stress to prevent slumping after forming, 2) strongly shear thinning behavior (pseudoplasticity) to allow forming under high shear stress, and 3) sufficiently high solids loading to obtain a system with reasonable shrinkage characteristics.

Previous work established the approximate mix viscosity required for ram pressing. Two statistically designed experiments were then formulated to address the more fundamental parameters but on production scale equipment at an external vendor's facility.

These experiments addressed the type of carbon source used as a sintering aid and the method by which the material was prepared. The intent was to determine whether decreasing the number of steps in the preparation process would result in better process control and product quality. Table 60 shows the Experiment No. 1 matrix which consists of a Taguchi L8 and a Taguchi L4.

Table 60

Composition Experiment No. 1 to Investigate Effect of Mix Ingredients, Powder Processing, and Viscosity

L8 Column No.		1	2	4	7
Design Order	Carbon Source	Powder Prep.	Binder Amt.	Viscosity	Binder Type
1	C (-)	A (-)	Lo (-)	Lo (-)	K (-)
2	C (-)	A (-)	Lo (-)	Hi (+)	S (+)
3	C (-)	A (-)	Hi (+)	Lo (-)	S (+)
4	C (-)	A (-)	Hi (+)	Hi (+)	K (-)
5	C (-)	B (+)	Lo (-)	Lo (-)	S (+)
6	C (-)	B (+)	Lo (-)	Hi (+)	K (-)
7	C (-)	B (+)	Hi (+)	Lo (-)	K (-)
8	C (-)	B (+)	Hi (+)	Hi (+)	S (+)
L4 Column No.			1	2	
1	D (+)	A (-)	Lo (-)	Lo (-)	
2	D (+)	A (-)	Lo (-)	Hi (+)	
3	D (+)	A (-)	Hi (+)	Lo (-)	
4	D (+)	A (-)	Hi (+)	Hi (+)	

A sufficient quantity of SiC powder was allocated for the backshroud development program to eliminate powder lots as a variable.

During initial experiments with the two types of carbon sources, a dispersion problem was encountered with carbon source D . This was resolved through the use of a higher than normal concentration of dispersant.

Powder was processed per preparation methods A and B. Eight experimental 25 pound mixes in the L8 experiment were processed through extrusion, ram processing, and drying. Four to eight dish-like plates were molded from each batch and subsequently dried on a previously established cycle. All of the samples exhibited severe drying cracks both externally and internally via X-ray.

Even though many of the response variables could not be evaluated because the samples were not sintered, a comparison of the two powder preparation methods was made. Method A produced a coarser, less uniform material which was unstable in that viscosity increased with age. In addition, this material had a greater tendency to stick to the ram pressing molds and green density values were lower.

Based upon these results, Carborundum elected to cancel the L4 column of this experiment and proposed an expanded Experiment No. 2 which would include various binder systems and drying parameters for each specific binder system.

In view of the processing difficulties encountered, Carborundum looked at viable alternatives and identified near net shape cold pressing and green machining. This approach became viable in the period subsequent to the start-up of the ram pressing activity and as a result of the purchase and installation of a 600 ton hydraulic press.

At this time, however, GAPD indicated that a redesign was being initiated on some engine components, including the backshroud. Until this is completed and the backshroud is redefined, fabrication was put on hold.

3.0 Wave Spring (CBBC)

The objective of this task was the development of a low cost fabrication process for high quality, reproducible wave springs with predictable properties.

Three configurations described below were under consideration:

P/N	I.D.	Wall	Thickness	Wave Amplitude
3612423	6.235"	.200"	.040"	.200"
3612424	6.235"	.200"	.140"	.165"
3612425	6.120"	.402"	.100"	.170"

Although similar in configuration, these wave springs have thicknesses and wave form amplitudes which suggested two potential fabrication methods. For the thinnest component a plastic extrusion and stamping process appeared viable. For the thickest component a dry pressing process was identified.

The fabrication process for the intermediate thickness wave spring was to be selected based upon the outcome of the above development efforts.

The major issues in the fabrication of these configurations and which are addressed in the workplan are:

- o Dimensional control of size and tolerance.
- o Elimination of distortion on sintering.
- o Formation of accurate wave form contour.
- o Low strength of "green" component due to very small cross sections.
- o Significant cost of diamond machining from blanks due to the wave form configurations.
- o Reproducibility of optimum properties.

In order to provide finished components for initial evaluation by GAPD, wave springs of all three designs were fabricated during 1987 and early 1988 using isopressing/green machining and final machining. All parts were green machined into flat rings which were O.D., I.D., and wave ground after sintering and NDE. Specific care was taken to minimize stresses within the parts through annealing prior to and after machining.

During contract Years I and II an extrusion/stamping process was investigated for the thinnest wave spring (P/N 3612423) and a dry pressing process was investigated for the thickest wave spring (P/N 3612424).

3.1 Extrusion/Stamping - Wave Spring P/N 3612423

Plastic extrusion and stamping were chosen because of the high green strength of this material which is of extreme significance for P/N 3612423 and its 0.040" thickness and 0.200" amplitude. Development was initiated in accordance with the workplan tasks listed below:

Task I: Fabrication of Sheet Stock
Task II: Processing of Flat Rings
Task III: Fabrication of MOR Bars
Task IV: Processing of Waved Rings
Task V: Evaluation of Process and Configuration
Task VI: Fabrication of Engine Quality Components

Even though GAPD deleted P/N's 3612423 and 3612424 from the workplan, Carborundum proposed to continue this effort since extrusion/stamping appeared viable for fabricating the .100" thick P/N 3612425. The following revised set of tasks was formulated:

Task I: Process Optimization
Task II: Processing of Waved Rings
Task III: Process Verification
Task IV: Fabrication of Engine Quality Components

Prior to initiating any of these tasks, Carborundum was directed on February 10 to terminate all wave spring activities as the remaining P/N 3612425 was deleted from the AGT 101 engine.

3.2 Dry Pressing - Wave Spring P/N 3612424

P/N 3612424 was originally selected for dry press processing because of its more rugged thickness (0.140") and its minimum wave amplitude (0.160"). When this P/N was cancelled at the end of the last contract year and efforts were transferred to P/N 3612425 only, Carborundum proposed to assess this process for the latter. P/N 3612425 has a greater wall thickness but is thinner and has more wave amplitude. Rather than fabricate a new die for this wave spring, the use of tooling for P/N 3612424 was proposed and the revised series of tasks was developed as follows:

Task I: Demonstration of 0.100" Pressed Thickness Capability
Task II: Procurement and Qualification of Tooling for Flat Rings (P/N 3612425)
Task III: Fabrication of MOR Test Bars
Task IV: Fabrication of Waved Rings
Task V: Fabrication of Engine Quality Components

Some of the ongoing activity relative to the preceding wave spring and applicable to the new P/N 3612425 was continued.

Additional dry pressed wave springs, P/N 3612424, were sintered on graphite wave form mandrels. Wave amplitude ranged from 0.146" to 0.150" on three springs, however, it was not uniform. The amplitude increased from the O.D. to the I.D. possibly due to higher than predicted shrinkage (lower green density samples) and buckling on the mandrel. Further sintering trials were planned.

4.0 Test Specimens (CBBD)

4.1 Test Specimens for Material/Process Characterization

The two sets of 250 test bars fabricated using the developed injection molding and ram pressing processes were postponed so as to correspond with the processing of engine quality components. These engine deliverables were rescheduled to 1990 so that major emphasis in 1989 could be directed at gaining a better understanding of processes and materials.

4.2 Test Specimens for NDE Development

The objective of this task was the characterization of Hexoloy SA SiC material fabricated by the various processes being developed under this program. As part of this task, procedures for introducing both high and low density seeded defects into injection molded billets were to be developed. During this report period, sintered SiC and graphite spheres were fabricated and four different size ranges were screened for seeding materials. The size ranges are:

Nominal Size(μm)	Mesh	Microns
50	-270/+325	- 53 + 44
100	-140/+170	-105 + 88
300	- 45/+ 50	-355 +297
500	- 35/+ 40	-500 +420

Fourteen billets (5.5" x 1.5" x 0.35") were injection molded from a standard SX-05 composition that contained 1% graphite screened to -35/+40 mesh (420μm-500μm). All 14 billets were evaluated by X-ray where the low density graphite showed up as small dark spots uniformly distributed throughout the samples. A higher intensity background light was needed to see the spots in the negatives. Visual comparison of the spots to a dot standard indicated that the particles were somewhere between 321μm and 635μm, meaning the particles did not break down during compounding.

This experiment showed that X-ray can easily detect voids or low density inclusions in the 420μm-500μm size range.

A second set of 14 billets was seeded with sintered spray dried SiC screened to -45/+50 mesh (297μm-350μm). The molded billets were examined by X-ray where the inclusions showed up as irregular-shaped bright spots scattered throughout the billet. The size of the bright spots, as determined by visual comparison to dot standards, ranged from less than 125μm to approximately 500μm. The reason for the large fraction of particles smaller than 297μm was believed to result from the breaking up of the spray dried material during compounding.

A second SX-05 mix was seeded with SiC grit sieved to -140/+170 mesh (88μm-105μm). The grit was used instead of the spray dried SiC because it is less likely to break up during compounding. Fourteen billets were molded with the mix and subsequently evaluated by X-ray. The X-ray negatives revealed numerous bright spots throughout all of the billets. Several of the large inclusions were removed from one of the billets and were found to be metallic (they were magnetic). Apparently the abrasive SiC grit added to the mix abraded the screw and barrel of the injection molding machine, contaminating the billet with metal.

Future activity directed at the identification of both types of high density inclusions in both molded and sintered SA SiC is planned.

4.3 NDE Development

Real-time Radiography

NDE development activities using real-time radiography were conducted to provide a method to detect inclusions in green injection molded SiC. Billets were produced using sintered SiC spheres as defect seeds. Sintered SiC was chosen since it has a much lower linear attenuation coefficient than any of the other identified sources of contamination. The linear attenuation coefficients for 100 kV X-ray source are as follows:

SiC	58.3/cm
Yellow Brass (67% Cu, 33% Zn)	1922.2/cm
316 Stainless Steel	1388.3/cm
(3% Mo, 18% Cr, 2% Mn, 14% Ni, 1% Si, 62% Fe)	

Techniques developed for detecting sintered SiC contamination will be applicable for higher attenuating materials since they would provide an X-ray with much higher contrast between the contaminants and green SiC.

Detecting inclusions in injection molded SiC and identifying their source is important for the production of reliable components. Real-time radiography is useful for this purpose since the part orientation can be easily varied to give the best viewing angle for detection. Another advantage is that the images are detected electronically and the signals can be digitized, thus making possible quantitative measurements of the X-ray transmission of the inclusion and thus classification into metallic and ceramic inclusions.

Measurements were made on the detectability of inclusions in a 5.5" x 1.5" .375" green injection molded billet that had been seeded with SiC particles. The particulate was difficult to see when viewing the direct video image, but could be detected when viewing an image formed by averaging at least 16 video fields. The visibility is enhanced by expanding the contrast and the maximum expansion can only be done when spatial variations in the response of the image convertor/intensifier and video chain are removed. This is easily done by subtracting a blurred version of the image from itself. The resulting image shows inclusions as dark spots which range from 200μm-500μm in diameter.

The system can be calibrated in terms of X-ray absorption if there are known changes in thickness in the field. Billets examined as above for inclusions contained two depressions on the surface from the injection molding push-out pins. These indentations which represented a 2-1/2% reduction in thickness could be readily detected. The change in video signal in that region could be equated to an equivalent change in SiC thickness. This could be used to distinguish between metallic and SiC inclusions.

Quantitative measurements of X-ray transmission can also be done on film if there is a reference material exposed on the same film. A proposed technique is to make a reference from several particles of various sizes of typical inclusion materials and encapsulate them between plastic films so that it can be used on each sample radiographed. By digitizing the films, the transmission change for an unknown inclusion can be compared to the same size reference, thus identifying the type of inclusion.

X-Ray Tomography (CT)

The use of X-ray tomography (CT) for evaluation of density uniformity in green and sintered components requires calibration standards of known uniformity. These in turn can then be used to assess the algorithms used in the CT data processing to remove the effects of beam hardening. Beam hardening is the change in the spectral distribution of an X-ray beam as it traverses through a part. It makes the outer edges of a part appear denser than the interior. One of the difficulties in evaluating the accuracy of these algorithms is having ceramic test samples with known uniformity. One solution is to use another material with similar X-ray absorption characteristics such as aluminum. Since the absorption spectra are not identical, the accuracy of this substitution must be checked.

These measurements were performed on an industrial tomography system at Scientific Measurement Systems in Austin, Texas using a prototype of the machine which was delivered to the BP Research Center-Warrensville in September 1989. Previous calibrations for beam hardening were done at 225 kV with a 30°-60°-90° wedge of 2024 aluminum positioned so that the 15 cm side opposite the 30° angle was parallel to the beam. A thin brass filter was used to preharden the beam. This data was used to correct the measured CT density distribution which should be uniform in a sintered isopressed rectangular bar of SiC oriented either as a 2.5 by 5.0 cm cross section, or as a 15.0 by 2.5 cm cross section. With the smaller cross section, the beam hardening correction didn't remove the apparent low density area in the center. For the higher aspect ratio case, the algorithm over corrected and made the regions where shorter path lengths overlap appear too dense (Figure 94).

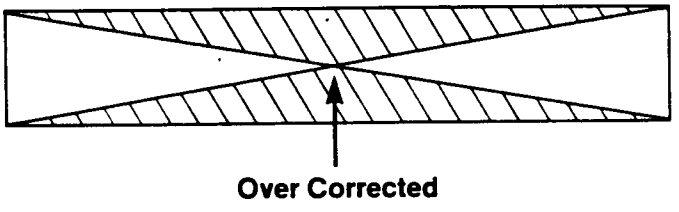

Figure 94. Over Corrected Beam Hardening Illustration

One reason why aluminum may not be a better match to SiC is the 2%-3% of copper added as an alloying element. This increases the absorption and it becomes important to test the beam hardening corrections with uniform materials of controllable concentrations.

This is best done using water solutions of X-ray absorbing salts such as potassium iodide (KI). A plexiglass container with the same interior dimensions as the 30°-60°-90° aluminum wedge was filled with a 10 wt% solution of KI. The transmission through the 0 to 15 cm path length was measured and used as an input to the algorithm for the beam hardening corrections. This technique was then applied to scans of 3%, 10%, and 16% KI solutions in a styrofoam cup. While a profile through the circular cross section of a 10% solution is uniform after applying the beam hardening correction, the 3% solution is over corrected, i.e., the corrected density appears lower at the outer edge than at the center. The opposite happens for the 16% solution as it is under corrected and still appears somewhat beam hardened.

4.4 Tensile Rupture Specimens

Fabrication of the required tensile rupture specimens was initiated during this reporting period. Fifty cylindrical billets were isopressed, green machined, sintered and delivered to the machining vendor.

C3

APPENDIX III

ANNUAL TECHNICAL PROGRESS REPORT
GARRETT CERAMIC COMPONENTS DIVISION

ADVANCED TURBINE TECHNOLOGY APPLICATIONS PROJECT

GARRETT CERAMIC COMPONENTS 1989 ANNUAL TECHNICAL PROGRESS REPORT FOR GARRETT AUXILIARY POWER DIVISION

I. INTRODUCTION

The objective of this 37 month technical effort begun in July 1988 is to develop a fabrication process with the potential for low-cost, mass production of AGT101 turbine rotors using Garrett Ceramic Components GN-10 silicon nitride. Pressure slip casting will be the primary fabrication approach. Materials and components will be extensively characterized and NDE methods developed and evaluated for improved process control and material/component qualification. In Task A, fabrication of the AGT-101 rotor using GN-10 silicon nitride and pressure slip casting will be developed. In Task C, GN-10 test specimens and NDE seeded defect standards will be fabricated by pressure slip casting.

II. TECHNICAL PROGRESS SUMMARY

TASK A. FABRICATION OF AGT-101 ROTOR BY PRESSURE SLIPCASTING

SUBTASK A.A FABRICATE ROTORS AND BILLETS USING BASELINE PROCESS

The initial evaluation conducted under Subtask A.A was an evaluation of casting of the AGT101 rotor using baseline GN-10 slip with no pressure assist during casting, so that subsequent effect of pressure slip casting could be determined. Non-pressure assisted slip casting of AGT101 rotors was performed during August through October 1988. The results observed were that rotors required 2.5 days to be fully cast. Extensive gas evolution in the slip was observed during casting, which resulted in extensive large porosity in the cast rotors. The baseline GN-10 slip became unstable after 10 to 12 hours and gelled, forming low cast density structures and resulted in extensive differential casting and drying shrinkages, which led to extensive rotor blade, hub, and shaft cracking. No blades were left attached to the rotor after mold removal. An example of a non-pressure assist cast rotor is shown in Figure 95.

Experiments conducted from September 1988 through January 1989 evaluated pressure casting of AGT101 rotors using the baseline GN-10 slip. The addition of pressure during casting reduced rotor casting times by 80 percent, down to 12 to 14 hours. Many blades remained attached to the rotors after mold removal and an extensive reduction in gas evolution was observed. A typical baseline pressure cast rotor is shown in Figure 95. Pressure slip casting of small billets (typically 0.375 to 0.5" thick) also revealed that pressure casting produces a much more homogeneous green density compact (much less

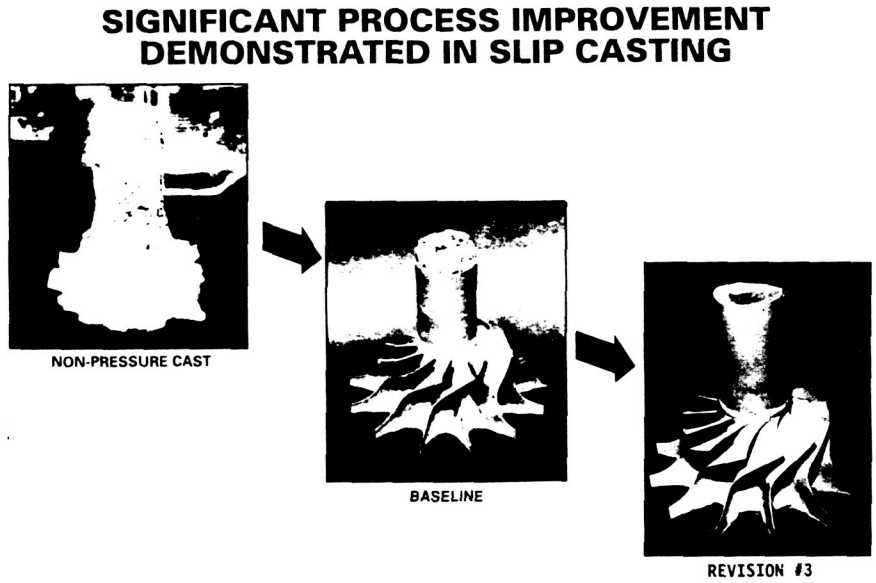

Figure 95. GN-10 AGT101 Rotors a) Non-Pressure Cast Baseline, b) Baseline Pressure Cast, c) Slip Revision #3 Processed.

drying warpage resulted) besides the extensive reduction in casting time. It was determined that pressure assisted casting does not result in substantial increases in green density.

Problems that still existed with the baseline rotor slipcasting process were that gas evolution of the slip during casting still existed, the baseline slip still became unstable after 10 - 12 hours leading to gelling and subsequent poor microstructures and differential drying shrinkage. These problems led to blade, hub, and shaft cracking during casting and mold removal. It was determined that the baseline slip was not reproducible, i.e. its properties were not repeatable.

In addition, it was determined that subsequent processing steps also created defects. The baseline drying and calcining steps also resulted in rotor and billet crack formation. The baseline encapsulation HIP process resulted in an extensive surface reaction layer and surface pitting.

Sixteen rotors in all were cast using the baseline slip casting process and seven were encapsulation-HIPed using the baseline HIP process. An evaluation of green density distribution across the baseline rotors from blade tip to blade tip and from hub bottom to shaft top revealed less than a 0.5% green density gradient across the rotor horizontally throughout the rotor but a 13% drop in

density from the rotor hub bottom to the shaft top due to slip instability, gelling and gas evolution. The green density gradient was eliminated during encapsulation-HIPing but the differential shrinkage resulted in poor HIPed rotor dimensional control due to the greater shrinkage at the rotor shaft top compared to the hub bottom.

Three HIPed rotors were cutup for mechanical property evaluation, along with numerous small thickness billets. The resulting mechanical properties are presented in Table 61. For the billets, results from two different machine shops are presented. After testing of bars from machine shop 1, it was determined that many bars were failing from machined flaws such as gouges and chipped chamfers. An evaluation of machine shop 2 bars revealed better and more consistent machined surface bars and the resulting increase in room temperature average strength, maximum strength values, Weibull values, and decrease in standard deviation. Examination of 2200 and 2500°F fast fracture strengths generated from billet source test bars indicates no significant difference between bars machined at each of the two machine shops. This is expected since high temperature air testing results in surface oxidation of the silicon nitride material, filling in machine damaged defects such as chips, cracks, and pits with SiO_2 and forcing the critical flaw to other sources. Four baseline rotors were delivered to GAPD in February 1989 for evaluation of the then current rotor fabrication process capability.

A comparison of baseline billet and rotor mechanical properties reveals an extensive reduction in strength at all temperatures for rotors, shown in Figure 96. This is the result of the poor green microstructures formed by slip outgassing and gelling during the extensive time required for casting the baseline rotors compared to billets, and baseline drying and calcining cycles which resulted in crack formation. The slip does not become unstable enough to affect billet green microstructures during the billet short casting times (0.75 to 1.0 hour) and the billets, being much thinner than rotors, were less susceptible to inadequate drying and calcining cycles. Rotor test bar fractography reveals that many failure origins occurred at pores, agglomerates, and vestiges of small cracks.

Allied-Signal Research and Technology initiated in-depth microstructural characterization on both baseline rotor and billet materials using STEM in 1989. The baseline rotors were examined from hub bottom to shaft top and from hub center to blade tip for any microstructure variations, including chemical and phase variances. The results are to be available in early 1990.

TABLE 61. Fast Fracture Mechanical Property Data Summary.

SOURCE	TESTED AT	MACHINE SHOP	AVG	MIN	MAX	STD. DEV.	NO.	WEIBULL
BASELINE SLIP PROCESS — BASELINE HIP PROCESS								
ROOM TEMPERATURE								
BILLET	GCCD	1	113.2	80.0	130.8	12.0	35	12.0
BILLET	GAPD	1	109.5	80.8	138.0	13.3	30	9.0
BILLET	GCCD	2	131.7	114.9	143.7	8.4	14	19.0
ROTOR	GCCD	2	92.3	57.5	122.7	18.9	23	5.7
2200°F								
BILLET	GAPD	1	95.4	65.6	108.0	13.2	30	17.1
BILLET	GCCD	2	90.4	85.2	101.1	5.8	5	----
ROTOR	GCCD	2	70.8	58.7	83.6	10.5	5	----
2500°F								
BILLET	GAPD	1	64.6	56.2	76.7	7.4	10	----
BILLET	GAPD	1	59.1	55.0	67.5	4.4	10	----
BILLET	GAPD	2	59.3	53.0	67.4	4.7	10	----
ROTOR	GCCD	2	39.2	36.4	41.9	2.2	5	----
BASELINE SLIP PROCESS — REVISED HIP PROCESS #1								
ROOM TEMPERATURE								
BILLET	GAPD	2	133.2	118.7	151.2	12.0	11	----
BILLET	GCCD	2	130.2	93.4	153.9	13.7	35	11.7
2200°F								
BILLET	GAPD	2	108.7	101.7	113.2	3.9	12	----
BILLET	GCCD	2	98.0	84.3	112.1	.6	9	----
2500°F								
BILLET	GAPD	2	70.8	60.2	81.2	7.0	10	----
REVISION #3 SLIP PROCESS — REVISED HIP PROCESS #1								
ROOM TEMPERATURE								
BILLET	GCCD	2	128.2	97.7	145.8	11.7	28	12.9
ROTOR	GCCD	2	128.3	98.7	145.1	11.9	29	12.6
2200°F								
BILLET	GCCD	2	92.7	86.4	99.4	4.1	9	----
ROTOR	GCCD	2	95.8	80.5	106.4	8.7	6	----
2500°F								
BILLET	GCCD	2	56.8	51.3	62.5	3.4	10	----
ROTOR	GCCD	2	65.9	60.6	70.1	3.2	6	----

Table 61. Continued

REVISION #15 SLIP PROCESS REVISED HIP PROCESS #1

SOURCE	TESTED AT	MACHINE SHOP	AVG	MIN	MAX	STD. DEV.	NO.	WEIBULL
ROOM TEMPERATURE								
BILLET	GCCD	2		BEING DETERMINED				
ROTOR	GCCD	2	126.1	101.0	145.7	12.0	28	12.3
2200°F								
BILLET	GCCD	2		BEING DETERMINED				
ROTOR	GCCD	2	89.5	77.8	96.2	5.4	10	----
2500°F								
BILLET	GCCD	2		BEING DETERMINED				
ROTOR	GCCD	2	53.9	49.9	57.8	2.4	10	----

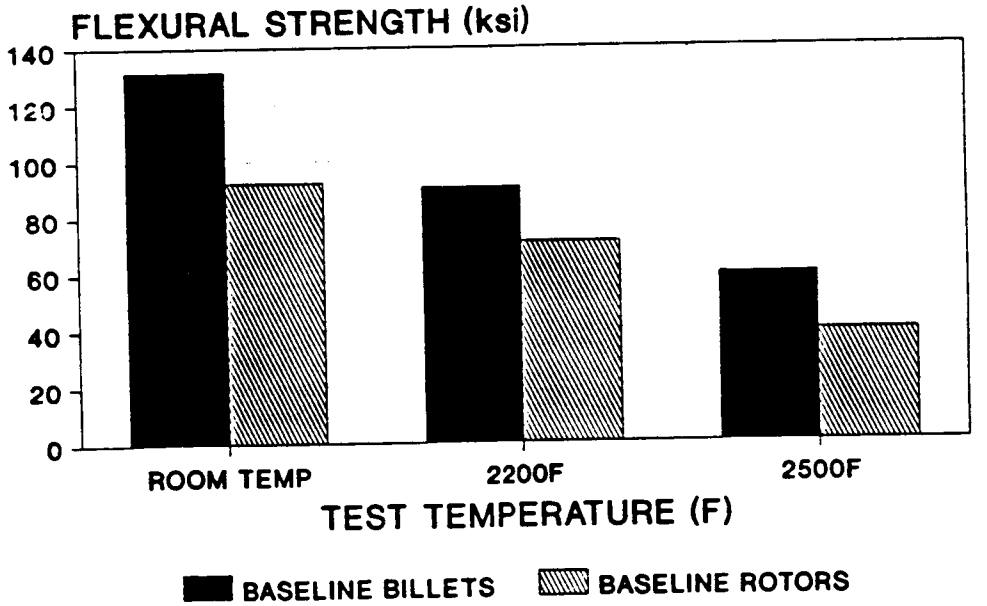

Figure 96. Comparison of Baseline Slip Process Billet and Rotor Mechanical Properties.

It was determined that extensive improvements in GN-10 slip properties and reproducibility, drying and calcining procedures, and encapsulation-HIP process were required in order to reproducibly fabricate defect-free AGT101 net-shape rotors with the required mechanical properties and dimensions.

SUBTASK A.B SLIPCAST ROTOR PROCESS DEVELOPMENT 1

The purpose of Subtask A.B was to take the problems identified in the fabrication of GN-10 AGT101 rotors using the baseline slip and HIP processes and investigate their elimination using iterative process development, and designed experiments where appropriate. Subtask A.B was begun in late 1988.

During early 1989, work focussed on slip preparation process improvement. A significant slip preparation process improvement, referred to as slip process revision #3, resulted in a GN-10 slip with greatly improved stability and reproducibility. This was achieved by refinement in slip preparation procedures, including much tighter control of slip dispersant addition procedures and controlled addition of slip pH adjustment additives. The improvement in slip property reproducibility is shown in Figure 3, where a statistical process monitoring chart shows the reduction in slip specific gravity variation using the revision #3 process compared to the baseline slip preparation process. A typical slip process revision #3 cast rotor is shown in Figure 95.

It was also determined that measured slip and process property variations were also due to inadequate characterization equipment use and calibration procedures. Rigorous measurement and calibration procedures were implemented and resulted in accurate and reproducible property measurements.

Drying and calcining cycles also were modified and resulted in reductions in crack formation during rotor drying and calcining treatments and elimination of drying and calcining cracks of billets.

Baseline pressure slipcast billets were encapsulation-HIPed using a modified HIP process (HIP process revision #1) where the intermediate layer encapsulant coating was modified and hold time at maximum temperature reduced. The revision #1 HIP process resulted in much improved as-HIPed surfaces (less reaction layer and pitting) and also resulted in increases in 2200 and 2500°F strengths, as shown in Table 61.

Approximately 15 slip process revision #3 rotors were slip cast. Six slip revision #3 rotors and many small slip revision #3 billets were encapsulation-HIPed using the improved HIP process

ORIGINAL PAGE IS
OF POOR QUALITY

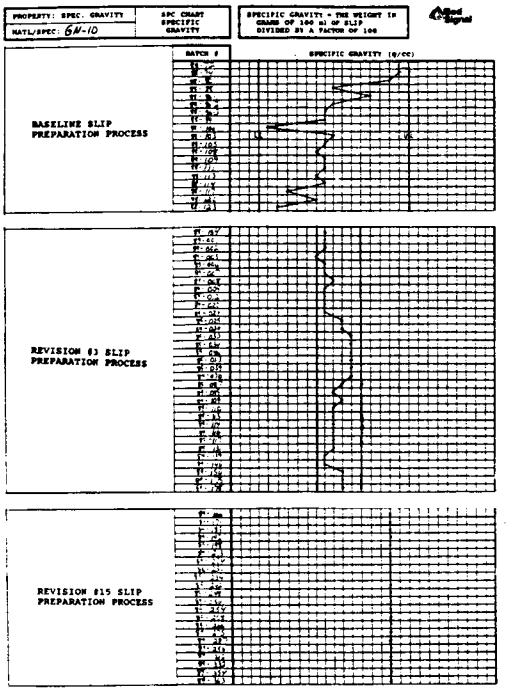

Figure 97. SPC Charting of Critical Slip Properties Such as Specific Gravity Documents Slip Process Improvements.

revision #1. Three rotors and many billets were cutup into test bars and mechanical properties evaluated. The results are shown in Table 61.Equivalent strengths were achieved in slip revision #3 billets and rotors, shown in Figure 98 (rotor test bars are cut from the rotor hub section so that the test bar lengths parallel the shaft), indicating that microstructure improvements in the rotor hub due to slip revision #3 property improvements generated equivalent green microstructures to small thickness billets. A comparison of baseline and slip process revision #3 billet properties (Figure 99) shows equivalent strengths, which is expected since the short casting time for billets, whether baseline or revision #3 slip derived, avoids slip instability problems. Comparison of baseline and slip revision #3 rotor mechanical properties (Figure100)shows a substantial increase in slip process revision #3 rotor strengths at all temperatures due to the improvement in slip stability at long casting times (more than 1 hour) and subsequent improvement in cast green microstructure.

There were, however, a number of problems stilled observed with the revision #3 slip process. The revision #3 slip still gelled after approximately 10 to 12 hours resulting in shaft rotor sections with poor microstructures. Some blade, hub, and shaft cracking still occurred during casting and mold removal due to differential casting and drying shrinkage caused by inadequate slip stability. The improved rotor drying process still resulted in some cracking in

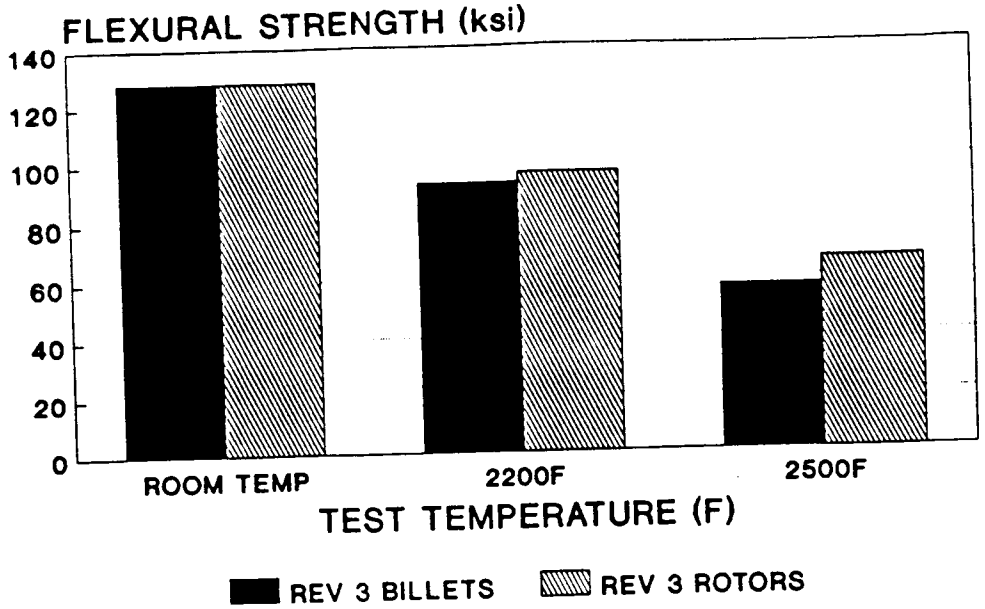

Figure 98. Comparison of Slip Process Revision #3 Billet and Rotor Mechanical Properties.

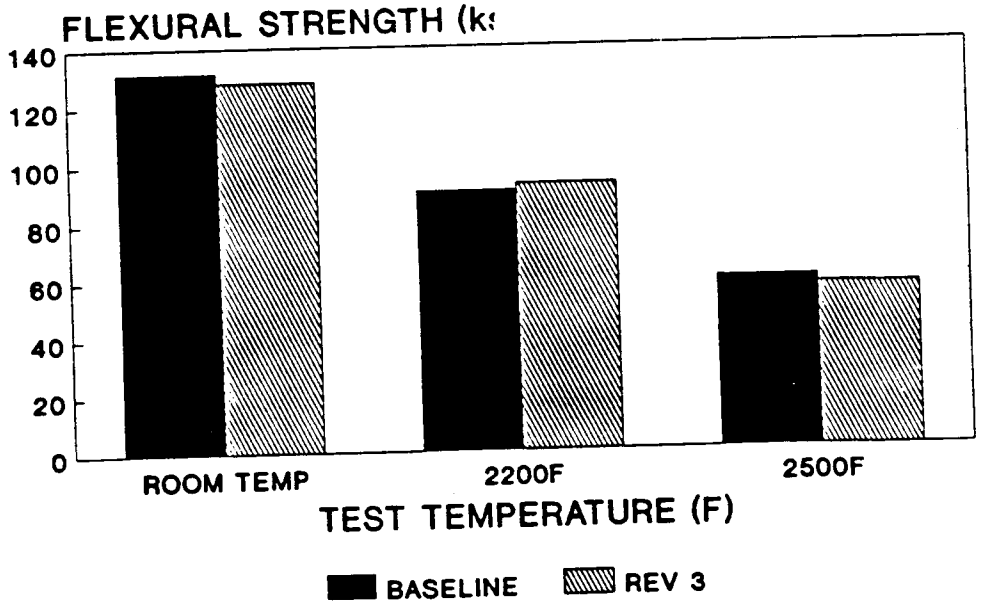

Figure 99. Effect of Slip Preparation Process on GN-10 Billet Mechanical Properties.

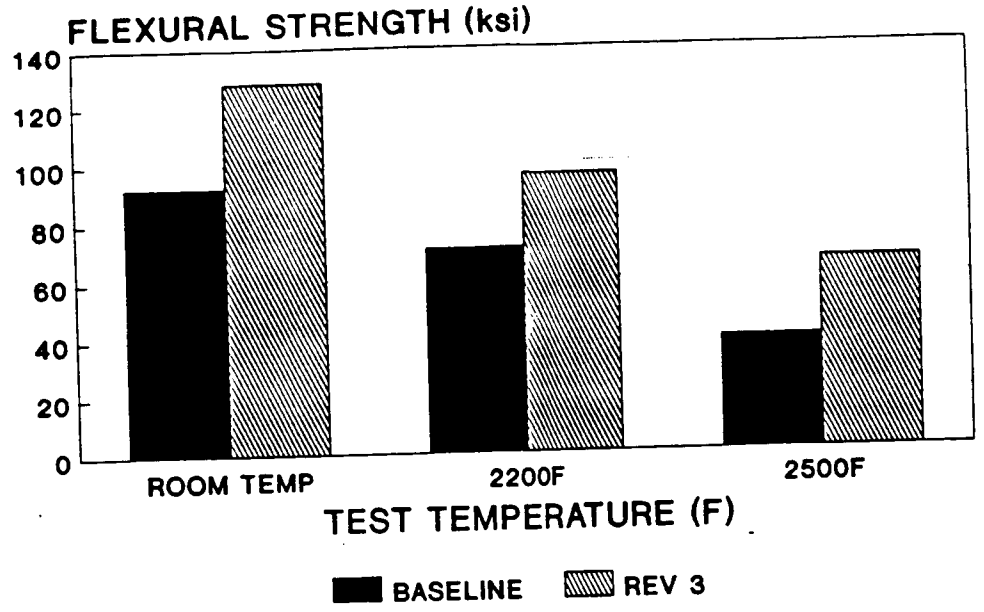

Figure 100. Effect of Slip Preparation Process on AGT101 Rotor Mechanical Properties.

hub, blade, and shaft sections. The rotor vertical green density gradient was reduced to 9.1% but needed to be reduced much further to allow rotor net-shape fabrication dimensional control. Experiments were initiated to explore lower and higher slip solids content effects on the vertical green density gradient. Two solids contents lower than the baseline and one solids content higher than the baseline were evaluated (see Table 62). The lowest solids content resulted in the lowest vertical green density gradient (3.5%) but this was still not acceptable. In addition the higher solids content slip resulted in a higher density gradient and lower maximum green density than the baseline solids content. This result is indicative of a slip not fully dispersed or stabilized, since it would be expected that a stable higher solids content slip below the dilatent rheology solids content limit would generate higher cast densities and lower density gradients due to greater suspension powder packing and subsequent smaller required particle rearrangement needed during cast layer formation.

In summary rotor mechanical properties in the rotor hub section were equivalent with billets and acceptable but process improvements were needed to result in reproducible defect-free AGT101 rotors with required dimensions.

Iterative experiments were initiated in March 1989 to examine improvements in the revision #3 slip preparation process which would eliminate the rotor problems detected. Through screening experiments

TABLE 62. Density Gradient Reduction Progress Summary.

BASELINE PRESSURE SLIPCAST ROTORS
SOLIDS CONTENT LEVEL 1
CASTING PRESSURE LEVEL 1

RESULT - 13.8% DENSITY GRADIENT
62.9% TD MAXIMUM DENSITY ACHIEVED

SLIP PREPARATION REVISION #3 SEMIROTORS
EFFECT OF SOLIDS CONTENT

SOLIDS LEVEL	CASTING PRESSURE LEVEL	DENSITY GRADIENT	MAXIMUM %TD DENSITY ACHIEVED
2	1	3.5	60.0
3	1	6.1	61.7
1	1	9.1	64.8
4	1	13.3	62.9

SLIP PREPARATION REVISION #15 ROTORS
EFFECT OF SOLIDS CONTENT

SOLIDS LEVEL	CASTING PRESSURE LEVEL	DENSITY GRADIENT	MAXIMUM %TD DENSITY ACHIEVED
1	1	5.9	65.6
5	1	3.5	66.6
6	1	2.3	67.2

EFFECT OF CASTING PRESSURE

SOLIDS LEVEL	CASTING PRESSURE LEVEL	DENSITY GRADIENT	MAXIMUM %TD DENSITY ACHIEVED
5	1	3.5	66.6
5	2	3.5	66.9
5	3	3.2	67.1

FURTHER INCREASES IN CASTING PRESSURE AND SOLIDS CONTENT

SOLIDS LEVEL	CASTING PRESSURE LEVEL	DENSITY GRADIENT	MAXIMUM %TD DENSITY ACHIEVED
7	2	1.8	66.9
7	3	0.9	67.3

SOLIDS CONTENT: LEVEL 2 < 3 < 1 < 5 < 4 < 6 < 7
CASTING PRESSURE: LEVEL 1 < 2 < 3

it was determined that sintering aid A was reacting in the aqueous environment, causing gas evolution, gelling, and slip instability. Substitution of a less reactive sintering aid A powder resulted in elimination of slip gas evolution and slip gelling with a great increase in slip stability. Modifications to the slip preparation process were also made based on the results of a second screening experiment, where it was determined that sintering aide suspensions needed to be aged before the GN-10 slip was prepared. A designed experiment was used to determine optimum aging times. The combination of these slip process improvements was named slip preparation process revision #15. The extensive improvement in slip stability generated using the revision #15 slip process is indicated in Figure 97, where revision #15 slip specific gravity varied very little compared to baseline and revision #3 slip processes.

Many billets and approximately 50 revision #15 rotors have been pressure cast in 1989. The as-cast yield of defect-free rotors has increased dramatically to greater than 80%. Rotor drying and calcining processes were further improved using iterative experiments. It was determined that the calcining cycle cooling rate was too rapid, thermally shocking rotors. Reduction in cooling rate eliminated this defect formation.

Six rotors were HIPed using the revision #1 HIP process. Figure 101 shows five revision 15 rotors after HIPing. The rotors were inspected after HIPing and no hub or shaft defects were detected. Three rotors were cutup for mechanical properties characterization. The results are shown in Table 61. Figure 102 compares baseline, revision #3, and revision #15 slip processed rotor properties. Slip revision #3 and #15 rotors have equivalent room and 2200°F properties. The slip revision #15 2500°F rotor strengths are slightly lower than revision #3 strengths. This is expected due to the fact that the improved slip revision #15 slip stability results in longer casting times (for equivalent slip solids contents and casting pressures), which expose the silicon nitride powder to aqueous surface hydroxylation for longer times. This results in higher grain boundary oxide contents and subsequent lower high temperature strengths.

The improved slip stabilities generated by slip revisions #3 and #15 lead to more reproducible rotor properties, as indicated by rotor room temperature properties shown in Table 63. For each slip process revision, the three rotors described were fabricated a minimum of one week apart, and more typically over two weeks apart. The baseline rotors show widely varying average strengths and miminum and maximum strengths. The slip revision #3 and #15 rotors average strengths vary less than 8 ksi, minimum strengths are above 100 ksi and maximum strengths are in the 140 ksi range.

Measurement of the green vertical density gradient in slip revision #15 rotors prepared using baseline slip solids content and

HIPed GN-10 AGT101 ROTORS
PREPARED USING SLIP PROCESS REVISION 15

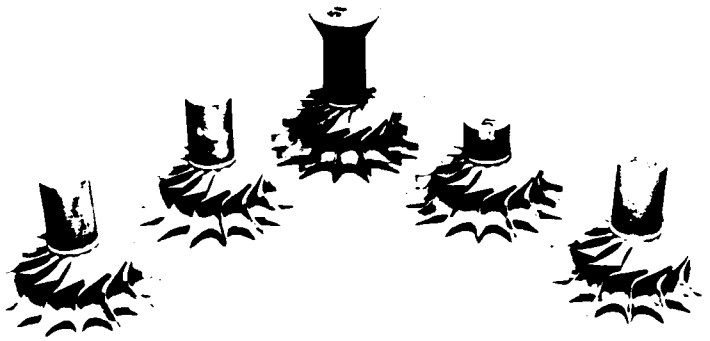

Figure 101. HIPed GN-10 AGT101 Rotors Prepared Using Slip Process Revision #15.

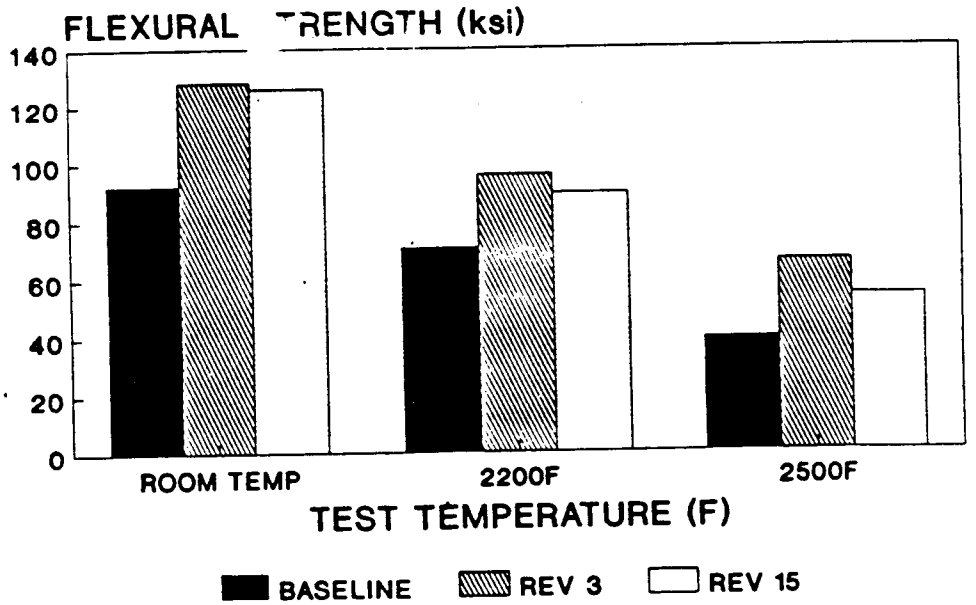

Figure 102. Effect of Slip Preparation Process on AGT101 Rotor Mechanical Properties.

TABLE 63. COMPARISON OF BASELINE, SLIP PROCESS REVISION 3, AND SLIP PROCESS REVISION 15 ROTOR ROOM TEMPERATURE FLEXURAL STRENGTHS AND CONSISTENCY.

BASELINE ROTORS	AVG	MIN	MAX	STD DEV	NUMBER TESTED
NO. 7	78.7	57.5	105.7	16.5	9
NO. 8	94.7	81.6	119.5	14.7	6
NO. 12	105.9	84.7	122.7	12.6	8
REVISION 3 ROTORS					
NO. 38	128.6	104.9	145.0	11.7	10
NO. 43	130.9	112.9	142.5	9.0	10
NO. 46	125.0	98.7	145.1	13.9	9
REVISION 15 ROTORS					
NO. 55	131.1	101.0	145.7	13.4	9
NO. 61	122.9	104.2	138.1	11.7	10
NO. 63	124.6	106.9	134.3	8.6	10

casting pressure showed a reduction in the gradient to 5.9% (Table 62). The improvement in rotor vertical green density gradient reduction with slip process improvement is shown in Figure 103. Improved slip stability results in more stable and consistent cast solids formation throughout the rotor casting process. Further reductions in the vertical green density gradient were explored by investigating higher slip revision #15 solids contents and rotor casting pressures in a matrix experiment. The results are shown in Table 62 and Figure 104. The stability of the revision #15 slip allows increasing rotor casting pressure and slip solids content to interactively reduce the slip process revision #15 vertical green density gradient to below 1%. Experiments were underway late in 1989 to determine the effect of 3.5% and 0.9% vertical density gradients on subsequent HIPed rotor dimensions using rods 1.5" diameter rods machined from revision #15 slip processed rotors.

Examination of the slip revision #15 and HIP process revision #1 rotor fabrication process revealed areas in need of further improvement in November 1989. Drying yield of slip process #15 rotors was approximately 80% and further improvements in reproducibility and drying consistency were needed. Iterative experiments were ongoing through the end of 1989 to improve rotor drying. Experiments at the end of 1989 also focussed on further improvements in revision #15 slip reproducibility and total rotor process yield. With the achievement of nearly defect-free rotors, dimensional measurements were initiated to determine blade shape conformance (it must be noted that the GN-10 AGT101 rotors are

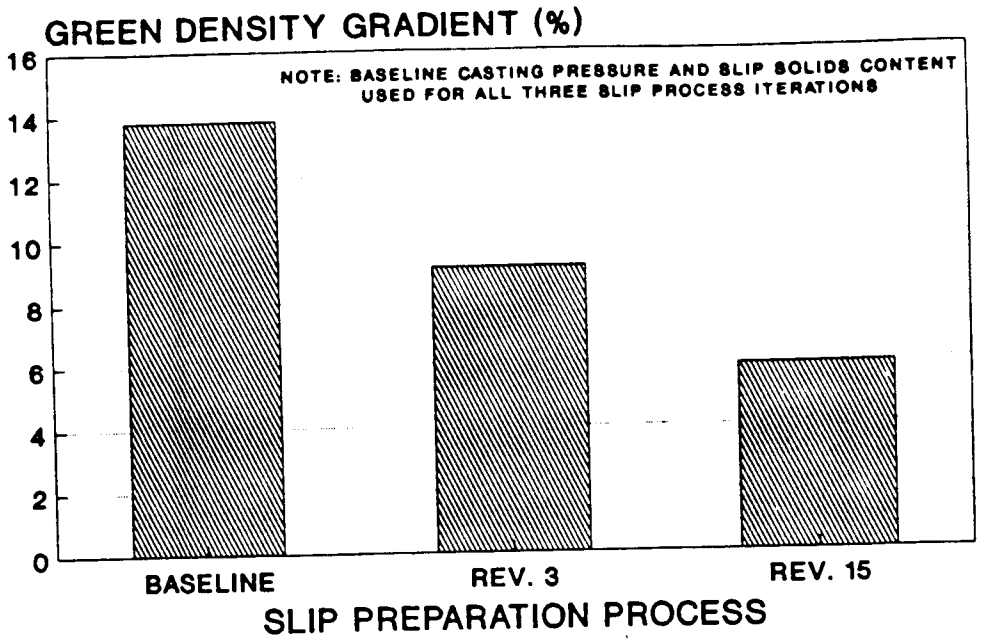

Figure 103. Rotor Vertical Green Density Gradient Reduction With Slip Preparation Process Improvement.

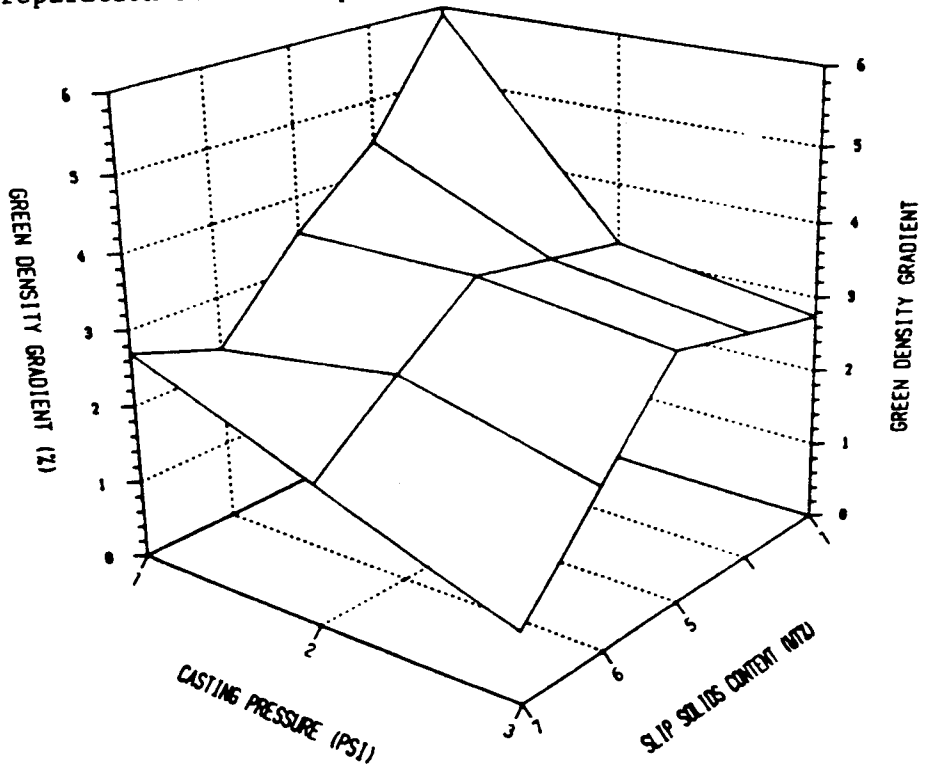

Figure 104. Slip Process Revision #15 Rotor Green Density Gradient Reduction With Increasing Slip Solids Content and Casting Pressure.

approximately 4% oversize due to the use of the original AGT program rotor tooling). Revision #1 encapsulation-HIPed revision #15 rotors still exhibited unacceptable surface roughness and pitting and experiments were initiated to investigate improved encapsulants and HIP process conditions.

Slip process revision #15 plates were cast in late 1989 that had extremely flat surfaces due to revision #15 slip stability. These plates were HIPed using the revision #1 HIP process and were being machined into as-processed surface test bars for evaluation of as-processed surface mechanical properties at the end of 1989.

A unique and very useful in-process characterization tool was developed in 1989 for examination of the rotor casting process. Microfocus realtime X-ray fluoroscopy was used to examine the AGT101 rotor slip/cast solids interface progression in-situ during casting non-destructively. An example of a slip revision #3 rotor monitoring experiment is shown in Figure105. Garrett Ceramic Component's unique pressure casting rigs are X-ray transparent and the whole rig can be placed in the X-ray inspection chamber. This in-process NDE technique has allowed characterization of the critical casting front spatially and temporally and determination of defect (e.g. crack) origins and causes.

An investigation of porous plastic mold technology was also initiated in 1989 as a potential replacement for plaster molds, which have a number of undesirable properties including weak mechanical strength, difficult porosity distribution reproducibility, and limited lifetimes. Porous plastic was also being explored as a potential mold material for all-surface dewatering during pressure slip casting of rotors. Currently Garrett Ceramic Components uses a uniaxial dewatering process. All-surface dewatering would potentially reduce casting times. Work to-date has centered on porous plastic mold evaluation for casting of flat surface billets. Equivalent casting rates and green cast densities have been achieved compared to plaster molds. Work also was initiated on mold release development since some cast part adherence was observed when using porous plastic molds.

Work was also initiated in September 1989 on screening of GN-10 slip through finer screens than the baseline process. Revision #3 slip was successfully screened through openings one-third the size of the baseline screens. Billets were cast and HIPed and were being cutup into test bars for evaluation at the end of 1989.

With the improvement in slip stability and reproducibility and subsequent rotor forming process reproducibility, it was decided that the GN-10 rotor pressure slip casting process was reproducible enough that designed experiments intended to explore process parameter boundary limits could be designed and implemented without process instabilities causing unacceptable errors in resulting

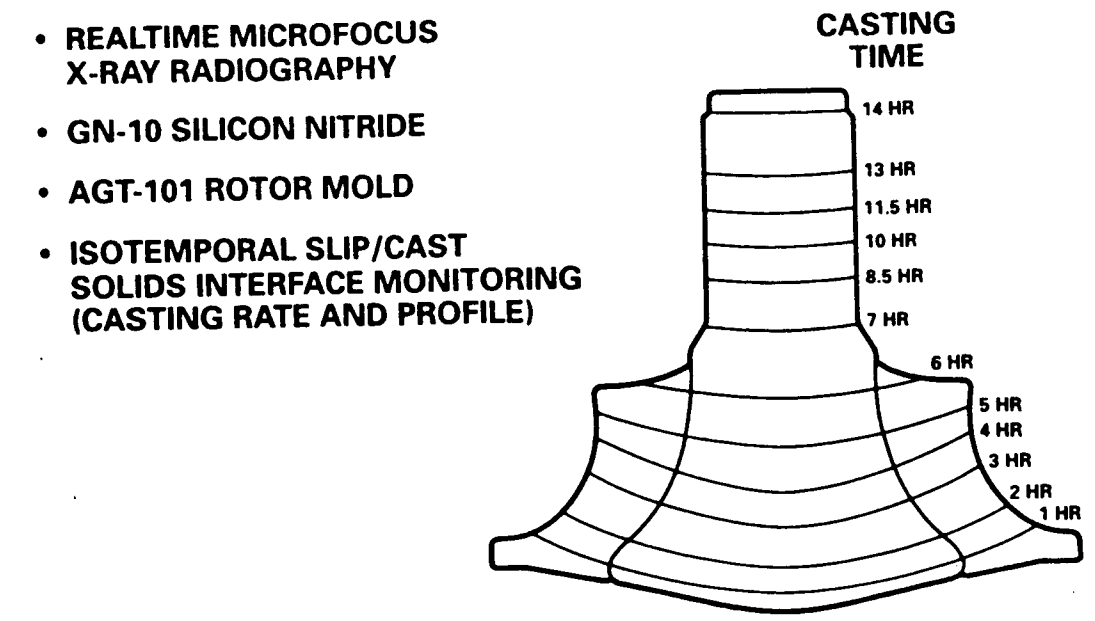

Figure 105. In-Situ NDE Examination of Pressure Casting Process.

interpretation. The initial boundary limit designed experiments are listed in Table 64. Due to the licensing of the ASEA encapsulation-HIP process in late 1989 and subsequent investigation of potential improvements, the final experimental design is still being determined.

SUBTASK A.F SLIPCAST ROTOR COMPONENT QUALIFICATION/NDE DEVELOPMENT

A task was initiated in June 1989 at Allied-Signal Research and Technology to investigate in-situ monitoring of the AGT101 rotor casting process using ultrasonic attenuation and velocity measurements to monitor the rotor slip/cast solids interface during pressure casting. Efforts during 1989 focused on transducer and technique development. Ultrasonic attenuation and velocity were examined as a function of frequency for both the current Garrett ceramics AGT101 mold material and plaster. Part-to-part variation was examined as well as signal strength. GN-10 slip was also examined and the optimum operating frequency conditions were evaluated for slip examination in a noncasting environment. Efforts were to continue into 1990.

Realtime and film microfocus X-ray fluoroscopy techniques were being developed in 1989. J. Minter of Garrett Auxiliary Power Division provided training and X-ray implementation support. Development of GN-10 silicon nitride penetrameters and step block gauges was initiated in 1989. In late 1989 three penetrameters were fabricated from GN-10 HIPed test bars. The penetrameters were

Table 64. GN-10 AGT101 Rotor Development Slip Revision #15 Processing Parameter Boundary Limit Determination Designed Experiments.

NO.	EXPERIMENT	DESIGN
1	DISPERSANT OPTIMIZATION	L_8
2	SLIP PREPARATION PROCEDURE	L_{16}
3	PRESSURE CASTING PARAMETERS	L_9
4	MOLD REMOVAL OPTIMIZATION	L_8
5	DRYING PROCESS OPTIMIZATION	L_9
6	CALCINING PROCESS OPTIMIZATION	L_9
7	ENCAPSULATION-HIP PARAMETERS	TBD

machined to three different thicknesses - 0.010", 0.020", and 0.050". Three different size holes were laser drilled into each penetrameter ranging from 0.003" to 0.060" diameter. At the end of 1989 the penetrameters were being examined for 2T detectability limits.

TASK C FABRICATION OF TEST SPECIMENS AND NDE STANDARDS

SUBTASK C.A FABRICATION OF MATERIAL EVALUATION TEST SPECIMENS

The objective of this subtask was to fabricate a set of 250 test bars of pressure slipcast GN-10 baseline slip and HIP processed silicon nitride for delivery to and subsequent evaluation by Garrett Auxiliary Power Division of baseline GN-10 mechanical properties. The test bars were delivered in February 1989. They consisted of:

200 - 0.25" by 0.125" by 2" Flexure Test Bars
20 - 0.25" by 0.25" by 2" Fracture Toughness Bars
30 - 0.25" by 0.5" by 4" Large Flexure Test Bars

SUBTASK C.C FABRICATION OF SLIPCAST DEFECT SEEDED BILLETS FOR NDE DEVELOPMENT

The NDE seeded defect specimens jointly designed by Garrett Ceramic Components and Garrett Auxiliary Power Division were initially fabricated in early 1989. The design is shown in Figure 106. The green specimens were investigated at Garrett Ceramic

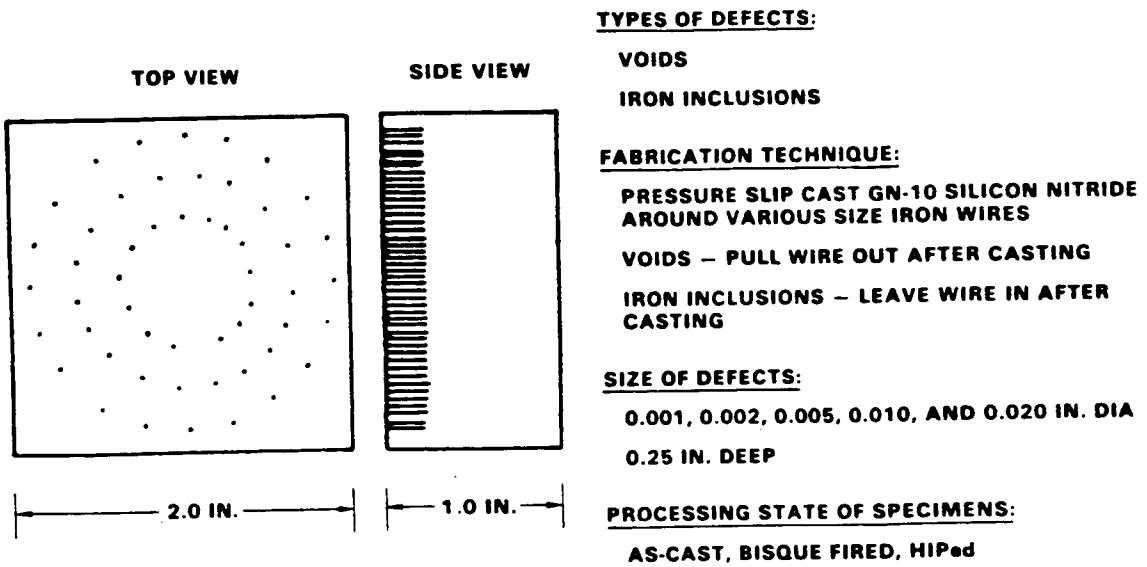

Figure 106. NDE Seeded Defect Specimen Configuration

Components using microfocus X-ray fluoroscopy. The green specimens were then delivered to Garrett Auxiliary Power Division for inspection, after which one green specimen was to be destructively analyzed by both groups and the remaining specimens processed through calcination, inspection, and then encapsulation-HIP and inspection. J. Minter of Garrett Auxiliary Power Division determined that ultrasonic inspection of the green seeded defect billets was not feasible due to their fragility and inability to be exposed to water (the ultrasonic inspection technique signal coupling medium). The green specimens were being prepared at Garrett Ceramic Components at the end of 1989 for calcination and subsequent inspection.

SUBTASK C.D FABRICATE TENSILE TEST SPECIMENS

Subtask C.D was initiated in 1989 to determine suitable tensile bar fabrication techniques that would be representative of Garrett Ceramic Components' AGT101 rotor pressure casting fabrication process. Subsequent delivery of 5 tensile specimens would be made tc Garrett Auxiliary Power Division when GN-10 properties were deemed reproducible and acceptable by GAPD. Two approaches were taken to explore potential fabrication routes for tensile bars. Large plates (9" by 5" by 1") of pressure slipcast revision #15 GN-10 were fabricated and HIPed in late 1989 for subsequent cutup into tensile test bars. The test bars fabricated by this technique are not necessarily representative of AGT101 rotor geometry or properties and will be compared with those fabricated by the other techniques whose development was initiated in late 1989 - vertical cylindrical

molds made from proprietary mold material, and porous plastic. The vertical cast rods should be more representative of the casting geometry and process used for AGT101 rotor fabrication.

GAS TURBINE DISTRIBUTION LIST
MAY 10, 1990

Jet Propulsion Laboratory
4800 Oak Grove Drive
Pasadena, CA 91103

National Institute of Standards & Technology
Attn: S. M. Wiederhorn
Inorganic Materials Division
Gaithersburg, MD 20899

NASA Lewis Research Center
21000 Brookpark Road
Cleveland, OH 44135
Attn: J. P. Gyekenyesi, MD 6-1
Library, MS 60-3 (3 copies)
C. L. Ball, MS 86-1
P. T. Kerwin, MS 86-6
J. A. Ziemianski, MS 86-1
Technology Utilization, MS 7-3
D. P. Fleming, MS 23-3
S. Levine, MS 49-3
R. Firestone, MS 500-305
T. P. Herbell, MS 49-3
H. E. Sliney, MS 23-2
T. Strom, MS 86-6 (10 copies)
J. R. Rollbuher, MS 77-10
R. C. Evans, MS 86-6
E. A. Willis, MS 86-1

Mr. R. Bradley
Oak Ridge National Laboratory
P. O. Box 2008
Oak Ridge, TN 37830

The Carborundum Company
Attn: Dr. J. W. Hinton
P. O. Box 1054
Niagara Falls, NY 14302

Wright Patterson Air Force Base
Attn: NASA Lewis Liaison Officer
AF APL/DO
Wright Patterson AFB, OH 45433

NASA Headquarters
Washington, DC 20546
Attn: RP/R. Anderson

U.S. Army Materials Technology Laboratory
405 Arsenal Street
Watertown, MA 02172
Attn: R. Katz
G. Quinn, MS-EMC

U. S. Department of Energy
Forrestal Building
Washington, DC 20585
Attn: R. J. Gottschall, MS 5H-063
A. A. Chesnes, MS 5G-046
R. T. Alpaugh, MS 5G-046
S. B. Kramer, MS 5G-064 (6 copies)

Wright Patterson Air Force Base
Attn: Mr. Dale Hudson, AFWAL/POTC
Wright Patterson AFB, OH 45433

Ms. Sharon White
Division 8453
Sandia National Laboratories
P. O. Box 969
Livermore, CA 94550

NASA Scientific & Technical Facility
P. O. Box 8757
B.W.I. Airport, MD 21240
(NOTE: Send 2 copies with
Authorization Form FF427)

Aviation Applied Technology Directorate
U. S. Army Research and Technology Labs
AVSCOM
Fort Eustis, VA 23604-55
Attn: William S. Taylor

U. S. DOE - TIC
P. O. Box 62
Oak Ridge, TN 37830
(NOTE: Send 2 copies with
Form RA-246)

DTNSRDC, Code 2752
Annapolis, MD 21402
Attn: Mark Cervi

Sandia National Laboratories
P. O. Box 5800
Albuquerque, NM 87185
Attn: Kevin L. Linker, 6217

Williams Research Corporation
2280 West Maple Road
Walled Lake, MI 48088
Attn: P. Rempes

Mr. George S. Wing
Seaport Village, Suite 2A
123 W. Torrance Boulevard
Redondo Beach, CA 90277

AVCO Corporation
550 South Main Street
Stratford, CT 06497
Attn: Library

Solar Turbines International
2200 Pacific Highway
San Diego, CA 92138
Attn: Library

U.O.P. Inc.
Materials Science Division
10 U.O.P. Plaza
Des Plains, IL 60016
Attn: Dr. G. R. Lester, Director

Wallace Murray Corporation
1125 Brookside Avenue
P. O. Box 80-B
Indianapolis, IN 46206
Attn: R. C. Bremer, Jr.

St. Elmo Hybrids
1048 Van de Venter Street
West Palm Beach, FL 33405
Attn: E. M. Long

General Motors Corporation
Detroit Diesel Allison
P. O. Box 894
Indianapolis, IN 46206
Attn: P. W. Heitman, W-5
H. E. Helms, T-19
P. Haley, S-51

Teledyne Continental
P. O. Box 6971
Toledo, OH 43612
Attn: Library

Mr. H. Franklin Hostetler
Brush Wellman, Inc.
1200 Hanna Building
Cleveland, OH 44115

General Electric Company
Aircraft Engine Group
1000 Western Avenue
Lynn, MA 01910
Attn: A. Bellin (374A8)

IIT Research Institute
10 West 35 Street
Chicago, IL 60616
Attn: D. Larson (Library)

Howmet Turbine Component Corp.
1600 S. Warner Road
Whitehall, MI 49461
Attn: John K. Thorne

Aerospace Corporation
2260 East El Segundo Blvd.
El Segundo, CA 90245
Attn: W. Roessler

Westinghouse R&D Center
1310 Beulah Road
Pittsburgh, PA 15235
Attn: Mr. Roy Bratton

Prof. Alan Epstein
Room 31-266
MIT
Cambridge, MA 02139

Mr. Graham Espin
Rolls Royce, Inc.
1201 Pennsylvania Avenue, NW
Washington, DC 20004

Ferro Corporation Technical Center
7500 E. Pleasant Valley Road
Independence, OH 44131
Attn: Mr. Donald Beale

Vought Corporation
P. O. Box 226144
Dallas, TX 75266
Attn: Dr. John L. Porter

General Electric Company
Aircraft Engine Group
Cincinnati, OH 45215
Attn: Mr. Warren Nelson, MS H-99

Norton Company
1 New Bond Street
Worcester, MA 01606
Attn: E. A. Sundburg

Cabot Corporation
Boyertown Technical Library
County Line Road
Boyertown, PA 19512

Coors Porcelain Company
600 9th Street
Golden, CO 80401
Attn: L. E. Coubrough

Corning Glass Works
Advanced Engine Components Department
Erwin Ceramics Plant
Corning, NY 14830
Attn: G. Papa

GTE Laboratories
40 Sylvan Road
Waltham, MA 02154
Attn: Dr. L. J. Bowen

Kyocera International Incorporated
8611 Balboa Avenue
San Diego, CA 92123

Pure Carbon Incorporated
St. Marys, PA 15857
Attn: W. R. Shobert

Mr. Martin R. Young
Bldg. #1, Room 3003
Ford Motor Company
20000 Rotunda Drive
Dearborn, MI 48121

SRI International
Menlo Park, CA 94025
Attn: Mr. David Rowcliffe

TRW, Inc.
23555 Euclid Avenue
Cleveland, OH 44117
Attn: Mr. John Reidy (T/M 2707)

Eaton Corporation
Engineering & Research Center
26201 Northwestern Highway
P. O. Box 766
Southfield, MI 48037
Attn: Mr. Lamont Eltinge

General Electric Company
Research & Development Center
P. O. Box 8
Schenectady, NY 12301
Attn: Dr. Curtis A. Johnson

Hamilton Standard
Bradley Field Road
Windsor Locks, CT 06096
Attn: Mr. A. Brouillet, MS 1A-2-6

Library of Congress
Room LM413
101 Independence Avenue, S.E.
Washington, DC 20540
Attn: Mr. Jack Moteff

Garrett Ceramic Components Division
19800 Van Ness Avenue
Torrance, CA 90509
Attn: Maxine Savitz

Commander
Applied Technology Laboratory (AVSCOM)
Attn: DAVDL-ATL (Roger Ferguson)
Fort Eustis, VA 23604-5577

Sunstrand Turbomach
Advanced Technology Group
4400 Ruffin Road
P. O. Box 85757
San Diego, CA 92138-5757
Attn: Tibor Bornemisza

Ceramics Division
Institute for Materials Science
and Engineering
National Institute of Standards & Technology
Gaithersburg, MD 20899
Attn: Stephen M. Hsu

EG&G
P. O. Box 1625
Idaho Falls, ID 83415
Attn: Mr. Basil Barna, M.S. ILF

G. E. Turbine Technology Department
1 River Road
Building 53, Room 322
Schenectady, NY 12345
Attn: Mr. Ken Beebe

Norton/TRW Ceramics
Goddard Road
Northboro, MA 01532-1545
Attn: B. J. McEntire

Torrington Company
Corporate Research
59 Field Street
Torrington, CT 06790
Attn: Mr. W. Chmura

Turbine Components Corporation
Technology Group
Box 431
Commerce Street
Branford, CT 08405
Attn: G. William Goward

James Cooper
Teledyne Continental Motors
P. O. Box 60
Mobile, AL 36601

Donald Anson
Battelle Columbus Laboratory
505 King Avenue
Columbus, OH 43201

1. Report No.	2. Government Accession No.	3. Recipient's Catalog No.
NASA CR-185240		

4. Title and Subtitle	5. Report Date
Advanced Turbine Technology Applications Project (ATTAP) - 1989 Annual Report	February 1990
	6. Performing Organization Code 99193
7. Author(s)	8. Performing Organization Report No.
Engineering Staff of Garrett Auxiliary Power Division, A Unit of Allied-Signal Aerospace Company	31-8071(02)
	10. Work Unit No.
9. Performing Organization Name and Address	11. Contract or Grant No.
Garrett Auxiliary Power Division 2739 E. Washington Street Phoenix, Arizona 85034	DEN3-335
	13. Type of Report and Period Covered
12. Sponsoring Agency Name and Address	Annual Report 1989
U.S. Department of Energy Office of Transportation Systems, Heat Engine Propulsion Division, Washington, D.C. 20585	14. Sponsoring Agency Code DOE/NASA/0335-2

15. Supplementary Notes

Annual Report under Interagency Agreement
Project Manager: T.N. Strom, Propulsion Systems Division
NASA-Lewis Research Center, Clevelend, Ohio 44135

16. Abstract

This report is the second in a series of Annual Technical Summary Reports for the Advanced Turbine Technology Applications Project (ATTAP), authorized under NASA Contract DEN3-335 and sponsored by the U.S. Department of Energy. The report was prepared by Garrett Auxiliary Power Division (GAPD) a unit of Allied-Signal Aerospace Company. The report includes information provided by Garrett Ceramic Components Division (GCCD), the Norton/TRW Ceramics Company (NTC), and the Carborundum Company, all subcontractors to GAPD on the ATTAP. The project is administered by Mr. Thomas Strom, Project Manager, NASA-Lewis Research Center, Cleveland, OH. This report covers plans and progress on ceramics development for commercial automotive applications over the period January 1 through December 31, 1989.

Project effort conducted under this contract is part of the DOE Gas Turbine Highway Vehicle System program. This program is directed to provide the U.S. automotive industry the high-risk, long-range technology necessary to produce gas turbine engines for automobiles with reduced fuel consumption, reduced environmental impact, and a decreased reliance on scarce materials and resources. The program is oriented toward developing the high-risk technology of ceramic structural component design and fabrication, such that industry can carry this technology forward to production in the 1990s. The ATTAP test bed engine, carried over from the previous AGT101 project, is being used for verification testing of the durability of next generation ceramic components, and their suitability for service at Reference Powertrain Design conditions.

This document reports the technical effort conducted by GAPD and the ATTAP subcontractors over the second year of the project. Topics covered include ceramic processing definition and refinement, design improvements to the ATTAP test bed engine and test rigs and the methodology development of ceramic impact and fracture mechanisms. Appendices include reports by ATTAP subcontractors in the development of silicon nitride and silicon carbide families of materials and processes.

17. Key Words (Suggested by Author(s))	18. Distribution Statement
Ceramic-Engine Ceramic-Technology	Unclassified-Unlimited Subject Category 85 DOE Category UC-96

19. Security Classif. (of this report)	20. Security Classif. (of this page)	21. No. of Pages	22. Price*
Unclassified	Unclassified	197	A10

* For sale by the National Technical Information Service, Springfield, Virginia 22161